University of Alberta

Investigations into Differences between Vaccinia and Myxoma Virus Plaquing Properties Identifies Strategies for Increasing the Oncolytic Efficacy of Myxoma Virus

by

Chad Robert Irwin

A thesis submitted to the Faculty of Graduate Studies and Research
in partial fulfillment of the requirements for the degree of

Doctor in Philosophy

in

Virology

Medical Microbiology and Immunology

Fall 2013
Edmonton, Alberta

DEDICATION

I dedicate this to the memory of my father, Donald Robert Irwin (October 24, 1958 – December 24, 2012), and my grandfather Kenneth Fritz Bauman (February 9, 1936 – February 15, 2010).

ABSTRACT

Despite both being poxviruses, vaccinia (VACV) and myxoma (MYXV) form very different plaque types. VACV plaques are large and show a central clearing of cells, while MYXV plaques are smaller and result in a clumping of cells. VACV spread is promoted by the formation of an enveloped form of virus (EV) and localized actin rearrangements (called actin tails), which push EV from a cell. Since mutations in genes that catalyze these processes often reduce VACV plaque size (i.e. mutants are more MYXV-like), we investigated the relative efficiency of these viruses to produce actin tails. MYXV forms far fewer actin tails than VACV. Bioinformatics identified MYXV counterparts to these VACV genes - minus one. MYXV lacks a F11 homolog. F11 promotes VACV spread by disrupting cortical actin through inhibition of RhoA-mDia1 signaling. We hypothesized the absence of a MYXV F11 homolog explains these plaquing differences and therefore generated a recombinant MYXV that expresses F11. This virus formed larger plaques, grew to higher levels, and induced a number of cellular morphological changes not observed in control MYXV strains. These included cell rounding, disruption of cortical actin, and more actin tails. F11+ MYXV formed smaller plaques and less actin tails than VACV, suggesting that while an absence of F11 partially explains why MYXV forms smaller plaques than VACV other differences likely exist.

MYXV naturally has oncolytic abilities, but does not spread well outside of lagomorphs, which could limit its abilities to treat cancer. We thought that enhanced spread conferred by F11 might increase MYXV's oncolytic effectiveness. $F11^{+}$ MYXV showed enhanced abilities to control tumor growth and prolong survival in xenografted mice bearing human mammary tumors. This virus also spread more efficiently from an injected tumor, to a second untreated tumor. We could mimic F11's stimulatory effects on MYXV growth in cell culture by pharmacological inhibition or siRNA-mediated

silencing of key regulators of the actin cytoskeleton. This suggests that chemical disruption of actin could enhance wildtype MYXV's oncolytic capacity. Since all viruses must overcome barriers to exit, like cortical actin, this approach could be used to improve the effectiveness of other oncolytic viruses.

ACKNOWLEDGEMENTS:

I would like to thank my supervisor, Dr. Evans, for taking a chance on me first as a summer student, then as a technician, and finally as a graduate student. I have learned an incredible amount during my time working for you, and am grateful for that. I also appreciate the independence you gave me to take this project in ways that we would never have predicted when I began grad school. Thank you to my committee members, Drs. Smiley and Wozniak, for your helpful suggestions.

I was also fortunate to work with an excellent group of people. Thank you to James, Don, and Wendy for teaching me a great number of skills when I first started in the lab. I could not have been successful as a graduate student without your knowledge, patience, and friendship. I would like to thank Nicole for her being a technician extraordinaire. Your hard work was invaluable to the success of this project. Furthermore, your humor made all those long days in the animal facility bearable. Thank you to Kate and Mary for your expertise in setting up these animal experiments. Danielle, Lindsay, Megan, Branawan, Li, and Wondim, thank you for making the lab a fun place to be.

Elisabeth, Sarah, Joel, Camille, Dee, Nick, and Chelsea, I enjoyed our coffees, lunches, volleyball games, and any other random event we partook in. Thanks for being there with me on this roller coaster ride. I'd also like to thank Kristin for her support and, for teaching me that sometimes you need to take a break, even if it means tromping through the Andes, or jumping off a mountain.

Thank you to Drs. Barry, Condit, McFadden, Moss, Ogg, and Way for providing reagents and other technical expertise. Also thank you to members of the Hitt, Shmulevtiz, and Barry labs for your ideas, and for being fun travelling companions to conferences. Thank you to Kim for being a great mentor and friend, I learned a lot being a teaching assistant for you. Also thanks to the office staff (Anne, Debbie, and Tabitha), and washup staff (San, Yadwiga) for all that you do that keeps the department running smoothly.

Funding from CIHR, NSERC, ACF, and AIHS supported this work. I was also fortunate to be supported by an NSERC CGS M, ACF graduate student scholarship, and a Queen Elizabeth II scholarship.

Lastly, I would like to thank my mom Sheila, and my siblings Byron (Mandy) and Nicole (Lance). I could not have done this without your support, at both the best and worst of times.

TABLE OF CONTENTS

LIST OF FIGURES

LIST OF TABLES

LIST OF ABREVIATIONS

ADF	actin depolymerization factor
AKT	protein kinase B
ATM	Ataxia telangiectasia mutated
Arp2/3	actin related protein 2/3 complex
BSA	bovine serum albumin
Cdc42	Cell division control protein 42
CEV	Cell-associated enveloped virus
DAPI	4', 6' diamidino-2-phenylindole
DDAO	7-hydroxy-9H(I,3-dichloro-9,9-dimethylacridin-2-one
DDAOG	9H-(1,3-dichloro-9,9-dimethylacridin-2-one-7-yl) β-D-Galactopyranoside
DMEM	Dulbecco's minimal essential media
DNA	deoxyribonucleic acid
DIC	differential interference contrast
EDTA	Ethylenediaminetetraacetic acid
EFC	Entry/fusion complex
Erk1/2	mitogen-activated protein kinase 1
EV	enveloped virus, also known as extracellular enveloped virus (EEV)
GAP	GTPase activating protein
GDI	GDP disassociation inhibitors
GEF	guanine exchange factor
GFP	green fluorescent protein
Grb2	growth factor receptor-bound protein 2
GST	glutathione-S-transferase
hpi	hours post-infection
IFN	interferon
IHD	International Health Department
IL	Interleukin
IV	immature virus
LacZ	β-galactosidase
LB	Lysogeny broth
LIMK	LIM domain kinase
MALDI-TOF	Matrix-assisted laser desorption/ionization -time of flight
mDia1	mammalian diaphaneous formin – 1 (also known as Dia1 or DIAPH1)
MEM	minimal essential medium
MLC	myosin light chain
MOI	multiplicity of infection
mRNA	messenger ribonucleic acid
MYXV	myxoma virus
MV	mature virus, also known as intracellular mature virus (IMV)
MVA	modified vaccinia Ankara
N.A.	Numerical aperature
Nck2	NCK adaptor protein 2
N-WASP	neural Wiskott-Aldrich syndrome protein

PAGE	polyacrylamide gel electrophoresis
PAK1	p21 protein (Cdc42/Rac1)-activated kinase 1
PBS	phosphate buffered saline
PBS A	phosphate buffered saline without calcium or magnesium
PBS Complete	phosphate buffered saline with calcium and magnesium
PBS-T	phosphate buffered saline with 0.1 % tween-20
PCR	polymerase chain reaction
PFU	plaque forming unit
PLD1	Phospholipase D1
PP2A	Protein Phosphatase 2A
p53	tumor protein 53
Rac1	ras-related C3 botulinum toxin substrate 1
Rb	retinoblastoma protein
Rho	ras homolog family member
ROCK	Rho-associated protein kinase
RNA	ribonucleic acid
rpm	rotations per minute
SCAR	Suppressor of cyclic AMP receptor
SCR	Short consensus repeat
SDS	Sodium dodecyl sulfate
S.E.M.	standard error of the mean
siRNA	small interfering RNA
SNARE	Soluble NSF attachment protein receptor
STAT-1/3	Signal-transducer and activator of transcription protein- 1/3
TNF	Tumor necrosis factor
TrFP	Tomato Red fluorescent protein
UV	ultra-violet
VACV	Vaccinia virus
WASP	Wiskott-Aldrich syndrome protein
WAVE	Wiskott-Alrrich syndrome protein family member 1
WV	wrapped virus, also known as intracellular enveloped virus (IEV)
WR	Western Reserve
WT	wildtype
X-Gal	5-Bromo-4-chloro-3-indolyl-β-D-galactosidase
YFP	Yellow fluorescent protein
YLDV	Yaba-like disease virus

CHAPTER 1: INTRODUCTION

1.1 Pathogen Manipulation of the Cytoskeleton:

The cytoskeleton plays an important role in virtually all aspects in the birth, life and death of an eukaryotic cell. In addition to playing an important structural role, the dynamic nature of the cytoskeleton is important for processes such as cell adhesion[4], motility[5], division[3,6,7], and for the endocytosis[8] or exocytosis[8-10] of molecules. The cytoskeleton is also involved in the intracellular transport of molecules and alterations in it can lead to potent changes in gene expression or the induction of apoptosis[11-13]. Given the diverse number of processes that the cytoskeleton is involved in, it is not surprising that its disregulation can be associated with diseases such as cancer, or that many pathogens target the cytoskeleton to facilitate their propagation (reviewed in [14-23]).

Three classes of polymers largely make up the cytoskeleton. These are microtubules, intermediate filaments and microfilaments. These polymers differ in their size and composition with microtubules being the largest in diameter at ~24 nm, intermediate filaments at ~ 10 nm, and microfilaments the smallest with a diameter of ~ 7 nm[24]. Microtubules and microfilaments are mostly homopolymers of proteins (tubulin and actin, respectively) and are highly dynamic structures, which are greatly involved in processes requiring movement. By contrast intermediate filaments tend to be more stable, can be formed from multiple types of subunits and tend to play more of a structural role (e.g. nuclear membrane)[24]. These polymers and their roles are the subject of numerous reviews ([24,25]).

One family of viruses that manipulates the cytoskeleton to aid in their growth are the poxviruses. Members of this family have been shown to activate components of the actin cytoskeleton to facilitate their entry, use microtubules for their intracellular movement, and alter the actin cytoskeleton to promote their exit and efficient spread. The work presented here focuses on two particular poxviruses, vaccinia virus (VACV)

and myxoma virus (MYXV) and explores whether differences in their spread properties are due to differences in their abilities to manipulate the actin cytoskeleton.

1.2: Actin Microfilaments:

Microfilaments are made from actin monomers (also known as globular or G-actin). In mammals six isoforms of actin exist, of which two are ubiquitously expressed (β and γ)[26]. While actin is one of the most abundant cellular proteins, comprising between 1-10% of the total protein mass of a cell[27], G-actin does not spontaneously form microfilaments (also known as filamentous or F-actin)[28]. The proper localization, formation, and turnover of microfilaments are tightly regulated processes whereby multiple mechanisms collectively contribute to microfilament stability (**Figure 1.1)**.

Actin dimers and trimers are highly unstable and *in vitro* tend to disassociate rather than form[29]. This is thought to minimize the spontaneous formation of microfilaments. The initial formation of a microfilament is catalyzed by three classes of proteins (Formins, Spires, and the Arp2/3 actin nucleating complex), which are thought to stabilize actin dimers and trimers until more actin monomers can be added, after which the actin polymer is far more stable[29-33]. Polymerization occurs in a directional manner where actin monomers are added to one end (the plus or barbed end) at a rate much faster than the other (the negative or pointed end). This directional addition is an energy intensive process that is driven by ATP hydrolysis by actin[28]. When bound to ATP, actin adopts a conformation that prefers negative end addition to the growing microfilament. Following addition, actin monomers promote ATP hydrolysis to form ADP-bound F-actin[28].

While polymerization occurs at the negative end of a microfilament the removal of ADP bound actin monomers (depolymerization) occurs at the plus end[28]. The relative rate of plus end addition to negative end removal of actin monomers determines the length of a microfilament. An additional mechanism whereby microfilament length is

influenced, is by proteins that modulate this addition and removal. ATP-bound actin monomers can be bound by proteins (e.g. profilin) that promote their addition to the plus end of microfilaments[28,34]. Alternatively proteins such as thymosin-β4 can bind ATP-actin monomers and prevent their addition to microfilaments[28]. Cofilin or actin depolymerization factor (ADF) proteins can facilitate the removal of ADP-actin monomers from the negative end, promoting microfilament shortening[28]. Profilin can then convert ADP-G-actin back to the polymerization-ready, ATP-bound, state[35]. Microfilaments ends can also be bound by proteins which prevent the addition or removal of actin monomers (e.g. CapZ binding the negative end or tropomodulin binding the plus end)[28,35,36]. Proteins such as gelosins, which cleave microfilaments, can also enhance microfilament turnover[28].

Microfilaments often exist in networks, which increase their mechanical strength. Some formin proteins (e.g. mDia1) can promote the formation of bundles of microfilaments, while other proteins such as α-actinin can result in cross-linking between microfilaments. Alternatively the Arp2/3 complex of proteins can bind to a microfilament and promote the formation of a side chain of F-actin [31,37]. Microfilaments can also be bound to membranes or membrane-bound proteins, through interactions with proteins such as myosin, or ezrin [28,38]. While myosin proteins can use microfilaments as tracks for the transport of molecules, these interactions also provide the mechanical force underlying processes such as cell motility.

1.3 Rho GTPase Regulation of the Actin Cytoskeleton:

Central to the proper spatial and temporal regulation of the actin cytoskeleton are several Rho GTPases. In humans at least 20 members, divided into eight subfamilies, are known to exist [39,40]. While this family of proteins are involved in many processes (reviewed in [21,40]) the Cdc42, Rac1, or RhoA-related subfamilies are of particular importance for their roles in cytoskeleton rearrangements.

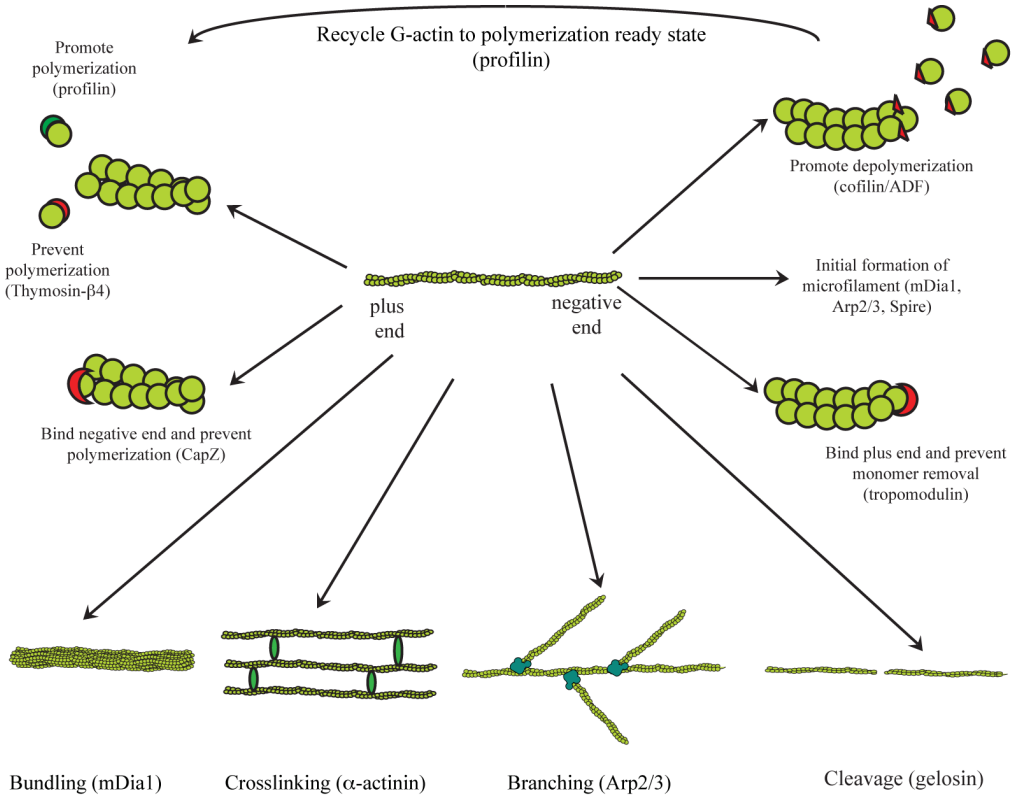

Figure 1.1: Factors regulating the formation, structure, and stability of actin microfilaments. Actin exists as monomers (G-actin) or in polymers called microfilaments or F-actin. The formation and dynamic nature of microfilaments is regulated by a number of factors. The initial formation of microfilaments is dependent on factors such as mDia1, Arp2/3, or Spires. Actin monomers are added to the plus end of a microfilament and removed from the negative end. Factors can bind actin monomers and promote (profilin) or prevent (Thymosin-β4) their addition to growing microfilaments. Microfilaments can also be incorporated into networks by proteins such as mDia1, α-actinin or Arp2/3. Factors can also promote microfilament stability by preventing monomer removal (tropomodulin). Microfilaments can be cleaved into fragments (gelosin) or have actin monomers removed from the plus end. Factors such as cofilin or ADF promote actin monomer removal. Actin monomers can then be converted back to a polymerization ready state by factors such as profilin.

1.3.1 Regulation of Rho GTPase Activity:

An important characteristic of Rac1,Cdc42 and RhoA are that these proteins are functionally active when bound to GTP and inactive when bound to GDP [41,42]. The intrinsic GTPase activity of these proteins allows them to convert from an active signaling state to an inactive state by the hydrolysis of GTP to GDP. Three classes of proteins modulate this "on/off" state (reviewed in[42]). These are guanine exchange factors

(GEFs), GTPase activating proteins (GAPs), and GDP disassociation inhibitors (GDIs). GEFs promote the activation of Rho GTPases by increasing the rate of GDP-GTP exchange, while GAPs promote inactivation of Rho GTPases, by increasing the intrinsic GTPase activity of the proteins.

Rho GTPases are post-translationally modified to contain lipid chains, which allows for their association with cell membranes, where GEFs and GAPs can modulate their activity. GDIs can prevent Rho GTPases from associating with membranes by binding these lipid moieties[42]. As such GDIs keep Rho GTPases in a GDP bound inactive state. In turn, this inhibition can be overcome by proteins, which displace GDIs[41]. Different GAPs, GEFs, and GDIs have been shown to modulate the activity of different Rho GTPases. This, combined with differences in the signaling molecules that activate GAPs, GEFs, and GDIs, allows for Rho GTPases to modulate distinct and often localized effects.

1.3.2 Rho GTPases Involved in Actin Cytoskeleton Rearrangements and their Regulation of Cell Movement:

Directional cell migration requires the coordination of multiple processes throughout the cell, including cycles of protrusion and retraction[43]. Rac1-related proteins, of which only Rac1 is ubiquitously expressed[40], are important for coordinating processes at the leading edge of a migrating cell, which result in the formation of protrusions called lamellopedia. The RhoA-related family of proteins contains three members: RhoA, RhoB and RhoC, of which RhoA is the best characterized[22,44]. RhoA is important in coordinating processes related to cellular contraction and appears to be particularly important throughout the central portion and lagging end of a migrating cell. Rac1 and RhoA are thought to be capable of coordinating these processes due to their mutually antagonistic properties (i.e. active Rac1 inhibits RhoA activation and *vice versa*) **(Figure 1.2).**

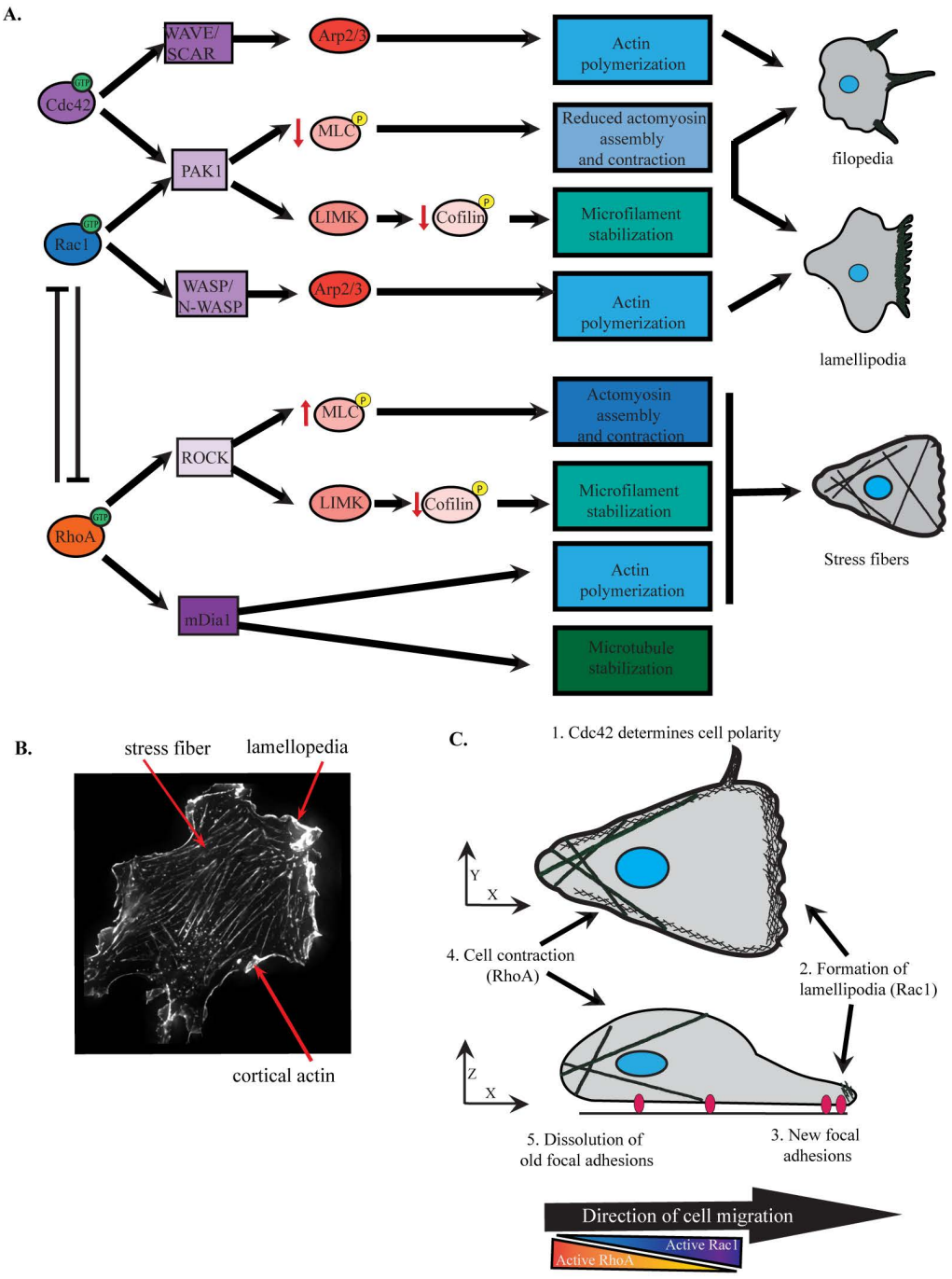

Figure 1.2: Rho GTPase regulation of actin polymerization and cell motility **(A)** Three subfamilies of Rho GTPases are particularly important for regulating actin polymerization. Active Cdc42 is important for the determination of cell polarity and filopedia. Active Rac1is important for the formation of laemellipodia at the leading end of a cell, while RhoA is important for the formation of actin stress fibers and processes at the lagging end of a migrating cell (see text for additional information). **(B)** Primary rabbit corneal fibroblast stained for actin using phalloidin. Various actin structures important for this work are highlighted. **(C)** Process of cell migration. Cdc42 activation aids in determination of cell polarity after which a series of protrusions and contractions coordinated by Rac1 and RhoA aid in directional cell migration. Panel A and C are adapted and modified from [45,46].

Cdc42 related proteins, of which only Cdc42 is ubiquitously expressed[40], are important for the formation of filopedia, which are localized in actin rich protrusion are important for processes such as macropinocytosis[47]. Cdc42 also appears to be important for the initial establishment of cell polarity as dominant negative mutants of Cdc42 result in lamellopedia found around the entire cell periphery rather than on one side of a migrating cell (reviewed in[48]).

Although different triggers modulate Rac1 and Cdc42 activation, there are some similarities in the effects promoted by these proteins. Of particular interest, both Cdc42 and Rac1 can activate the Arp2/3 actin nucleating complexes, although they do so through different effectors (WASP/N-WASP for Cdc42 and WAVE/SCAR for Rac1)[46,49]. Arp2/3 mediated microfilament formation is further stabilized by the ability of both Rac1 and Cdc42 to activate PAK1. This causes the activation of LIMK, which phosphorylates and inactivates cofilin. Rac1 and Cdc42 activation also result in a localized downregulation of actin-myosin contractions, which aid in the formation of lamelopedia and filopedia.

RhoA is important for coordinating the formation of focal adhesions, actin myosin contraction (stress fibers), and lagging end retraction[4,5,21,22,40,44,46,49,50]. These processes collectively provide the mechanical force necessary to move a cell forward. Active RhoA executes these morphological changes primarily through two effector proteins: Rho-associated protein kinase 1 (ROCK) and mammalian Diaphanous formin-1 (also known as mDia1, DIAPH1 or Dia1). The activation of mDia1 promotes the nucleation of microfilaments along with formation of microfilament bundles[29,30,32-34,44]. ROCK also promotes the formation of microfilaments by activating LIMK, which in turn inactivates cofilin[4,13,21,22,28,33,44,50]. Additionally, ROCK1 promotes the phosphorylation and activation of MLC, and proteins such as Ezrin. Active MLC promotes the formation

of actin bundles, and actin-myosin contraction, while active Ezrin anchors actin to the cell's plasma membrane[38]. In cell culture these structures are known as stress fibers[51].

RhoA activated mDia1 also appears to be important for coordinating these actin cytoskeletal rearrangements with those in the microtubule network (reviewed in[52]). Although the mechanism is unknown, mDia1 stabilizes microtubules, which contributes to the directionality of cell movement.

1.3.3 Rho GTPase involvement in exocytosis:

Rho GTPases, and elements of the actin cytoskeleton, also play important roles in regulating exocytosis, with Cdc42, Rac1 and RhoA all implicated in this process[8,10,53,54]. Inactive Rac1, Cdc42 and active RhoA have been implicated in preventing vesicle fusion, while active Rac1, Cdc42 and inactive RhoA have been suggested to promote vesicle fusion with the plasma membrane[55]. Active RhoA is thought to inhibit vesicle release by stabilizing local actin filaments, while active Rac1 promotes vesicle release by promoting membrane fusion by activating a lipase (PLD1)[55]. The exact role of Cdc42 in regulating vesicle release is unknown, but it has been suggested that they may serve to regulate SNARE proteins[55].

1.4 Poxviruses:

Many viruses, including some poxviruses, target elements of Rho GTPase signaling to promote their own spread. Poxviruses are a diverse family of viruses, which are characterized by the following properties. Poxviruses form brick-shaped virions when viewed at by electron microscopy, and are unusual in that unlike most other families of DNA viruses they replicate exclusively in the cytoplasm[3]. Poxviruses employ relatively large genomes (upwards of 300 kb in some species), and contain many genes[3]. Genome comparisons of poxviruses have identified a conserved set of essential genes in the center of the genome, while the ends of the genomes can vary greatly by virus. These ends primarily encode the immunoregulatory and species-specific viral factors.

The International Committee on the Taxonomy of Viruses (ICTV) has subdivided poxviruses into two subfamilies, the *Chordopoxvirinae*, and the *Entomopoxvirinae*, which infect vertebrates and insects, respectively. These subfamilies can be further subdivided into nine genera for the *Chordopoxvirinae* and three genera for the *Entomopoxvirinae*[1,3]. Viruses are assigned to genera based on a number of criteria, including: host-range, disease pathology, serological cross-reactivity between members, and nucleotide sequence similarity[1]. There also exist a number of unclassified poxviruses (e.g. crocodile and squirrel poxviruses), which have been suggested to represent prototype members of yet to be classified genera[1,56].

For the work presented here, two particular viruses are of interest. The first is vaccinia virus (VACV), which is the prototype for the *Orthopoxvirus* genus, and is the most commonly studied poxvirus. The second virus is the *Leporipoxvirus* genus prototype, myxoma virus (MYXV).

1.5 Vaccinia virus:

VACV is the prototypical *Orthopoxvirus*. This genus is one only two genera that includes members whose native hosts are humans, the other being *Molluscipoxvirus,* and its only member Molluscum contagiosum[1,3]. There are periodic reports of humans being infected with two zoonotic orthopoxviruses: monkeypox (native to regions of Africa) and cowpox (endemic in Europe). VACV is probably best recognized for its use as the vaccine that was used to eradicate smallpox, which is caused by variola virus (also an *Orthopoxvirus*). Smallpox is primarily a human disease, although other non-human primates can be infected with it in laboratory settings. The absence of an animal reservoir for variola is thought to be a contributing factor behind the successful eradication of smallpox in the latter half of the 20th century.

In contrast to the narrow tropism of variola, and most other poxviruses, VACV is capable of establishing a productive infection in a wide array of animals including mice,

non-human primates, rabbits, and humans. While its ancestral source and native host remains uncertain[57,58], its long history of use as the smallpox vaccine, and relative safety in healthy individuals has made VACV the model for research into poxvirus biology. VACV is also being pursued for use as vector for a number of other vaccines including HIV[59] or Hepatitis B[60] and C[61], or for a cancer therapeutic. Although displaying oncolytic properties, it replicates in a wide range of human cells, and is not naturally selective for cancer. Much work has been undertaken in trying to increase VACV specificity for dividing cancer cells by mutating genes involved in promoting growth in non-dividing tissues[62-66]. Indeed, VACV mutants devoid of certain nucleotide biosynthesis genes and/or the viral growth factor have shown great promise in clinical trials[66,67].

1.6 Myxoma virus:

In addition to MYXV (the genus prototype), the *Leporipoxvirus* genus has three natural members and one laboratory-derived recombinant. These are: Shope fibroma virus (also called rabbit fibroma virus) [SFV], hare fibroma virus [FIBV] and squirrel fibroma virus [SQFV][1,3,68]. A laboratory recombination event between Shope fibroma and MYXV has also resulted in the formation of a virus known as malignant rabbit fibroma virus (MRV)[69-71]. In their native host these viruses are characterized by causing a benign localized tumour-like lesion, known as a fibroma, on the skin of an infected host. These tumor like lesions are ultimately cleared by the hosts immune system[68,72].

While MYXV causes a relatively benign infection its native hosts, the South American (*Sylvilagus brasiliienes*) and North American hares (*Sylvilagus bachnani*), it is more commonly known for its pathology in its non-native hosts[68]. In European rabbits (*Oryctolagus cuniculus*) MYXV causes a systemic and lethal disease, called myxomatosis, where rabbits succumb to organ failure and secondary bacterial infections associated with viral disregulation of the immune system[72]. Indeed the first description of a disease caused by MYXV was not in its native hosts, but in a laboratory colony of

imported European rabbits in Uruguay in 1896 (reviewed in[73,74]). It would not be for another 40 years that the natural reservoir of MYXV would be identified[72]. While the genetics underlying the differences in MYXV pathology between European and American lagomorphs is unknown, the systemic spread in European rabbits is thought to be due to the viruses' ability to replicate in leukocytes, which aids in virus transport to new sites[75].

During the early years of MYXV research, repeated attempts to infect a wide array of non-lagomorph hosts (including humans) failed to cause productive infections[72,74]. The fact that MYXV is highly specific for lagomorphs, and caused a devastating disease in European rabbits, gave rise to the idea that MXYV could be used as a biological control for European rabbits. In Australia, rabbits were introduced by European settlers, and in the absence of natural predators, had became a major pest within 20 years of introduction[72]. The Moses strain of MYXV (also known as the Standard Laboratory strain, or SLS) was field tested in 1950[72,76]. Flood conditions, combined with the fact that the major vector for MXYV transmission is arthropods (mosquitoes or fleas), lead to rapid spread of MXYV from these field stations. Within a few years the virus had spread across the continent. The results were devastating to the rabbit population, with reductions of greater than 90% observed in some locations[76,77]. The use of MYXV as a biological control was repeated in Europe, with the release of the Lausanne strain of MYXV, first isolated in Brazil in 1949, into France in 1952[78]. Over the next few years the virus spread throughout continental Europe and Great Britain, possibly aided by farmers [72].

While initially having devastating effects on rabbit populations, a rise of host-resistance, combined with virus attenuation, lead to their eventual recovery[79]. Both host and virus remain endemic in Australia and Europe to this day. This history serves as a classic illustration of host-pathogen co-evolution in a natural environment[78,80,81].

One interesting property of MYXV is that while it does not cause disease in humans, it can replicate in, and kill some human cancers. The oncolytic properties and mechanisms behind this break in tropism will be discussed in greater detail in section 1.12.

1.7 Poxvirus Life Cycle Based on Studies using Vaccinia Virus:

Much of what is known about the life cycle of poxviruses has come from studying VACV. While much of what has been learned from these studies is applicable to other poxviruses, some differences do exist. The next couple of sections will review the poxvirus life cycle based on studies using VACV (**Figure 1.3)**, with particular focus given to factors that contribute to efficient VACV exit and spread. A subsequent section will compare the life cycle of VACV with the what is known about the lesser characterized MYXV, and how differences in the plaquing properties of these viruses lead us to investigate whether there were differences in the abilities of these viruses to exit and spread from cells.

In comparison to many other viruses, the entry process of poxviruses is quite complex and poorly understood. This is due, in part, to the existence of more than one type of infectious virus, multiple proteins involved in binding virus to cells, and multiple entry pathways. These processes are facilitated by a large complex of viral proteins. Due to the different modes of poxvirus entry, production of infectious virus from an already infected cell will be first discussed and then followed by an overview of the different modes of viral entry.

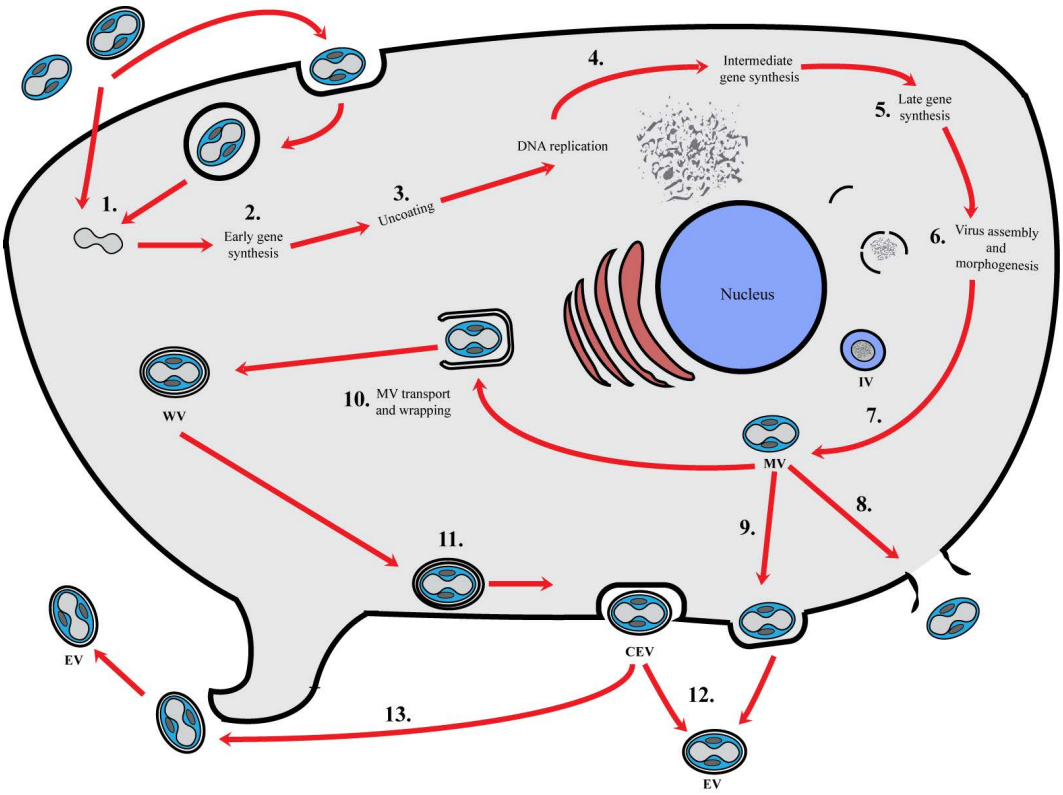

Figure 1.3: Poxvirus life cycle: **(1)** Mature virus (MV) and enveloped virus (EV) bind cells and enter either through direct fusion or endocytosis ultimately releasing a viral core into the cell. **(2)** Early mRNAs are expressed which provide factors for immune evasion, uncoating, DNA replication and intermediate gene expression **(3)** uncoating **(4)** DNA replication occurs along with intermediate gene expression, which provides factors necessary for late gene expression **(5)** Following DNA synthesis late gene expression occurs which produces structural proteins and enzymes that are packaged in virions and necessary for the next round of infection **(6)** virus assembly occurs beginning with the formation of crescent shaped structures, followed by the formation of spheroid immature virus (IV). **(7)** IV undergo a number of maturation steps (see text) to produce infectious MV. MV can undertake one of several potential fates. MV can be released via **(8)** lysis or **(9)** budding**.** **(10)** MV can also transport via microtubules and acquire two sets of lipid membranes from either the trans-Golgi network or endosomes to form wrapped virus (WV) **(11)** WV transport via microtubules to the cell surface where the outer WV membrane fuses with the plasma membrane, releasing a double-membraned virus to the cell exterior. Cell-associated enveloped virus (CEV) can either disassociate to form enveloped virus (EV) **(12)** or catalyze the formation of actin projectiles through an outside-in signaling cascade **(13) .** Figure adapted and modified from [2,3]

1.7.1 Poxvirus Uncoating, Gene Expression and DNA Replication:

Regardless of the mode of entry, a proteinacous virus structure (known as a core), which surrounds the viral genome and contains a number of viral enzymes, is released from viral capsids into the cytoplasm. Cores then traffic via microtubules to sites

near the nucleus and microtubule organizing center (MTOC)[82,83]. Here the virus establishes an area, known as a viral factory (also known as a virosome or B-Type inclusion). This area is largely devoid of cellular organelles and is the site where viral replication and assembly occurs.

Even before virus cores reach sites where viral factories will be established, they are thought to be expressing, and extruding viral mRNAs[3,84]. This class of genes (called early) is thought to represent roughly half the genes encoded by the VACV genome[3,85], and include genes whose products are necessary for uncoating[86], DNA metabolism and replication, factors necessary for the expression of intermediate genes, and a plethora of proteins involved in aiding in virus evasion of the immune system.

Following uncoating, early gene products are thought to gain access to the viral genome, allowing for the start of DNA replication. At the same time as DNA replication occurs, a new class of intermediate genes is expressed. This provides factors necessary for late gene expression, which marks the end of DNA replication. Late genes encode a number of structural proteins, as well as enzymes, which are packaged into virions and are necessary for the establishment of the next infection cycle.

Distinct promoter sequence motifs differentiate each class of viral genes [87,88]. However, a number of genes are transcribed throughout infection (e.g. A33R, A36R, B5R)[89]. In these situations, combinations of early, intermediate, and late promoters are found in tandem, upstream of the open reading frame[87]. Promoter consensus sequences have been used to generate hybrid early/late promoters which have been useful tools for expressing transgenes from recombinant poxviruses[88].

1.7.2 Virus Assembly and Morphogenesis:

The formation of infectious virus, following DNA replication, is perhaps the most complex part of the poxvirus life-cycle, with at least 70 viral proteins being implicated in the production of infectious mature virus (MV)[90]. Although the source of

virus membrane lipids remains disputed, it is generally accepted that MV are surrounded by a single lipid bilayer[2]. These lipid layers form over a protein-scaffold made up of D13 trimers[91] and are initially seen in electron micrographs as crescent shapes. These crescents expand and eventually form spheres, into which are packaged viral genomes and enzymes[90,92].

These spheroid-shaped structures, usually called immature virions (IV) then undergo a number of maturation steps, which converts them into an infectious brick-shaped mature virion (MV). During this process the D13-scaffold is lost[93,94], proteases cleave some viral proteins (reviewed by Condit *et al.*[90]), a virus encoded redox system oxidizes disulfide bonds [95,96], and additional viral proteins (e.g. H3[97] and A27[98]) are recruited. At the end of this process MV consist of a core, containing the genome, surrounded by a single lipid bilayer containing approximately 20 viral proteins[90]. On either side of the dumbbell shaped core are protein rich structures (known as lateral bodies), which contain the enzymes necessary for initiating the next round of infection. Now infectious, MV can undergo one of many possible fates before infecting another cell.

The vast majority of infectious virus exists as MVs and are generally thought to be released from cells upon lysis[2]. However, a fraction of MVs undergo an additional form of maturation, which permits their release prior to cell lysis. This starts when MVs are transported away from viral factories and acquire two additional sets of lipid bilayers, as well as several additional viral proteins, not found in MVs[99,100 101-103]. This triple layered virion, now known as a wrapped virus or WV, is then transported *via* microtubules to the cell periphery [104-106], where the outer WV membrane fuses with the cell membrane. This releases a now double membrane virus (known as an enveloped virus or EV) to the cell periphery. Here, cell-associated EV (CEV) can initiate a signaling cascade that promotes the polymerization of actin underneath the virion. These structures,

known as actin projectiles or actin tails can then push the EV away from the cell, facilitating its detachment from the cell. EV can then proceed to infect a neighbouring cell. It should be noted that MVs, WVs, EVs are also referred to intracellular mature virus (IMV), intracellular enveloped virus (IEV) or extracellular enveloped virus (EEV), respectively[107]. The biological roles and genes responsible for EV and actin projectile formation will be discussed in greater detail in sections 1.8 and 1.9.

There also exist reports of MV budding at the cell surface at late times of infection[108,109]. This also gives rise to a virus with similar membrane structure as an EV (i.e. two sets of lipid bilayers). However, it is unknown whether this form of virus has similar functions and protein composition as EV.

1.7.3 Poxvirus Entry:

Although great strides have been made in recent years in understanding how poxviruses enter cells, it still remains one of the more poorly understood aspects of the VACV life cycle. This is due to the existence of multiple binding and entry pathways, the observation that different strains seem to bind and enter cells through different mechanisms, and the fact that MVs and EVs have different numbers of membranes.

MV binding to the cell surface is greatly diminished in cells lacking glycosaminoglycans, or that have been treated with proteinase, suggesting that glycosaminoglycans and yet to be identified cell proteins act as receptors for MV[110-113]. Three viral proteins have been implicated in binding to glycosaminoglycans: A27 and H3 have been implicated in binding heparin sulfate, and D8 in binding chondroitin sulfate[114-117]. While L1 is implicated in entry, it may also play a role in virus binding to unidentified cellular proteins, while A26 has been shown to bind laminins[118,119]. A26 and A27 are not found in all strains of VACV, which may explain some of the differences in binding between poxviruses[112,120,121]. Given that MV and EVs share no common surface proteins, it may not be surprising that they display differences in their binding. While the

receptors and proteins implicated in EV binding to cells are unknown (unlike MVs), EV binding to cells is not inhibited following cell treatment with proteinases[110].

Both MVs and EVs are thought to have the capacity to enter by direct fusion with the cell surface. The entry of MV is also dependent upon at least 11 viral proteins which form the entry/fusion complex (EFC). This complex mediates the fusion of the MV membrane with the cell membranes, which releases the viral core into the cell interior (reviewed in[107,112,113]). While this seems fairly straightforward for MV, and would release the core into the cytoplasm, this mode of entry is complicated in EVs by membrane topology. The outer layer creates a topological problem and also masks the EFC. This is overcome in part due to the fragility of the EV membrane. Upon contact with the cell the outer membrane of the EV can become disrupted resulting in the exposure of a MV, and the EFC, to the cell surface[122]. This induced fragility is thought to involve two EV specific proteins (A34 and B5), as well as interactions with the glycosaminoglycans on the cell surface[122,123].

Virions are also capable of entering cells *via* macropinocytosis. This seems to vary by virus strain with the Western Reserve (WR) strain entering by a process that requires membrane blebbing, Rac1 and PAK1 activation, and may mimic how apoptotic bodies are recycled[124,125]. The IHD-J strain of VACV seems to enter through a process that requires filopedia formation and Cdc42 activation[126]. Both strains transiently activate RhoA but it is uncertain how this aids in virus entry, as constitutively active RhoA mutants inhibit virus entry, while dominant negative versions have little effect on entry[126]. While macropinocytosis may serve to promote virus bypass of the cytoskeleton it represents another membrane barrier to core entry into the cytoplasm. Virus escape depends on endosomal acidification, as inhibition of this acidification inhibits[125]. It is thought that the outer EV membrane may become disrupted under these conditions and

that low pH activates the EFC, which promotes virion fusion with the endosomal membrane[113,126,127].

Differences in the expression of A25 and A26 may explain differences in the mode of entry of poxviruses[121,124]. A25 and A26 are thought to serve as pH-sensitive fusion suppressors, which inhibit EFC activity at neutral pH (i.e at the cell surface) but allow for fusion at low pH (i.e. in endosomes)[128]. Thus strains that encode A25 and A26 are thought to prefer entry by endocytosis, while strains that lack these proteins are thought to prefer entry by membrane fusion. Differences in A26 may also explaining differences in strain activation of Rac1/Cdc42 signaling, as A26 binds laminins[118] and activated laminins can lead to Rho GTPase signaling activation[129].

1.8 Role of Different Types of Virions in Vaccinia Virus Spread:

As discussed in previous sections VACV forms two types of infectious virus MV and EVs. But what advantage does the virus gain by producing these multiple forms of virus? After all EV seems to have a number of advantages over MV. Unlike MV, EV can induce the formation of actin tails, which is implicated in rapid spread *in vitro* and important *in vivo,* as shown by the fact that mutants unable to form actin tails are attenuated (discussed in more detail in sections 1.9). EV also appear to have a lower particle to PFU ratio than MV, suggesting that they may be more infectious[110].

In plaque assays, VACV forms comet-like tails of secondary plaques, which spread in a unidirectional manner from the primary plaque. EV are important for comet-tail formation as EV mutants do not usually form comet tails. Further, the treatment of infected cells with antiserum against EV proteins, but not MV proteins, also inhibits comet tail formation as well as decreasing the primary plaque size[130]. EV mutants are also attenuated *in vivo*, and in many cases where infected organs have been examined, show decreased spread to these tissues **(Table 1.1).** Collectively, these data suggest that EVs are important for efficient intra-host spread.

Analysis of serum from humans and animals receiving live smallpox vaccine, reveals numerous MV-specific antibodies, while antibodies against only two EV proteins (A33 and B5) have been reported (reviewed in[130 131]). This combined with observations that much higher concentrations of EV-specific *versus* MV-specific antibodies are needed to achieve virus neutralization, has lead to the idea that EV may serve to hide the more immunogenic MV proteins[130]. EV membranes have also been reported to incorporate host immunoregulatory proteins such as the complement control protein, or associate with a virus-encoded complement control protein. These are thought to aid in EV resistance to complement[132-134].

So why do poxviruses not exclusively form EV? One possibility is that producing two types of virus permits maximal virus production. WV production peaks much sooner than MV. By 8 h post-infection, WV comprise 37% of the total intracellular virus population, while at 24 h post-infection it represents ~ 1% [135]. Despite reports of the recycling of WV outer membranes, the decrease in proportion of WV as infection progresses may result of the depletion of lipid membranes[135-139]. Late in infection it has been reported that the microtubule-organizing center (MTOC) of VACV-infected cells becomes disrupted[140]. Given that WV formation depends upon microtubule structures this may also contribute to a decrease in WV formation.

The relative abundance of MV at late stages of infection suggests that it may represent a means of maximizing virus production in an environment that has reduced resources to produce the "better-quality" EV virus. However, there is a body of evidence that while EV is important for efficient intra-host spread of the virus, MV are important for the transmission of virus between hosts.

Many poxviruses transmit through aerosols or skin abrasions. MV are stable in the presence of a wide array of environmental insults that it would encounter in these transmission routes, including temperature, desiccation, and the presence of a number of

detergents (reviewed in [130]). In contrast the outer membrane of EV is relatively fragile, likely a necessity for initiating a successful infection, and is disrupted upon exposure to many of these conditions. Although not observed in VACV or MYXV, some poxviruses (e.g. cowpox or ectromelia) can incorporate MV into protein-rich complexes called A-type inclusion bodies [141]. These are thought to provide additional protection for MV transmission. The failure to form inclusion bodies containing VACV has been attributed to a truncation of the A26L gene[142].

1.9 VACV Genes Necessary for the Production of WV, EVs, and Actin Projectiles:

As discussed previously EVs are important for the rapid spread of VACV in cell culture, and promote virulence *in vivo*. To date, eight viral genes (A27L, A33R, A34R, A36R, B5R, E2L, F12L, F13L) have been implicated in the production of EVs and their associated actin projectile formation. F11L has also been implicated in aiding virus spread by disrupting cortical actin, which promotes WV reaching the cell surface[143]. Deletions reduce plaque size, and in viruses tested for virulence these viruses are attenuated. Table 1.1 summarizes these virus phenotypes. Two other virus proteins (K2 and A56) are also associated with EVs but do not appear to play a role in their generation or spread, as mutant K2L or A56R viruses form normal size plaques. Rather they appear to play a role in preventing cell-cell fusion, and in anchoring other immune evasion proteins to EVs [133,144]. This section will summarize the roles of viral genes in the formation of EVs and actin projectiles.

1.9.1 VACV Genes Implicated in WV Formation and Intracellular Transport:

Subsets of MVs are transported via microtubules from viral factories to sites near the trans-Golgi network. This transport is dependent upon the MV-associated protein A27[99,100]. Once here MVs can acquire two sets of lipid membranes, derived from either the trans-Golgi network or from endosomes, and form WVs. The exact details are still unknown but MV wrapping requires F13, in concert with B5, A27, and possibly E2.

Deletions of F13L, B5R and repression of A27L, all result in a drastic reduction in WV formation[145-147]. A point mutation in A27L has been identified that allows normal MV transport but has a defect in WV formation[100]. This suggests that A27 may have a direct role in WV wrapping in addition to promoting MV transport to the sites of wrapping.

F13 plays a key role in the formation of WVs. It localizes to the trans-Golgi network and to vesicles and is important for the proper localization of other viral proteins such as B5 [104,148,149]. F13 shows homology to both the HIV-1 Env protein and the mammalian phospholipase D (PLD). HIV-1 Env is important for the development of viral envelopes and is thought to promote formation of virus envelope by recruiting vesicles to sites of virus assembly *via* an interaction with the endosomal protein TIP-47 [150,151]. Like HIV-1 Env, VACV F13 also interacts with TIP-47, and if one disrupts this interaction, either by mutations or with the *Orthopoxvirus*-specific drug (ST-246), it drastically reduces WV formation [152-160].

The PLD domain of F13 shows broad lipase activity and inhibiting this activity, either through mutations or with a PLD inhibitor (butanol-1), drastically reduces the formation of WVs[161]. Why this activity is important for WV formation is unknown. However, mammalian PLDs play an important role in regulating vesicular budding from the trans-Golgi network, suggesting that F13 may also play a similar role.

Two other viral proteins are also implicated in WV formation. B5 mutants, more specifically carboxy-terminus mutants, show a decrease in WV formation[146,147,162]. How B5 contributes to WV formation is currently unknown. While it is agreed that E2L is important for EV production, as evident by decreased production of CEVs and EVs in E2L mutants, whether E2 is important for WV formation is disputed. While Dodi *et al*. and Morgan *et al.* found E2L mutants formed WVs, Dodding *et al.* found E2L mutants had defects in WV formation[163-165]. Further work is required to clarify these

Table 1.1: VACV genes involved in EV/actin tail production[f]

Gene	Deletion Mutant Phenotype							Protein Interactions	Reference
	Plaque Size	MV	WV	CEV	EV	Actin tails	Virulence		
A27L[a]	Small	Normal	None	None	None	?	Not tested	Microtubules, A26	99,142
A33R	Small	Normal	Normal	Normal	Increased	None	Attenuated	A36, B5	166-175
A34R	Small	Normal	Normal	Reduced	Increased but reduced infectivity	None	Attenuated	A36, B5	123,132,173,176-181
A36R[b]	Small	Normal	Normal	Normal	Reduced	None	Attenuated	A33, A34, B5, E2, F12, Grb2, Nck1, Abl and Src kinases	170,182-193
A56R[c]	Normal	Normal	Normal	Normal	Normal	Normal	Attenuated	K2, C3	133,134,144,194,195
B5R	Small	Normal	Reduced	Reduced	Reduced	Few	Attenuated	A33, A34, A36	106,146,147,162,167,168,176,190,196-203
E2L	Small	Normal	?	Reduced	Reduced	Reduced	Not tested	F12, A36	163-165
F11L[d]	Small	Normal	Normal	Reduced	Reduced	Few	Attenuated	RhoA	143,204,205
F12L[e]	Small	Normal	Normal	None	Reduced	None	Attenuated	A36, E2, kinesin-1	165,206,207
F13L	Small	Normal	Reduced	Reduced	Reduced	None	Attenuated	TIP-47, Rab9	139,145,149,153,160,161,208-210
K2L	Normal	Normal	Normal	Normal	Normal	Normal	Normal virulence	A56, C3	195,211-213

[a] associated with MVs, not in WV/EV membranes
[b] found only in outer WV membrane and not in EV
[c] A56 deficient virus form normal size plaques but have synicitia
[d] not found in virions
[e] associated with outer WV membrane only and not found in EV
[f] adapted and modified from[130]

discrepancies.

Although A33 and A34 are not essential for the formation of WV membranes, they are needed along with B5 for the proper localization of other viral proteins to WV membranes. A34 also appears to play an important role in the rate of EV formation. The E_{151} allele of A34 is naturally found in the IHD strains of VACV, while the K_{151} allele is found in all other strains[179]. This difference is thought to explain the increased rate of EV formation and larger comet tails produced by the IHD strains in comparison to other strains[182]. A33, A34 and B5 are thought to form a complex that is important for each others proper glycosylation and incorporation into WV membranes. This is supported by

the observation that, in the absence of any one of these proteins, the remaining two show glycosylation defects, and fail to localize to WV membranes[173,175,176,180,181]. B5 is thought to play a central role in the formation of this complex, as it interacts with A33[175] and A34[176], while A33 and A34 do not appear to interact as judged by co-immunoprecipitation techniques[173]

While A33, A34 and B5 localize to both sets of WV membranes, they appear to direct VACV A36 exclusively to the outer WV membrane[148,170,188,214,215]. This is suggested by the observation that A36 fails to localize to WVs in the absence of either A33[170] or A34[181], and it co-immunoprecipitates with both proteins. In turn, A36 interacts with E2[163] and F12[165], and these interactions are probably needed to recruit F12 to the outer WV membrane[184].

WVs traffic to the cell periphery via microtubules [106,186,207]. This transport requires F12, which resembles the kinesin light chain and has been shown to interact with kinesin-1 (an important motor protein for microtubule transport)[165]. This interaction is important for the movement of WVs along microtubules to the cell surface, as mutating F12L to abolish this interaction prevents WV transport to the cell periphery[165,207]. A36 and E2 deficient viruses also show decreased rates of WV transport[163,186]. It has been suggested that these decreases are due to A36 and E2 playing a role in facilitating F12's association with WV membranes[163,184]. Once WVs reach the cell periphery, the outer WV membrane fuses with the inner leaflet of the cell membrane, which leaves the now double-membraned EV on the cell exterior. This creates the CEV form of the virus.

1.9.2 VACV Genes Involved in Actin Projectile Formation:

Actin projectiles or actin tails, are formed when CEV comes in contact with other viral proteins expressed on the surface of an infected cell. These actin projectiles are thought to provide the mechanical force necessary to drive EV away from the surface of a cell[182]. Actin projectiles can repulse an incoming EV, thus preventing it from infecting a

cell already infected by another virus, pushing it away until it encounters an uninfected cell [89,216]. These projectiles can form in cells undergoing early stages of infection (i.e. not yet producing infectious virus) and are thought to explain why VACV plaques spread much faster than simple replication kinetics would predict. While the generation of new infectious VACV particles take ~ 6 h, it has been observed that, on average, wild-type VACV spreads to a new cell at a rate of approximately one every ~ 1.2 h [89]. In comparison VACV strains defective in WV or actin projectile formation spread at rates similar to what replication kinetics would predict (~ 1 cell/5-6 h). This shows that these processes are important for rapid virus spread[89].

Actin projectiles are also thought to provide mechanical force to promote an exiting EVs disassociation from a cell[182]. This is inferred from the observation that a VACV A36 mutant strain showed increased number of CEVs and decreases in the amount of virus in the surrounding media[182].

Deletion of A33R, A34R or A36R completely abolishes actin projectiles, while B5R mutants severely reduce their frequency. A36 is thought to serve as a scaffold for the recruitment of the Arp2/3 actin nucleation complex (discussed in section 1.2). Phosphorylation of two tyrosine residues in A36 is thought to be important for this process. Phosphorylation of A36 Y112 allows for the recruitment of Nck, and the phosphorylation of Y132 allows for the recruitment of Grb2 [189,217,218]. These adaptor proteins then stabilize an interaction with N-WASP, which in turn recruits Arp2/3, which can then polymerize actin underneath the extracellular virion[217,219,220]. These phosphorylation-dependent interactions are important as the mutation of both Y112 and Y132 completely block actin projectile formation and decreases EV production[182,218]. While the mutation of either amino acid residue causes a reduction in actin tails, the Y112F substitution has a greater affect than a Y132F[218]. This suggests that recruiting Nck2 is more important than Grb2 for actin projectile formation.

Src family kinases (Src, Yes, Fyn) and Abl-tyrosine kinases (Abl, Arg) also localize to actin tails, and have been implicated in phosphorylating A36[221]. The growth of virus in cell lines lacking these kinases, or expressing dominant negative versions of these proteins, causes a reduction in A36 phosphorylation, and decreases actin tail formation[185,218,221,222]. Pharmacological inhibitors of Src (PP1) or Abl kinases (PD-166326 or STI-571) have also been show to decrease actin tail formation[218,221].

While all three genes are essential for actin projectile formation, A33R and A36R are expressed both early and late in infection, while A34R is expressed only late in infection[89]. The expression of A33R and A36R at early times (i.e. when A34 is not present) is important for promoting virus spread. In the absence of A34, A33 and A36 localize to the cell surface and ectopic expression of only A33 and A36 in uninfected cells can result in actin projectile formation upon adding purified EVs[89,216]. The current model explaining this data suggests that at early times in infection A33 and A36 are localized to the cell surface, where they can repel incoming EV, thus preventing superinfection. However, at late times of infection, when A34 is expressed, these proteins would become localized to WVs. As a result, A36 and A33 would become concentrated underneath exiting CEV, maximizing actin projectile formation and favouring new virus disassociation[182,183].

The ability of purified EV to induce actin projectile formation, suggests that EV can induce an outside-in signaling cascade to initiate actin projectile formation. EV-associated B5 has been implicated in promoting this. B5 is a type I membrane protein, with four short consensus repeats (SCR) near its amino-terminus. Deletion of SCR4, or a point mutation in this region of B5 (P189S), still allows for normal formation of WV[221]. However, these mutations result in a reduction in actin projectile formation, and SRC kinase activation [168,196,197]. Further, unlike wild-type virus, the addition of these mutant EVs to cell lines expressing A33 and A36 fails to induce actin projectile formation[216].

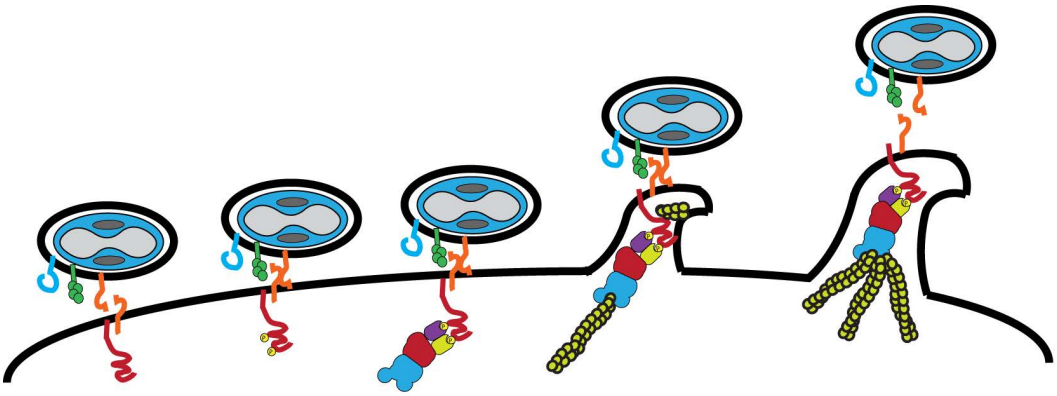

1.EV contact with infected cell | 2. Phosphorylation of A36 by Src and Abl kinases (Requires A33 and EV surface B5) | 3. Recruitment of actin nucleating machinery | 4. Actin projectile formation | 5. EV detaches from cell

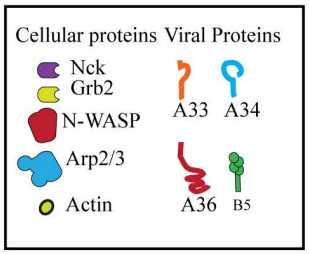

Figure 1.4 Model for VACV actin projectile formation: Upon coming in contact with an infected cell, EV activate an outside-in signaling cascade which results in the phosphorylation of A36 by Src or Abl kinases. This phosphorylation event requires B5 and is influenced by A33. Phosphorylated A36 can then recruit Nck and Grb2 proteins, which serve as adapters to recruit N-WASP, and the Arp2/3 actin nucleating complex. Arp2/3 then catalyzes the polymerization of actin which pushes the cell-associated EV away from the cell. EV then disassociate and proceed to infect another cell. Actin projectile formation requires cell-surface A33 and A36 and EV bound B5 and can either 1) promote an exiting EVs disassociationg or B) prevent superinfection by repulsing an incoming EV.

These observations suggest that B5 serves as signaling molecule to initiate SRC phosphorylation and subsequent actin projectile formation.

The role of A33 in actin projectile formation is still not fully understood. Like A36, A33 localizes to cell membranes in the absence of any other viral proteins[89]. A33 can be phosphorylated at serine residues, and in the absence of A33, a decrease in tyrosine phosphorylation of A36 is observed [170]. A transient interaction between A33 and B5 appears to be important for regulating actin projectile formation and EV release.

Mutations that abolish this interaction, either carboxy-terminal truncations of A33 or point mutations in B5 (P189S), decrease actin projectile formation, but enhances EV release and comet tail formation[166-168,197]. Mutations that stabilize the interaction of A33 and B5 still allow for actin projectile formation, but mutant virus display a small plaque phenotype[174,175]. Although additional experiments are needed an enticing model would be that cell-associated A33 serves as a receptor, which transiently interacts with EV-bound B5 to relay a signal that causes phosphorylation of A36. Phosphorylated A36 then recruits the actin nucleating machinery, forming actin projectiles to push away EV, after which cell-associated A33 and EV-bound B5 no longer interact, favouring in the disassociation of the virion. The EV can then go on to infect an additional cell and start a new round of infection.

1.10 Disruption of RhoA Signaling Promotes EV Release and Actin Projectile Formation:

VACV EV exit shows some similarities with exocytosis, in that the actin cytoskeleton represents a barrier that both vesicles and WVs must traverse in order to reach the plasma membrane of cells[9,143]. As discussed in section 1.3 Rho GTPases are critical for maintaining cytoskeletal integrity. VACV is thought to aid in EV release by disrupting the actin cytoskeleton *via* inhibition of elements of this signaling pathway.

The use of constitutively active and inactive versions of Cdc42, Rac1, and RhoA suggests that disruption of RhoA signaling is important for VACV release. Constitutively-active RhoA reduced VACV actin projectile formation and decreased VACV release, while constitutively active versions of Cdc42 or Rac1 had little effect on these processes[204].

VACV infection causes decreases in the active levels of Cdc42, Rac1 and RhoA. While the mechanism and biological significance behind VACV mediated decreases in active Cdc42 and Rac1 is unknown, VACV F11 is important for the disruption of RhoA

signaling[204]. In the absence of F11, increases in active RhoA are observed in VACV infected cells[205]. F11L mutant viruses exhibit decreases in plaque size, decreased actin projectile formation, and reduced EV production[205,223].

F11 decreases the active levels of RhoA and directly binds to RhoA to inhibit downstream signaling[224]. The interaction between active RhoA and F11 is mediated by a region near the carboxy-terminal of F11, which resembles a region of cellular ROCK1 that binds to RhoA[224]. While this interaction presumably disrupts RhoA signaling to both ROCK1 and mDia1, the disruption of RhoA signaling to mDia1 seems to be more important for promoting VACV spread[143,224]. Disruption of ROCK1 signaling, using the chemical inhibitor Y-27632, or transient transfection of mutant versions of the gene, has little effect on VACV actin projectile formation or EV release[143]. In contrast transfection of constitutively-active mDia1 drastically reduces the numbers of actin projectiles and virus release[143]. In agreement with VACV release being promoted by disruption of RhoA-mDia1 signaling VACV infection results in decreases in processes controlled by active mDia1, primarily a decrease in the numbers of actin stress fibers and an increase in microtubules reaching the cell periphery[143,204]. These alterations are thought to help WV reach the cell plasma membrane, and then cell surface. The externalized EV can then form actin projectiles and be released.

VACV infection has also been shown to induce two types of cell movement. The first form is cell migration, while the second type involves long projections[84]. F11 has been implicated in the induction of cell migration, a process that occurs at early times in infection[223,224]. While the reintroduction of F11L into the MVA strain of VACV induces cell motility, it does not affect plaque size[225]. MVA has a mutated copy of F11L as well as mutations in other actin projectile promoting genes. Thus whether cell migration plays a role in viral spread, or is a byproduct of F11L inhibition of RhoA signaling to facilitate EV exit is unclear.

The factors responsible for the induction of cellular projections, also called cytoplasmic corridors, are unknown at this time. It is known that it depends upon late gene synthesis but not on the formation of WVs[84,226,227]. The biological significance of this phenomenon is also unclear.

1.11 Comparison of Myxoma and Vaccinia Virus Life Cycles:

Plaque assays for animal viruses were first described over 60 years ago[228]. It has been known for almost as long that while VACV forms large lytic plaques, containing a central clearing surrounded by a ring of infected cells, that MYXV mostly produces a clumping of infected cells, in something called a focus[229-234]. In some circumstances, small plaques are formed by MYXV. This has been observed relatively late in infection (after 7 days), and when virus are grown under agar[229,231]. Even so these lytic plaques are rare, representing less than 1% of foci observed with the Lausanne strain of MYXV [231]. While MYXV and VACV display drastically different plaquing properties, the relatively few studies that have examined the life cycle of MYXV suggest many similarities between these viruses. Some differences in terms of entry and the rate of virus production have still been observed. Unlike the WR strain of VACV, MYXV entry is less affected by siRNA-mediated silencing of PAK1, or by inhibitors of endosomal acidification [235]. This suggests that MYXV prefers a direct fusion mode of entry rather than entry by the endocytic pathway (see section 1.7.3).

Once inside a cell, the life cycles of MYXV and VACV follow similar stages to produce infectious virus. Like VACV, MYXV replicates in cytoplasmic factories near the nucleus and undergoes similar stages of morphogenesis, with crescents, IVs, MVs, WVs and EVs all being observed by electron microscopy[72,236-240]. In terms of shape and size, MYXV and VACV virions are indistinguishable, with MVs of both viruses having dimensions of ~ 300nm × 230nm × 75nm[238,241]. Despite showing essentially no serum cross-reactivity (a single unidentified MYXV core protein appears to cross-react with

VACV derived anti-sera[72]), the MVs of MYXV and VACV appear to be quite similar in their protein composition.

Our laboratory previously used MALDI-TOF mass spectrometry to analyze the composition of MYXV MV. These studies suggest that the composition of MYXV MV is similar to that of VACV, with MYXV encoding homologs of most of the known MV proteins identified in purified VACV [242,243]. This technique also suggested that several MYXV MV proteins undergo similar proteolytic cleavage events as their VACV counterparts, although while VACV A10 is processed to three proteins, its MYXV homolog (M099) likely is cleaved only twice [243]. Included in the lipid layer of MYXV MVs are homologs to J1R, H3L and A27L (M060R, M071L, M115L, respectively), which are implicated in virion binding to the cell surface (see section 1.7.3) [243]. MYXV homologs of F13L (M022L) and A34R (M122R) have been shown to be found associated with MYXV EVs[239,244].

Although MYXV undergoes similar morphogenesis stages as VACV, the VACV life cycle appears to run faster than that of MYXV. While no direct comparison of these viruses life cycles have been performed, in VACV MVs begin to appear between 5 and 6 h.p.i. [135], while MYXV MVs are seen between 8 and 12 h.p.i [239]. With both viruses, CEVs and EVs are evident by 16 h.p.i, although in MYXV CEVs exhibit a "marked increase" after 20 h.p.i [239]. Like VACV, actin projectiles and cytoplasmic corridors between infected cells have been observed in MYXV infections [219,239].

We asked the question: despite both being poxviruses, why do VACV and MYXV display such drastically different plaquing phenotypes? Given the importance that EVs and actin projectiles play in promoting the efficient spread of VACV, we started the work presented in Chapter 3 by comparing the amounts of actin projectiles formed by these viruses. We found that in all cell lines tested, VACV-infected cells showed that significantly more actin projectiles than MYXV. A genome comparison of MYXV and

VACV showed that MYXV encodes homologs of most of the VACV genes implicated in EV/actin projectile formation. While not a homolog of A36, MYXV M125 can complement actin projectile formation in an A36R-deficient strain of VACV, suggesting an orthologous function[219]. In Chapter 4 we show M125R is required for actin projectile formation in MYXV-infected cells, and VACV A36R can complement that this deficiency. We also failed to identify a MYXV homolog of VACV F11L. In Chapter 3 we show that a recombinant MYXV encoding F11L, but not other VACV EV-specific genes (A33R, A34R, A36R, or B5R) exhibits a larger plaque than WT MYXV. This suggests that one factor, which contributes the differences between plaques formed by VACV and MXYV, is that MYXV lacks a homolog of VACV F11L.

1.12 Myxoma Virus as an Oncolytic Virus:

MYXV is somewhat of a conundrum in that while it causes tumor-like lesions in its native host; it has oncolytic properties in some non-native cells/hosts. These seemingly counter-intuitive properties have been largely attributed to differences in MYXVs ability to modulate immune-sensing and cellular proliferation pathways in different hosts. The avirulence of MXYV in non-lagomorphs is thought to be due to the ability of these hosts to induce an anti-viral state in response to MYXV infection.

1.12.1 The Immune System Defines Myxoma Virus Tropism

Tumor necrosis factor (TNF) and interferons (IFN) can act in both an autocrine or paracrine fashion to create an antiviral response. IFNs bind to the interferon receptor (IFNAR) and can activate a number of different pathways, including the Janus kinase (JAK), STAT-1/3, and Erk1/2 pathways. These can collectively induce the expression of a number of genes, which have antiviral or antiproliferative properties (reviewed in[245]). TNF binds the TNF receptor (TNFR) and has been implicated in inducing many responses, including inflammatory and apoptotic responses (reviewed in [246]). Poxviruses are renowned for their ability to disrupt these signaling pathways to promote their own

growth, and MYXV is no exception. While MYXV can manipulate many aspects of TNF and IFN signaling in rabbits, it does not appear to have the same ability to circumvent these pathways in non-lagomorphs. These differences are thought to be a major determinant of MYXV tropism.

Infecting primary human and murine fibroblasts with MYXV induces the expression of both TNF and type I IFNs[247-250]. This induction is thought to be driven by the detection of viral RNA or DNA through the retinoic acid inducible gene I (RIG-I) and/or Toll-like receptors (TLRs) 7 and 9[247,249,250]. MYXV can partially offset the effects of type I IFNs (IFNα and β) in human cells, by inhibiting the phosphorylation reactions that are needed to activate the Janus kinase Tyk2 by using a yet-to-be identified viral protein[251]. This may explain why MYXV growth is only partially inhibited in human fibroblasts in the presence of type I IFN[251].

While MYXV encodes a protein, which binds and inhibits rabbit TNF- α it does not have the same ability to bind to non-lagomorph versions of this cytokine[252-254]. Despite this, MYXV replication in primary human fibroblasts is only partially inhibited in the presence of human TNF- α [248,255]. However, MYXV growth is completely abolished in primary human fibroblasts upon exposure to both TNF- α and IFN- β[255]. This synergistic inhibition is attributed to the induction of additional cellular genes, which neither cytokine induces alone[256]. Collectively, these data suggest that MYXV tropism in non-rabbits is determined by the host's immune system. This is further supported by observations that MYXV can replicate in cells deficient in components of these innate immune responses and cause lethal disease in STAT-1 deficient mice[248].

1.12.2 Defects in Cancer Cells Support Myxoma Virus Growth:

Viruses and cancer cells face similar obstacles, in that they must evade the immune system in order to be survive. Cancer cells are thought to accomplish this by using one of two methods. The first method occurs at the cellular level, where alterations

in the cancer cell limit its recognition or killing by immune cells. Many cancer cells show decreased levels of pro-apototic proteins, immunoregulatory receptors (e.g. TNF, IFNR, STATs), or factors like MHC-1 (reviewed in [257-259]). These mutations collectively prevent cancer cells from being recognized and killed by immune cells.

Cancer cells can also evade destruction by the immune system by limiting the recruitment of immune cells to the tumor microenvironment, or by altering the activity and viability of these cells within the tumor. These changes come largely due to alterations in the levels of cytokines and are the subject of multiple reviews ([260-262]). While genetic alterations in tumors aids in evasion from the immune system, they also presumably create a more favorable environment for MYXV growth.

It has been known since the 1950s that MXYV can replicate in guinea pig cancerous tissue[263]. However, it wasn't until almost 50 years later that knowledge about cancer cell immune defects combined with a new understanding of how the immune system affects MYXV growth, lead to the discovery that MYXV had oncolytic properties in human cancer cells. Sypula and colleagues screened the NCI-60 panel of human cancer cells and found that most of these cell lines supported MYXV growth [264].MYXV does not appear to have preference for replication in a particular type of cancer.. Rather, MYXV growth in cancer cells appears to be influenced by the fact that many transformed cells have lost the ability to induce an antiviral state in response to both TNF and/or IFN [256].

The tumor suppressor status and the protein kinase B (AKT) activity of the cell also influences MYXV replication. Cancer cells with defective tumor suppressors (p53, ATM or Rb) have been shown to support higher levels of MYXV growth [265]. A higher level of the phosphorylated active form of AKT has also been linked with elevated levels of MYXV growth[266-269]. Disregulation of these pathways has been linked to promoting cell survival and proliferation through a number of means, many of which could aid viral

growth. These include inhibiting apoptosis and down regulating immunoregulatory proteins (reviewed in[270,271])

MYXV is also able to influence elements of cell-signaling pathways, which promotes its growth in cancer cells. One protein that plays a key role in this is M-T5 (M005). M-T5 has been shown to promote the phosphorylation and re-distribution of AKT from the nucleus to the cytoplasm of infected cells [272]. Cell arrest at G_o can trigger apoptosis, and M-T5 is thought to aid in preventing this by mediating the degradation of the cell's checkpoint regulator p27. This, in turn, promotes cell cycle progression from G_o to G_1[273]. M-T5 deficient MYXV show a reduced tropism for some cancer cells, suggesting that these manipulations of cell signaling are important for virus replication[264]. Cancer cells which remain permissive for MYXV in the absence of M-T5 are reported to already have high levels of phospho-AKT[266-268,274].

1.12.3 Models Evaluating the Oncolytic Efficacy of Myxoma Virus:

MYXV shows promise for the treatment of a number of hematological malignancies (e.g. leukemia's), which are currently treated with chemotherapeutic agents. While these are often initially successful, drug-resistant relapses frequently occur. In these cases high doses of radiation are often then used. While these treatments destroy cancerous hematopoietic cells, they also destroys normal ones. As such grafts of hematopoietic stem cells are then used to reconstitute the immune system following radiotherapy. These cells can be either cells that were extracted from the patient prior to radiation therapy, or from a MHC-matched donor. Both sources have potential problems. Donor cells can potentially attack host organs, while using the patient's own cells risks re-introducing cancerous cells. One option is to try to purge these cells of cancerous cells before re-introduction (reviewed in[62,275]) and MYXV seems capable of selectively doing this. Pre-treating cancerous blood cells (leukemic or multiple melanoma) with MYXV before introducing them into immunocompromised mice has greatly reduced the rate of

tumor reformation[276-279]. Interestingly, MYXV appears to show specificity for binding to cancerous hematopoetic cells, while leaving normal primary human cells unaffected, and can reduce the grafting of cancerous cells, but not normal cells in mice [278-280].

While MYXV appears to be well adapted for the *ex vivo* treatment of hematological malignancies it is less encouraging for the treatment of solid tumors or metastases. In the 1950's MYXV was evaluated for its oncolytic properties in Guinea Pig models of Daels sarcomas[263]. While it showed efficacy *in vitro,* MYXV had little efficacy *in vivo,* something the authors attributed to the immune system limiting virus replication [263,281]. These less-than encouraging results may explain why it was not for almost another 50 years, when the molecular basis for MYXV growth in cancer cells was better understood, that any further studies were performed to examine the use of MYXV as an oncolytic agent.

Since the early 2000s, MYXV has been evaluated for oncolytic efficacy in a number of solid tumor models. These have included both immunocompromised and immunocompetent animals. When administered intratumorally, MYXV has been shown to significantly delay growth of experimental human gliomas, medullablastomas, or rhaboid tumors that were established in the brains of nude mice [282-284]. In some of these cases (e.g. some mice bearing U87-gliomas or Daoy medullablastomas) cures were observed [282,283]. MYXV treatment has also shown some efficacy in the treatment of solid tumors in immunocompetent hosts. Intratumoral injections of MYXV into C57/BL6 mice bearing subcutaneous B16F10 tumors reduces tumor growth rates [285]. However, while MYXV is capable of replicating in, and killing, rat RC38 gliomas *in vitro*, it has little efficacy when administered intratumorally in animal models[286].

While MYXV shows some promise when injected intratumorally into solid tumors, it appears to have a limited capacity to home in on cancer cells when administered intravenously, and to spread between tumors. While displaying oncolytic

activity when injected directly into a U87 glioma, MYXV does not appear to spread to and affect the growth of a second, contralateral tumor which did not receive a virus injection [282]. MYXV also appears incapable of spreading systemically to cure B16F10 lung metastases in C57/BL6 mice [285].

MYXV is safe in non-lagomorphs, appears to show specificity to cancer cells, and displays oncolytic efficacy in a number of tumor models. However, it does not appear to spread well from the site of introduction to other metastatic sites. This suggests that there is room to improve the oncolytic efficacy of MYXV.

1.12.4 Approaches for Increasing the Oncolytic Efficacy of Myxoma Virus:

A number of approaches have been undertaken in attempts to improve MYXV as an oncolytic virus. These have focused on modulating the immune response, the AKT status of cells, or the delivery route.

Active AKT can be dephosphorylated and converted to an inactive form by the phosphatase PP2A. Treatment of cancer cells with the PP2A inhibitors okadaic acid or endothall, can promote MYXV growth in some cancer cells, which are normally non-permissive for MYXV[287]. The use of the immunosuppressant/cancer therapeutic drug rapamycin can also increase MYXV tropism in cancer cells. Its use has also been shown to synergistically enhance the oncolytic efficacy of MYXV in animal models of experimental medullablastomas, gliomas, and brain tumor-initiating stem cells [269,283,285,286,288,289]. Rapamycin is thought to aid MYXV growth by abrogating elements of the type I IFN response[286], and by promoting phosphorylation of AKT[287]. Our laboratory has also recently performed a genome-wide siRNA screen in human MDA-MB-231 adenocarcinomas. This screen identified a number of genes that when silenced promoted MYXV growth [290]. This suggests that additional pathways could be targeted to enhance the oncolytic activity of MXYV.

As discussed in section 1.12.2, tumors are microenvironments that either exclude immune cells, or secrete factors that inhibit immune cell normal activity. It is widely accepted that combining the oncolytic activity of viruses, with their tendency to recruit immune cells to the sites of infection, may allow for better clearance of tumors (reviewed in [291]). Interleukin-12 (IL-12) is an important activator of NK-cells and cytotoxic T-cells, and its expression has been linked with antitumorgenic properties [292]. A conditionally replicating HSV-1 expressing IL-12 has been shown to display increased tumor control properties[293,294]. A recombinant strain of MYXV expressing human IL-12 has also been shown not to cause myxomatosis in European rabbits [295]. It has been suggested that this IL-12 virus may be a more effective oncolytic virus, although no *in vivo* studies have been performed to investigate this possibility. Similar suggestions have been made for the use of a strain of MYXV expressing IL-15 [296].

Altering the route of virus delivery can also enhance the effectiveness of MYXV. While an intravenous injection of virus does not prolong the survival of animals bearing brain tumors, intratumoral injection or virus delivery to the central nervous system does [284,286]. The use of cell delivery vectors has also been shown to increase the oncolytic efficacy of MYXV. Adult stem cells have been shown to traffic to tumors and some of these cells can be infected by MYXV [297,298]. The non-intratumoral injection of adipose-derived and MYXV-infected adult stem cells showed better virus delivery to, and distribution in, malignant gliomas than virus treatment alone. This, in turn, enhanced the survival of these mice[298].

While no attempts to increase the oncolytic efficacy of MYXV through enhancing its spread capabilities have been attempted, it has been shown that the efficacy of other oncolytic viruses can be improved if they exhibit enhanced spread. Reoviruses bearing mutations in the σ1 or λ2 capsid genes show increased plaque size and display enhanced control of B16 melanomas in C57BL/6 mice [299]. The introduction of the IHD-J

allele of A34R (E_{151}) into the wildtype WR strain of VACV also enhances the tumor control properties in C57/BL6 mice bearing subcutaneous CMT64 tumors or BALB/c mice bearing subcutaneous JC tumors, derived from murine lung or mammary cancer cell lines (See section 1.9 for discussion of A34R) [300]. Further, this virus showed increased spread to distant tumors, and was better able to control metastatic 4T1 cancer in BALB/c mice[300] . Similar increases in efficacy were observed in a C57BL/6 model of MC38 colon cancer when this variant A34R allele was introduced into the VV-DD (JX-929) strain [301]. VV-DD is recombinant VACV (Wyeth strain), which also lacks thymidine kinase and the viral growth factor [65].

Given that the oncolytic efficacy of other these viruses can be improved by enhancing their spread properties, and that our F11L-expressing MYXV (Chapter 3) showed increased spread in rabbits and monkey cell lines, we wondered if F11L-expressing MYXV would display increased efficacy as an oncolytic virus. In chapter 5 I describe how we established a tumor model for evaluating the oncolytic abilities of MYXV. In Chapter 6 I describe how we tested if F11 expression affects the oncolytic abilities of MYXV. Furthermore, given that F11 inhibits elements of the Rho signaling pathway to promote disruptions in the actin cytoskeleton, I also tested whether chemical or genetic disruption of the actin cytoskeleton can be used to enhance MYXV growth.

1.13 Project Overview and Rationale:

In cell culture poxviruses form one of two types of plaques. The first type is a large lytic plaque, where a circle of infected cells surrounds a large cell-free central clearing. These type of plaques are commonly made by viruses like VACV. The second type of plaque is that formed by viruses like MYXV. These plaques (often called foci) are smaller, expand at a slower rate than the first type of plaque, and tend to cause clumping of infected cells.

We started this work by asking the question why, despite both being poxviruses, do VACV and MXYV form such clearly different plaque types in cell culture? While one can envision many reasons that could explain these differences, we focussed on examining differences in exit and spread between these viruses. Effective VACV spread is dependent upon the formation of EV and actin projectiles, and mutations in many of the genes responsible for these processes reduce plaque size and virus yields (i.e. confer a more MYXV-like phenotype). In work presented in Chapter 3 I show that MYXV-infected cells form far fewer actin projectiles than VACV-infected cells. Comparison of the genomes of these two viruses identified clear MYXV homologs/orthologs for the majority of VACV genes involved in these processes. Exceptions were to VACV A36R, B5R and F11L.

Although more closely related to another VACV protein, C3L, MYXV M144R shows homology to B5R. Additional bioinformatics analyzes (hydrophobicity and localization profiles) suggest that M144 is likely a homolog of B5R. Despite limited sequence homology M125R can complement actin projectile formation in A36R-deficient VACV, suggesting an orthologous function[219]. In Chapter 4, I showed the importance of M125R for MYXV actin projectile formation, through the generation and characterization of a M125R-deficient strain of MYXV.

In contrast to all other genes, we could not find a MYXV homolog of VACV F11L. This lead us to hypothesize that the absence of a MYXV homolog of VACV F11L might contribute the smaller plaques formed by MYXV. I found that a recombinant strain of MYXV encoding VACV F11L enhanced actin projectile formation, virus titers and exhibited a larger plaque size. This was not observed in MYXV encoding A33R, A34R, A36R, B5R or any combination of these four genes. This F11L^{+} MYXV also induced a number of alterations to the actin cytoskeleton that have been associated with the F11 activity including disruption of cortical actin, cell-rounding and altered cell migration.

These observations were confirmed in a number of monkey and rabbit cell lines including freshly isolated primary rabbit cornea fibroblasts. While the addition of F11 enhanced plaque size of MYXV, these plaques were significantly smaller than those formed by VACV, which suggests other genes regulating plaque size remain to be discovered and which are different in these two viruses.

Around the time I was pursuing these studies, reports surfaced showing the oncolytic efficacy of VACV could be improved by increasing its ability to spread[300]. Given that MYXV also has oncolytic properties, we wondered if the enhanced spread observed by our F11L$^+$ strain of MYXV would produce a more effective oncolytic virus. In Chapter 6 I show that F11L$^+$ MYXV can replicate to higher levels in many human cancer cells, and in some cases causes more effective viral-mediated killing. In MDA-MB-231 adenocarcinomas, we confirmed similar alterations to the actin cytoskeleton as those observed in rabbit and monkey cells. We then established a MDA-MB-231 tumor model in NIH-III mice to evaluate the oncolytic efficacy of MYXV. In Chapter 5 I discuss the process used to optimize this model, including a study of virus doses and development of non-invasive animal imaging techniques for the tracking of cancer cells and virus using an IVIS Spectrum small animal imager. In Chapter 6 I show that the effects caused by F11L in cell culture translates to delayed tumor growth and prolonged survival of mice. Furthermore, in a bilateral tumor model, where mice had MDA-MB-231 tumors established in opposite mammary fat pads, we observed that the F11L expression produced greater tumor control of the secondary uninjected tumor. This was associated with more MYXV in the non-injected tumor.

F11 disrupts cortical actin by disrupting RhoA signaling[143,204,224]. We were also able to mimic these genetically induced effects by using pharmacological inhibitors of actin polymerization, or siRNA-mediated depletion of key regulators of cortical actin

(RhoA, RhoC, mDia1 or LIMK2). While these enhanced WT MYXV growth, they had little effect on F11L^{+} MYXV.

Collectively the work presented in this thesis suggest that one factor explaining the drastic differences in plaquing properties between MYXV and VACV is the absence of a MYXV homolog to VACV F11L. Introducing this gene into MYXV enhanced viral spread. We can translate this enhanced growth into more effective oncolytic activity. Furthermore, F11 inhibtis RhoA signalling, which is a pathway commonly disregulated in cancer cells, suggesting that it may be possible to combine inhibitors of this pathway to enhance the efficacy of many oncolytic viruses.

CHAPTER 2: MATERIALS AND METHODS

2.1 Plasmid Generation and Related Molecular Biology Techniques:

This section describes techniques that were used to generate a number of plasmids, which would be used for either the creation of recombinant viruses (Section 2.3.2) or transient transfections of virus-infected cells (Section 2.5.2.2). Typically, the generation of a plasmid started with PCR amplification of a region of DNA, usually from a viral DNA template. PCR products of the appropriate size, as confirmed by agarose gel electrophoresis, were then Topo® TA cloned into the PCR 2.1 TOPO vector, and transformed into *Escherichia coli (E.coli)*. From the resulting bacterial colonies, plasmids were isolated by "mini-prep" techniques and plasmids containing the desired DNA were confirmed through a combination of restriction digest analysis and sequencing. The DNA of interest was isolated through restriction enzyme digests and agarose gel purification, and then sub-cloned into similarly digested destination vectors. The bacterial transformation, plasmid isolation and confirmation process was repeated until the final construct was generated, which was confirmed by sequencing. Any plasmid that was to be used for an experiment in mammalian cells was first purified using a Qiagen Maxi-Prep kit.

2.1.1 Polymerase Chain Reaction:

Polymerase chain reactions (PCR) were used to amplify regions of DNA that were to be used for either cloning or diagnostic analysis of recombinant viruses. *Taq* polymerase (Fermentas) was used to amplify DNA regions for diagnostic PCR, or for DNA destined for cloning that was less than 1 kb in length. In order to minimize the likelihood of obtaining PCR products with mutations, PCR products larger than 1 kb was amplified using Roche's Expand high-fidelity polymerase. PCR reactions comprised of 50µl aliquots containing template DNA (25ng of viral template or 1ng of plasmid DNA) and 15 pmol of each primer. Reactions using *Taq* polymerase were performed in 10mM

TrisHCl pH 8.8, 50mM KCl, 0.08% (v/v) NP-40, 2.5mM $MgCl_2$,0.2mM of each dNTP, and used 1U of enzyme. Reactions using Expand high-fidelity polymerase were performed in proprietary buffer with 2.5mM $MgCl_2$ and using 2.6 U of enzyme. PCR reactions were performed in a Biometra T-gradient thermocycler and started with an initial denaturation step of 2 mins at 94^{o}C. This was followed by 30 cycles consisting of a 30s at 94^{o}C step, a 30s annealing step, whose temperature was determined by taking the primers annealing temperature and subtracting 5^{o}C, and an elongation step at 72^{o}C. The length of the elongation step was calculated by using 1 min for every kb in size that the PCR product was. Following these cycles a final elongation step of 7 mins was performed. **Table 2.1** lists the primers used in these studies.

2.1.2 Agarose Gel Electrophoresis and Gel-Purification of DNA:

DNA fragments were analyzed by gel electrophoresis. For this DNA was mixed with 10× gel loading buffer and this mixture was then loaded on to a 1X TAE agarose gel (40mM Tris-acetate, 1mM EDTA, containing 1:20 000 SYBR safe DNA stain). The concentration of agarose varied from 0.8-1.2% depending on the size of the fragments that were to be resolved. Following separation by electrophoresis (using ~80V/cm), DNA was visualized using a Kodak Gel Logic 200L imager.

When a fragment of DNA was to be purified by gel extraction, the desired band was the cut out of the agarose gel and purified using a QiaQuick gel extraction kit, as per the manufacturer's instruction.

2.1.3 Restriction Enzyme Digests:

Restriction enzyme digests were typically done in 20µl reactions containing the appropriate buffer, ~0.5-1.0 µg of DNA, and 1-5 U of the desired restriction enzyme. Restriction enzymes were purchased from Fermentas, with the exception of *PacI* which was initially purchased from New England Biotechnology (NEB). Digests were allowed

to proceed for at least 1 h at 37°C, and in some situations overnight. When DNA was to be used for subcloning these reactions were scaled up proportionally.

Table 2.1: Primers used in these studies

Gene amplified	primer sequence (5'→3')[1]	Template:
VACV-A33R	Fwd: GCGGCCGCTTGTGTTAAAACAATGAACTAA Rev: GCGGCCGCTTAGTTCATTGTTTTAACAC	VACV WR genomic DNA: 143220-143888 (forward strand)
VACV-A34R	Fwd: GCGGCCGCTATTTATTTTTGTACATTAATAA Rev: GCGGCCGCTAACGACTTATTATTAATTA	VACV WR genomic DNA: 143889-144449 (forward strand)
VACV-A36R	Fwd: TTAATTAATAAAGTTGTAAAGTAAATAATAAAACA Rev: TTAATTAATCACACCAATGATACGACC	VACV WR genomic DNA: 144993-145724 (forward strand)
VACV-B5R	Fwd: GCGGCCGCCTATTAAAATATAAAATCTAAGTAGGAT Rev: GCGGCCGCTTACGGTAGCAATTTATGGAA	VACV WR genomic DNA: 168274-169327 (forward strand)
VACV-F11L	Fwd: GCGGCCGCCAGATGGTAAAATTATAAAAAG Rev: GCGGCCGCTTACAAACGAAAGTCCAGGTTTG	VACV Copenhagen genomic DNA 37801-38847 (reverse strand)[2]
EcoGPT	Fwd: GCGGCCGCGCTCGAAAGGAGGAACTATATCC Rev: TTAATTAATCTCGATCCGGAGCATGCAA	pTM3
mCherry[3]	Fwd:TTAATTA**AAAATTGAAATTTTATTTTTTTTTTTGG AATATAAATA***ATGGTGAGCAGGGCGAGGA* Rev: TTAATTAAGCTCGAGATCTGAGTCCG	pmCherry-C1
MYXV-M127L	Fwd: CGTAGTAGAACGTTAAACGAATGCG Rev: AACTCGGTCGCGTTAAATTTCTT	analysis of recombinants
MYXV-ΔM127L	Fwd: TTAGAGGGGCTACGAGACGTGG Rev: CGGATGCGTCGACGTAATAGA	analysis of recombinants
M125R-Flag[4]	Fwd: GCGGCCGCAGCTGTTCATTGTGTACG Rev: GCGGCCGCCTA**CTTGTCGTCATCGTCTTTGTAGTC** AGATACGGCCGTTTCTGT	MYXV Lau genomic DNA: 139361-140313 (forward strand)
MYXV-ΔM125R	Fwd: TACGGTTTATGCCCCATTGAG Rev: CGTTCAGACGATGTTCCATGA	analysis of recombinants
VACV-A34R Tyr101-Ala140	Fwd: GGATCCTATTGGGTAAGTTTAAAAAAG Rev: GAATTCAGCATCCGTCGTACTGTTTA	VACV WR genomic DNA
VACV-A36R Thr 142-Glu214	Fwd: GGATCCACGGAGACTGTTGAAGTACT Rev:GAATTCTTCTATATCATCGTGTTCATGA	VACV WR genomic DNA
Notes:		
1: underlined sequence denotes restriction enzyme sites **2: Our lab VACV WR strain contains a 13 amino acid addition of F11L at the 3' end of the gene which does not match the reported sequence, thus Copenhagen DNA was used as a template** **3: Bold sequence denotes synthetic early late promoter** **4: Bold sequence denotes FLAG-epitope tag sequence**		

2.1.4. TOPO® TA Cloning and DNA Ligations:

Fragments of DNA that were to be ligated together were first purified from restriction enzyme reactions by agarose gel purification as described in section 2.1.2.

When non-directional cloning was to be used, the digested vector was first subjected to an overnight incubation with shrimp alkaline phosphatase (SAP) (Fermentas).

Following DNA quantification, DNA was ligated at a 3:1 ratio of molecules of insert to vector using T4 DNA ligase (Fermentas). The reactions were allowed to proceed for either 4 h at room temperature or overnight at 16^{o}C, after which 1-2µl (~10-20ng of DNA) were used to transform electrocompetent *E. coli* as described in section 2.1.5.

PCR fragments were often ligated into a vector using TOPO® TA cloning. For this, PCR products (which had non-template 5'A) were mixed with TOPO PCR 2.1 vector, which has VACV topoisomerase covalently linked to the molecule. The reaction was allowed to proceed for 5 min after which 1µl of the reaction was used to transform *E. coli* as described in section 2.1.5

2.1.5 Transformation and Propagation of *E.coli*:

Electrocompetent *DH5α E.coli* (F- φ80*lacZΔM15 Δ(lacZYA-argF) U169 recA1 endA1 hsdR17 (r^{k}-, m^{k}+) phoA supE44 λ- thi-1 gyrA96 relA1*) were prepared by growing a culture in Luria-broth (LB) to mid-log (OD_{600} ~0.6). Centrifugations and washes in 10% glycerol were used to remove residual ions and concentrate the bacteria, after which they were frozen until use. When warranted, commercially available electrocompetent DH10B' *(*F– *mcr*A Δ(*mrr-hsd*RMS-*mcr*BC) Φ80*lac*ZΔM15 Δ*lac*X74 *rec*A1 *end*A1 *ara*D139 Δ(*ara leu*) 7697 *gal*U *gal*K *rps*L *nup*G λ–) with high transformation efficiency (Invitrogen) were used instead.

To transform *E. coli* a mixture of bacteria and DNA were transferred to a pre-chilled 0.1cm BioRad electroporation cuvette, and then subjected to a 1.80kV pulse for 4-5ms using a BioRad electroporater. Following this, 0.25mL of SOC recovery media (Invitrogen) was added. Bacteria were allowed to recover, and express plasmid-encoded antibiotic resistance gene(s), at 37^{o}C for 1h, after which bacteria were plated on LB agar plates containing the appropriate antibiotic. Bacteria were then grown overnight to allow

for the formation of colonies. When blue/white selection was being utilized, 40 µl of 40 mg/mL X-Gal was added to the plate prior to bacterial plating.

2.1.6 Plasmid Isolation:

Plasmid DNA was normally isolated from 1.5 mL of an overnight bacterial culture using a commercially available "mini-prep" kit (Fermentas) as per the manufacturer's instructions. DNA, destined for the transfection of mammalian cells, was purified free of endotoxins from 100 mL overnight bacterial cultures using a Qiagen Maxi-Prep Kit, as per the manufacturer's instructions.

2.1.7 DNA Sequencing and Vector Map Construction:

All final constructs were sequenced. Sequencing reactions were performed by the Applied Genomics Centre (TAGC) (University of Alberta), and compared to a reference sequence using Sequencher (v4). Plasmid vector maps were generated using either Vector NTI (v9) or MacVector (v11.0). A list of the plasmids used in these studies are outlined in table 2.2.

2.2. Cell-culture:

This section pertains to the cell lines used, procedures for isolation of primary cells, and techniques used for culturing the mammalian cells that were used in these studies. A list of the cell lines used in these experiments, their sources, and the cell culture media used in their propagation are outlined in **Table 2.3.** The media, supplements and fetal bovine serum (FBS) were obtained from GIBCO. All cells were routinely tested, and found to be negative for mycoplasma by PCR (Invitrogen).

Table 2.2 Plasmids generated in these studies

Plasmid	Plasmid Backbone	Use
CIpA33R-Topo	Topo PCR 2.1	Construction of CIpLGPT-A33R
CIpA34R-Topo	Topo PCR 2.1	Construction of CIpLGPT-A34R
CIpA36R-Topo	Topo PCR 2.1	Construction of CIpLGPT-A36R
CIpB5R-Topo	Topo PCR 2.1	Construction of CIpLGPT-B5R, construction of CIpLGPT-A36R/B5R, used for
CIpA33R/A34R-Topo	Topo PCR 2.1	Construction of CIpLGPT-A33R/A34R
CIpF11L-Topo	Topo PCR 2.1	Construction of CIplGLPT-F11L and CIpLGPTmCherry-F11L
CIpE/LmCherry	Topo PCR 2.1	Construction of CIpLGPTmCherry
CIpEcoGPT	Topo PCR 2.1	Construction of CIpLGPT and CIdelM125RGPT
pLAB		Construction of CIpLGPT , constructed by geneart, contains homology to 5' and 3' ends of M127L
CIpLGPT	pLAB	Construction of CIpLGPT-A33R , -A34R, -A36R -B5R, -A33R/A34R, - A36R/B5R, and CIpLGPTmCherry, construction of ΔM127L virus
CIpLGPTmCherry	CIpLGPT	Construction of CIpLGPTmCherry-F11L, Construction of ΔM127L-mCh virus
CIpLGPT-A33R	CIpLGPT	Construction of MYXV-A33R
CIpLGPT-A34R	CIpLGPT	Construction of MYXV-A34R
CIpLGPT-A36R	CIpLGPT	Construction of CIpLGPT-A36R/B5R, Construction of MYXV-A36R
CIpLGPT-B5R	CIpLGPT	Construction of MYXV-B5R
CIpLGPT-A33R/A34R	CIpLGPT	Construction of MYXV-A33R/A34R
CIplGPT-A36R/B5R	CIpLGPT	Construction of MYXV-A36R/B5R
CIpLGPT-F11L	CIpLGPT	Construction of MYXV-F11L
CIpLGPTmCherry-F11L	CIpLGPTmCherry	Construction of MYXV-F11L-mCh
CIpGEX2T-A34R	pGEX-2T	Protein expression for A34 antibody generation
CIpGEX2T-A36R	pGEX-2T	Protein expression for A36 antibody generation
delM125R		Construction of CIdelM125R-GPT , constructed by geneart, contains homology to 5' and 3' ends of M127L
CI-delM125R-GPT		Constuction of delM125R virus
CI-M125R-FLAG	Topo PCR 2.1	M125R gene with C-terminal FLAG tag under native promoter, used for transient transfections

2.2.1 General Cell-Culture Techniques:

Unless stated otherwise, cells were passaged as follows: 150mm dishes of cell monolayers were passaged upon reaching ~90-95% confluency. To do this, the media were aspirated and the cells washed with Versene (0.72% NaCl, 0.02% KCl, 0.01% Na_2HPO_4, 5mM EDTA pH 8.0) containing 0.25% trypsin (Gibco), after which versene was added to cells, and the cells incubated at 37^{o}C until they detached from the dish. The trypsin was inactivated by adding serum-containing media to the versene/cell mixture.

When cell counts were needed, a 10ul aliquot was taken, mixed 1:1 with trypan blue dye (Invitrogen), and cell numbers determined using either a hemocytometer or a Countess automated cell counter (Invitrogen). The cells were then diluted to the desired number and added to tissue culture plates.

2.2.2 Cell Bank Generation:

To generate banks of cell-lines, the cells were detached from tissue culture plates as described in section 2.2.1. The cells were then pelleted at 800 rpm (100~g) using a Beckman Allegra X-22R centrifuge, resuspended in 10% DMSO (Invitrogen) in FBS, cells quantified (as described in section 2.2.1), and diluted to a desired cell number (typically 1-2 $\times$ 10^6 cells/mL). Cells were then aliquoted and gradually frozen overnight at -80^{o}C using an isopropanol-freezing container before being transferred to liquid nitrogen for long term storage.

To thaw cells stored in liquid nitrogen, a tube was removed from storage, rapidly thawed at 37^{o}C in a water bath, and then added to pre-warmed media. The cells were allowed to attach for at least 4 h before the media was aspirated, and replaced with fresh culture media.

Table 2.3: Cell lines used in these studies

Cell Line	Cell type	Source	Media
BGMK	Monkey Kidney epithelium	Diagnostic Hybrids	MEM + 10% FBS
SIRC	Rabbit Cornea fibroblast	ATCC	MEM + 10% FBS
RK13	Rabbit kidney fibroblast	ATCC	MEM + 10% FBS
U87-MG	Human glioblastoma	ATCC	MEM + 10% FBS, +1% Sodium pyruvate
U118-MG	Human glioblastoma	ATCC	DMEM+10% FBS
Daoy	Human medullablastoma	ATCC	DMEM+10% FBS
Capan-2	Human pancreatic pdenocarcinoma	ATCC	DMEM+10% FBS
PANC-1	Human pancreatic epitheliod carcinoma	ATCC	DMEM+10% FBS
HeLa (S3)	Human cervical adenocarcinoma	ATCC	DMEM+10% FBS
MDA-MB-231 (D3H2LN)	Human mammary adenocarcinoma	Caliper Scientific	MEM + 10% FBS, +1% Sodium pyruvate
MDA-MB-468	Human mammary adenocarcinoma	M.Hitt (U of A)	1:1 DMEM/F12+10% FBS
MCF7	Human mammary adenocarcinoma	M.Hitt (U of A)	DMEM+10% FBS
MTHJ	Murine mammary adenocarcinoma	M.Hitt (U of A)	DMEM + 10% FBS
AY-27	Racine urothelial carcinoma	M.Hitt (U of A)	RPMI 1640 + 10% FBS
HEK-293T	Human kidney epithelium	T.Hobman (U of A)	DMEM + 10% FBS
KU-7	Human urothelial carcinoma	M.Hitt (U of A)	DMEM + 10% FBS
BSC40	Monkey kidney fibroblast	ATCC	MEM + 5% FBS

Note: All media was supplemented with 1% non-essential amino acids, 1% L-glutamine, 1% antibiotic/antimycotic

2.2.3 Isolation of Primary Rabbit Corneal Fibroblasts:

Procedures for isolation and culturing of primary rabbit corneal fibroblasts were modified from protocols established by Chan and Haschke and Griffth *et al* [302,303]. Corneas were isolated from a European rabbit, which had been euthanized for an unrelated experiment. The corneas were washed with PBS containing 2%

antibiotic/antimycotic and stored in DMEM at 37°C overnight. Corneas were then cut into small pieces (~1 mm^3), and digested twice with 4 mg/mL Type 1A Collagenase (Sigma) in PBS for a total of 5 h at 37°C. The resulting cell mixture was then centrifuged at 1800 rpm for 12 min, and then the cells were cultured in DMEM + 10% FBS. All of the experiments performed using these cells were done within one passage of isolating the cells, and passaging and cell banks were generated as described in sections 2.2.1 and 2.2.2.

2.3 Virus Stains Utilized in These Studies:

This section pertains to the viruses used and generated in these studies, as well as the protocols used to grow, purify, titrate and UV-inactivate any stocks. **Table 2.4** outlines the viruses used in these studies, as well as their sources and any notable characteristics.

2.3.1 Generation of Recombinant Viruses:

To generate recombinant MYXV 60 mm dishes of BGMK cells were infected with MYXVvLacZ at a MOI of 2. After 1 h the inoculum was replaced with serum and antibiotic free medium (Opti-MEM from Invitrogen), and after another the hour cells were transfected with DNA. Transfection reactions consisted of 2µg of linearized plasmid, which had been incubated with 10µl of lipofectamine 2000 (Invitrogen) in opti-MEM for 30 mins prior to transfection.

After 24-48 h the virus-cell mixture was harvested, and subjected to three rounds of freeze-thaw. Virus was then plated on 60 mm dishes of BGMK cells and after 1 h, the inoculum replaced with fresh media. To select recombinants encoding the *EcoGPT* cassette media containing 25 µg/mL mycophenolic acid, 15 µg/mL hypoxanthine and 250 µg/mL xanthine was used. Following two rounds of liquid drug selection, virus was subjected to an additional three rounds of purification by picking plaques. This was performed as follows: after infecting cells for 1 h the virus inoculum was replaced with a

1:1 mixture of 2×DMEM and 1.7% Nobel agar. The agar was allowed to solidify and the plates incubated at 37^{o}C until virus foci were visible. This took 3-7 days. Virus were then isolated from plaques using a P-1000 tip, placed in PBS complete, subjected to three freeze-thaw cycles, and replated.

In situations where recombinant viruses expressed mCherry fluorescent protein, the presence of this marker was confirmed by fluorescence microscopy using an inverted Zeiss microscope. Following agar selection, the viruses, were amplified by repeated passage on BGMK cells until titers of ~10^6 pfu/mL were obtained, after which each recombinant virus was assayed for purity, as described in the next section. In general three separate recombinants for each strain were followed through to this stage.

2.3.2 Analysis of Recombinant Viruses by PCR:

Recombinant virus purity was confirmed by PCR analysis. For this ,60 mm dishes were infected with each recombinant virus at MOI ≅ 1 for 24 h. After which media was replaced with 1mL cell lysis buffer (1.2% SDS, 50mM Tris pH 8.0, 4mM EDTA, 4mM $CaCl_2$ and 0.2mg/mL proteinase K (Fermentas)) and then incubated 4h-18h at 37^{o}C.

This mixture was extracted with buffer-saturated phenol (Invitrogen) and centrifuged at 18 000 ×G for 10 mins. The aqueous layer was transferred to a new tube and the DNA precipitated with cold 95 % ethanol (2:1 volume) and 3 M sodium acetate pH 5.2 (1:20 volume), and centrifuged for 30 min at 18 000 ×G. The pellet was washed with 70% ethanol, and the DNA resuspended in H_2O. DNA was quantified and diluted to 25ng/µL and 1 µL of DNA used in a 50µL PCR reaction. At least two PCR reactions using different primer pairs were used to confirm the structure of each virus.

If analysis showed evidence of residual WT virus, the recombinant virus was subjected to additional rounds of agar purification and the process repeated until a pure

population of recombinant virus was obtained. In situations where a gene had been introduced (e.g. MYXV-F11L-mCh) the sequence of the introduced gene was confirmed by sequencing the PCR product.

Table: 2.4 Viruses used in these studies

Virus	Source	Characteristics	Reference
		Vaccinia virus strains	
Western Reserve	ATTC	Wild-type virus	
ΔJ2R	Our Lab	Expresses β-galacosidase	63
A5L-YFP	B.Moss	YFP tagged A5L, phenotypically WT	304
		Myxoma virus strains	
Lausanne	ATTC	Wild-type virus	
LacZ	G.McFadden	Intergenic insertion of β-galacosidase, phenotypically wild-type	305
GFP-TrFP	G.McFadden	Expresses GFP (early) and TrFP (early and late)	255
PL K/O	Our lab	Complete deletion of M127L	306
MT4-	M.Barry	Lacks both copies of M-T4 (M004L/R)	307
		Recombinant myxoma virus strains generated in these studies (all strains are GPT$^+$ and with the exception of ΔM125R lack a functional M127L)	
ΔM127L			
ΔM127L-mCh		Expresses mCherry	
MYXV-A33R		Expresses VACV A33R	
MYXV-A34R		Expresses VACV A34R	
MYXV-A36R		Expresses VACV A36R	
MYXV-B5R		Expresses VACV B5R	
MYXV – A33R/A34R		Expresses VACV A33R and A34R	
MYXV- A36R/B5R		Expresses VACV A36R and B5R	
MYXV – F11L		Expresses VACV F11L	
MYXV – F11L-mCh		Expresses VACV F11L and mCherry	
ΔM125R		Disrupted M125R	

2.3.3 Virus Titration:

Virus titers were determined as follows: ten-fold serial dilutions of virus in PBS complete were prepared and then 0.5 mL was added to each well of a 6-well dish of BGMK cells. The dilutions were plated in triplicate for the titration of virus stocks, or in duplicate for the titration of virus from experiments. The virus were absorbed for 1 h before the inoculum was replaced with fresh medium and the dishes returned to the incubator.

MYXV viruses encoding beta-galactosidase were cultured 2-3 days and fixed by a 5 min incubation with 2 % formaldehyde in PBS. The cells were washed with PBS and a solution containing 5mM $K_3Fe(CN)_6$, 5mM $K_4Fe(CN)_6$, 2mM $MgCl_2$ and 0.5mg/mL X-gal in PBS was added. The plates were then incubated at 37oC for 4-18 h which caused the encoded beta-galactosidase to turn the plaques blue. The X-gal solution was then aspirated, the plaques washed with water, and plaques counted.

When viruses lacked β-galactosidase, the virus were stained with crystal violet. In these situations, the MYXV was grown for 5 days, or 2 days for VACV, after which the medium was aspirated and the cells fixed and stained with a solution containing 15 % ethanol, 2 % glacial acetic acid, 2 % formaldehyde and 0.5 % crystal violet. The cells were fixed for 20-30 min before being washed with water, and plaques counted.

2.3.4 Generation, Purification, and UV-Inactivation of Virus Stocks:

High titer virus stocks were generated in a manner similar to those outlined by Smallwood *et al.*[308] BGMK cells grown in roller bottles each containing ~10^8 cells per bottle (Corning) were infected at a MOI=0.05, and then cultured for 72-96 h. At this point the medium was decanted, the cells washed with PBS A, and incubated with 40 mL of versene/trypsin until the cells detached. The cells were pelleted by centrifugation (2000 × G for 10 min), and the pellet resuspended in 5 mL per bottle of 10 mM Tris-HCl pH 8.0. The virus was then released from cells by using a combination of freeze-thaw and dounce-homogenization. Cellular debris was removed by centriguation (2000 × G for 10 min), the supernatant transferred to a new tube, and the pellet re-extracted with buffer, dounce-homogenization and centrifugation. The pooled supernatants were then applied to the top of an equal volume of 36% sucrose in 10mM Tris-HCl pH 8.0, centrifuged for 80 min at 26 500 × G using a JS13.1 rotor. The virus pellet was re-suspended in PBS A, and any residual debris removed by centrifugation of 5 min at 2000 × G. The virus stocks were then titered, diluted to working concentrations, and aliquoted.

To generate UV-inactivated stocks of virus, virus was exposed to a UV-lamp for 2 h at a dose rate of ~ 7.5 J/sec/m^2. Virus inactivation was confirmed by plaquing. We detected no plaques when 10^9 pfu were plated, suggesting this treatment was effective.

2.4 Analysis of Virus Growth Properties:

2.4.1 Single and Multi-Step Growth Curves:

For low MOI multi-step analysis of virus growth 60 mm dishes of nearly confluent cells were infected at a MOI of 0.01 (~ 0.5 - 3 x 10^4 pfu). Following 1 h infection medium was added. At indicated times, the virus-cell mixture was harvested by scrapping cells into the medium. Virus was then released from cells by freeze-thaw and tittered on BGMK cells. A similar approach was taken for high MOI, single-step, growth-curves, except that MOI =5 (~ 1x10^7 pfu) was used and cells were washed once with complete PBS after infection and prior to the addition of medium. The results of three independent experiments (mean ±S.E.M.) are reported.

2.4.2 Virus Release Experiments:

To measure the proportion of virus released into the cell medium, cells were infected at a MOI=10 for Rk13 cells or MOI=5 for MDA-MB-231 cells, after which the virus inoculum was removed, any unbound virus removed by 2 washes with complete PBS and fresh medium was added. The medium was removed 24 h later and centrifuged for 10 min at 1000 × G. The supernatant was then transferred to a new microfuge tube and tittered. This represents the soluble (aka released) virus population. To determine the total virus, the cell layer was scraped into complete PBS, freeze-thawed, and then tittered. The amount of released virus, as a percent of total virus (released + cellular virus) was then calculated. The results of three independent experiments are shown.

2.4.3: Cell Viability Assays:

To determine the effects of virus on cell viability, 96 well-plates were seeded with 5-10 ×10^4 cells/well. The next day the cells in one well were counted, and the

remaining cells infected with the indicated MOI of each virus. At the indicated times, alamar blue (resaurin salt) was added to a concentration of 44μM and cells incubated for 2h at 37^{o}C. A Fluorstar Optima plate reader was then used with filter settings of 544nm excitation and 590nm emission. The fluorescence signal is reported as a percentage of the signal obtained from uninfected cells. Three separate wells per experimental condition were used and each experiment was performed three times.

2.5 Microscopy and Associated Techniques:

2.5.1 Live Cell Microscopy:

Live cell microscopy was performed using a personal Delta-Vision microscope at 10 X magnification (N.A. = 0.30). These experiments used confluent BGMK cell monolayers, which had been grown overnight on glass-bottom 35 mm dishes (World Precision Instruments, Sarasota FL). All experiments were performed in the absence of CO_2, on a stage heated to 37^{o}C, and used phenol red-free MEM supplemented with 10mM HEPES pH 7.3. Live cell microscopy was used to visualize either the rates of plaque growth (section 2.5.1.1) or virus-induced cell motility (section 2.5.1.2).

2.5.1.1 Use of Live Cell Microscopy to Analyze Plaque Growth:

To examine rates of plaque growth, each dish of BGMK cells was infected with ~ 20-50 pfu of virus. The infection was allowed to proceed to until virus expressed fluorescent proteins were visible. For A5L-YFP VACV this was 6 h post-infection and for recombinant strains of MYXV the mCherry signal was visible at 18 h post-infection. At this point imaging was started and fluorescent and phase-contrast images of each plaque taken at 10 min intervals for either 18h (VACV) or 30 h (MYXV). Between four and seven plaques were imaged for each virus, and the plaque size for each virus calculated using Image J (v1.44i; National Institutes of Health).

To determine the maximal plaque growth rates, the change in plaque size over each measured interval of time (dX/dT) was calculated, plotted versus the time, and the

maximum amplitude calculated from a fit to a curve assumed to be log-Gaussian in shape. These experiments were performed in phenol-free MEM supplemented with 10mM HEPES pH 7.3 and in the presence of 10% FBS.

2.5.1.2 Use of Live Cell Microscopy to Examine Cell Motility:

To perform the cell migration assays, a P-200 micropipette tip was used to introduce a scratch into a monolayer of confluent BGMK cells. The cells were then infected at a MOI=5 and imaged at 5 minute intervals for 24 h in serum-free medium. The experiment was repeated on at least two separate occasions, with multiple fields of view imaged on each occasion.

2.5.2 Fixed Cell Immunofluorescent Microscopy:

2.5.2.1 General Protocol

For microscopy performed on fixed cells the cells were prepared as follows: circular coverslips (1.5 mm thickness) were sterilized by using 95 % ethanol and fire and placed in 24-well tissue culture dishes. Cells were added, and allowed to grow overnight, and then infected (or mock-infected). The experiments which used MDA-MB-231 cell used a MOI=10, all other cell lines were infected with a MOI=5. The inoculum was replaced with fresh medium after 1 h, and the infection allowed to proceed until the desired time.

In situations where imaging was done on cells that had been transfected with plasmid DNA, the cells were transfected with 150 ng of DNA using 1 µl of lipofectamine (in a total of 100 µl) at 2 h post-infection. These transfection reagents were performed in Opti-MEM (Gibco).

To fix cells, the medium was removed and replaced with 4% paraformaldehyde in PBS. The cells were incubated on ice for 20 min, and then the aldehyde radicals neutralized, and the cells permeabilized using 0.1M glycine in PBS with 0.1% tween-20 (PBS-T). The coverslips were then washed three times with PBS-T, blocked for 30 mins

with 3% BSA in PBS-T, and then incubated with primary antibody (diluted in blocking solution) for either 2 h at room-temperature or overnight at 4^{o}C. The unbound primary antibody was removed using three PBS-T washes, and then the cells incubated for 1 h with secondary antibody. Monoclonal mouse antibodies were usually detected using a Cy5-conjugated antibodies and polyclonal rabbit antibodies were detected using AlexaFluor 594-conjugated antibodies. The antibodies, and concentrations used, are listed in table 2.5. The cells were counterstained with 0.3 U/mL phalloidin (usually conjugated to AlexaFluor488) and 5ng/mL DAPI, to detect actin and DNA, respectively. Following six washes with PBS-T, the coverslips were mounted in Mowiol mounting medium (0.1mg/mL Mowiol, 0.1M PBS pH7.4, 25% glycerol, 2.4% triethylenediamine (DABCO)). The cells were then imaged using a Delta-vision microscope at either 20X (N.A. = 0.75), 60× (N.A. = 1.42), or 100× magnification (N.A. =1.40). In situations where Z-stack images were taken, the files were processed using a deconvolution algorithm and conservative ratio settings, and a single plane composite image was generated using software supplied with the microscope (SoftWorx v4.1.2).

In situations where only actin and DNA were imaged, the cells were fixed and processed as described above, except that the BSA blocking and antibody incubation steps were skipped.

2.5.2.2 Quantification of Actin Stress Fibers, Cell area and Actin projectiles:

The measurement of actin stress fibers, virus-induced actin projectiles, and cell areas was done using three separate experiments, where 50 cells were examined for each sample per experiment (i.e. n=150). The exception to this was when actin projectiles were quantified in primary rabbit corneal fibroblasts, where the experiment was performed twice (i.e. n=100).

These studies used the aforementioned Delta-vision microscope at either 60 × or 100 × magnification or a Zeiss Axioscope 2 microscope at 100 × magnification

(N.A.=0.75). To determine the cell area, the images were exported and the area of each cell determined using Image J. Data presented represents mean ± S.E.M.

2.6 Western Blot Analysis:

To analyze the expression of viral and cell proteins lysates were made using 60 and 150 mm dishes, respectively. Lysates were produced by removing the medium, and washing and scraping the cells into cold PBS-A. The cells were recovered by centrifugation at 1000 × G for 10 min, resuspended in the buffers described below, and lysed on ice for 30 min. When protein concentration was required, the cells were lysed in NP-40 buffer (150mM NaCl, 50mM Tris pH 8.0, 0.5% NP-40, 5 mM EDTA). In other situations, the cells were lysed in RIPA buffer (50mM Tris pH 8.0, 150 mM NaCl, 1% NP-40, 0.5% sodium deoxycholate, 0.1% SDS). The lysates were centrifuged for 30 min at 18 000×G and the supernatant transferred to a new tube.

Protein quantities were determined using a BioRad Bradford assay. Briefly, a sample of lysate was added to a solution of 1× Bradford colourmetric reagent, and incubated for 5-15 min at room temperature the absorbance was determined using a DU370 spectrophotometer (Beckman) at 595 nm, and the protein concentration calculated by a comparison with BSA samples of known concentration.

Prior to SDS-PAGE analysis, the lysates were mixed with ¼ volume of 4× SDS-PAGE loading buffer (0.4% SDS, 0.4% β-mercaptoethanol, 40% glycerol, 50mM Tris pH 6.8, 1mg/mL bromophenol), boiled for 5 min, and briefly centrifuged. After being separated the proteins were transferred to nitrocellulose membranes using 65 V for 2h or 25 V overnight in a buffer containing 192mM glycine, 25mM Tris pH 8.3 and 10% methanol and a BioRad Mini Trans Blot transfer apparatus.

The membranes were subsequently blocked for 30 min at room-temperature in Licor blocking buffer (diluted 1:1 with PBS), and then hybridized to the diluted primary antibodies for 2 h at room-temperature or overnight at 4^{o}C, also in Licor blocking buffer.

The primary antibody was then removed and the membranes washed three times with PBS-T before being incubated for 1-2 h at room temperature with IR-dye conjugated secondary antibodies in PBS-T. A list of antibodies, their sources, and the concentrations used are shown in table 2.5. The membranes were finally washed three times with PBS-T and twice with PBS, and the antigen-antibody complexes detected using a Licor Odyssey imager.

To perform quantitative western blotting Licor software was used to outline the bands and calculate the integrated intensity values. To normalize for any variances in sample loading the ratio of the desired protein to cellular β-actin was always calculated from the same membrane. When, possible, this was done by using two antibodies derived from different IR-fluorophores. When this was not possible, the protein to be quantified was probed first. The membrane was then stripped using commercially available stripping buffer (Licor), and re-probed for β-actin.

2.7 **SiRNA Silencing Experiments:**

All siRNA experiments were performed in MDA-MB-231 cells. The siRNAs were purchased from Qiagen, and were transfected into cells using Dharmafect 4 transfection reagent. The siRNAs used for these experiments were as follows. For RhoA gene silencing, hsRhoA-6 siRNA (SI02664211) and hsRhoA-7 (SI0264267) were used. The RhoC targeting siRNAs were hsRhoC-5 siRNA (SI02663906) and hsRhoC-6 (SI02663913). LIMK2 targeting siRNAs were hsLIMK2-7 siRNA (SI02665334) and hsLIMK2-8 (SI02758490). The siRNAs used to silence mDia1 were hsDIAPH1-1 siRNA (SI00073920), hsDIAPH1-2 siRNA (SI0073927), hsDIAPH1-3 siRNA (SI00073934), and hsDIAPH1-4 siRNA (SI00073941). Qiagen had experimentally verified siRNAs against RhoA, RhoC, LIMK2 but not against mDia1. Qiagen AllStars Negative Control siRNAs were used as a control and are reported to have no mammalian targets.

To analyze the degree of "knockdown", and determine optimal siRNA concentrations 24 well dishes were seeded with 2×10^5 cells per well and allowed to grow overnight. The siRNA containing mixtures were prepared as follows. For each reaction, 1 µl of Dharmafect transfection reagent was added to 49 µl of Opti-MEM. This mixture was incubated for 5 min at room temperature before being added to 50 µl of siRNA dissolved in Opti-MEM. The siRNA and transfection reagent mix was then incubated for 20 min at room temperature, before being added to the cells. Three hours later, 400 µl of MEM (without antibiotics and antimycotics), was added to each well. After 48 h the cells were lysed in 150 µl of RIPA buffer and processed as described in section 2.6. Two separate wells were pooled together and 40 µl of lysate electrophoresed on SDS-PAGE gels. All of the siRNAs produced high levels of knockdown at even the lowest concentrations tested (10 nM) and subsequent experiments used these concentrations. All siRNAs targeting mDia1 knocked down mDia1 proteins levels, but subsequent experiments used only hsDIAPH1-1 and hsDIAPH1-3 siRNAs.

For experiments that examined the effects of gene silencing on viral yields, 6 well (35 mm) dishes were used. The number of cells and the transfection reactions were scaled up 4-fold but otherwise performed as described above. After 48 h exposure to the siRNAs, the cells were infected at a MOI=0.1 and the infection allowed to proceed for another 48 h before virus was harvested and titered on BGMK cells. The change in yield was then determined relative to the cells transfected with All-Stars siRNA controls.

2.8 Drug Studies:

Latrunculin B and Y-27632 were purchased from Sigma. Latrunculin B was dissolved in DMSO and Y-27632 in H_2O. For experiments using these drugs, the cells were infected at MOI=10 for microscopy, or MOI=0.1 for yield experiments. The infection was allowed to proceed for either 4 h, for Y-27632, or 8 h for Latrunculin B, before the medium was replaced with fresh medium containing drug, or the appropriate

Table 2.5 Antibodies used in these studies

Primary antibodies					
Protein directed against	**Species of origin**	**Source**	**Catalog number**	**Western Blot dilution**	**Immunofluorescence dilution**
VACV A33	Mouse	B.Moss		1/1000	1/500
VACV A34	Rabbit	These studies	Appendix	1/10 000	1/1000 - 1/2000
VACV A36	Rabbit	M.Way			1/500
VACV A36	Rabbit	These studies	Appendix	1/5000	
VACV B5	Mouse	S. Isaacs		1/20000	1/10000
VACV F11	Rabbit	R. Condit		1/1000	
MYXV M-T4	Rabbit	M. Barry		1/5000	
GST	Mouse	Our Lab		1/1000	
β-actin	Mouse	Sigma	A5441	1/15000 - 1/20000	
RhoA	Mouse	Santa Cruz Biotechnology	sc-4180	1/500	
RhoC	Rabbit	Cell Signaling	D40E4	1/500	
mDia1	Goat	Santa Cruz Biotechnology	sc-10886	1/200	
LIMK2	Rabbit	Santa Cruz Biotechnology	sc-5577	1/200	
ROCK1	Mouse	Santa Cruz Biotechnology	sc-17794	1/200	
Ezrin	Mouse	Santa Cruz Biotechnology	sc-58758	1/500	
Cofilin	Rabbit	Santa Cruz Biotechnology	sc-33779	1/500	
mCherry	Rabbit	Clontech	632475	1/1000	
FLAG (M2)	Mouse	Sigma	F1804	1/1000	
FLAG (M2)	Rabbit	Sigma	F7425		1/500

Western blot secondary antibodies (used at 1/20 000 dilution)			
Species directed against	**Species of orign**	**Source**	**Catalog number**
α-Mouse IR800	Goat	Licor	926-32210
α-Mouse IR800	Donkey	Licor	926-32212
α-Goat IR680	Donkey	Licor	926-32224
α-Rabbit IR680	Goat	Licor	926-32221

Immunofluorescent secondary antibodies (used at 1/1000 dilution)			
Species directed against	**Species of origin**	**Source**	**Catalog number**
α-Mouse AF488	Goat	Molecular Probes (Invitrogen)	A21202
α-Mouse AF594	Goat	Molecular Probes (Invitrogen)	A11005
α-Mouse Cy5	Goat	Molecular Probes (Invitrogen)	A10524
α-Rabbit AF488	Goat	Molecular Probes (Invitrogen)	A11008
α-Rabbit AF594	Goat	Molecular Probes (Invitrogen)	A21207
α-Rabbit Cy5	Goat	Molecular Probes (Invitrogen)	A10523

solvent control. For microscopy, infections were allowed to proceed for a total of 20 h before the cells were fixed, processed and visualized as described in section 2.5.1**.** For virus yield experiments, the infection was allowed to proceed for a total of 48 h, before cells were harvested, lysed by freeze-thaw, and tittered on BGMK cells.

2.9 Animal studies:

2.9.1 Establishment of Xenograft Tumors in NIH-III mice:

Six-to-eight week old female NIH-III mice (Crl: NIH-*Lyst*$^{bg\text{-}J}$ *Foxni*^{nu} *Btk*^{xid})) were purchased from Charles River and allowed to acclimatize of 7-10 days before beginning the experiment. Mice were feed an alfalfa free diet (Teklad Global 14% Protein Rodent Maintenance diet (Harlan Laboratories)), as chlorophyll has been reported to fluoresce at wavelengths that may interfere with the *in vivo* imaging of fluorescent proteins. All animal work was approved by University of Alberta committees according to guidelines issued by the Canadian Council on Animal Care (http://www.ccac.ca/en).

Human mammary adenocarcinoma cells expressing firefly luciferase (MDA-MB-231-luc) were prepared for injection as follows. Large (150 mm) dishes of cells were grown as described in section 2.2.1. The cells were then trypsinized, pooled in 50 mL conical tubes, and centrifuged at ~ 200 × G for 7 min at 4^{o}C. The medium was removed, the cells washed with PBS and then resuspended in PBS A. The cells were counted (section 2.2.1) and diluted to 8×10^{7} cells/mL in PBS A. Mice were sedated with isofluorane, and immediately prior to injection the cells were mixed 1:1 with BD matrigel (BD Biosciences). A 27-gauge needle was then used to subcutaneously deliver 50 µl of the cell mixture (2×10^{6} cells) into a mammary fat pad. The mice were then returned to their cage and allowed to recover. The process for tumor establishment was the same regardless of whether one or two tumors were being established. In the single tumor model, tumors were established in one right mammary fat pad.

2.9.2. Virus Delivery and Animal Monitoring:

After the cells were injected, the mice were monitored daily until tumors became palpable, approximately 10-15 days after injection. At this point the mice were sedated and tumor length, width, and height measured by calipers. Tumor volume was calculated using the formula $1/24 \times \pi \times m_1 \times (m_2 + m_3)^2$, where m_1 was the longest dimension, m_2 the next, and m_3 the smallest. From these volumes, mice were sorted into cohorts, each having roughly equal mean tumor volumes.

One to two days later, treatment with virus began. For this, the mice were sedated; tumor dimensions measured, and then 50µl of live or UV-inactivated virus delivered intratumorally, using a 25-gauge needle. In mice bearing two tumors, the one located in the right mammary fat pad was injected, and the other one left untreated. Mice were then returned to their cage and allowed to recover.

For each experiment, three doses of virus were administered over a 5-7 day period. The dose of virus administered varied by experiment and ranged from 1×10^5 pfu to 5×10^7 pfu, which was the maximum amount of virus that could be produced in the allowable volumes.

During the injection period, and for two weeks after the last injection, mice were monitored twice daily. After this mice were monitored once daily through to the end of the experiment. Mice were weighed, and had their tumor(s) measured twice weekly. In experiments where mice had a single tumor the mice were followed through until tumor volume reached $1500mm^3$, after which mice were removed from the study and euthanized with CO_2 gas. These data were used to calculate survival curves.

In bilateral tumor models, mice were monitored for a period of six weeks following the first injection of virus. At this point the mice were imaged (described in section 2.9.3), euthanized, and the organs assayed for viral titers (described in section 2.9.4)

2.9.3 *In Vivo* Imaging of Mice:

An IVIS Spectrum small animal imager running Living Color version 4 software (Caliper Life Sciences) was used for *in vivo* imaging of mice. This imager can detect bioluminescent signals, as well as many different fluorescent proteins. For imaging, mice were anaesthetized using 5% isofluorane before being transferred to a heated stage, where they were kept unconscious using 1-2% isofluorane during the imaging period. When bioluminescent and fluorescent imaging was to be performed on the same animal, fluorescent imaging was performed first, and was followed by the injection of luciferin and bioluminescent imaging.

2.9.3.1 Bioluminescent Imaging of Mice:

The MDA-MB-231-luc cancer cells used to establish tumors express firefly luciferase under control of a SV-40 promoter. This allowed tumors to be visualized following intra-peritoneal (IP) injection of the potassium salt of D-luciferin (Caliper Life Sciences) at 150 mg/kg. Injections were performed using a 27 gauge needle while mice were anaesthetized on the imager stage. Imaging was started immediately and pictures taken at 1 min intervals for a total of 10 min. The bioluminescent signal is reported as radiant efficiency (photons/sec/cm^2/str). This represents a software standardized scale, and allows for the comparison of images across various time points. To quantify a luciferase signal, the tumor was outlined and the Living Color software was used to measure the total flux in units of photons/sec.

2.9.3.2 Fluorescent Imaging of Mice:

The IVIS Spectrum imager can image many different fluorescent markers. We tried multiple different markers (both fluorescent and small molecule) before deciding on using a virus-encoded mCherry fluorescent protein to track virus *in vivo*.

The fluorescent proteins were imaged using auto-exposure settings and the recommended filter sets. For imaging the fluorescent substrate DDAOG and its product

DDAO (see section 5.2.3), mice were first injected in the tail vein with 100µl of DDAOG (dissolved in 1:1 DMSO to PBS). DDAOG was purchased from Sigma.

The mCherry fluorescent protein was chosen for subsequent animal imaging and conditions providing the best signal to noise were determined (see section 5.2.4). To quantify mCherry signal the tumor was outlined and the total radiant efficiency (p/s)/ ($\mu W/cm^2$) measured at 570nm excitation and 680nm emission settings.

2.9.4 Detection of Virus in Tissues:

To measure virus titers in organs and tumors, a GentleMacs tissue disassociater was used. Following tumor removal, the tumors were stored frozen at -80^{O}C until assayed. At this point the tumors were thawed, cut into small pieces (~ 2mm in each dimension), and transferred to a pre-weighed GentleMacs C-type tube. The mass of the tumor was calculated and 4mL of buffer (10mM Tris pH 8.0, 5mM EDTA pH 8.0) added for every gram of tumor. Each tissue was then disrupted, and the virus released, by subjecting the tissue to a 45 sec "protein" cycle on the GentleMacs machine. Each tube was then centrifuged for 10 min at 1000 × G, and the supernatant assayed for virus (section 2.3.3). Organs were processed in a similar manner except that 3 mL of buffer was used for each organ. Virus levels were reported as pfu/g of tumor or pfu/organ.

2.10 Statistical Analysis:

Statistical analysis of data was performed using Graphpad Prism (v5.01). Analysis of variance (ANOVA) tests with either one-way post-Tukey column comparisons, or two-way Bonferroni post-tests, were used to compare data comprising multiple viruses or time points. For analysis comparing two groups of data a student T-test, either paired or unpaired depending on the situation, was used. Survival curve comparisons were calculated using the Log-Rank (Mantel-Cox) test built into Prism's software. $P < 0.05$ was considered significant and statistically significant results reported as: * $P<0.05$, ** $P<0.01$, and *** $P<0.001$.

CHAPTER 3: GENETICS UNDERLYING DIFFERENCES IN PLAQUE MORPHOLOGY BETWEEN MYXOMA AND VACCINIA VIRUSES

A version of the data presented in this chapter has been published:

Irwin C.R. and Evans D.H. (2012) Modulation of the myxoma virus plaque phenotype by vaccinia virus protein F11. Journal of Virology. **86:** 7167-7179

All of the experiments presented in this chapter were performed by myself, and the original manuscript was written by myself with editorial contributions from my supervisor, Dr. Evans.

3.1 INTRODUCTION:

Despite both being poxviruses it has been known since at least the 1950s that vaccinia and myxoma viruses display differences in their plaquing behaviours. VACV forms large primary lytic plaques, characterized by a central clearing of cells. As VACV infection proceeds, smaller secondary plaques are often observed in pattern known as a "comet tail." In contrast MYXV infection of cells in culture results in a clustering of cells in something known as a "focus", with secondary infections being observed in much rarer frequency than VACV. So why is it that one poxvirus (VACV) can form plaques while another (MYXV) forms foci? While one could envision a number of possible factors that could explain these differences, the work presented in this chapter focuses on comparing differences in factors known to be involved in efficient exit and formation of actin projectiles, both are properties that are involved in efficient VACV spread, but poorly characterized in MYXV.

3.2 RESULTS:

3.2.1 Differences in the plaquing, growth properties and frequency of actin projectile formation of vaccinia and myxoma viruses:

We began this work by re-examining and quantifying observational differences between MYXV and VACV. Wild type strains of MYXV (Lausanne) or VACV (WR or IHD-W) were plated on BGMK cells and fixed and stained with crystal violet at two, three or four days post-infection. In addition β-galactosidase expressing recombinant viruses were similarly plated, and fixed and stained with X-Gal at two days post-infection. By two days post-infection, primary VACV plaques were approximately 10 fold larger than MYXV foci. Further, a number of secondary VACV plaques were observable. **(Figure 3.1)** In comparison to the WR strain of VACV, a greater number of secondary plaques/comet tails is observed in the IHD-W strain **(Figure 3.1A)**. These differences have been attributed to a single amino acid difference in the A34R gene[179].

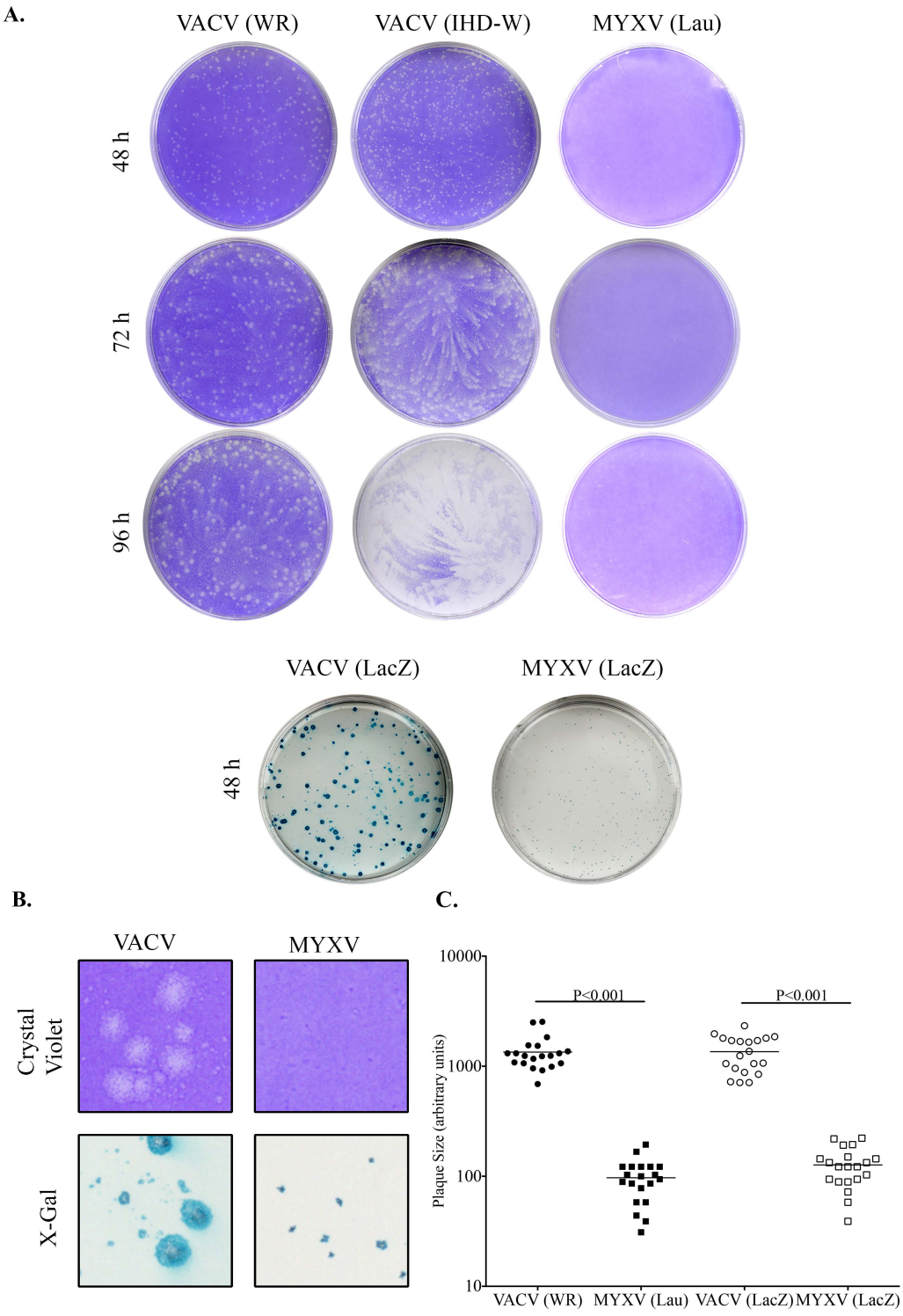

Figure 3.1: Comparison of plaquing properties of VACV and MYXV on BGMK cells: (A) 60mm dishes of BGMK cells were infected with ~200 pfu of the indicated virus and fixed and stained at various times with either crystal violet or a X-Gal containing stain. **(B)** 5X magnification of plaques at 48 h from (A) **(C)** Quantification of relative areas of plaque size of 20 randomly selected plaques at 48 h from (A)

The MYXV-LacZ virus has β-galactosidase inserted in an intergenic region between M011L and M012L, and has been shown to behave identically to its parental Lausane strain[305]. This, combined with observations that MYXV-LacZ formed foci of equal size as its parental strain, and that the presence of β-galactosidase made virus detection much easier, especially at early times, lead us to use MYXV-LacZ as our "wild-type" strain for all future experiments.

We also compared the growth properties of MXYV and VACV in BGMK cells using high MOI single-step growth and low MOI multi-step growth curves (**Figure 3.2).** Despite having similar growth kinetics at early time points VACV grew to higher titers than MYXV, reaching titers of 10-100 × higher levels by 24 to 48 h post-infection.

Efficient VACV spread has been attributed to a number of factors, including the formation of multiple forms of infectious virions, and the manipulation of the actin cytoskeleton. While MVs are released primarily following cell lysis, EV can be released prior to cell-lysis by fusion of its outer membrane with the cellular plasma membrane. Extracellular but still cell-associated EV, can undergo one of two fates. They can disassociate and proceed to infect another cell. Alternatively, EV can initiate a signalling cascade, which results in the rearrangement of actin underneath of the EV. These rearrangements, known as actin projectiles, push EV away from the infected cells. Actin projectiles have also been shown to prevent EV from re-infecting an already infected cell[89]. Collectively, these processes have been shown to contribute to VACVs rapid spread, and formation of secondary plaques/comet tails.

No direct comparison of the various forms of virions produced by MYXV and VACV has been performed. However, a number of groups have reported that, like VACV, MYXV is capable of forming these different forms of enveloped virions. MYXV has also been shown to form actin projectiles[219,239]. Given the importance that

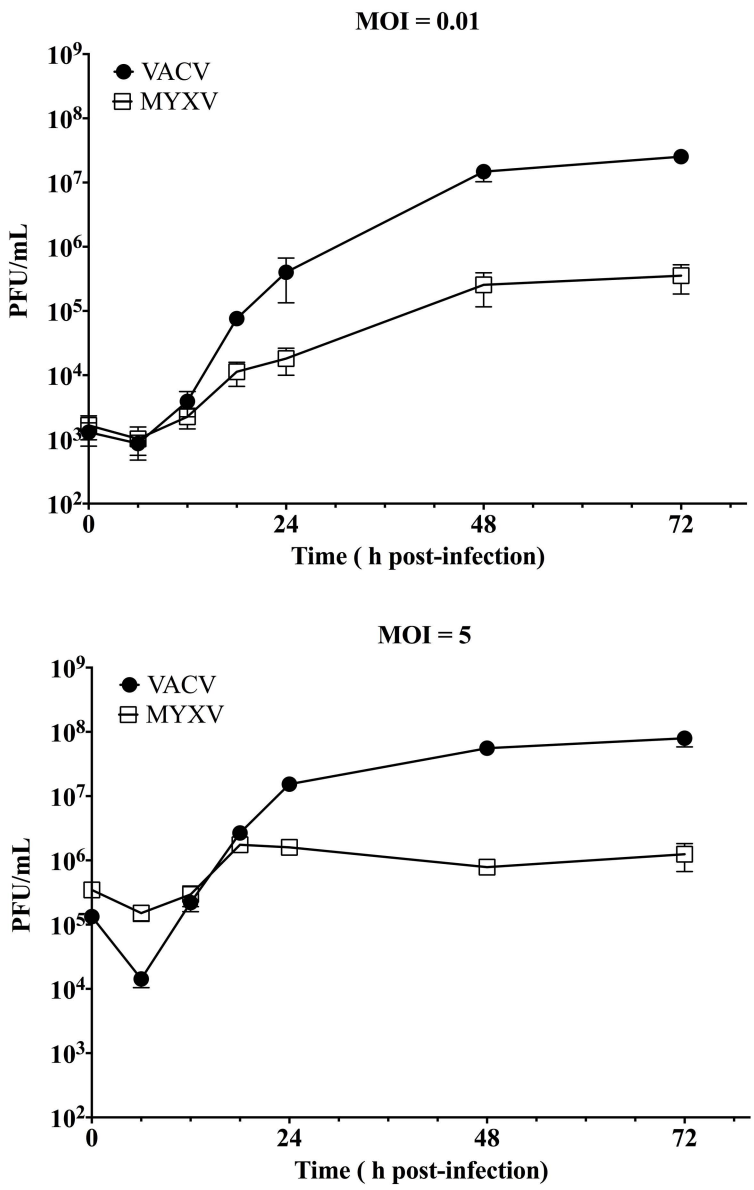

Figure 3.2: Comparison of the growth of MYXV and VACV at low and high MOI conditions 60 mm dishes of BGMK cells were infected with either VACV or MYXV at either **(A)** MOI = 0.01 or (B) MOI = 5. Virus was harvested at indicated times and titered on BGMK cells. The mean ± S.E.M. from three independent experiments are shown.

actin projectiles have in rapid spread of VACV, we sought to determine if the differences in MYXV and VACV spread could be attributed to differences in actin projectiles.

For this we infected coverslips of BGMK cells with either MYXV or VACV, fixed them at 20 h post-infection, stained them for actin using AlexaFluor488 conjugated phalloidin, and DNA using DAPI, and then visualized the cells by fluorescent microscopy. Two striking differences between MYXV- and VACV-infected cells were noted. The first was that VACV-infected cells are smaller and more "rounded-up" than MYXV-infected cells. The second difference was that actin projectiles were much more abundant in VACV-infected cells **(Figure 3.3A).** These projectiles were quantified and it was found that VACV infected cells had 2.0 ± 0.3 actin projectiles per cell *versus* 0.2± 0.1 per MYXV infected cell ($P<0.001$). It is possible that these differences may have been a result of VACV being able to more efficiently engage monkey cell actin machinery than the rabbit-specific MYXV. To test this, we repeated these experiments in two rabbit cells lines, RK13 and SIRC, which are also highly permissive for both viruses. In both these cells VACV-infected cells displayed significantly more actin projectiles than MYXV-infected cells (**Figure 3.3B and C)**. The most abundant actin projectiles were observed in RK13 cells. In these cells VACV induced 7.2±0.5 actin projectiles per cell *versus* 0.5 ± 0.1 for MYXV infected cells, $P<0.001$).

These observations suggested that the differences between the plaquing behaviour of MYXV and VACV were not the result of growing these two viruses, which have different tropisms, on non-optimal cells, but rather due to MYXV defects in the EV/actin projectile formation pathway.

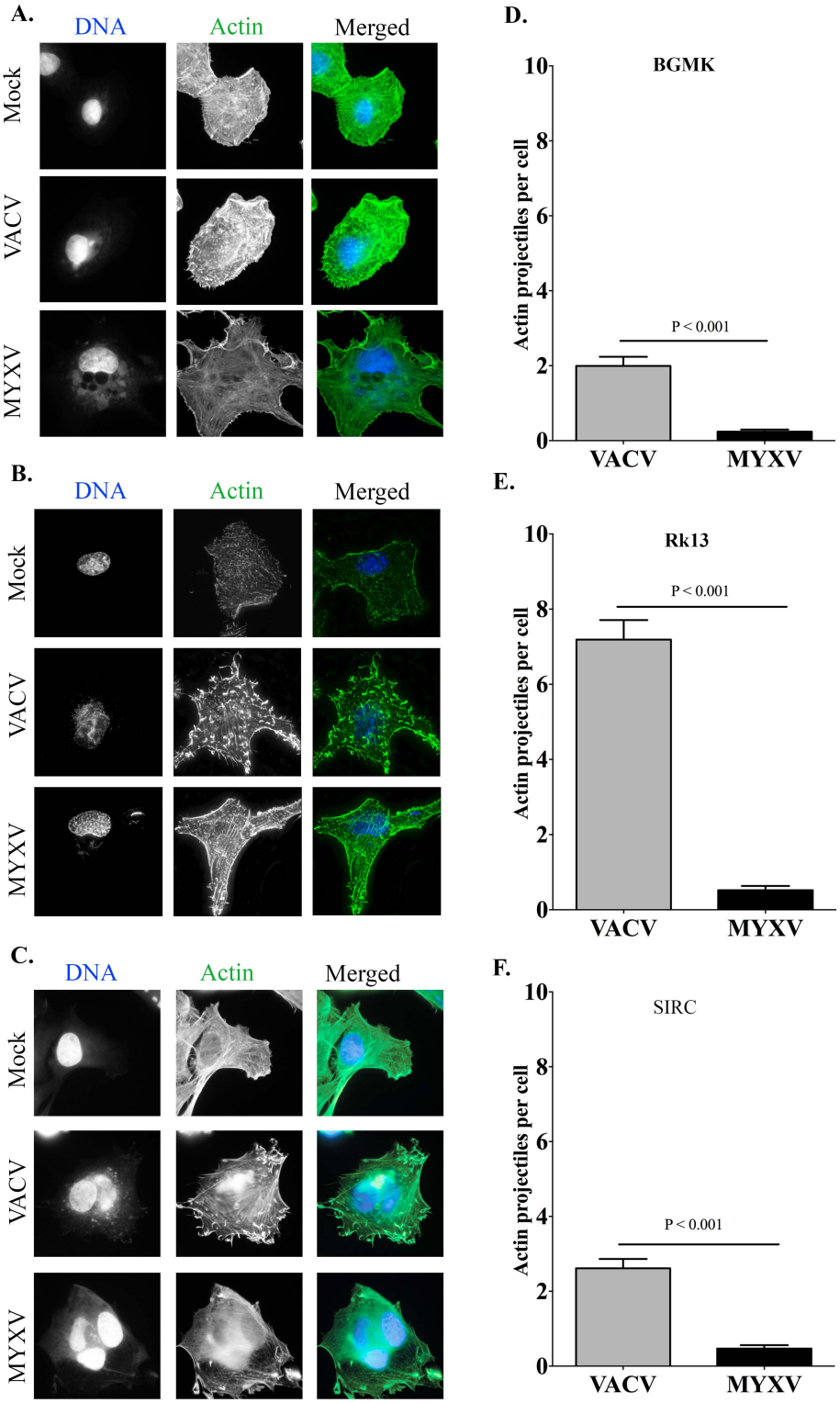

Figure 3.3: Quantification of actin projectiles formed by VACV and MYXV: BGMK (A), RK13(B) or SIRC (C) cells were infected with VACV or MYXV (or mock infected), after 20 h cells were fixed and stained for actin or DNA using AlexaFluor488-phalloidin and DAPI. Cells were then visualized at 100 X magnification using a Delta-vision microscope. Panels A-C show representative images. Panels D-F shows the mean actin projectiles formed per cell plus S.E.M., as determined from 100 cells for each virus.

3.2.2 Genome Comparisons of MYXV and VACV:

The formation/release of EV, combined with the production of actin projectiles, plays a key role in spreading VACV. To date nine genes have been implicated in these processes (A27L, A33R, A34R, A36R, B5R, E2L, F11L, F12L and F13L) (See section 1.9). Interestingly, none of these genes are essential for VACV viability, but when mutated result in smaller plaques, decreases in viral yields, and often a reduction in the number of actin projectiles. In other words, mutations in these genes confer a more "MYXV-like" phenotype upon VACV.

Thus, we decided to analyze the genome of MYXV for homologs of the aforementioned VACV genes implicated in these processes. In addition, we also searched for MYXV homologs to VACV genes involved in virion binding to the cell surface, and entry. The results of these searches are presented in **Table 3.1**. BlastP searches revealed likely homologs of the majority of proteins involved in these processes. An exception in genes involved in virion binding is the absence of a homolog to the acid-sensitive suppressor fusion protein(s) A25/A26, which could potentially explain differences in MYXV/VACV binding and entry[235,276].

Concerning genes involved in WV formation/exit and the production of actin projectiles, MYXV homologs of VACV A27L, A33R, A34R, E2L, F12L, and F13L are found. These are M115L, M121R, M122R, M028L, M021L and M022L, respectively. Furthermore, many of these genes are located in positions syntenic to their VACV counterparts. Homologs of A36R and B5R are less easily identified, as discussed below. In addition, we could not find any evidence of a MYXV homolog of VACV F11L (discussed more in section 3.2.4).

BLASTP searches do not uniquely identify a MYXV homolog to A36R, with both M123R and M125R showing low levels of similarity. However, M125R has been shown to be a functional ortholog to A36R as it complements actin projectile formation

in an A36R-deficient VACV strain[219]. The role of M125R in the context of a MYXV infection will be discussed in further detail in Chapter 4.

Whether MYXV encodes a homolog to B5R is less clear. M144R shows 42% similarity to B5R and is located in a syntenic position. This suggests that these genes are likely homologous. However, M144R also resembles the VACV complement control protein encoded by C3L. This is further confounded by the fact that B5R and C3L have

Table 3.1: VACV genes implicated in controlling virus spread and their MYXV homologs

Genes implicated in virion binding to the cell surface			Entry/fusion complex genes			Genes implicated in EV formation and spread		
VACV	**MYXV**	**Amino acid percent similarity[#]**	**VACV**	**MYXV**	**Amino acid percent similarity**	**VACV**	**MYXV**	**Amino acid percent similarity**
A25L YP 233027.1	ND[†]	N/A	**A16L** YP 233018.1	**M106L** NP 051820.1	65	**A27L** YP 233032.1	**M115L** NP 051829.1	64
A26L YP 233030.1	ND	N/A	**A21L** YP 233022.1	**M110L** NP 051824.1	77	**A33R** YP 233038.1	**M121R** NP 051835.1	57
A27L YP 233032.1	**M115L** NP 051829.1	64[††]	**A28L** YP 233033.1	**M116L** NP 051751.1	68	**A34R** YP 233039.1	**M122R** NP 051836.1	67
D8L YP 232995.1	**M083L** NP_051797.1	50	**F9L** YP 232930.1	**M019L** NP 051733.1	70	**A36R** YP 233041.1	**M125R** NP 051839.1	<25%
H3L YP 232983.1	**M071L** NP 051785.1	62	**G3L** YP 232961.1	**M046L** NP 051760.1	69	**B5R** YP 233069.1	**M144R** NP 051858.1	42
			G9R YP 232969.1	**M054R** NP 051768.1	64	**E2L** YP 232940.1	**M028L** NP 051742.1	62
			H2R YP 232982.1	**M070R** NP 051784.1	81	**F11L** YP 232932.1	ND	N/A
			I2L YP 232953.1	**M039L** NP 051753.1	67	**F12L** YP 232933.1	**M021L** NP 051735.1	57
			J5L YP 232979.1	**M067L** NP 051781.1	79	**F13L** YP 232932.1	**M022L** NP 051736.1	72
			L1R YP 232970.1	**M055R** NP 051769.1	87			
			L5R YP 232974.1	**M059R** NP 051773.1	69			
			O3L YP 910498.1	**M037L** NP 051751.1	81			

*** bold denotes gene, NCBI reference sequence is listed below**
[#] determined by NCBI BLAST P analysis (http://blast.ncbi.nlm.nih.gov/Blast.cgi)
[†]ND = Homologous gene not detected
[††]Based upon an alignment of the C-terminus of these proteins, M115L contains a 78 amino acid residues N-terminal extension when compared to A27L

homology to one another. However, while C3 is secreted, B5 is a type I membrane protein, with a trans-membrane domain near its carboxy-terminus. We compared the secretion and hydrophobicity profiles of M144 with B5 and C3 using Expasy SecretromeP (http://www.expasy.org/proteomics/post-translational_modification) and ProtScale (http://www.expasy.org/ProtScale) programs. M144 lacks a secretion signal sequence and hydrophobicity analysis of these proteins shows M144 has a hydrophobicity profile more similar to B5 than to C3 (**Figure 3.4).** This suggested to us that M144 is likely a B5 homolog. It should be noted that subsequent to our initial comparisons of these genomes, an extensive analysis of *Chordopoxvirinae* viruses for B5 homologs also identified M144 as being distantly related to VACV B5[309]. This work also suggested that C3 may have emerged from B5 duplication.

3.2.3 The Effect of MYXV Expression of VACV A33R, A34R, A36R, and/or B5R on MYXV Growth Properties:

The absence of clear homologs of VACV A36R and B5R, combined with the observations that point mutations or truncations of A33R[168,197], B5R [168,197], A34R[179], or A36R[182] can alter VACV EV release and actin projectile formation, lead us to ponder whether the MYXV "defect" in actin projectile formation and spread is a result of a deficiency in one of these genes. Further, could this "defect" be complemented by expressing one or more of these VACV genes?

To address this question, we created a series of recombinant MYXV strains which expressed one or more of these VACV genes. We decided to insert these VACV genes into the M127L gene, which encodes a photolyase. We chose this location because our laboratory has previously shown that this gene is non-essential, and that mutating M127L had no effect on virus growth [306]. A series of plasmids were constructed that had the gene(s) of interest (under control of their native promoter), along with a selectable *EcoGPT* marker, cloned inside 2x200 bp of DNA sequence that matched the 5' and 3'

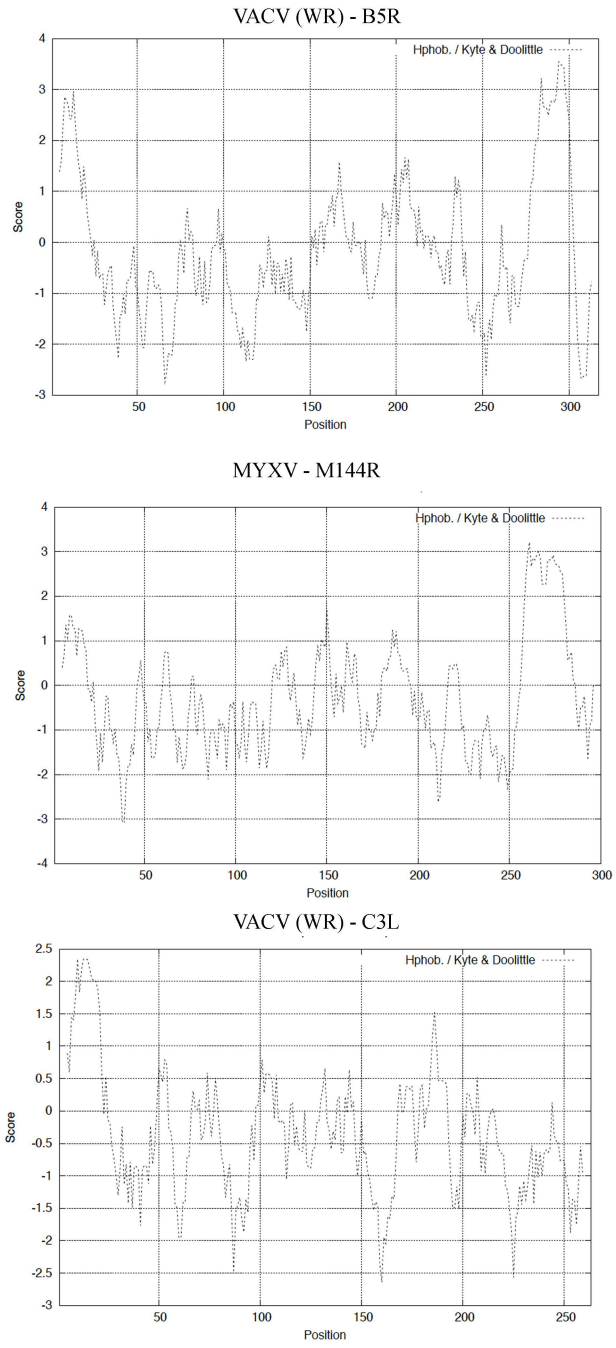

Figure 3.4: Comparison of the hydrophobicity profiles of M144R with B5R and C3L: Both VACV B5 and C3 proteins have short complement control regions at the amino-terminus. However, while C3 is secreted B5 contains a carboxy teriminal transmembrane domain. Given that M144 showed sequence homology to both C3 and B5 we compared the hydrophobicity profiles of these three proteins. For this, amino acid sequences were analyzed for hydrophobicity using a Kyte & Doolittle ProtoScale algorithim, available from EXPASY(http://web.expasy.org/protscale/). Similar to B5, M144 showed an increase in hydrophobicity near the C-terminus of the protein, which suggests the the presence of a transmembrane domain.

ends of the M127L gene. The methodology for the construction of these plasmids is discussed in **section 2.1**. These plasmids were then transfected into the β-galactosidase-expressing MYXV and recombinant viruses, which express A33R, A34R, A36R, B5R, A33R + A34R, and A36R + B5R were isolated. We also generated a virus (ΔM127L) which had only a disrupted photolyase gene to serve as a control in these experiments. A schematic description of these viruses is shown in **Figure 3.5.**

We anticipated that these proteins should be expressed to similar levels when expressed in MYXV, as in VACV. Although A33, A36 and B5 are also expressed early in infection, all of these VACV genes are expressed late in infection, and as such we analyzed their expression at late times in infection (24 h post-infection). Western blot analysis revealed that these proteins were indeed expressed from recombinant MYXV, and while similar levels of proteins appeared to be expressed some differences in the migration of A33 and A34 were observed (**Figure 3.5c).** We then went on to test if these VACV genes could modify the growth properties of MYXV.

The first parameter tested concerned whether one or more of these VACV genes altered the appearance of MYXV foci. BGMK cells were infected with ~ 100-200 pfu of MYXV. After 96 h, the cells were fixed and stained overnight with X-Gal. No visible alterations in the plaquing properties of these viruses were observed. I also used Image J software to determine the relative areas of 20 randomly-selected foci from each group, and these measurements supported these initial observations (**Figure 3.6).**

These viruses were also analyzed for any differences in growth properties using a multi-step low MOI (0.01) growth curve on BGMK cells. All of these viruses grow to levels similar to those of WT and the ΔM127L control viruses (**Figure 3.7).** We also sought to examine whether the presence of these VACV genes had any noticeable effect on the cellular morphology of MYXV-infected cells. For this, RK13 cells were infected at a MOI of 5 with the different viruses and the infection allowed to proceed for 20h

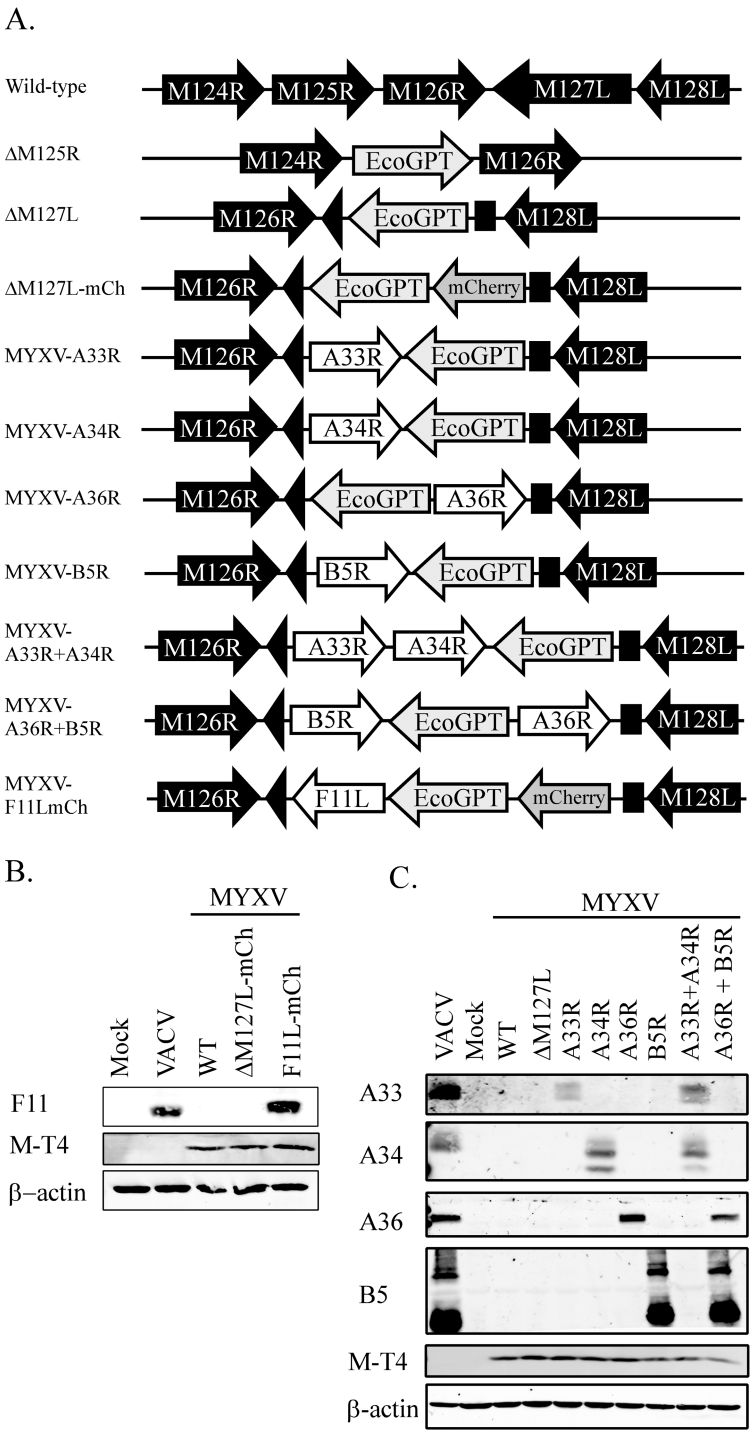

Figure 3.5: Recombinant viruses generated in this study. (A) A series of recombinant MYXV strains were constructed encoding the indicated VACV genes under the regulation of their native promoters and inserted in the MYXV photolyase gene (M127L). Recombinants were selected using mycophenolic acid resistance and/or mCherry fluorescence. A virus deficient in M125R was generated through a similar method. **(B)** Western blot analysis of F11 expression. F11 is an early gene, so BGMK cells were infected for 6 hr with the indicated viruses, harvested, and western blotted for VACV F11. **(C)** Western blot analysis of proteins produced late in infection. Cells were harvested 24 hr post-infection and blotted with antibodies directed against A33, A34, A36 or B5. MYXV M-T4, and cellular β-actin were used as loading controls in panels B and C.

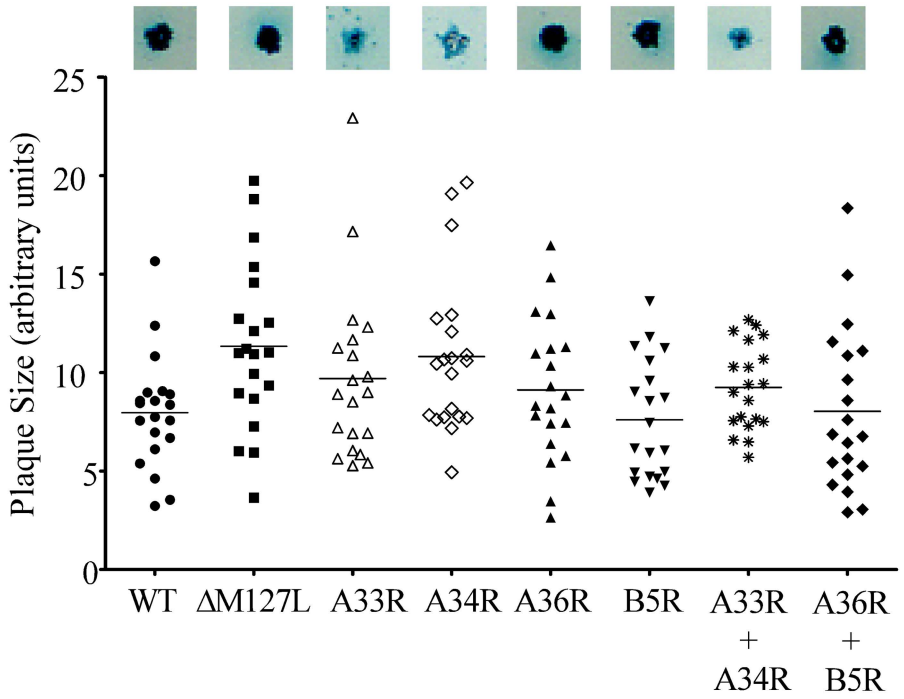

Figure 3.6: Effect of VACV A33R, A34R, A36R and/or B5R expression on plaquing properties of MYXV. BGMK cells were infected for 96 hr with the indicated viruses and the plaques stained with X-gal and then imaged. The median area of each group (20 plaques per group) is marked with a line, no statistical differences between any groups were seen. A representative plaque for each group is shown.

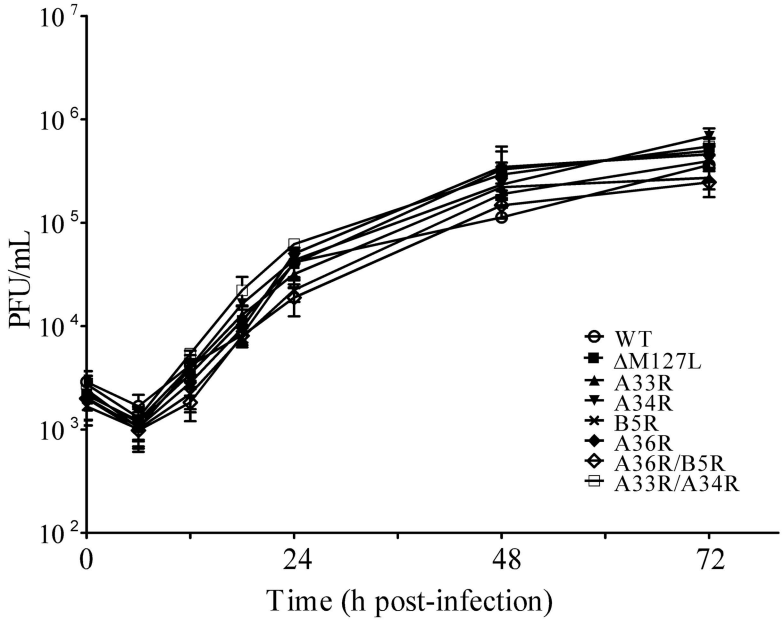

Figure 3.7: Effect of VACV A33R, A34R, A36R and/or B5R on growth of MYXV: 60mm dishes of BGMK cells were infected at a MOI of 0.01 and harvested at the indicated times. The figure shows mean titers plus S.E.M. from three independent experiments

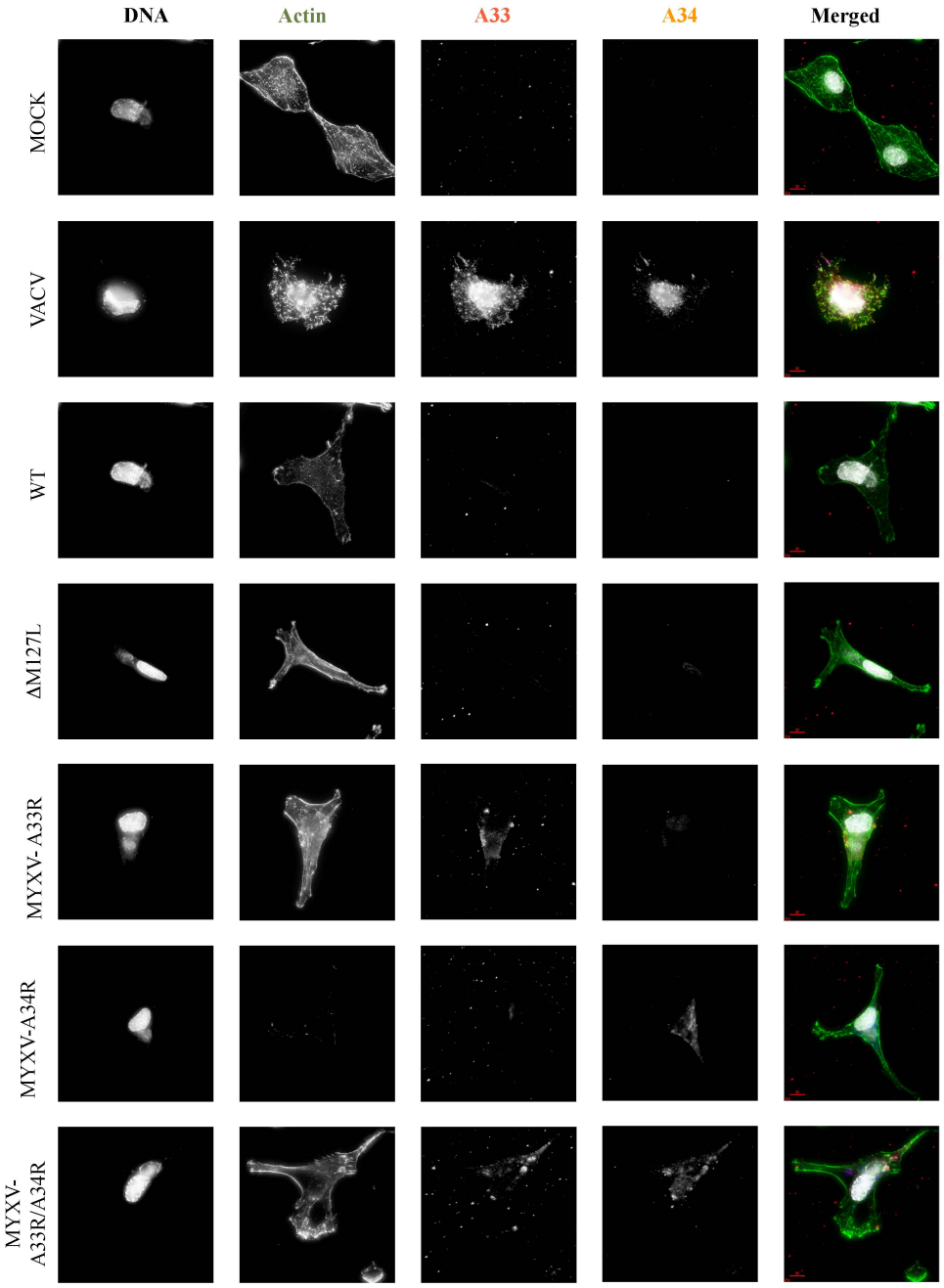

Figure 3.8: Expression of VACV A33R and/or A34R in MYXV-infected cells does not alter actin projectile formation. RK13 cells were infected with the indicated viruses at M.O.I.= 5, cultured for 20hr, fixed and then stained for DNA (DAPI) and actin (Alexa-fluor 488 phalloidin), and for the protein of interest using the indicated antibody plus Alexa-fluor 594 or Cy5-conjugated secondary antibodies. Cells were visualized at 60 X magnification.

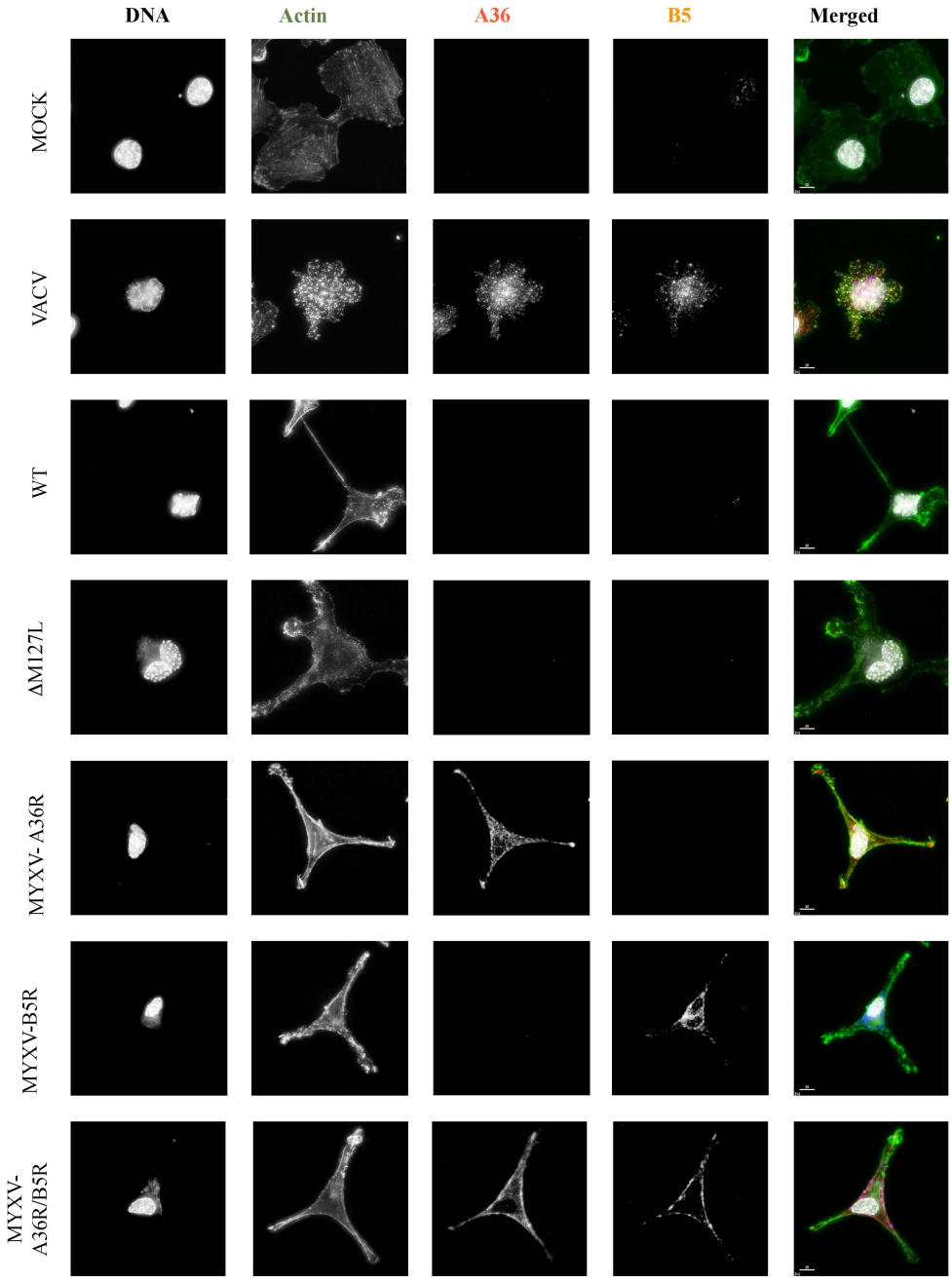

Figure 3.9: Expression of VACV A36R and/or B5R in MYXV-infected cells does not alter actin projectile formation. RK13 cells were infected with the indicated viruses at M.O.I.= 5, cultured for 20hr, fixed and then stained for DNA (DAPI) and actin (Alexa-fluor 488 phalloidin), and for the protein of interest using the indicated antibody plus Alexa-fluor 594 or Cy5-conjugated secondary antibodies. Cells were visualized at 60 X magnification.

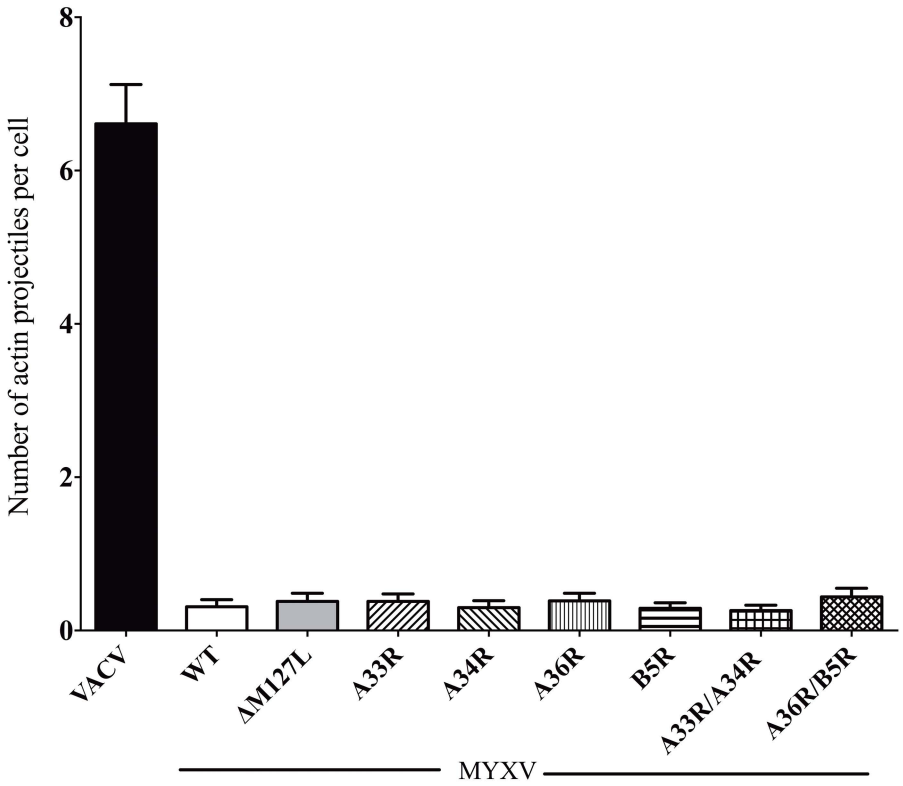

Figure 3.10: Quantification of actin projectiles produced by recombinant MYXV expressing VACV A33R, A34R, A36R, and/or B5R. Rk13 cells were infected with respective viruses at a MOI of 5 and fixed at 20 h post-infection, and stained for actin using phalloidin. A total of 100 cells (50 from 2 independent experiments) were imaged and a quantified from actin projectiles. The data presented represents the mean number of actin projectiles per cell plus S.E.M .

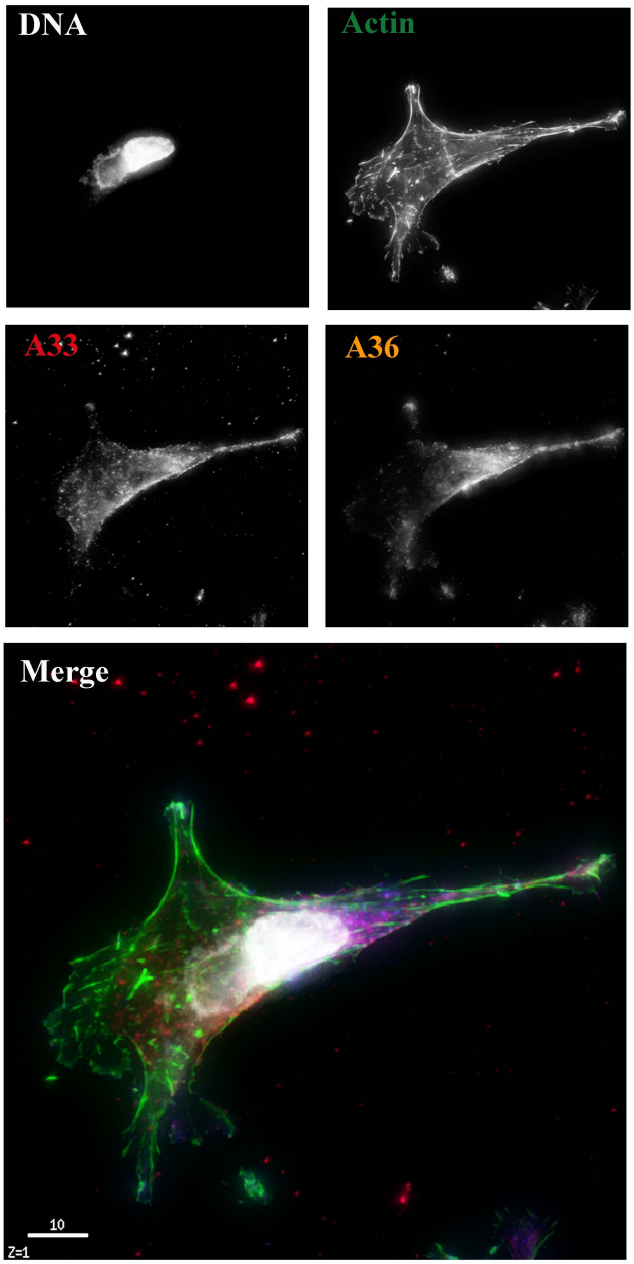

Figure 3.11: Expression of VACV A33R, A34R, A36R and B5R does not alter actin projectile formation in MYXV-infected cells. RK13 cells were co-infected with the MYXV-A33R+A34R and MYXV-A36R+B5R viruses at M.O.I.= 5, cultured for 20hr, fixed and then stained for DNA (DAPI) and actin (Alexa-fluor 488 phalloidin), and for the protein of interest using the indicated antibody plus Alexa-fluor 594 or Cy5-conjugated secondary antibodies. Antibodies directed against A33 and A36 were used to detect cells infected with both recombinant viruses. Cells were visualized at 60 X magnification.

before the cells were fixed, processed and immunostained for different proteins. Cells were then counterstained for actin and DNA using AlexaFluor488-conjugated phalloidin and DAPI, respectively, and imaged at 60 × magnification using a fluorescent microscope. Since A33- and A34-specific antibodies were derived from mouse and rabbit, respectively, cells were co-labeled for these proteins (**Figure 3.8).** The same was true for A36 and B5 (**Figure 3.9).** No noticeable change in the frequency of actin projectile formation was observed with these viruses, and this was supported by the quantification of actin projectiles from a population of cells infected with these viruses **(Figure 3.10).** Even in situations where all four VACV genes were expressed in the same MYXV-infected cell no change in the number of actin projectiles was observed (**Figure 3.11).** This was accomplished by co-infecting cells with the A33R/A34R and A36R/B5R MYXV viruses. Co-infected cells were identified by co-immunolabelling cells using the A33 and A36 antibodies.

Together, these data suggested that the differences observed between the plaquing properties of MYXV and VACV were not due to a "defect" in one of these MYXV homologs/orthologs, at least such a "defect" could not be complemented through the expression of one or more of these VACV genes.

3.2.4 The Effect of VACV F11L on MYXV Plaquing Properties:

We could not find any evidence that MYXV encodes a homolog to VACV F11L. Mutations in F11L have been shown to decrease actin projectile formation and VACV plaque size (i.e. creates a more "MYXV-like" phenotype)[205,223]. Where VACV encodes F10L, F11L, and F12L, in the syntenic location in MYXV one sees M020L (the F10L homolog, 82% similarity) followed immediately by M021L (the F12L homolog, 57% similarity).

We therefore examined what effect F11L has on MYXV. Initially, a recombinant strain was created using a similar strategy to those used for the A33R, A34R, A36R and

B5R viruses. We also created a strain of MYXV that expressed the mCherry fluorescent protein, under the control of a synthetic early/late hybrid poxvirus promoter. Experiments with this mCherry^{+} virus (F11L-mCh), along with a new control virus (ΔM127L-mCh) are presented here. F11 is an early gene, and the expression of F11 was tested at 6 h post-infection. Similar expression levels to that observed in VACV-infected cells were observed (**Figure 3.5B**). Some initial experiments were performed with the non-mCherry F11L^{+} virus and are presented in Appendix A.

Introducing F11L into MYXV caused a number of changes in the MYXV phenotype. The recombinant virus was created on BGMK cells, and it was obvious, even during the final stages of purification, that this virus formed larger foci **(Figure 3.12A)**. Measurement of F11L-mCh foci, showed that on BGMK cells they were about two-fold larger than those of the wild-type or control viruses (**Figure 3.12B).** While this increase in foci size was significant on BGMK cells, the differences were much more striking on SIRC and RK13 cells **(Figure 3.12A).** In both cases, F11L increased the foci size by approximately four-fold **(Figure 3.12C and D)**. Interestingly, we also observed a more VACV-like lytic plaque and the presence of secondary plaques. This was especially noticeable on SIRC cells.

To gain further insight into the kinetics of plaque formation we used live-cell microscopy to measure the rate of plaque expansion. For this, 35 mm glass bottom dishes containing confluent BGMK cells were infected with ~ 20-50 pfu of each virus. We used the virus encoded fluorescent proteins to track infected cells and therefore, in lieu of wildtype VACV, a version of the virus that expressed an A5L-YFP fusion protein was used [304]. For these experiments, infection was allowed to proceed until the fluorescent protein was visible, after which imaging was started. For VACV, imaging was started at 6 h post-infection and phase contrast (DIC) and YFP images taken at 10 min intervals for 18 h (until 24 h post-infection). Imaging ended with VACV strains at this time as the

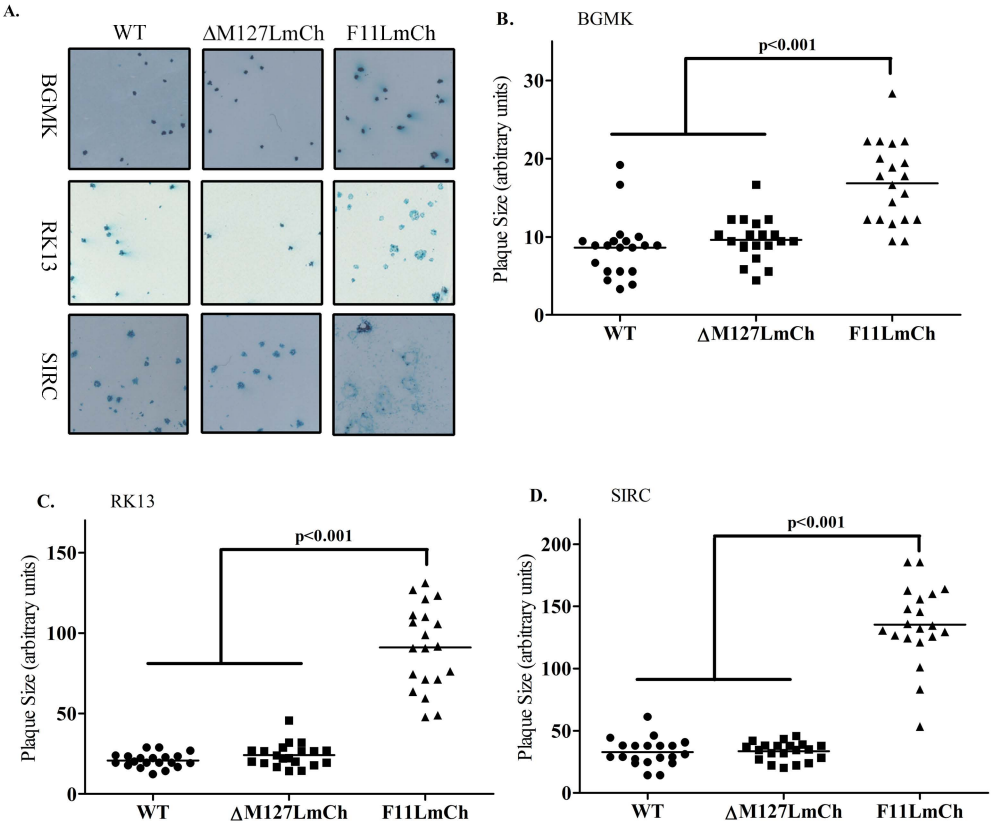

Figure 3.12: Effect of the VACV F11L gene on MYXV plaque size. (A) Plating properties. Viruses were cultured for 96 hr on BGMK, RK13, or SIRC cells and the plaques stained using X-gal. **(B, C and D)** Relative plaque area of viruses grown on BGMK **(B)**, RK13 **(C)** or SIRC **(D)** cells. Plaques were imaged and the areas determined using ImageJ. Each horizontal line on the scatter plot shows the median area of 20 randomly chosen plaques.

plaques expanded outside of the field of view. For the MYXV strains, imaging was started at 18 h and allowed to proceed for 30 h (phase contrast and mCherry images were also taken at 10 min intervals). For each virus, multiple plaques/foci were imaged, and from at least two separate plates, with n=5, n=7, and n=4 for A5L-YFP VACV, ΔM127L-mCh and F11L-mCh, respectively. Similar to what we observed in fixed cells we were able to observe some clearing of cells in the center of the plaques formed by F11L-mCh MYXV. **Figure 3.13** shows representative images of the plaques formed by each virus.

Fluorescent images were exported at 2 h intervals, and the area of these plaques calculated using Image J. These data were plotted and used to calculate the relative growth rates of plaques. F11L increased the growth rates of MYXV by approximately six-fold when compared to that of the ΔM127L-mCh control (5.8 ± 0.8 *versus* 1.0 ± 0.2 relative units). VACV plaques still spread 6-7 times faster than the F11LmCh virus, and about 40-fold faster (38.9 ± 6.8) than the ΔM127L-mCh control.

3.2.5 Effect of F11L on MYXV Growth:

We next tested if F11L had any effect on MYXV growth. For this we used a multi-step low MOI (MOI=0.01) growth curve analysis. In BGMK, RK13, and SIRC cells we saw that F11 caused a modest increase on MYXV growth (~5 fold). VACV still grew to ~10 fold higher levels than F11LmCh **(Figure 3.14B-D).** While F11 increased MYXV levels at low MOI situations, in single-step high MOI growth curves (MOI=5), all MYXV viruses grew to similar levels, regardless of whether F11L was present **(Figure 3.14A)**.

VACV F11 binds to and inhibits RhoA-mDia signalling pathways. This inhibition disrupts the actin cytoskeleton, and promotes microtubule dynamics [143,204,205]. This is thought to help WV reach the cell periphery, where the outer membrane can fuse with the plasma membrane and release the virus to the cell exterior, which in turn promotes virus release **(See section 1.9).** Given that F11L mutants release less virus into

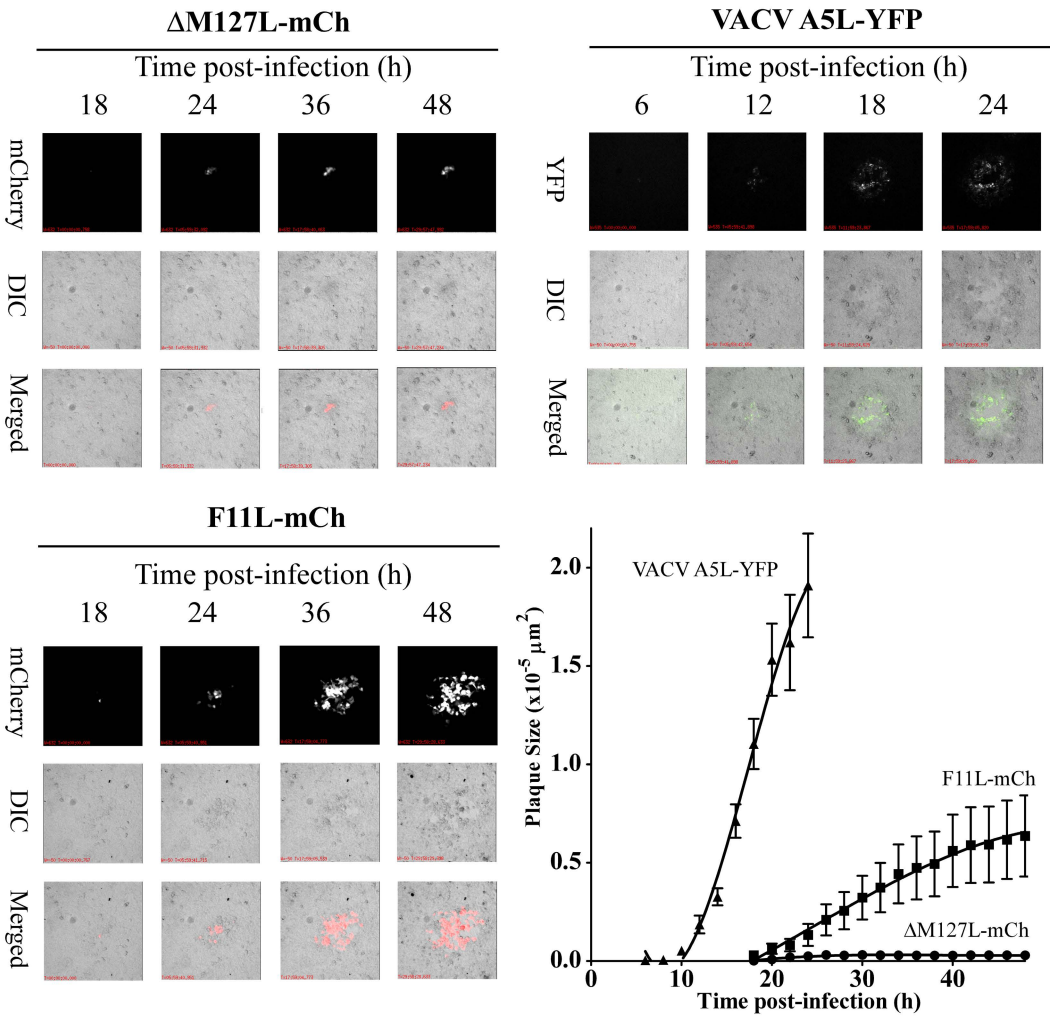

Figure 3.13: Effect of VACV F11L on MYXV plaque formation kinetics. BGMK cells were infected with the indicated viruses and the infection then allowed to progress until fluorescence became visible. This was 6 h post-infection for VACV and 18 h post-infection for the two MYXV strains. Live cell microscopic imaging was then initiated with fluorescent and differential interference contrast (DIC) images being recorded every 10 min over the next 18 or 30 h for VACV or MYXV, respectively. These were then merged to form time-lapse movies. The bottom right panel illustrates the different rates of plaque growth measured using 4-7 randomly selected plaques per virus. Time lapse videos of this data are available as supplemental vidoes S1-S3 in J Virol. 2012 Jul;86(13):7167-79. doi: 10.1128/JVI.06936-11.

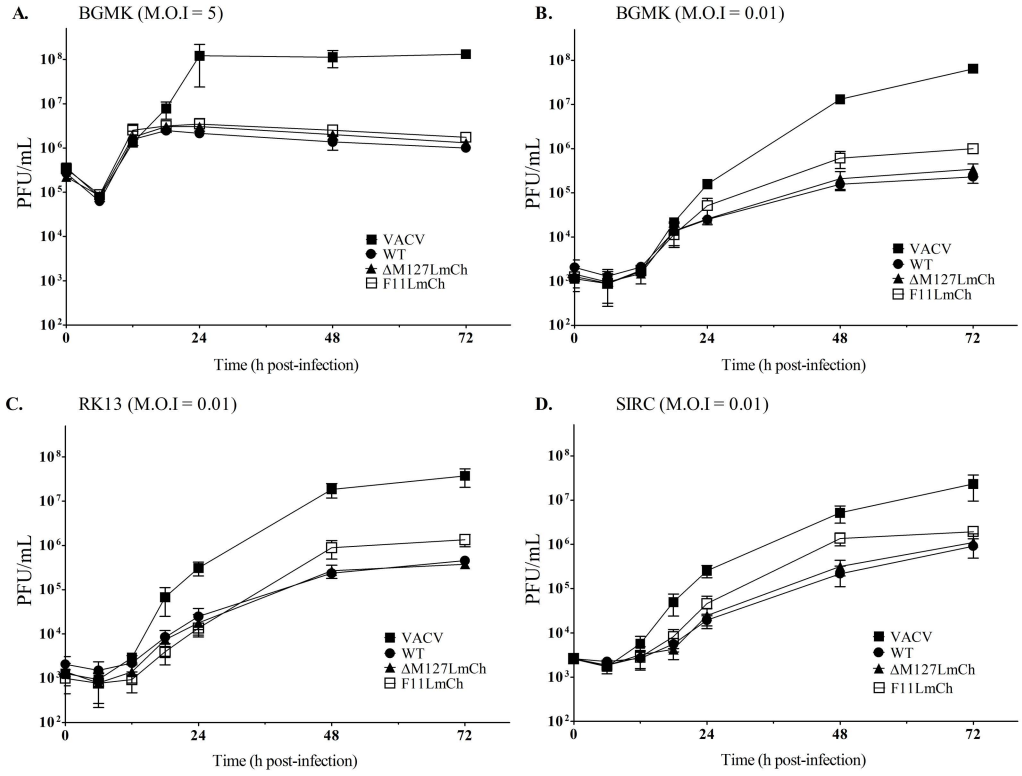

Figure 3.14: Effect of the VACV F11L gene on MYXV growth properties. (A) Single-step growth curve. BGMK cells were infected at MOI = 5 and then harvested at indicated times and titered. **(B, C and D)** Multi-step growth curves. BGMK **(B)**, RK13 cells **(C)** or SIRC cells **(D)**. Virus growth was measured as in A except that cells were infected at a MOI = 0.01. The figure shows mean titres plus the S.E.M. from three independent experiments.

the medium[205], we predicted that compared to VACV, MYXV should release less virus into the medium. Conversely the F11L$^+$ MYXV should be found in increased amounts in the medium.

To test the effect of F11L on MYXV virus release we used RK13 cells as these cells are reported to produce and release high levels of VACV EV[135]. For these experiments 60 mm dishes of RK13 cells were infected at a MOI = 10, left for 1 h, and any unbound virus removed with 2 PBS washes before adding medium. After 24 h, the medium was removed, centrifuged to remove any cellular debris and titered. The cell monolayer was harvested into PBS, lysed using three freeze-thaw cycles, and the virus titered. These values were then used to calculate the percent of total virus found in the medium (**Figure 3.15).** As predicted, less MYXV than VACV was found in the media. Interestingly, relative to that seen with WT MXYV, the disruption of M127L reduced the proportion of virus found in the medium (0.35% ± 0.08 *versus* 1.06%± 0.08 for WT, $P<0.01$). This does not appear to a result of a second site mutation as similar observations were seen with both the ΔM127L and ΔM127LmCh viruses. While this was observed in RK13 cells this was not observed in similar experiments performed with MDA-MB-231 cells (Chapter 6).

Regardless of the effect of disrupting M127L on virus release; it is clearly reversed by F11L. An approximately four-fold increase in the amount of virus in the medium, relative to the ΔM127LmCh control, was observed (1.43 ±0.15 *versus* 0.35% ± 0.08, $P<0.01$). Collectively, these data suggest that F11 does not increase the amount of virus produced, but rather increases the ability of the virus to exit the cell and spread.

3.2.6 The Effect of F11L on MYXV Cell Morphology, Cell Movement and Actin Projectile Formation:

F11 has also been shown to induce a number of morphological changes in infected cells. F11 is believed to disrupt the cortical actin layer, which causes a reduction

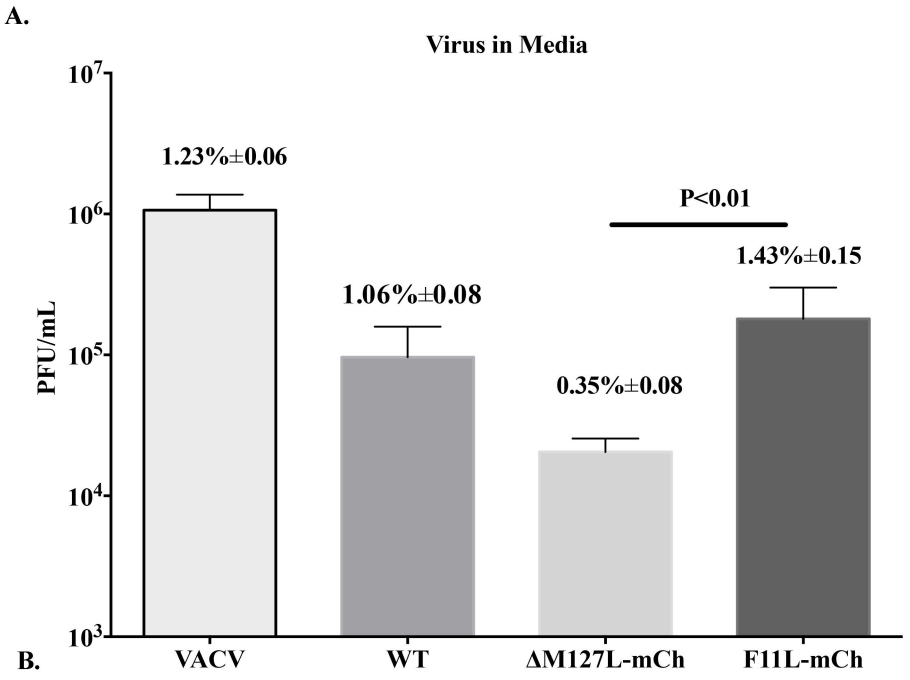

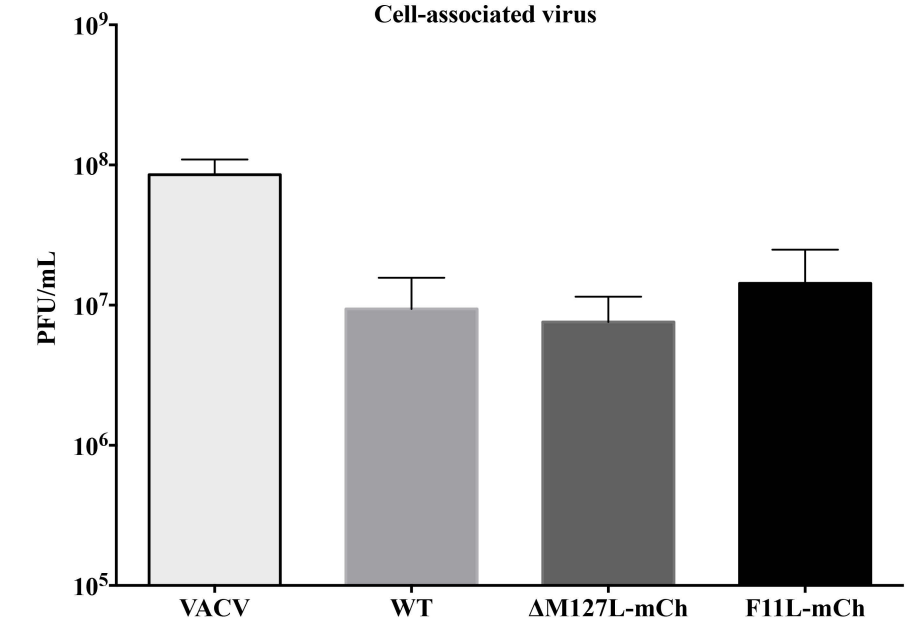

Figure 3.15: Effect of F11L on release of MYXV from RK13 cells. Rk13 cells were infected at a MOI=10 with respective viruses. After 24 h, media was removed, centrifuged to remove any cellular debris and titered. The values from these represent the media fraction (panel A). The cellular monolayer was harvested into PBS, subjected to three freeze-thaw cycles, and titered (Panel B). These numbers were then used calculate the fraction of total virus that was in the media, which is listed as mean percent plus S.E.M. (n=3) above the respective virus in panel A.

in actin stress fibres[143]. F11 has also been implicated in inducing cell-contraction and motility[223,224]. We wanted to test whether F11 expression caused similar changes to the morphology of MYXV-infected cells.

F11 is expressed early in VACV infection and many of the morphological changes associated with F11 have been reported to occur early as well. To test whether these alterations occurred when F11 was expressed *via* MYXV we infected RK13 cells, fixed them at 8 h post-infection, and stained for actin and DAPI as previously described. It should be noted that the F11 antibody cross-reacted with another protein, because of this we were unable to use this antibody in microscopy (Appendix figure A2). Upon imaging two morphological changes were immediately noted. The first was that in comparison to control/WT MYXV, cells infected with the F11L $^{+}$ MYXV were smaller, and more rounded. The second difference was that the actin cytoskeleton appeared more disrupted **(Figure 3.16A)**.

We took a random sampling of cells and measured the cell area and the number of actin stress fibres. While WT and control MYXV had no major effect on cell area (relative to uninfected cells) cells infected with VACV or F11L^{+} MYXV exhibited a ~40-50% reduction in cell area (**Figure 3.16B).** To measure the relative disruption of the cortical actin layer, we counted the number of central actin stress fibres. We found that, in comparison to the ΔM127L-mCh control virus, cells infected with F11LmCh virus had significantly fewer stress fibres (2.7±0.3 *versus* 8.6±0.5 per cell, P<0.001).

While there appeared to be an increase in the number of actin projectiles observed at 8 h post-infection, these differences were not significant (**Figure 3.16D).** However if the infected was allowed to proceed for 20 h we observed an approximately three-fold increase in the number of actin projectiles formed in cells infected with the F11LmCh virus, compared to the M127LmCh virus (1.8 ± 0.2 *versus* 0.6 ± 0.1, P<0.001). This was still significantly less than the number of actin projectiles observed on VACV

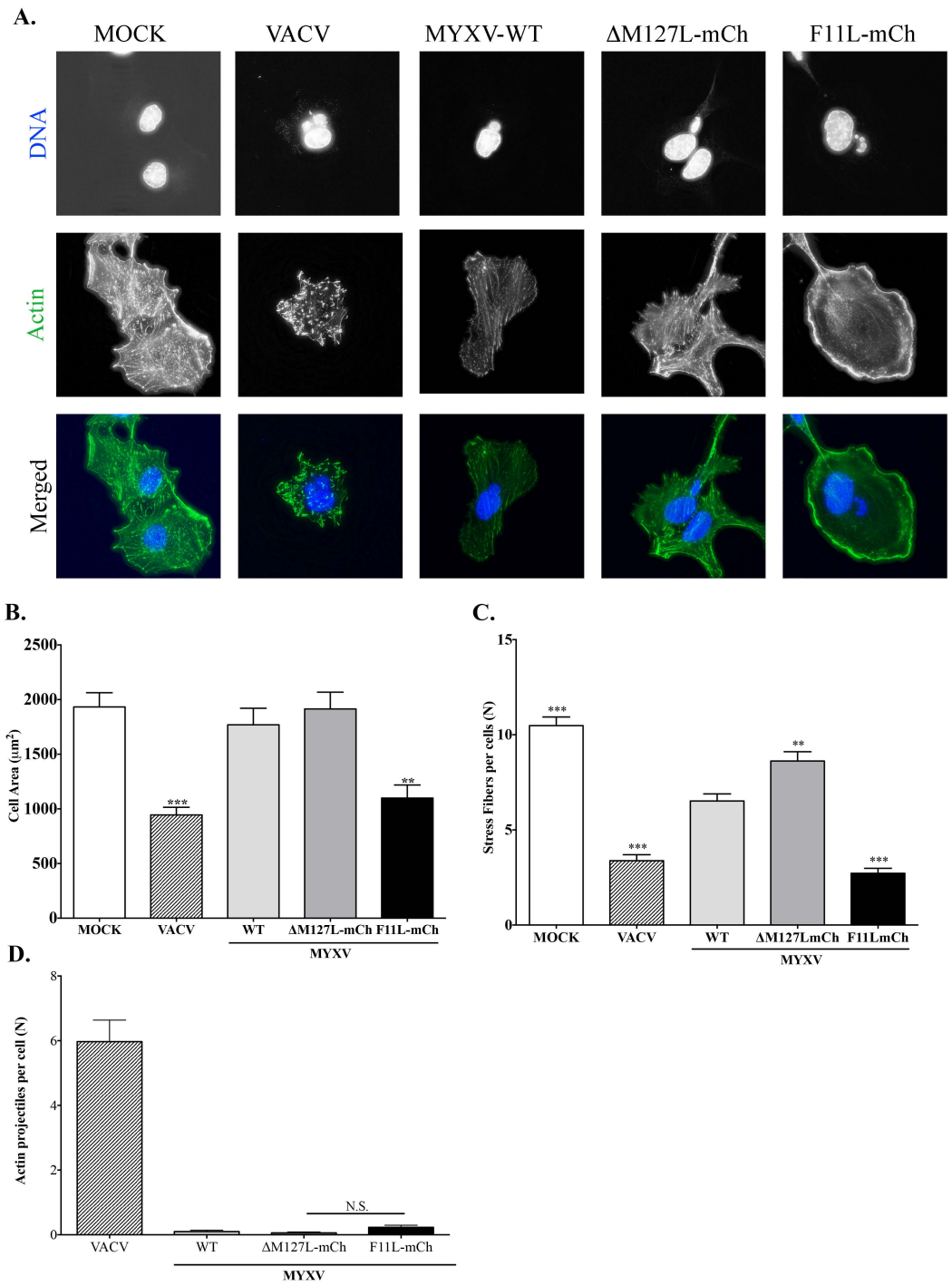

Figure 3.16: Effect of VACV F11L on the cell morphology of MYXV-infected cells. Rk13 cells were infected with respective viruses, fixed at 8 h post-infection, and stained for actin and DNA, using Alexa-Fluor488 phalloidin and DAPI, respectively. **(A)** Cells were visualized at 60 x magnification using a personal delta-vision **(B)** Quantification of the number of actin stress fibres at 8 h post-infection **(C)** Quantification of the cell area of infected cells at 8 h post-infection. Cell area was calculated using ImageJ. **(D)** Quantification of actin projectiles formed per cell. For all quantifications the numbers represent mean plus S.E.M, and are calculated from 50 cells per virus for each of two independent experiments (n = 100). Signficance reported is in comparison to WT MYXV.

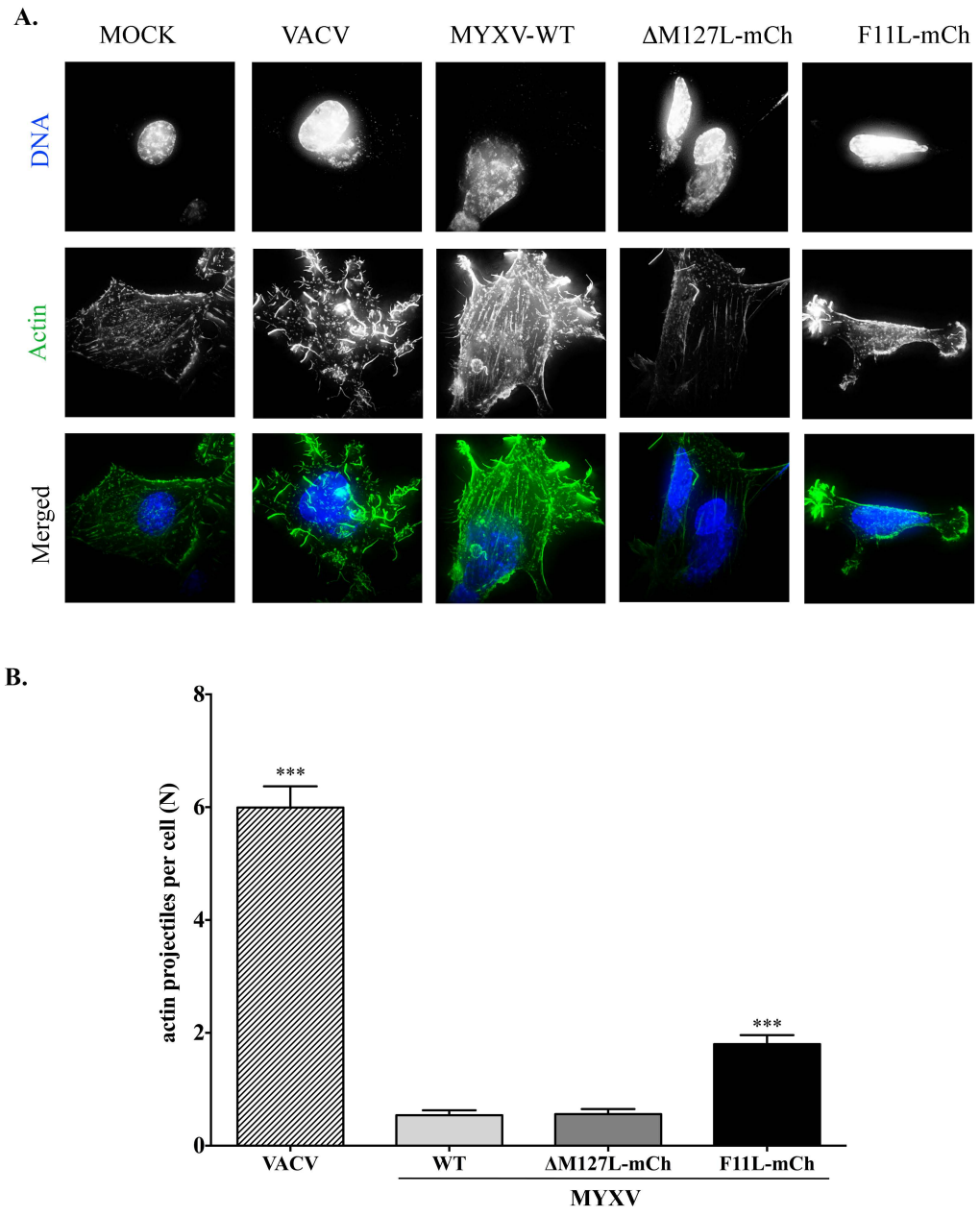

Figure 3.17: Effect of VACV F11L on the cell morphology of MYXV-infected Rk13 cells. Rk13 cells were infected with respective viruses, fixed at 20 h post-infection, and stained for actin and DNA, using Alexa-Fluor488 phalloidin and DAPI, respectively. **(A)** Cells were visualized at 100 x magnification using a personal delta-vision **(B)** Quantification of the number of actin projectiles formed at 20 h post-infection. Values shown represent the mean plus S.E.M.. using 50 infected cells per virus from each of three independent experiments (n = 150)

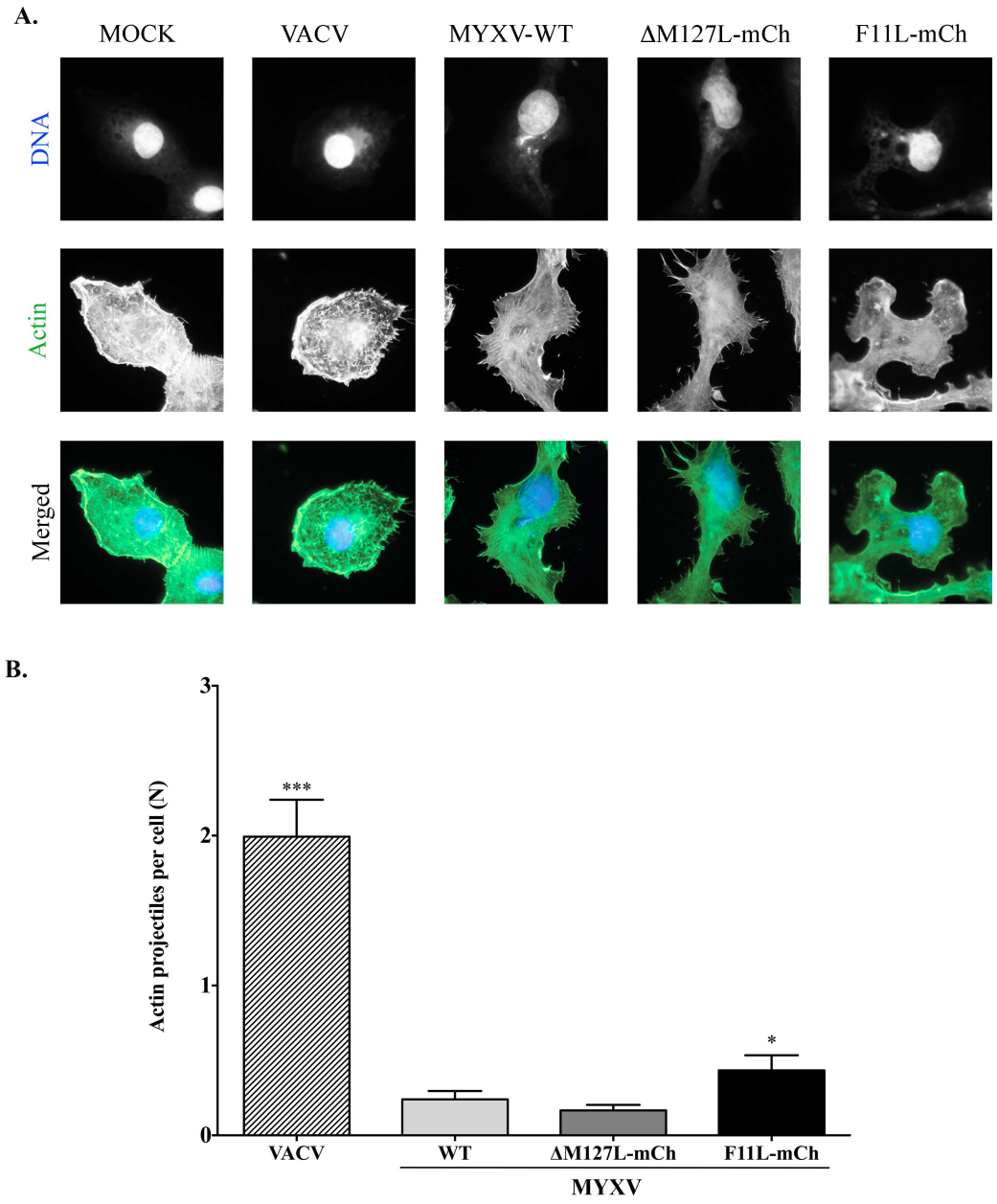

Figure 3.18: Effect of VACV F11L on the cell morphology of MYXV-infected BGMK cells. BGMK cells were infected with respective viruses, fixed at 20 h post-infection, and stained for actin and DNA, using Alexa-Fluor488 phalloidin and DAPI, respectively. **(A)** Cells were visualized at 100 x magnification using a personal delta-vision **(B)** Quantification of the number of actin projectiles formed at 20 h post-infection. Values shown represent the mean plus S.E.M.. using 50 infected cells per virus from each of three independent experiments (n = 150)

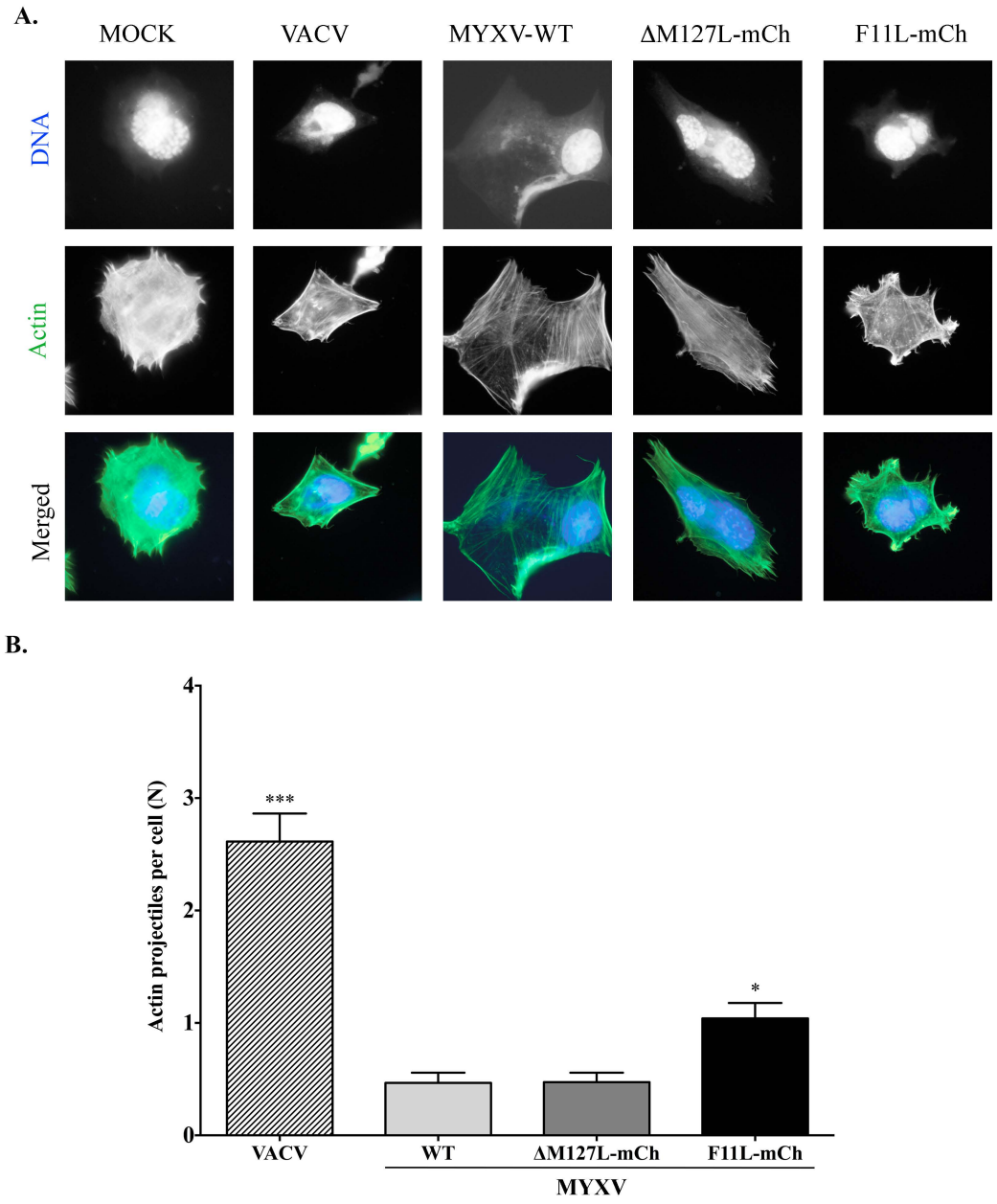

Figure 3.19: Effect of VACV F11L on the cell morphology of MYXV-infected SIRC cells. SIRC cells were infected with respective viruses, fixed at 20 h post-infection, and stained for actin and DNA, using Alexa-Fluor488 phalloidin and DAPI, respectively. **(A)** Cells were visualized at 100 x magnification using a personal delta-vision **(B)** Quantification of the number of actin projectiles formed at 20 h post-infection. Values shown represent the mean plus S.E.M.. using 50 infected cells per virus from each of three independent experiments (n = 150)

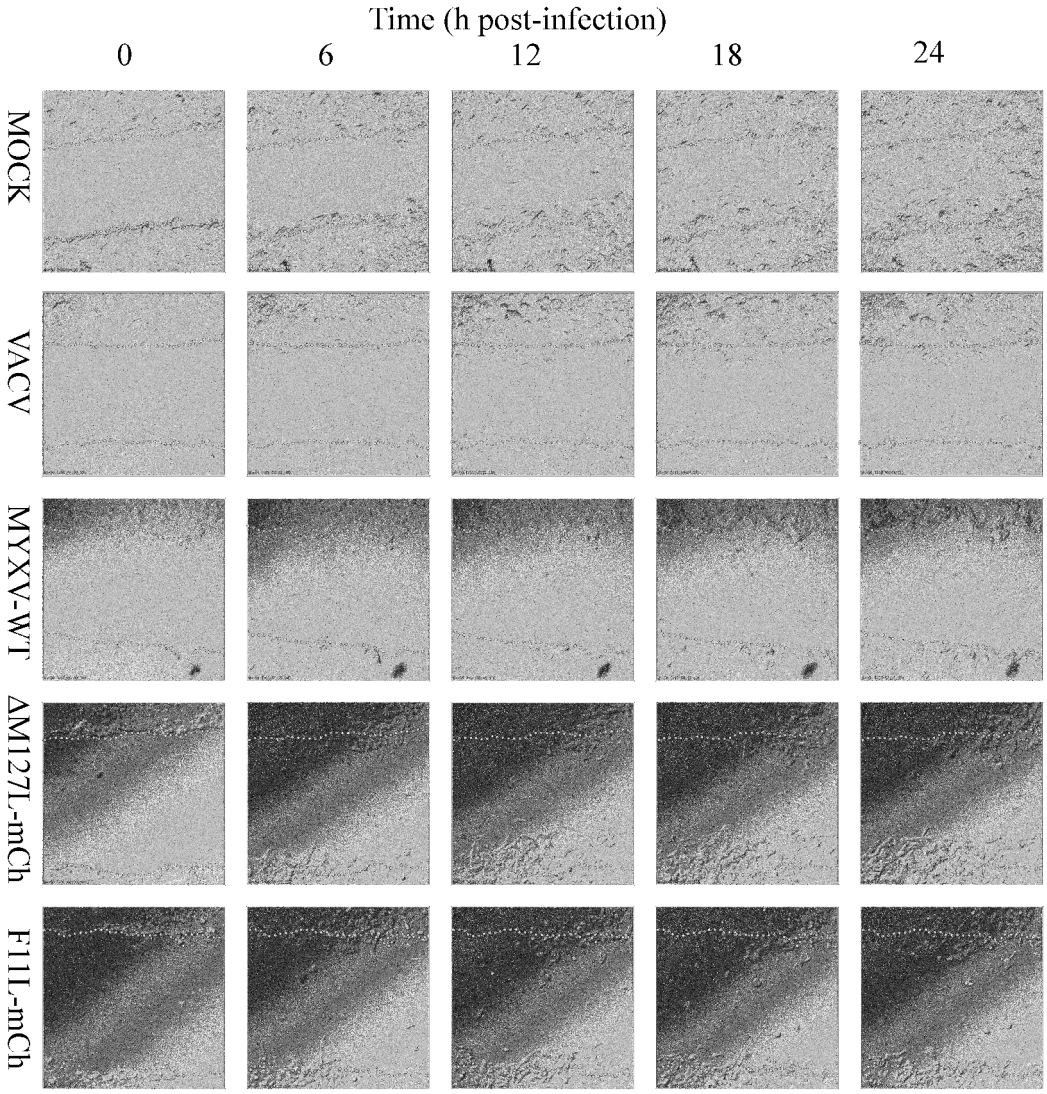

Figure 3.20: Effect of F11L-expressing MYXV on infected cell mobility. A pipette tip was used to introduce a scratch into a monolayer of BGMK cells and then the cells were infected (or mock-infected) with the indicated viruses at MOI=5. The subsequent movement of the cells was tracked using live-cell microscopy with an image being recorded every 5 minutes and incorporated into a time-lapse movies. The figure shows representative images taken from one of the six different fields of view (and two independent experiments) that were used to track each of the four different virus-infected cells, and uninfected control cells. Dotted lines denote the initial boundaries of the scratch. Time lapse videos of this data are available as supplemental videos S4-S8 in J Virol. 2012 Jul;86(13):7167-79. doi: 10.1128/JVI.06936-11.

infected cells (5.4 ± 0.4, P<0.001) **(Figure 3.17A).** Similar increases in the number of actin projectiles in F11LmCh-infected cells were also observed in BGMK and SIRC cells **(Figure 3.18 and 3.19).**

F11L inhibition of RhoA-mDia1 signalling causes an increase in cell motility[224]. This is supported by observations showing that repairing the F11L gene in VACV strain MVA induces cell motility while using siRNAs to knockdown F11 expression reduces the motility of wild-type VACV[223-225]. We predicted that, in comparison to VACV, MYXV should be unable to induce cell-motility while MYXV encoding F11L should gain the ability to induce cell motility.

To test these predictions we used live-cell microscopy to track cell movement into an area devoid of cells. In these assays, commonly called a wound-healing experiment, a P-200 pipette tip was used to introduce a scratch into a confluent monolayer of BGMK cells growing on a 35 mm glass bottom dish. The cells were then infected, or mock-infected, and placed on a pre-heated microscope stage. Cells were then imaged at 10× magnification, at 5 min intervals, for 24 h, in the absence of serum. Time-lapse movies were then generated. As predicted the WT or control MYXV did not appear to induce cell motility while cells infected with the F11LmCh MYXV were seen invading the "wound", albeit not to the extent seen with VACV (**Figure 3.20)**.

3.2.7 The Effect of F11L on MYXV Growth in Primary Rabbit Cornea Fibroblasts:

To this point our studies had used transformed or immortalized cell lines, and although we had used several cell lines it is possible that the differences seen between MYXV and VACV were the result of some unanticipated consequence of growing these viruses on culture-adapted cells. To address these concerns, we repeated several of these key experiments on primary rabbit cells. We chose to use primary rabbit cornea fibroblasts due to the relative ease of isolating and culturing them. In addition we had

data from virus growth on SIRC cells, an immortalized rabbit corneal fibroblast, which could serve as a comparison.

The isolated fibroblasts were immediately seeded into a 6-well dish, and infected 5 days later with ~20-50 pfu of each virus. Three days later fluorescent images of plaques were taken at 10× magnification (**Figure 3.21B)**. The cells were then fixed and the plaques visualized by X-Gal staining (**Figure 3.21A)**. We observed that F11 increased the size of the MYXV plaques. These plaques were more lytic in nature, with a central clearing of cells being observed.

We also tested whether F11 altered actin structures in MYXV-infected primary cells. For this, coverslips of primary cells were seeded immediately after isolation or after one passage and infected with respective viruses. The infection was allowed to continue for 20 h before the cells were fixed, stained for actin and DNA, and visualized by microscopy.

Similar to what we observed in other cell lines, VACV formed significantly more actin projectiles than WT MYXV (9.4 ± 0.9 actin projectiles per cell *versus* 0.4 ± 0.1, $P<0.0001$). We also saw that F11 caused a decrease in actin stress fibres, and an approximately three fold increase in the number of actin projectiles in F11LmCh MYXV. (1.5±0.2 actin projectiles per cell *versus* 0.5±0.1 for the ΔM127L-mCh control, $P<0.001$) **(Figure 3.21C,D).**

Collectively, the experiments using primary rabbit cornea fibroblasts are in agreement with those done with immortalized or transformed cell lines. This suggests that the differences in MYXV and VACV plaquing properties are not an artefact produced by growing these viruses on cell culture adapted cells, and that the absence of a MYXV homolog to F11 partially explains these differences.

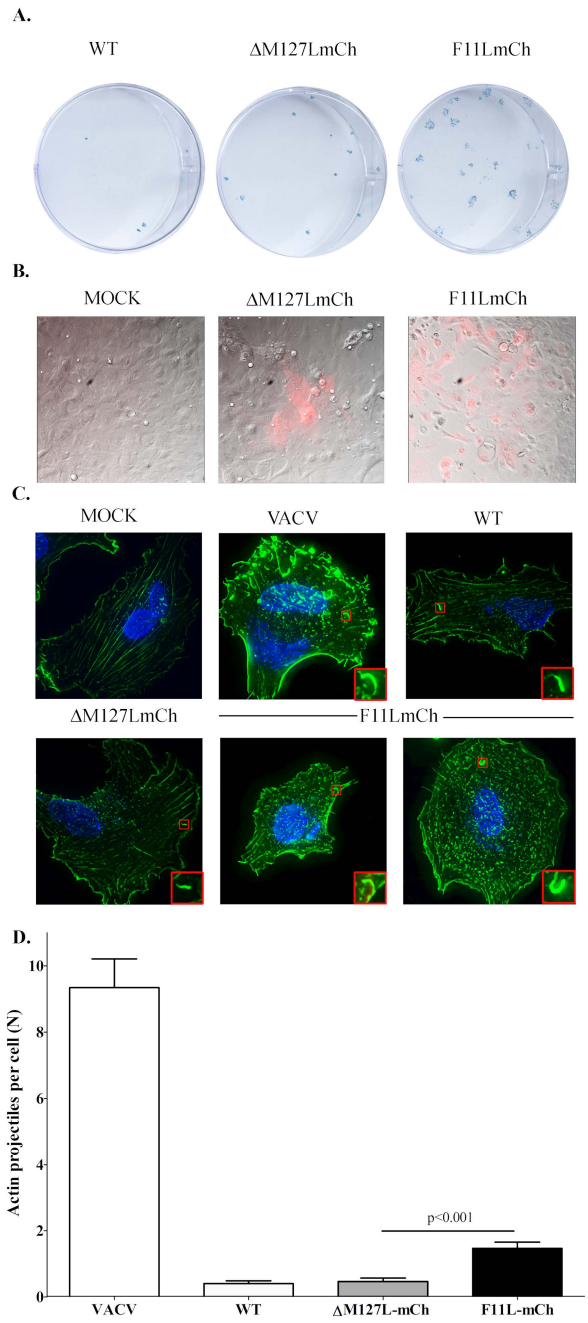

Figure 3.21: Effect of F11L on MYXV growth in primary rabbit cornea cells. Rabbit cornea cells were infected with the indicated viruses 3-5 days post harvest. **(A)** MYXV plaques visualized with β-galactosidase. Cells were infected with the indicated viruses for 72h before being fixed and stained with X-Gal. **(B)** MYXV plaques visualized using mCherry fluorescence. Cells were infected for 72 hr with the indicated viruses and then, prior to fixation and staining for β-galactosidase activity (Panel A), the plaques were imaged at 10× magnification using mCherry epifluorescence and DIC. The merged images are shown. **(C)** Cornea cells were infected (or mock-infected) for 20 hr with the indicated viruses at MOI=5, fixed and stained for both actin and DNA, and imaged (at 100× magnification) by fluorescence microscopy. Merged images are shown along with enlarged views of the actin projectiles (shown inset). **(D)** Quantification of the actin projectiles (seen in Panel C). The figure shows the mean + S.E.M. for the number of actin projectiles per cell from two independent experiments (n = 100, 50 from each experiment).

3.3 SUMMARY AND BRIEF DISCUSSION:

We started this work by asking, why does VACV form significantly larger plaques than MYXV? We found that VACV produces significantly more actin projectiles than MYXV and through bioinformatics identified MYXV homologs/orthologs to the majority of genes involved in these processes. An exception was the absence of a MYXV F11L homolog. We created a series of MYXV which expressed VACV genes and found that the expression of F11L, but not A33R, A34R,A36R, or B5R, increased MYXV foci size. Furthermore F11L expressing MYXV induced a number of morphological changes consistent with its known VACV role. This included cell-rounding and migration, disruption of the actin cytoskeleton and increased actin projectile formation and virus release into the media.

While $F11L^{+}$ MYXV showed increased plaque size these were still smaller than VACV. Furthermore, F11L-mCh formed significantly fewer actin projectiles than VACV. This suggests that while the absence of a F11L homolog partially explains why MYXV forms smaller plaques than VACV, there are additional, yet to be identified, differences that exist between these viruses.

CHAPTER 4: M125R IS ESSENTIAL FOR THE FORMATION OF ACTIN PROJECTILES BY MYXOMA VIRUS AND CAN BE COMPLEMENTED BY VACCINIA VIRUS A36R

A version of the data presented in this chapter has been published as supplemental data in:

Irwin C.R. and Evans D.H. (2012) Modulation of the myxoma virus plaque phenotype by vaccinia virus protein F11. Journal of Virology. **86:** 7167-7179

All of the experiments presented in this chapter were performed by myself, and the original manuscript was written by myself with editorial contributions from my supervisor, Dr. Evans.

4.1 INTRODUCTION:

In the previous chapter we found that while MYXV forms actin projectiles, it forms them much less efficiently than VACV. Bioinformatic comparisons of the genomes of these viruses revealed that MYXV encoded homologs to most of the VACV genes implicated in these processes. Three exceptions exist. We found no evidence of a MYXV homolog to VACV F11L, and homologs to A36R and B5R were less clear. Sequence alignment, combined with secretion and hydrophobicity profile analysis, suggests that M144 is likely a B5 homolog. This is supported by a recent analysis of numerous poxvirus genomes for B5 homologs[309].

Sequence alignment of M125R reveals very little similarity to VACV A36R. However, M125R is a homolog of Yaba-like disease poxvirus (YLDV) gene Y126R. This gene despite lacking sequence similarity to VACV A36R has been shown to have orthologous functions and can complement an actin projectile formation in an A36R deficient strain of VACV. Like Y126R, M125R can complement actin projectile formation, at least in transient transfections, in an A36R deficient strain of VACV. This suggests that M125R has orthologous functions to A36R[219].

We set out to investigate the roles of both M125R and M144R in the context of MYXV. However, I was only able to generate a MYXV mutant of M125R. The data presented in this chapter focuses on characterizing this mutant and collectively show that while M125R is essential for MYXV actin projectile formation, and contributes to MYXV foci size, it does not appear to have a major effect on virus growth. Furthermore, I show that VACV A36R can complement M125R in terms of actin projectile formation.

4.2 RESULTS:

4.2.1 Effect of Disrupting M125R on the Plaquing and Growth Properties of MXYV:

In VACV, A36R contributes to both virus growth and plaque size[188,192,193]. Given that M125R is thought to be an ortholog of VACV A36R, one would predict that disrupting M125R should result in smaller foci and lower yields of virus. To test this, we plated our ΔM125R MYXV along with wild-type MXYV, to test for any differences in plaque size. As predicted, disrupting M125R resulted in a smaller foci formation on a number of cell lines (BGMK, RK13, SIRC and BSC-40) (**Figure 4.1A).** Quantification of plaque size revealed that on average ΔM125R foci were ~ 2/3 the size of foci formed by WT MYXV. The exception to this was on BSC-40 cells, where WT MYXV foci were approximately five times the size of the ΔM125R MYXV **(Figure 4.1B)**

We also investigated whether M125R contributed to the growth of MYXV. For this we performed a multi-step low MOI (0.01) growth curve analysis on BGMK cells. Interestingly, the differences observed in plaque size between WT and ΔM125R MYXVs did not translate to any difference in virus production, with very similar yields of virus being observed **(Figure 4.2).**

4.2.2 Effect of Disrupting M125R on Actin Projectile Formation:

A36R is essential for the formation of actin projectiles in VACV-infected cells. We predicted that if M125R has orthologous functions to A36R, then cells infected with M125R-deficient MYXV would also be devoid of actin projectiles. To test this, we performed immunofluorescent microscopy on a number of cell lines (BGMK, RK13, SIRC and primary rabbit cornea fibroblasts) using conditions similar to those used to examine actin projectiles as described in Chapter 3. For each condition we screened 50 cells in three separate infections (i.e. n=150) but could find no evidence of actin

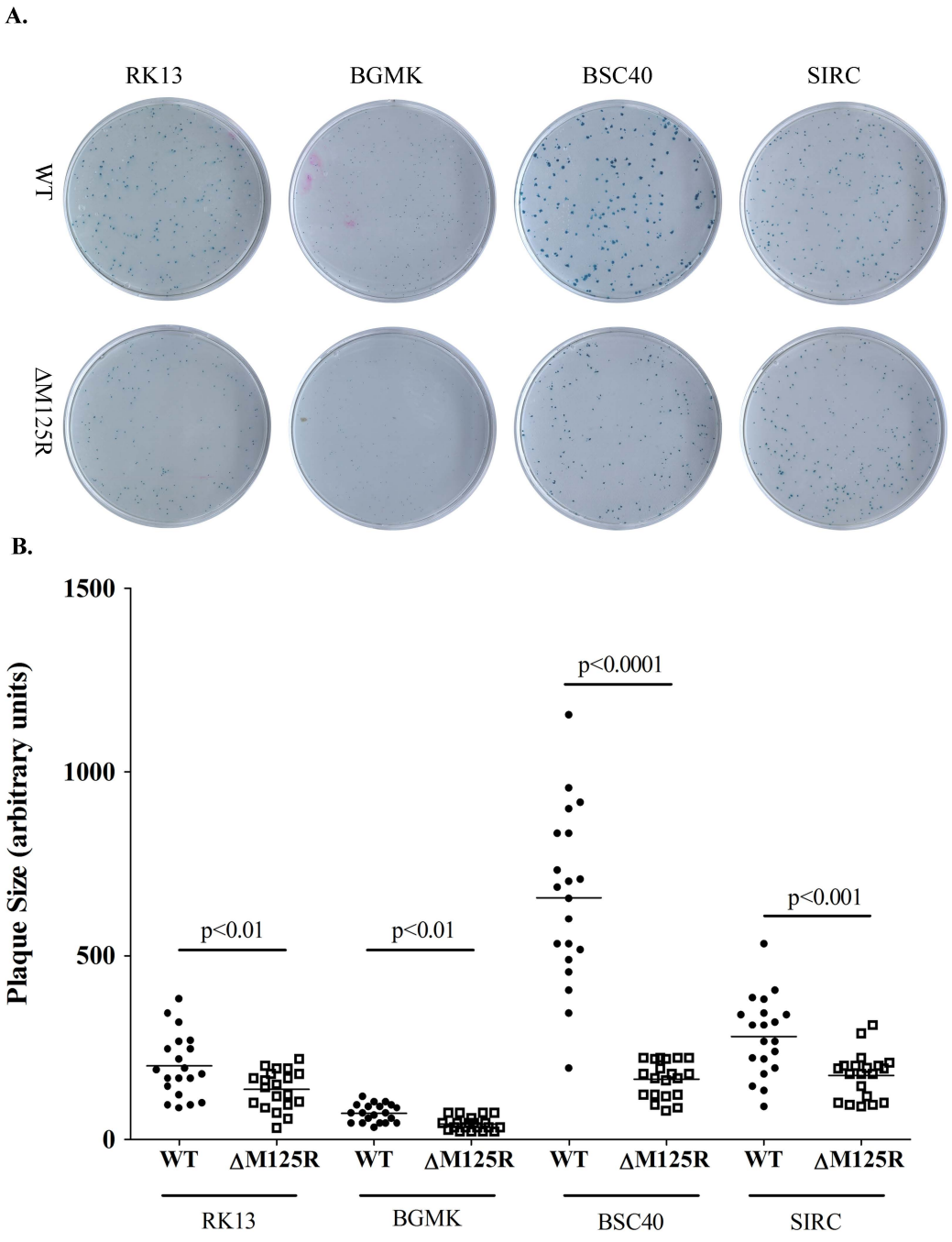

Figure 4.1: Effect of disrupting M125R on MYXV plaque properties: (A) Plaque properties. The indicated viruses were cultured for 96hr on RK13, BGMK, BSC40 or SIRC cells and then the dishes were fixed and stained with X-Gal. **(B)** Quantitation of plaque areas. The plaques were scanned into digital images and the areas determined using ImageJ. Each horizontal line on the scatter plot shows the median area of 20 randomly chosen plaques.

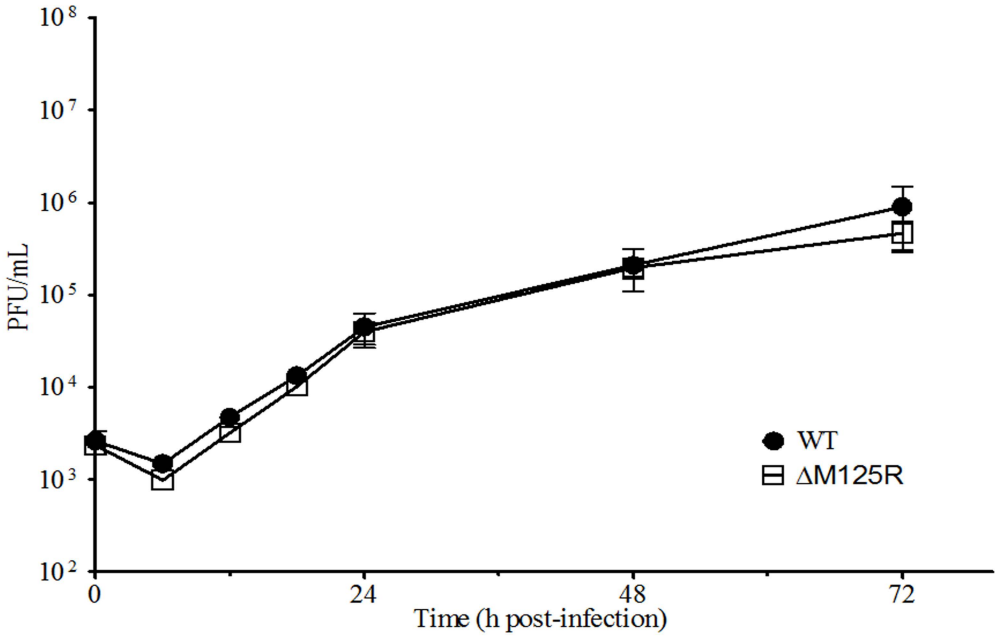

Figure 4.2: Effect of disrupting M125R on the MYXV growth in a multi-step growth curve: BGMK cells were infected with virus at M.O.I. = 0.01, harvested at the indicated times, and the progeny virus titered on BGMK cells. The figure shows mean titres plus the S.E.M. from three independent experiments.

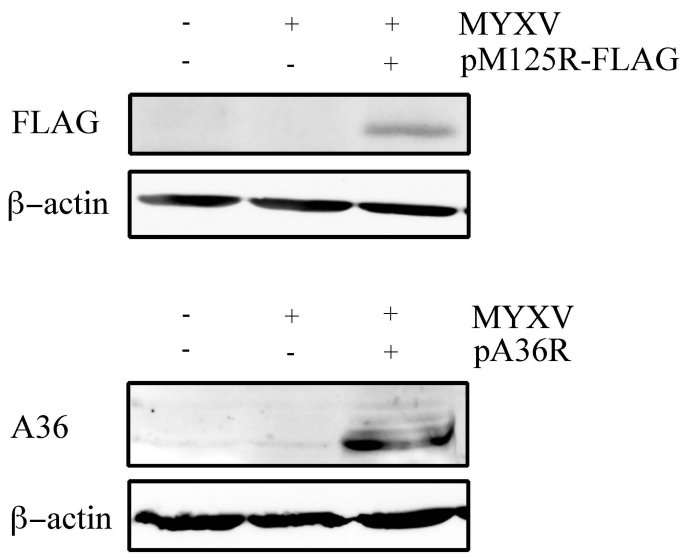

Figure 4.3 Expression of A36 or M125R-FLAG by western blot analysis: BGMK cells were infected with MYXV at a M.O.I. = 5 and transfected with 10μg of plasmid DNA 2hr after infection. The cells were harvested 22 hr later and blotted for either A36 or FLAG. Cellular β-actin was used as a loading control.

projectiles in cells infected with ΔM125R. This suggests that like its counterpart in VACV, M125R is essential for the production of actin projectiles in MYXV.

4.2.3 Complementation of Actin Projectile Deficiencies in ΔM125R-infected Cells by Transient Transfection of Plasmids Encoding FLAG-epitope Tagged M125R or VACV A36R:

Transient transfection of A36R-deficient VACV-infected cells with a plasmid encoding M125R can result in a restoration of actin projectile formation[219]. We wanted to see if the opposite was also true, i.e can a plasmid encoding VACV A36R restore actin projectile formation in cells infected with ΔM125R MYXV?

To do this I made use of a plasmid (pA36R) that had been made as an intermediary for the creation of the MYXV-A36R virus in Chapter 3. This plasmid has VACV A36R under the control of its native promoter. I also created a plasmid (pM125R-FLAG) that expressed C-terminal FLAG epitope tagged version of M125R, under its native promoter. I choose a C-terminal tag strategy as it has previously been shown that M125R can be successfully expressed when a C-terminal mCherry fluorescent protein fusion was used[219]. Both pA36R and pM125R-FLAG are in the same plasmid backbone (PCR-Topo2.1). The expression of proteins of the expected molecular weight was confirmed by western-blot analysis using WT MYXV cells that had been transfected with these plasmids **(Figure 4.3)**

These plasmids were then used to transfect RK13 cells infected with ΔM125R virus. At 20 h post-infection, cells were fixed and immunostained for either A36R (as done in chapter 3), or for FLAG (using a polyclonal anti-FLAG antibody), and then counterstained for actin or DNA. As a control for transfection, a FLAG-tagged version of VACV A50R (DNA-Ligase) was used. This gene would not be expected to have any effect on actin projectile formation.

The infected and transfected cells were then visualized by microscopy. Transfecting ΔM125R infected cells with either pM125R-FLAG or pA36R permitted the

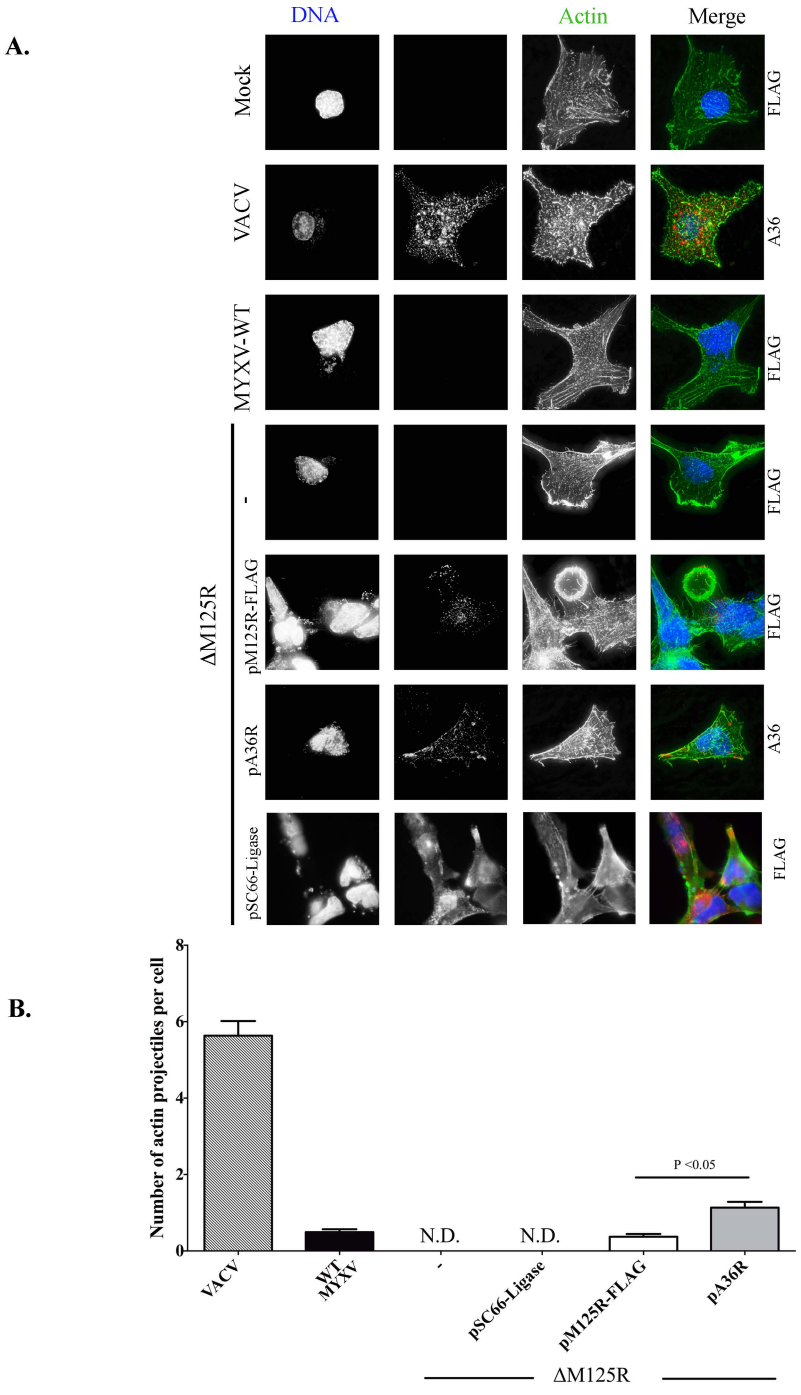

Figure 4.4: VACV A36R can complement actin projectile deficiency in ΔM125R-infected cells: **(A)**RK13 cells were infected at a M.O.I. of 5 and transfected 2 hr later with 150ng of plasmid DNA encoding either A36R or a C-terminal FLAG-epitope tagged form of M125R. Both proteins were expressed under the control of their native promoter. The cells were fixed at 20 hpi and stained using anti-A36 or anti-FLAG(M2) antibodies plus an Alexa-594 conjugated secondary antibody. The cells were counterstained for actin and DNA using Alexa-488 phalloidin and DAPI, respectively, and visualized at 100X. **(B)** Quantification of the actin projectiles shown from A. The figure shows the mean number of actin projectiles plus the S.E.M. Fifty infected/transfected cells were analyzed for each virus in each of three independent experiments (n=150).

formation of actin projectiles **(Figure 4.4).** I performed this experiment three times and counted the number of actin projectiles on a total of 150 transfected cells for each plasmid. I found that transfecting ΔM125R infected cells with pM125R-FLAG, restored the numbers of actin projectiles to levels similar to those observed in WT infected cells (0.4± 0.1 actin projectiles per cell *versus* 0.5 ± 0.1 for WT). Interestingly, transfecting ΔM125R-infected cells with pA36R produced significantly higher levels of actin projectiles (1.1±0.2 actin projectiles, $P<0.05$) (**Figure 4.5)**.

4.3 SUMMARY AND BRIEF DISCUSSION:

MYXV produces actin projectiles despite having no clear homolog of one of the VACV genes (A36R) known to be critical for their formation. M125R is homologous to YLDV Y126R, a gene that, like M125R, does not look much like VACV A36R. However, both Y126R and M125R are capable of catalyzing actin projectile formation, in cells infected with an A36R-deficient VACV. This suggests that all three proteins share orthologous functions.

Here we investigated the role of M125R in the context of a MYXV infection. We found that M125R was essential for the formation of actin projectiles and that disrupting it produced smaller foci. Interestingly, at least in BGMK cells, this did not translate to lower viral yields in a multi-step, low MOI growth curve.

I also showed that actin projectile formation can be restored in ΔM125R-infected cells by transfecting plasmids expressing either a FLAG-tagged version of M125R or VACV A36R. Interestingly, cells transfected with A36R produced more actin projectiles than those transfected with M125R. Whether these differences are due to differences in gene expression or that A36R is "better" at catalyzing actin projectile formation, cannot be inferred from these experiments alone. Regardless, these data show that M135R is essential for the formation of actin projectiles by MYXV and can be complemented by VACV A36R.

CHAPTER 5: OPTIMIZATION OF VIRUS DOSE AND *IN VIVO* IMAGING TECHNIQUES FOR EVALUATING THE ONCOLYTIC EFFICACY OF MYXOMA VIRUS IN A XENOGRAFT TUMOR MODEL OF MICE BEARING LUCIFERASE TAGGED HUMAN MDA-MB-231 BREAST CANCER CELLS

The data presented in this Chapter represents a body of unpublished data.

I was involved in all experiments presented in this Chapter. I would like to acknowledge the invaluable assistance of Nicole Favis, Kate Agopsowicz and Dr. Mary Hitt in these experiments. Kate assisted in the establishment of tumors in these initial experiments. Nicole was involved in virtually all aspects of these animal experiments and Dr. Hitt provided valuable advice in the design of these experiments.

5.1 INTRODUCTION:

MYXV has shown oncolytic efficacy in a number of animal tumor models. We sought to develop a platform for evaluating the efficacy of oncolytic viruses using a combination of traditional methods, such as caliper measurements, and more cutting-edge technologies, i.e. the use of a newly purchased IVIS Spectrum small animal imager. We decided to use an orthotopic xenograft model, wherein immunocompromised NIH-III mice bear tumors produced by a human mammary adenocarcinoma cell line (MDA-MB-231). We chose this model for a number of reasons. First, a firefly luciferase expressing version of this cell line is commercially available from Caliper Scientific (MDA-MB-231-D3H2LN) and Caliper has optimized conditions for establishing and tracking these tumors in mice. The immunocompromised NIH-III mice are also better suited for imaging as the absence of hair allows for better detection of both bioluminescent and fluorescent signals.

MDA-MB-231 cells also support an intermediate level of MYXV growth and, in subcutaneous tumor models, are not easily cured even with repeated doses of MYXV (1×10^8 pfu) (G.McFadden, personal communication). We hypothesized that this model would allow us to test whether our engineered viruses worked better or worse relative to WT viruses. We chose an orthotopic tumor model as it allowed for the direct delivery of virus to the tumor, although other avenues of delivery are possible. Furthermore, we could use calipers to monitor tumor growth.

In this chapter I describe the experiments used to determine the effective dose of MYXV in this model. I also show a number of experiments that were used to optimize the conditions for the imaging of luciferase-expressing MDA-MB-231 cells *in vivo,* as well as the methods for tracking viral replication. These experiments served to identify conditions that would be used to evaluate the oncolytic ability of recombinant MYXV (Chapter 6) and VACV (B. Gowrishankar *et al.,* unpublished.)

5.2 RESULTS:

Tumors were established by injecting the mammary fat pad of NIH-III mice with 2×10^6 luciferase expressing MDA-MB-231 cells. The tumors were allowed to grow until palpable, after which caliper measurements were used to determine tumor volume, and the mice were sorted into groups with similar mean tumor volumes. At this point, usually 10-17 days after implantations the experimental treatments could begin.

5.2.1: Determination of the Minimal Effective Dose of MYXV Virus:

Our first objective was to identify whether MYXV displayed any oncolytic efficacy in this model and, if so, what was the minimal effective dose of virus. To this effect we compared the rate of tumor growth in mice receiving PBS injections, with those receiving one of three different doses of live ΔM127L MYXV ($1\times 10^{6,}$ 5×10^6, or 2.5×10^7 pfu). One cohort received a UV-inactivated dose of ΔM127L virus at the highest dose used in these trials. However, the data acquired from this group are not shown, as this group contained less mice (3) and had one mouse that died during imaging due to problems with the anaesthetic system.

The other animals were injected intra-tumorally with three doses of virus over a one-week period. Tumor volumes were monitored, twice weekly, until two dimensions of the tumor were greater than 16mm long, one dimension greater than 20mm long, after which they were euthanized for compassionate reasons and scored as "dead". We also monitored mice for any signs of illness, or weight loss. In all conditions mice showed no signs of virus illness, and continued to gain weight throughout the experiment (**Figure 5.1A)**. This suggested that MYXV is safe in these mice.

It became noticeable within the first week following virus injection, even by visual examination, that mice infected wth live virus had tumors that were smaller. These tumors did grow over the next few weeks, but at a much slower rate than those receiving only PBS (**Figure 5.1B).** Although no instances of a cure were observed in these mice,

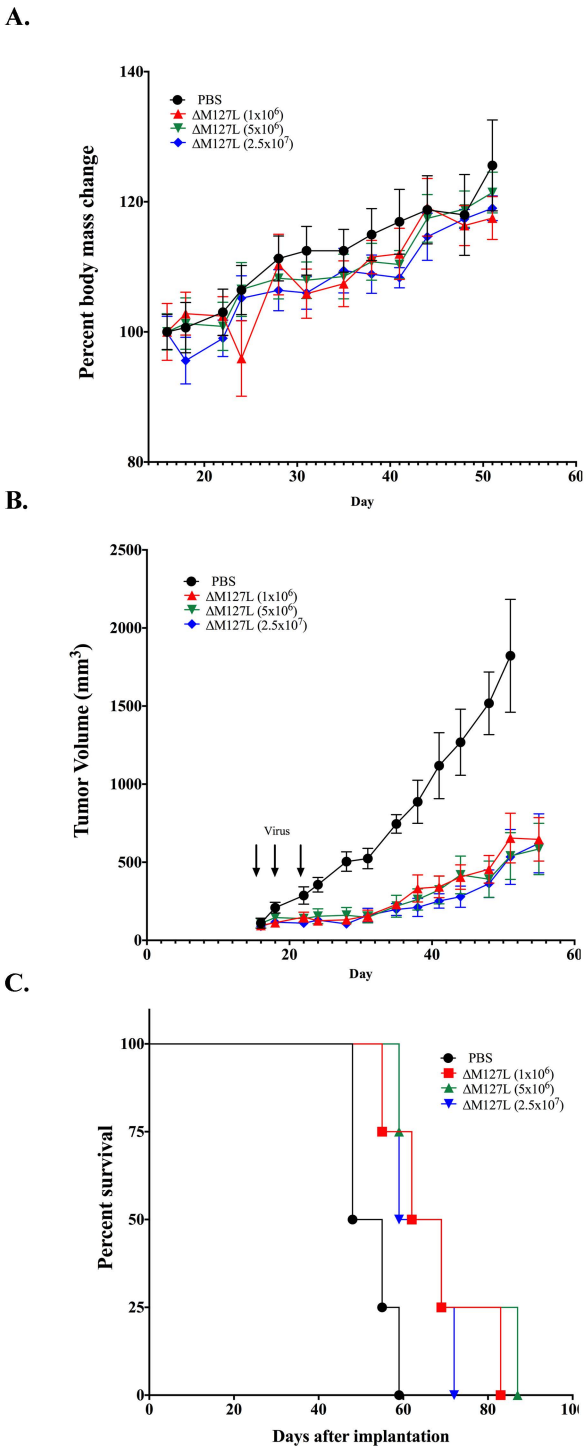

Figure 5.1: Evaluation of the oncolytic efficacy of MYXV in an orthotopic tumor model of NIH-III mice bearing tumors of human MDA-MB-231 cells. Tumors were allowed to establish for 15 days following the injection of 2 x10^6 luciferase expressing MDA-MB-231 cells into the mammary fat pad of NIH-III mice. Three intratumoral injections of MYXV (ΔM127L), over the course of 7 days, were then administered. **(A)** Mice were monitored for changes in body mass and **(B)** changes in tumor volume, as determined by caliper measurements. **(C)** Survival curves. Mice were removed from the study when their tumor was greater than 16 mm in two dimensions, or 20 mm in one dimension. For all groups presented here, an n of 4 was used.

these delayed tumor growth rates did translate into significantly longer survival times **(Figure 5.1C).**

Interestingly, amongst the groups receiving live virus, few differences were observed. These groups had similar rates of tumor growth **(Figure 5.1B),** and had almost identical median survivals (65.5 days, 65.5 days, and 64 days for the 1×10^6, 5×10^6, or 2.5×10^7 pfu doses, respectively). In contrast the PBS-receiving mice had a median survival of 51.5 days post tumor-implantation (**Figure 5.1C).** Taken as a whole, these experiments showed that MYXV was safe, and effective at delaying tumor growth and prolonging the survival of mice bearing MDA-MB-231 tumors. These experiments also showed that this efficacy was observed at even the lowest doses of virus used (1×10^6). In a subsequent experiment, we found that 1×10^6 pfu is likely the minimum effective, as we observed no statistical difference in the median survival of mice receiving doses of 1×10^5 pfu when compared to mice receiving UV-inactivated virus (**Figure A.3**).

Some additional pieces of information were obtained from these pilot studies that would prove useful in subsequent experiments. In comparison to mice that received PBS, mice that received live virus had tumors that tended to be "flatter". This suggested that the criteria for determining endpoint (tumor >20mm in one dimension, or >16 mm in two dimensions) may not have been the best for comparing different treatments, as at endpoint, mice receiving live virus would have tumors that had significantly smaller volumes than in control animal. We decided to alter the criteria for determining an endpoint in future experiments. We decided to use a fixed tumor volume ($1500mm^3$), as opposed to fixed dimensions. This value is still less than specified in the CCAC animal regulations, which permit a tumor burden being less than <10 % of body mass. This would be ~2000 mm^3 in our studies.

Another interesting observation was that at higher doses of virus, a greater number of mice formed scabs over the tumors. Whether this was caused by more killing of tumor cells, producing more necrotic tissue, is uncertain.

5.2.2 Optimization of Conditions for the Bioluminescent Imaging of Luciferase Tagged MDA-MB-231 Cancer Cells *In Vivo:*

Concurrent with the experiments presented in the previous section we also optimized the conditions for visualizing luciferase-tagged cancer cells. We were specifically concerned with establishing the timing of the maximum luciferase signal, and whether there was a correlation between the tumor volume, measured with calipers, and the luciferase signal.

To determine luciferin's metabolism kinetics, one mouse treated with PBS only, and two mice that received the highest dose of virus were used. Ten days after the first virus injection these mice were anaesthetized, placed on the stage of the IVIS spectrum imager, and then injected intraperitoneally (IP) with luciferin (200µl of 15mg/mL). Imaging was begun using auto-exposure settings and an image taken every minute for 20 minutes. The mice were then returned to their cages and monitored for recovery. The supplied software (Living Colors v4) was then used to analyze the bioluminescent signals. Outlines of the tumor signals were made and the total flux (photons/sec) plotted **(Figure 5.2)**. We observed that the luciferase signal changed over time with a peak in the 5-10 minute range post-infection (**Figure 5.2B).** In subsequent experiments we would image ~10 min post-injection.

Since we observed that mice receiving live virus had lower levels of luciferase activity and these mice had smaller tumor volumes, as determined by caliper measurements, we wanted to see if there was a correlation between the luciferase signal an tumor volume. To do this we imaged mice over several weeks. Occasionally we would observe a luciferase signal in a mouse on one day and not on another. This was despite

A.

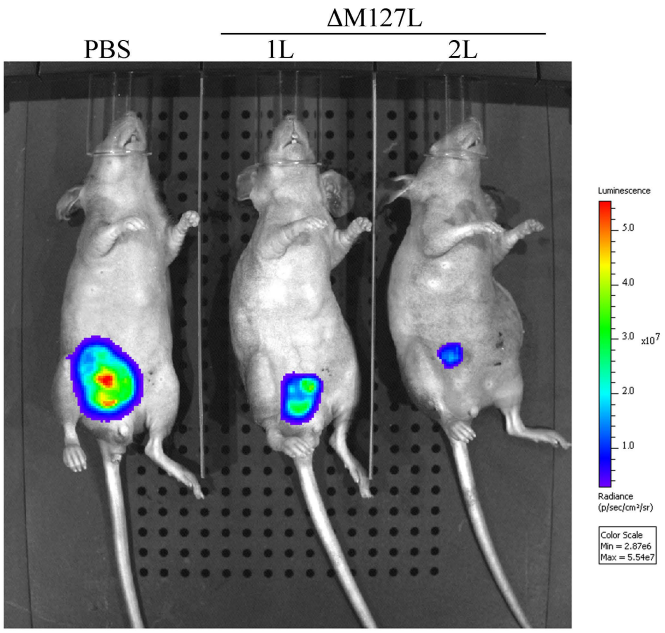

B.

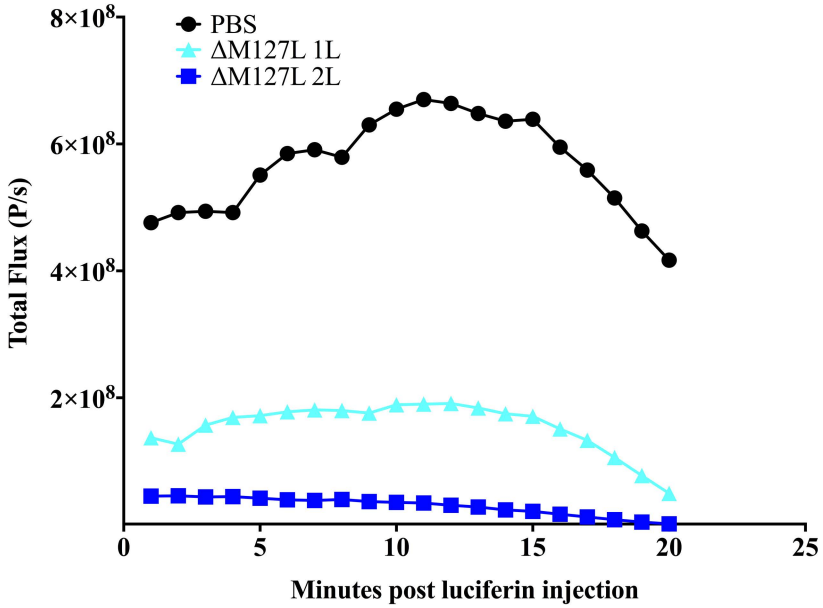

Figure 5.2: Determination of luciferase kinetics of NIH-III mice bearing luciferase-expressing MDA-MB-231 tumors. At 10 days post virus injection, three mice (one PBS and 2 receiving 2.5×107 pfu of ΔM127L) were anaesthetized and IP injected with 0.2 mL of 15mg/mL D-luciferin. Mice were then imaged at 1 min intervals for 20 mins. **(A)** Representative image at 10 mins. **(B)** To measure the luciferase signal at different times, Living color imaging software was used to outline and measure total flux (photons/second)

the continued presence of a tumor and testing various exposure times. Oddly, we would then see the return of the signal the next week. The reasons for this irregular luciferase signal detection remain obscure.

From a number of mice we determined the luciferase signal intensity for the tumor, and plotted it against tumor volume, as measured by calipers **(Figure 5.3).** Using a number of points from both infected and uninfected MYXV we observed a weak correlation between the luciferase signal (total flux) and tumor volume (R^2= 0.37). (**Figure 5.3A)** We noted that this correlation did improve somewhat if one looks at a subset of mice receiving only PBS, R^2 =0.71 **(Figure 5.3B).** In general, when luciferase signal was reliably detected, it was usually lower in mice receiving virus than in control animals (e.g. **Figure 5.2B).** We also occasionally detected the presence of secondary luciferase signals, suggesting the presence of metastases.

The lack of a strong correlation between a luciferase signal and the tumor volume, combined with the observation that scabs partially obscure the luciferase signal, lead us to conclude that calipers would remain a better method for monitoring tumor growth. It also avoids longer periods of sedation, needed for imaging, which sometimes killed the mice. However, the ability to detect metastases and other small tumors does make the IVIS imager a powerful tool to augment these more traditional approaches.

5.2.3: **Evaluation of DDAOG as a Substrate for Detection of Virus *In Vivo:***

Many recombinant viruses, including all of the recombinant MYXV generated in this thesis, encode a LacZ gene. While this allows for easy detection in cell-culture using X-Gal or ONPG reporter assays, few approaches for using β-galactosidase as a reporter *in vivo* exist. One substrate that has been reported to be used *in vivo* is 9H-(1,3-dichloro-9,9-dimethylacridin-2-one-7-yl) β-D-galactopyranoside (DDAOG)[310]. This substrate is cleaved by β-galactosidase to produce 7-hydroxy-9H(I,3-dichloro-9,9-dimethylacridin-2-one) (DDAO). DDAOG fluoresces at 600nm when excited with a light at 465 nm. When

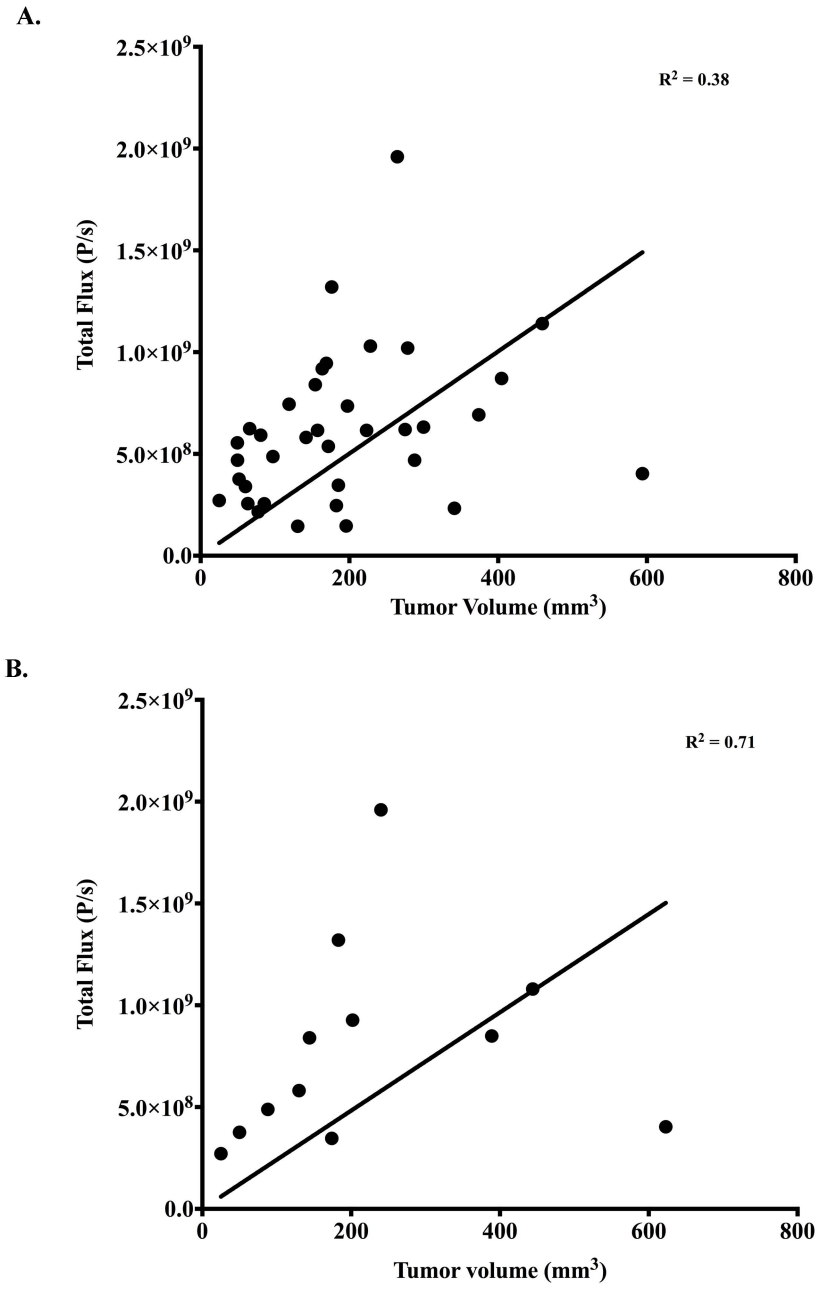

Figure 5.3: Relationship between tumor volume and luciferase signal in NIH-III mice. Weekly imaging with the IVIS Spectrum small animal imager was used to visualize bioluminescent signal following IP injection with D-luciferin. At ~ 10 min post-injection, luciferase levels (Total Flux) as described in Figure 5.2, were plotted against tumor volume. **(A)** correlation between tumor volume and luciferase signal of a mixed population of infected and uninfected mice. **(B)** Correlation of luciferase levels and tumor volume of a subset of **(A)** which received only PBS injections

DDAOG is cleaved by β-galactosidase the resulting DDAO has an emission spectrum that is red shifted (646nm excitations, 659nm emission)[310,311]. We hoped that by imaging mice at 640nm excitation/ 700 nm emission we could detect virus encoded β-galactosidase.

We first tested this compound in cells. For this a 96 well dish of either BGMK or MDA-MB-231 cells were infected with virus and then cultured for 4 days. DDAOG was added to a concentration of 10 μM, incubated for 2 h at 37^{o}C, and detected using the IVIS imager with 640nm excitation and 700nm emission filters. A MOI-dependent increase in signal was observed in infected cells, with a 5-10 fold increase in total radiant efficiency being observed at cells infected at a MOI of 1 (**Figure 5.4)**.

We then went on to test whether DDAOG could be used *in vivo*. Mice were given a tail vein injection of DDAOG (0.1 mL at 5 mg/mL), and the substrate allowed to metabolize for 10 mins before imaging was commenced. We took images using the filter pairs necessary for detecting DDAOG and DDAO (**Figure 5.5),** as well as a number of other filters surrounding the expected excitation/emission wavelengths. While there was some tissue auto-fluorescence observed at the wavelengths for detecting DDAOG, this was not seen at the wavelengths used for detecting DDAO. As expected in a mouse receiving PBS, no fluorescence was observed at wavelengths expected for visualization of DDAO. In one mouse, which had received virus, we observed some signal at the site of the tumor, but a significantly larger amount at the site of injection. In the other virus-treated mouse, no detectable amounts of DDAO signal was detected. We repeated these experiments, again unsuccessfully, leading us to conclude that DDAOG is not useful for detecting virus *in vivo.*

5.2.4 Detection of Virus-Encoded Fluorescent Proteins:

We next tested whether virus-encoded fluorescent proteins could be used to track virus *in vivo.* We had available recombinant strains of MYXV that expressed three

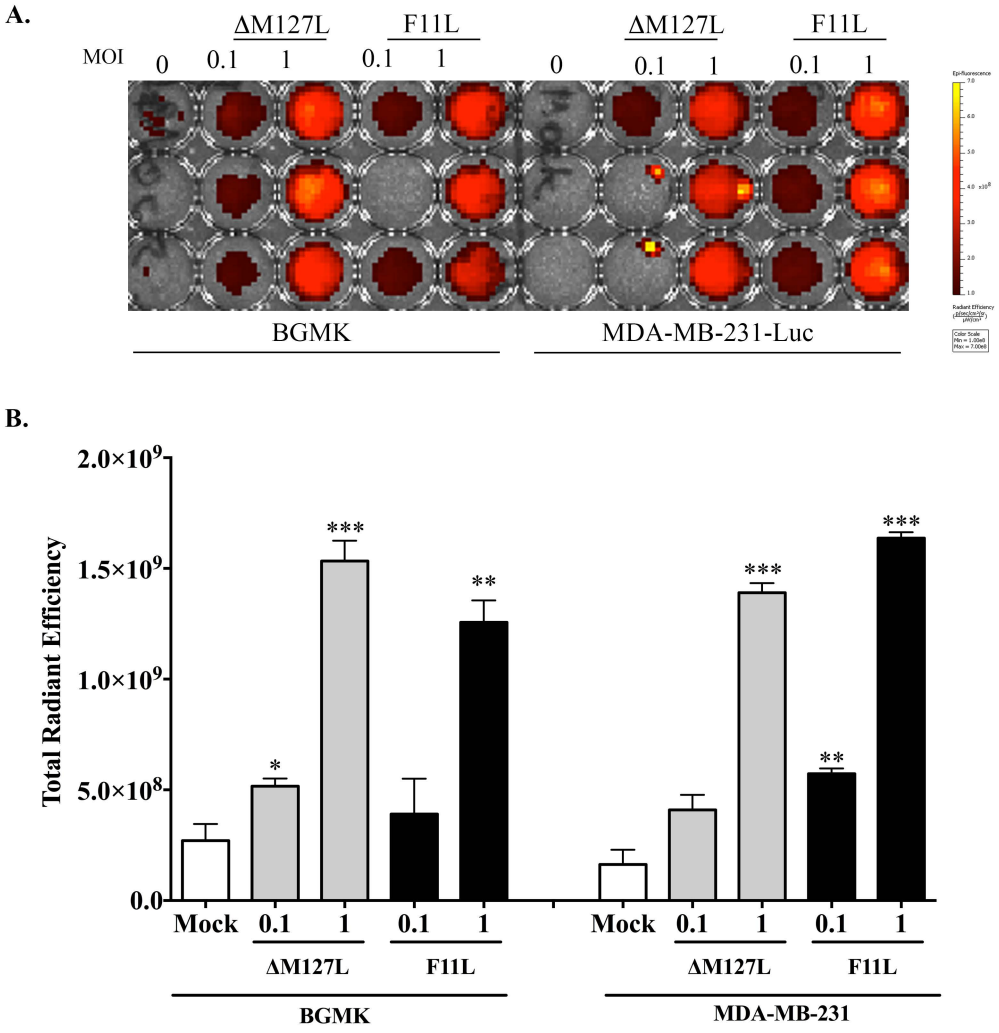

Figure 5.4: *In vitro* analysis of virally expressed β-galactosidase activity following DDAOG addition. A 96-well dish of BGMK or MDA-MB-231 cells was infected with β-galactosidase expressing MYXV at either a MOI of 0.1 or 1, and the infection allowed to proceed for 4 days. At this point DDAOG was added to a concentration of 10μM, and allowed to react for 2 h at 37°C. The plate was then visualized on an IVIS Spectrum imager using filter pairs of 640nm excitation/700nm emission, which span the wavelengths that DDAO (the product of DDAOGs cleavage by β-galactosidase) would be expected to be detected. **(A)** 96-well dish visualized by IVIS imager. (B) Quantification of the total radiant efficiency ([photon/sec]/[μW/cm^2]) of samples from A. Statistical significance reported is relative to the mock control for each cell line.

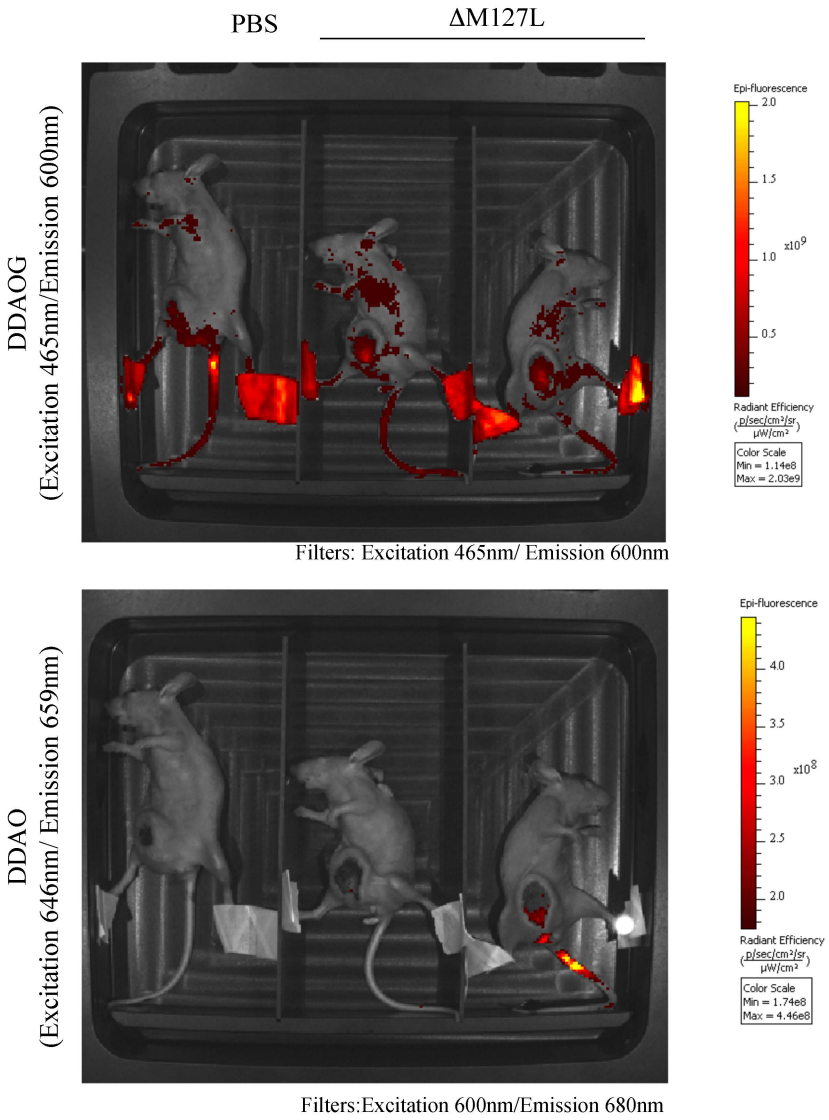

Figure 5.5: IVIS imaging of mice injected with DDAOG: Two mice that had been injected with β-galactosidase expressing MYXV, and one that had received an injection of PBS given 100µl of a 5mg/mL solution of DDAOG via tail-vein injection. After 10 mins mice were anaesthetized and placed on an IVIS imager, after which images were taken at filter combinations that detected either the injected substrate (DDAOG) or DDAO, which is produced upon β-galactosidase cleavage of DDAOG.

different fluorescent proteins: eGFP, mCherry, and/or TrFP. The vMYX-GFP-TrFP virus expresses green fluorescent protein (GFP) under the control of an early promoter, and Tomato Red fluorescent protein (TrFP) under the control of the P11K late viral promoter. This virus was obtained from G. McFadden and has been previously described [255]. The virus encoding an mCherry fluorescent protein (ΔM127L-mCh) was described in Chapter 3.

We took mice that were about to reach experimental endpoints and injected tumors with 2.5×10^7 pfu of virus. These virus were allowed to replicate for three days and then the mice were anaesthized and imaged, using filter pairs that permit the detection of eGFP, TrFP or mCherry fluorescent proteins (**Figure 5.6).** No eGFP or TrFP signals were detected, although this may not be surprising given that both these proteins have emission wavelengths < 600 nm. Caliper has reported that fluorescent proteins emitting at wavelengths <600 nm can be difficult to differentiate from the background, due to fluorescence from hemoglobin. However, we could detect a signal at wavelengths used for detecting mCherry fluorescent protein. This led us to conclude that mCherry-expressing viruses would likely be the best choice for our purposes.

Caliper has reported that the excitation/emission spectrum of many fluorescent proteins may red-shift *in vivo* compared with what is seen in culture. With the guidance of their technical support group, we imaged mice using different filter pairs, and compared the signal to the background signal in mice. This was done by outlining a tumor in a mouse receiving mCherry expressing virus, and determining the average radiant efficiency [p/s/cm²/sr] / [μW/cm²]. This was then divided by the signal detected in a similarly sized tumor from a mouse that did not receive live virus. The results from this analysis are summarized in **Table 5.1**. From these data we determined that an excitation filter of 570nm and emission filter of 680nm gave the best signal-to-background ratios. These wavelengths would be used for subsequent experiments.

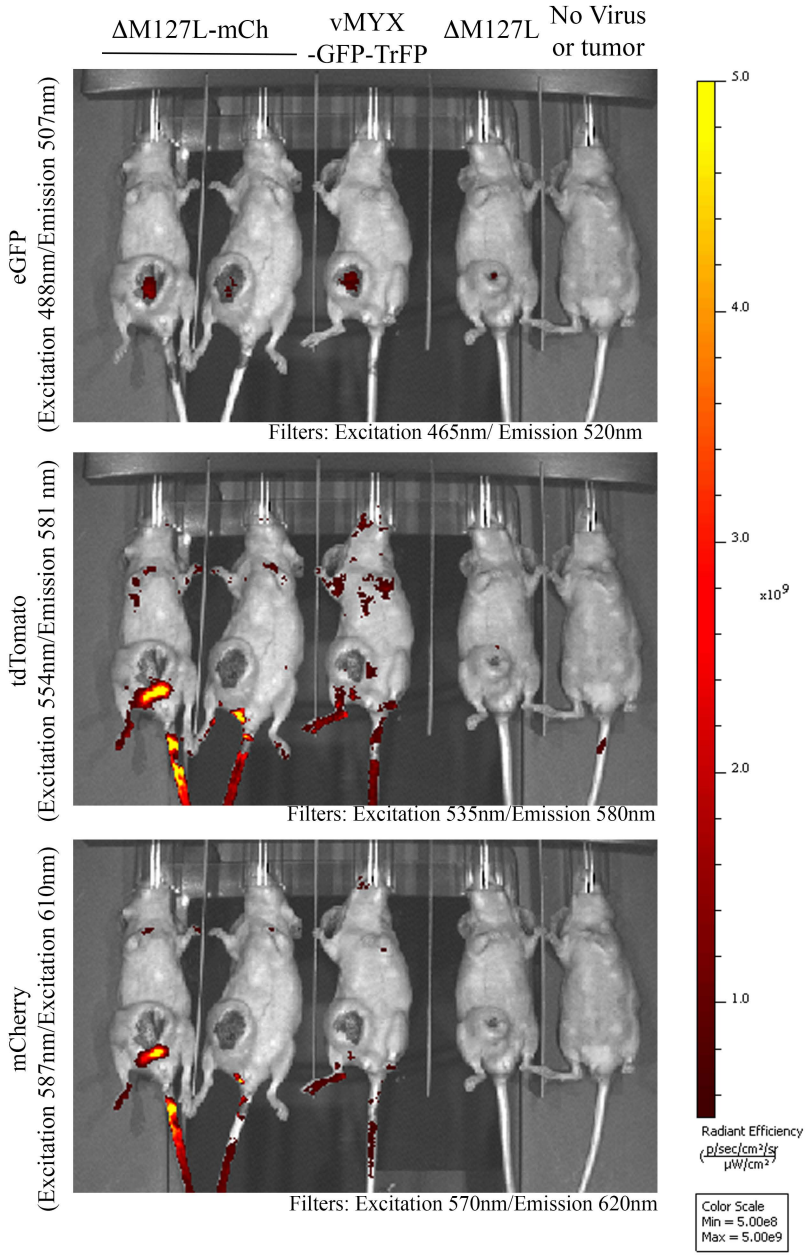

Figure 5.6: IVIS imaging of mice infected with recombinant MYXV expressing mCherry, tdTomato, or eGFP fluorescent proteins: MDA-MB-231 tumor bearing NIH-III mice were injected intratumorally with $2.5x10^7$ pfu of recombinant MYXV that expressed either mCherry or GFP and tdTomato fluorescent protein. After three days, mice were anaesthetized and imaged using filter pairs that detect either GFP, tdTomato, or mCherry. As controls a mouse that received an injection of a MYXV that did not express a fluorescent protein, or that did not have a tumor were imaged in parallel.

Table 5.1: Signal to noise ratio of virally encoded mCherry fluorescent protein at different emission/excitation spectrum [a,b]		
Emission (nm)	**Excitation (nm)**	
	500	570
560	1.45	-
580	1.53	-
600	1.71	-
620	2.03	5.74
640	3.08	4.81
660	2.29	5.55
680	2.82	7.15

[a] The filters used have a cutoff ± 10nm of indicated value

[b] Signal to noise was determined by calculating the ratio of total fluorescence in a tumor of a mouse infected with mCherry to one receiving UV-inactivated virus

5.3 SUMMARY AND BRIEF DISCUSSION:

In this chapter I set out to establish an animal model that would serve as a platform for evaluating the oncolytic efficacy of recombinant MXYV *in vivo*. We chose an orthotopic breast cancer model consisting of immunocompromised NIH-III mice bearing tumors established from human MDA-MB-231 cells. This model was attractive for several reasons: these cells support an intermediate level of MYXV growth, and are not readily cured by MYXV in a subcutaneous model. This should allow the model to differentiate between more or less effective oncolytic viruses.

We initially tested whether 1) MYXV showed any signs of toxicity, 2) whether it was effective at controlling tumor growth, and 3) if there is a minimum effective dose. We found no obvious signs of virus related toxicity. While no instances of a cure was observed in virus-treated mice, a significant delay in tumor growth rates and prolonged survival was observed in mice receiving live virus. This suggested to us that this model

would likely be effective for comparing the relative oncolytic activities of recombinant MYXV.

In addition to determining virus dosing conditions we also optimized the *in vivo* imaging techniques that are used for tracking cancer cells and virus. Although bioluminescent imaging provided an attractive tool for visualizing cancer cells, and can sometimes detects metastases that are not detectable with calipers, there were several problems that prevent its adoption as an alternative to calipers. First therle in the same mouse were issues with reproducibility, in that a luciferase signal was not always detectable in the same mouse from one day of imaging to the next. While we hoped that longer imaging times would alleviate this problem, these occasionally cause the loss of animals held under anesthesia for extended periods. Furthermore, we found that the scabs which formed on some tumors later in these trials sometimes occluded a luciferase signal. Collectively these concerns suggested that luciferase imaging, was not a replacement for caliper measurements, but could still be used to augment it.

We also evaluated how fluorescence could be used to detect virus *in vivo*. We found that a β-galactosidase substrate DDAOG could not be used *in vivo*, probably due to sensitivity and solubility problems. We also evaluated three different fluorescent proteins (eGFP, mCherry, and TrFP) and found that mCherry gave the best signal *in vivo*. Further optimization identified an excitation/emission filter combination that maximized signal-to noise- ratio. Together, these experiments established an animal model for evaluating the oncolytic efficacy of MYXV, and would serve as the basis of the studies outlined in the next chapter.

CHAPTER 6: MYXOMA VIRUS ONCOLYTIC EFFICIENCY CAN BE ENHANCED THROUGH CHEMICAL AND GENETIC DISRUPTION OF THE ACTIN CYTOSKELETON

A version of the data presented in this Chapter was recently submitted.

I was involved in all experiments presented here. Animal related experiments were performed with invaluable assistance from Nicole Favis while all other experiments were solely performed by myself. The first draft of this paper was written by myself, while the final draft had editorial contributions from Drs. Evans and Hitt.

6.1 INTRODUCTION:

While MYXV has shown oncolytic efficacy in a number of tumor models it does not appear to spread well from the site of introduction, a property that would be desirable for the treatment of metastatic cancers. This is best highlighted by a study where experimental gliomas were established in both hemispheres of the brains of nude mice. One tumor was directly injected with MYXV and was eradicated. However, no effect on the second contralateral tumor was observed[282].

It has been reported that the oncolytic efficacy of both VACV and reovirus can also be improved by increasing the abilities of these viruses to spread. Mutations in reovirus capsid proteins λ2 and σ1 proteins create virus variants that are more effective at controlling B16 melanomas in C57B/L6 mice[299]. Introducing a K151E point mutation into the VACV A34R gene has been shown to increase the efficacy of VACV in controlling tumor growth, in a number of models, and improves spread to tumors distant from the site of introduction[300,301]. This allele is naturally found in the IHD strains of VACV and causes increased production and dissemination of the EV form of VACV[179]. EV have been implicated in the intra-host spread of VACV (see section 1.8).

Since our F11-expressing MYXV, described in Chapter 3, would be expected to produce more EV, we asked the question: would MYXV encoding F11L be a more effective oncolytic virus? The work presented in this chapter investigates this possibility. Furthermore, given that F11 has been shown to disrupt the actin cytoskeleton through an inhibition of RhoA-mDia1 signaling, we tested whether disrupting the actin cytoskeleton, either through chemical or genetic approaches, could enhance the growth of MYXV in cancer cells.

6.2 RESULTS:

6.2.1 F11-expression Alters the Actin Cytoskeleton of MYXV-infected MDA-MB-231 Cells:

We started this work by investigating whether effects of F11 on the morphology of highly-permissive cells (Chapter 3) could also be seen in an MDA-MB-231 cancer cell line. We chose this cell line for the reasons presented in Chapter 5. MDA-MB-231 cells were infected with WT, ΔM127L-mCh, and F11L-mCh MYXV strains and western blots used to demonstrate expression of F11 and mCherry. The levels of mCherry expression also varied little between the ΔM127L-mCh and F11L-mCh viruses **(Figure 6.1A)**.

Similar to the observations made in other cell types (RK13, SIRC, BGMK and primary rabbit cells), we found that the actin cytoskeleton in MYXV-infected MDA-MB-231 cells was selectively altered by a recombinant MYXV encoding F11L. At early times in infection (8 h post-infection) we saw that F11L-mCh infected cells exhibited a decrease in central actin stress fibres when compared to cells infected with ΔM127L-mCh (3.4 ± 0.3 fibres per cell *versus* 10.3 ± 0.1 fibres per cell; $P<0.001$) **(Figure 6.1C)** Furthermore, these F11L-mCh infected cells were more rounded and smaller, with a surface area ~ 60% of that of all other cells. As I saw in other cell lines the WT and ΔM127LmCh infected cells had a similar surface area to those observed in uninfected cells(**Figure 6.1D).**

We also observed that at late times in infection (20 h) there was a significant increase in the number of actin projectiles formed by the F11L-mCh virus, when compared to ΔM127L-mCh infected cells (1.1±0.1 actin projectiles per cell *versus* 0.3±0.06; $P<0.001$) (**Figure 6.1E).** Analysis of the amount of virus released into the media was also performed at 24 h post-infection. While the total amount of virus released was lower than that observed with similar experiments performed in Rk13 cells (Chapter

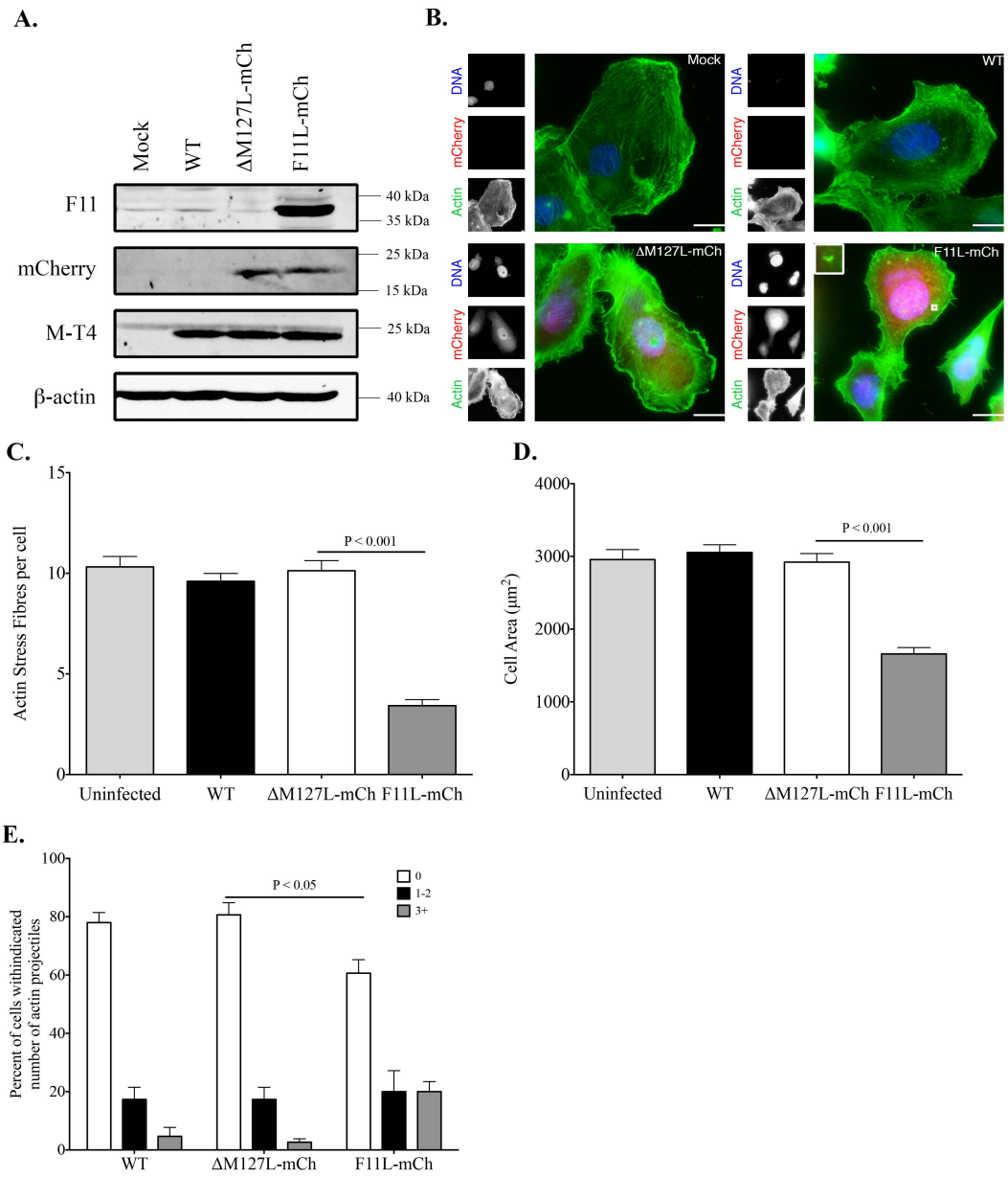

Figure 6.1: F11-dependent alterations in the structure of the actin cytoskeleton of MYXV infected MDA-MB-231 cells. (A) Western blot analysis of cells infected with the viruses used in this study. MDA-MB-231 cells were infected with the indicated viruses at MOI=10, harvested 6 h post-infection, and western blots used to detect virus-encoded F11 and mCherry, a MYXV gene product (M-T4), and cellular β-actin. **(B)** Fluorescent microscopy of MYXV-infected cells. MDA-MB-231 cells were infected with the indicated viruses at MOI=10, and fixed 20 h post-infection. The cells were stained with AlexaFluor 488-phalloidin or DAPI, to visualize actin and DNA, respectively and imaged at 60× magnification. **(C)** Effect of infection on actin stress fibers. The number of actin stress fibers in cells infected with the indicated viruses was determined at 8 h post-infection. **(D)** Effect of F11 on the cell area of MYXV infected cells at 8 h post-infection. **(E)** Effect of F11 on the frequency of actin projectile formation by MYXV. The percentage of infected cells at 20 h post-infection with a given number of actin projectiles. The data shown were generated from three experiments, and 50 cells analyzed in each experiment (n = 150). Actin projectiles are not common in MYXV-infected cells, one is shown enlarged (inset) in the bottom right-corner of panel B.

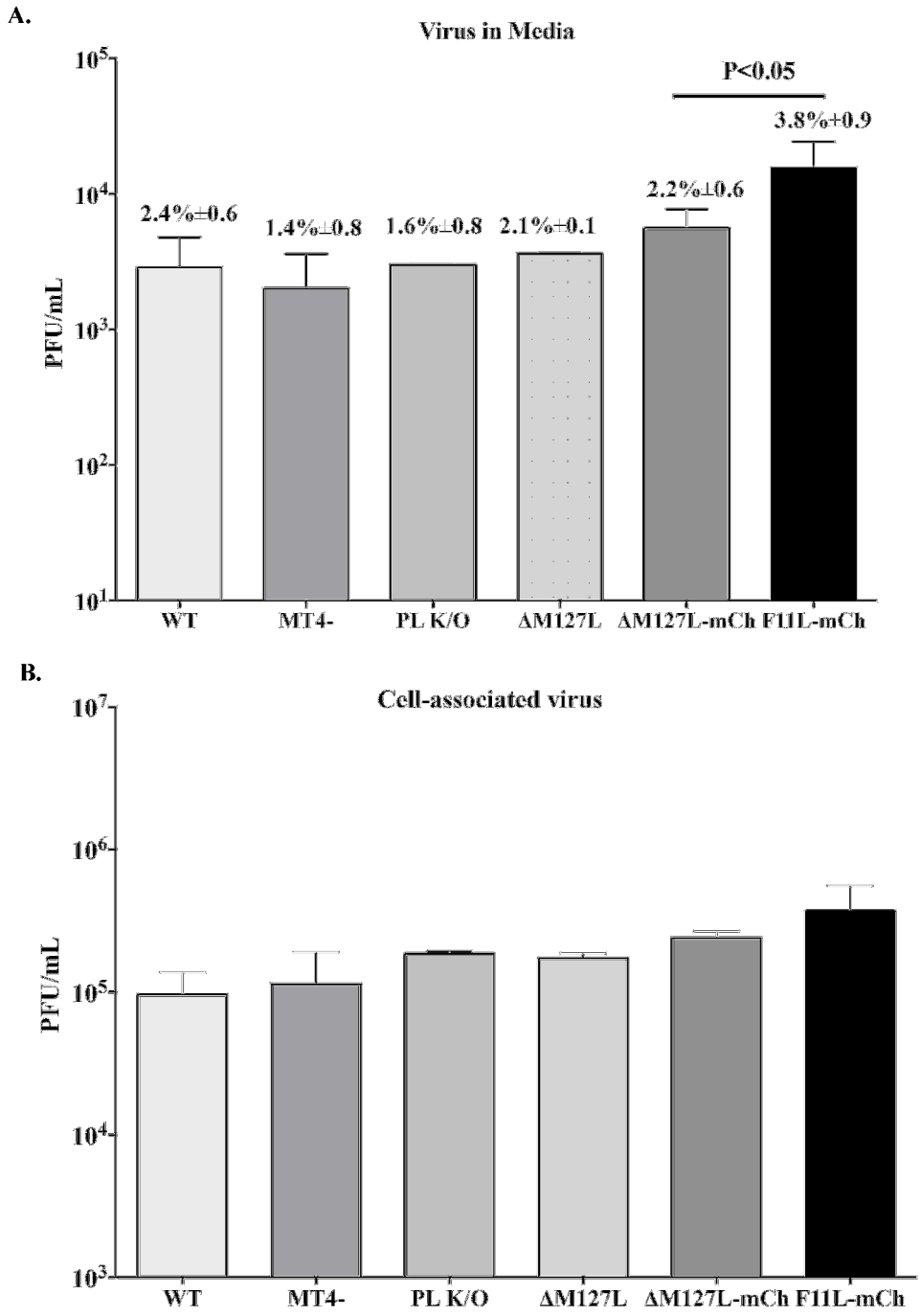

Figure 6.2: Effect of F11L on release of virus from MDA-MB-231 cells. MDA-MB-231 cells were infected at a MOI=5 with respective viruses. After 24 h, media was removed, centrifuged to remove any cellular debris and titered. The values from these represent the media fraction (panel A). The cellular monolayer was harvested into PBS, subjected to three freeze-thaw cycles, and titered (Panel B). These numbers were then used calculate the fraction of total virus that was in the media, which is listed as mean percent plus S.E.M. above the respective virus in panel A.

3) we found that the presence F11L increased the percentage of virus released into the medium of MDA-MB-231 cells. **(Figure 6.2).**

6.2.2 Drugs can be Used to Mimic the Effects of F11L on MYXV Growth in MDA-MB-231 cells:

In order to spread efficiently VACV must balance the needs to disrupt cortical actin (to promote EV exit), while ensuring the availability of actin for other processes (i.e. actin projectiles). Important insights into these processes have been provided through the use of chemical inhibitors like cytochalasin D [143,312] and latrunculin B [143]. While high concentrations of latrunculin B are detrimental to VACV release, low concentrations are stimulatory and can overcome the inhibitory effects of using dominant negative RhoA mutants [143]. Since F11 seems to act similarly to low concentrations of latrunculin B, we sought to see if we could use this compound to mimic the effects of F11. MDA-MB-231 cells were infected with the different viruses, cultured in the presence of latrunculin B, and the virus progeny titered. We saw that treating cells with low amounts of latrunculin B significantly increased the yields of WT and ΔM127L-mCh MYXV, but had no additional effects on the yield of the F11L-encoding strain **(Figure 6.3).** We also observed that treating cells with 0.1 μM latrunculin B enhanced the percentage of WT and ΔM127L-mCh infected cells with actin projectiles, but had little effect on F11L-mCh infected cells (**Figure 6.3).** Much as has been observed in VACV-infected cells [143], higher concentrations of latrunculin B (1 μM) appeared to reverse this increase in growth, although it is likely that this higher concentrations are toxic to the cells **(Figure 6.3).**

We next tested whether disrupting RhoA signaling could also enhance MYXV growth. Active RhoA signals primarily to two effectors: ROCK and mDia1 (See section 1.3). While F11 binds to RhoA and presumably disrupts both pathways, the disruption of the mDia1 branch seems more important for virus release[204,205,224]. Consistent with observations in VACV, we found that the use of the ROCK inhibitor Y-27632 had little

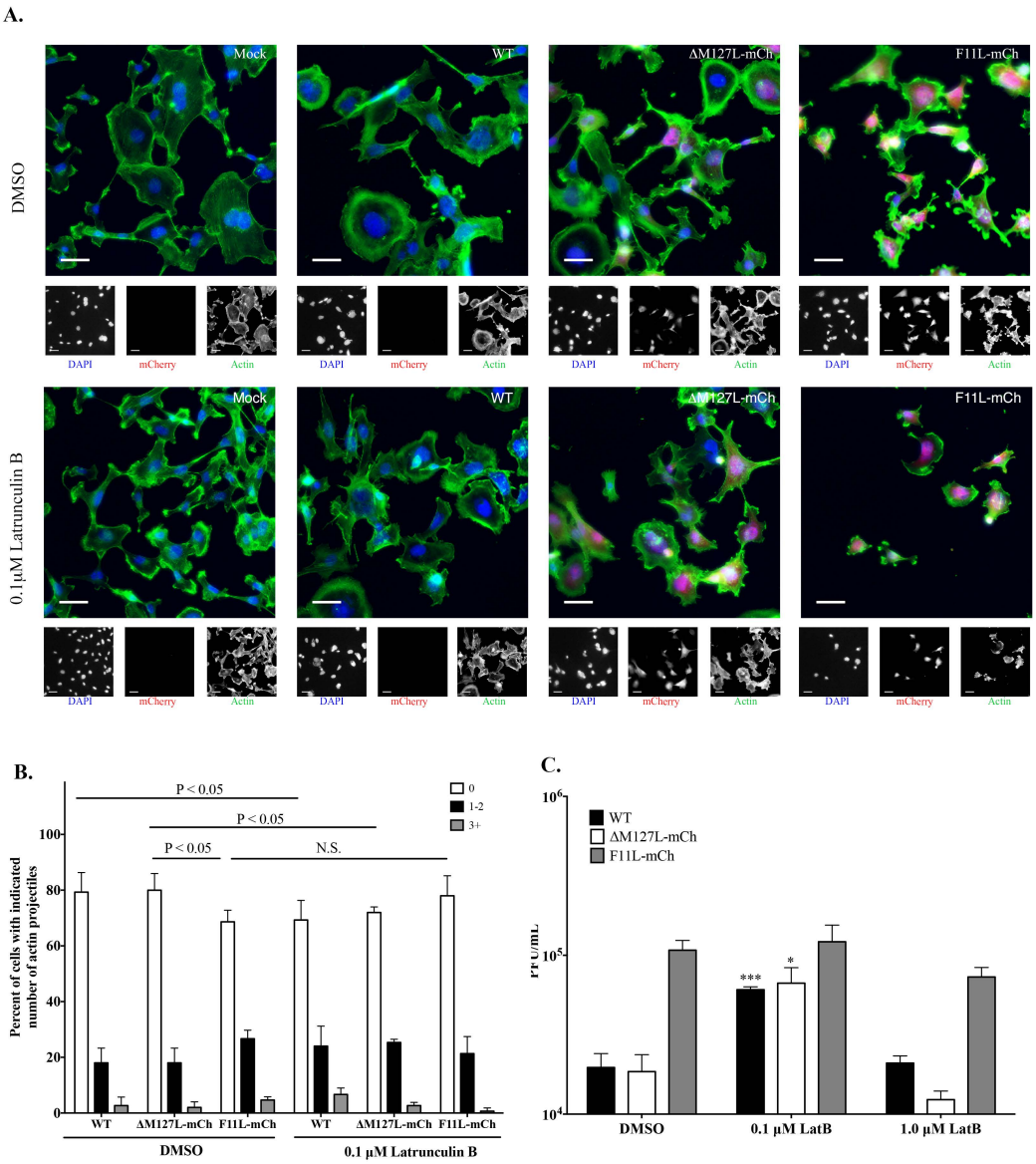

Figure 6.3: Effect of latrunculin B on MYXV: (A) Effect of latrunculin B on actin structures in MYXV-infected MDA-MB-231 cells. MDA-MB-231 cells grown to sub-confluency on glass coverslips and then infected with the indicated viruses at MOI=10. The cells were cultured for 8 h, the media replaced with fresh media containing 0.1 µM, 1.0µM latrunculin B, or the DMSO solvent, and the cells incubated for another 12 h and then fixed. Cells were then stained for actin and DNA and visualized at 20 x magnification. Note that due to toxicity the 1.0 µM latrunculin B samples could not be visualized **(B)** Quantification of actin projectiles from Panel A. The graph shows the mean percentage of cells (±S.E.M) exhibiting 0, 1-2, or ≥ 3 actin projectiles per cell. The results were compiled from three independent experiments, analyzing 50 cells per experiment (i.e. n=150). **(C)** Effect of latrunculin B on MYXV growth. MDA-MB-231 cells were infected with the indicated viruses at MOI=0.1. Eight hours later the media was replaced with fresh media containing 0.1 µM or 1 µM latrunculin B (or a DMSO control), cultured 48 h, and the resulting virus harvested and titered, the results from three independent experiments are shown.

effect on MYXV yields and actin projectile formation (**Figure 6.4).** This was despite the appearance of cellular projections consistent with ROCK inhibition.

We also used siRNA-mediated gene silencing to see what effect inhibiting other elements of the Rho signaling pathway might have on MYXV growth. We found that depleting cells of RhoA or mDia1 enhanced the growth of WT and ΔM127L-mCh viruses relative to that in cells treated with a non-targeting siRNA control, but had little effect on the growth of MYXV expressing F11L (**Figure 6.5)**. Western blots confirmed the effects of the two different siRNAs used to target each gene **(Figure 6.5).** We also examined the effect of RhoC and LIMK2 depletion on MYXV growth. Although they display differences in their downstream effects on cell morphology and migration, RhoA and C both bind mDia1 and promote the formation of actin stress-fibres ([44], reviewed in [22]). In a recent genome-wide screen, we identified LIMK2 as a gene that when silenced, appeared to promote MYXV growth in MDA-MB-231 cells (mDia1 was also identified in this screen)[290]. Activation of LIMK2, which is downstream of Rho and ROCK, has been shown to promote actin polymerization and actin stress fibre formation. This is due to LIMK2 phosphorylating and inactivating cofilin, thus preventing actin depolymerization [313]. Furthermore, the actin cytoskeleton of MDA-MB-231 cells can be disrupted by siRNA knockdown of LIMK2 [314]. We observed that silencing of RhoC and LIMK2 also caused an increase in the growth of WT and ΔM127L-mCh viruses with little effect on $F11L^+$ MYXV (**Figure 6.5)**. Together, these data suggest that MYXV growth can be enhanced by disruption of the actin cytoskeletal architecture using either pharmacological inhibitors, siRNA-dependent gene silencing, or by expressing a VACV-derived transgene (F11L).

6.2.3 Effect of F11L on MYXV Growth in Cancer Cells:

In Chapter 3 I showed that F11-expressing MYXV grows to approximately 5-fold higher titers in cell-lines which support high levels of MYXV growth (BGMK,

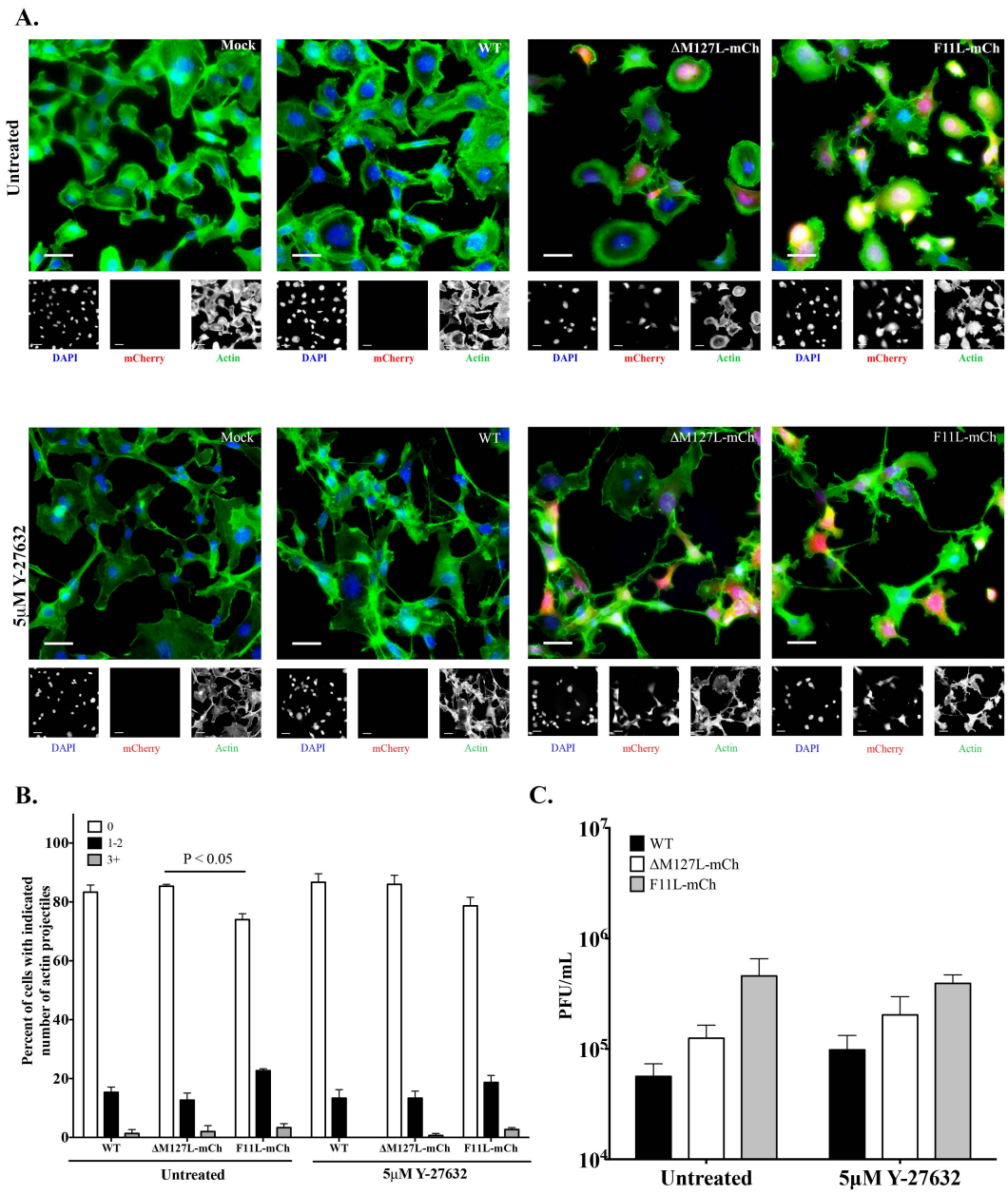

Figure 6.4: Effect of the ROCK1 inhibitor Y-27632 on MYXV: (A) Effect of Y-27632 on actin structures in MYXV-infected MDA-MB-231 cells. MDA-MB-231 cells were cultured and infected, after 4 h cells were the media was replaced with fresh media containing 0mM or 5mM drug and the infection allowed to proceed for an additional 16 h, after which cells were fixed and stained with AlexaFluor488-phalloidin or DAPI. Cells were then imaged at 20x magnification using a personal Delta-vision microscope. (B) Quantification of actin projectiles from Panel A. The graph shows the mean percentage of cells (±S.E.M) exhibiting 0, 1-2, or ≥ 3 actin projectiles per cell. The results were compiled from three independent experiments, analyzing 50 cells per experiment (i.e. n=150). (C) Effect of Y-27632 on MYXV growth. MDA-MB-231 cells were infected with indicated viruses at a MOI of 0.1. Four hours later media was replaced with fresth media contain either 0mM or 5mM Y-27632. Two days later virus was harvested and titered on BGMK cells. The mean plus S.E.M. from three independent experiments are shown.

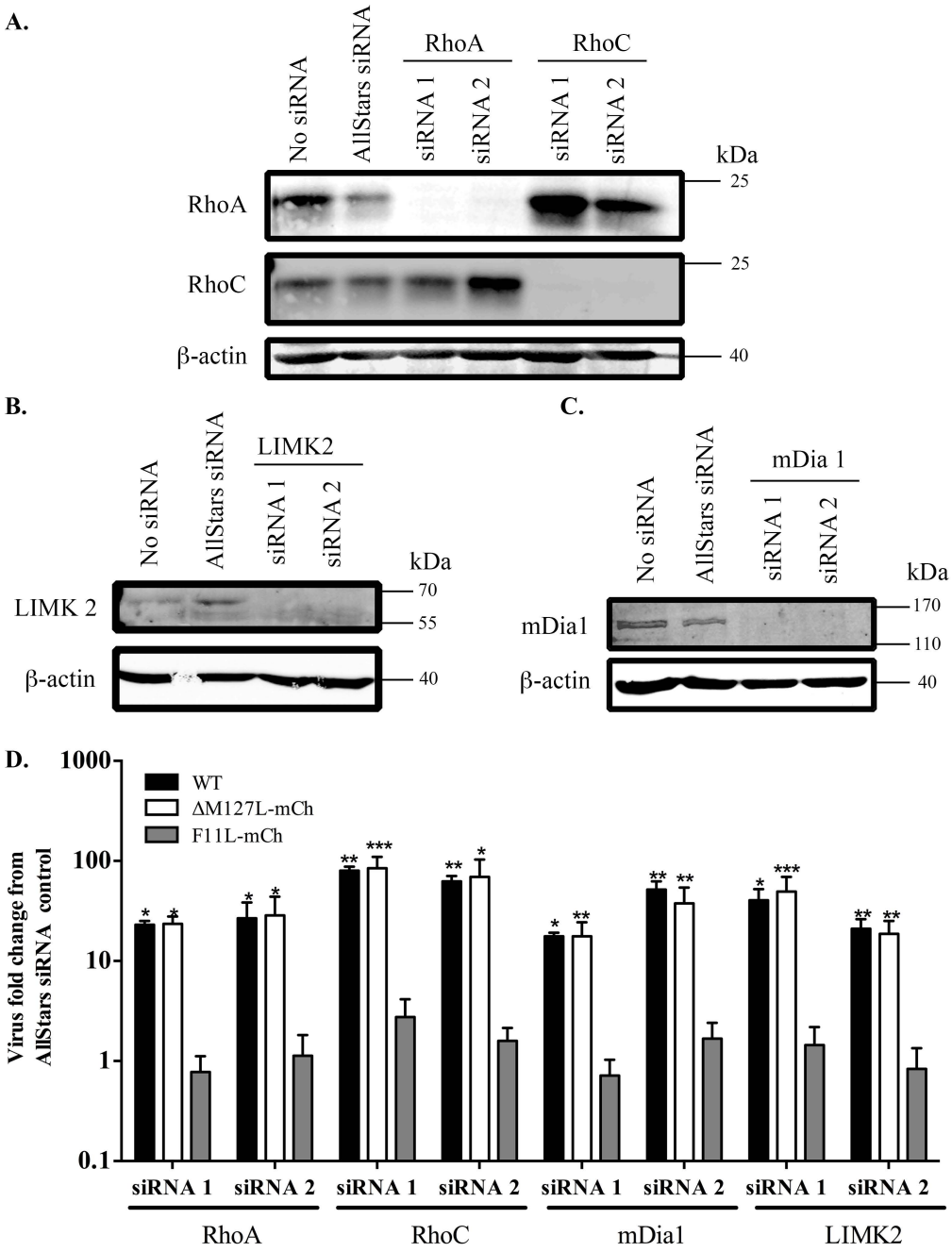

Figure 6.5: Effect of siRNA-mediated silencing of key regulators of the actin cytoskeleton on MYXV growth in MDA-MB-231 cells. MDA-MB-231 cells were transfected with the indicated siRNAs for 48 h, and then infected with virus at MOI=0.1. Two days later, the viruses were harvested and titered. For each siRNA treatment, we report the yield of virus measured relative to the amount of virus produced in cells that were transfected in parallel with a non-targeting AllStars siRNA control. **(A-C)** Demonstration of siRNA-mediated knockdown of protein expression by western-blot analysis. MDA-MB-231 cells were transfected with the indicated siRNAs and cultured for 48 h. The cells were then harvested, lysed and western blotted using antibodies directed against RhoA and RhoC **(A)**, mDia1 **(B)**, and LIMK2 **(C)**. **(D)** Change in virus levels in siRNA-treated sample relative to the virus levels in cells treated with AllStars siRNA control. The mean plus S.E.M. from three independent experiments are shown. Statistics shown compare the yield for each virus with those obtained in AllStars treated samples.

RK13, and SIRC). We wanted to see if this was also true in cancer cell lines, which normally support lower levels of MYXV growth. For this, a panel of cancer cells [10 human cancer cells, 1 murine (MTHJ) and 1 rat (AY-27)] was screened for changes in 1) viral yields and 2) plaque morphology. Hek293T and BGMK cells were also screened in these comparisons. To examine viral yields, cells were infected at a MOI of 0.01 and virus harvested at 24, 48, 72, and 96 h post-infection. The virus was then titered on BGMK cells (**Figure 6.7).** In almost all situations, F11-mCh MXYV grew better than WT or ΔM127L-mCh. Interestingly, this effect varied from cell line to cell line, with some cells (e.g. U87-MG) behaving much like BGMK cells and promoting ~5-fold increase in viral yield, whereas in other cell lines (e.g. MCF 7) the effect was much greater (~30-fold). Importantly, the F11L gene did not enhance virus growth in cells that are normally non-permissive for MYXV, such as HeLa or MTHJ, although it did stimulate sufficient growth in "non-permissive" lines like Daoy or Capan2 to create the appearance of a change in host range.

To complement these virus yield assays, we also looked for differences in virus spread on these cancer cell lines by infecting cells at a MOI of 0.1, allowing the infection to proceed for 96 h before fixing cells and staining them for viral β-galactosidase activity via X-Gal staining (**Figure 6.8).** In cell lines that appeared to show a change in host range from viral yield experiments, plaques were observed with all strains of MXYV. Furthermore, a greater number of $LacZ^+$ cells were observed in monolayers infected with F11L-mCh, when compared to WT or control strains, suggesting enhanced spread.

Rho signaling proteins are often up-regulated in cancer cells and so I wanted to see if there was a correlation between the effects of F11L on MYXV growth, and the levels of these proteins. Western blot analysis showed that the expression of RhoA and C varied greatly across cell lines. However, we did not find any obvious correlation between the effects of F11 on MYXV growth, and the levels of RhoA or RhoC, or any of

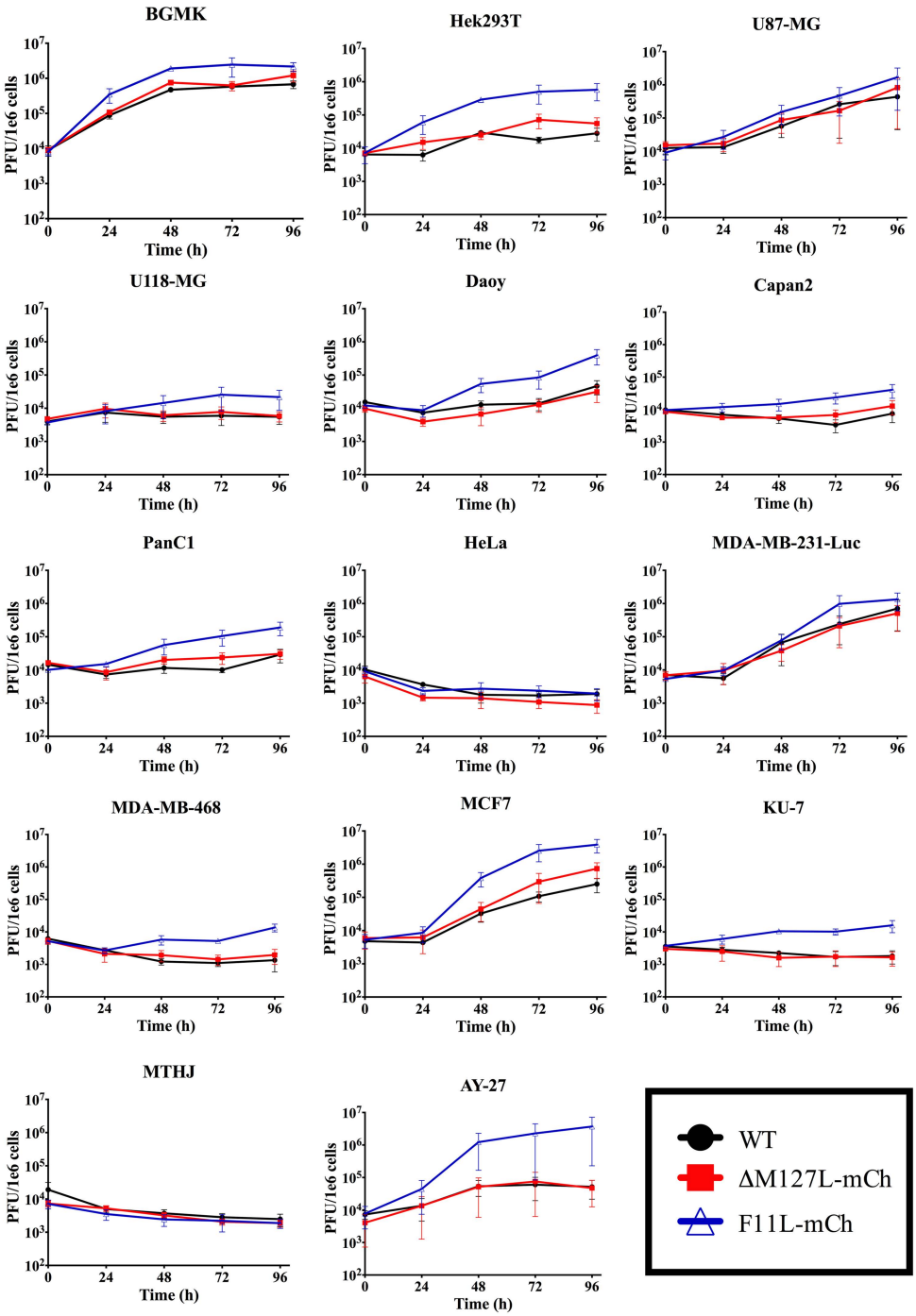

Figure 6.6: Effect of F11L expression on MYXV growth in cancer cells in low MOI condidtions. A panel of cancer cells were infected at a MOI of 0.01. At indicated times virus was harvested and titered on BGMK cells. The mean titer plus S.E.M., as normalized to PFU/1e6 cells, from three independent experiments are shown.

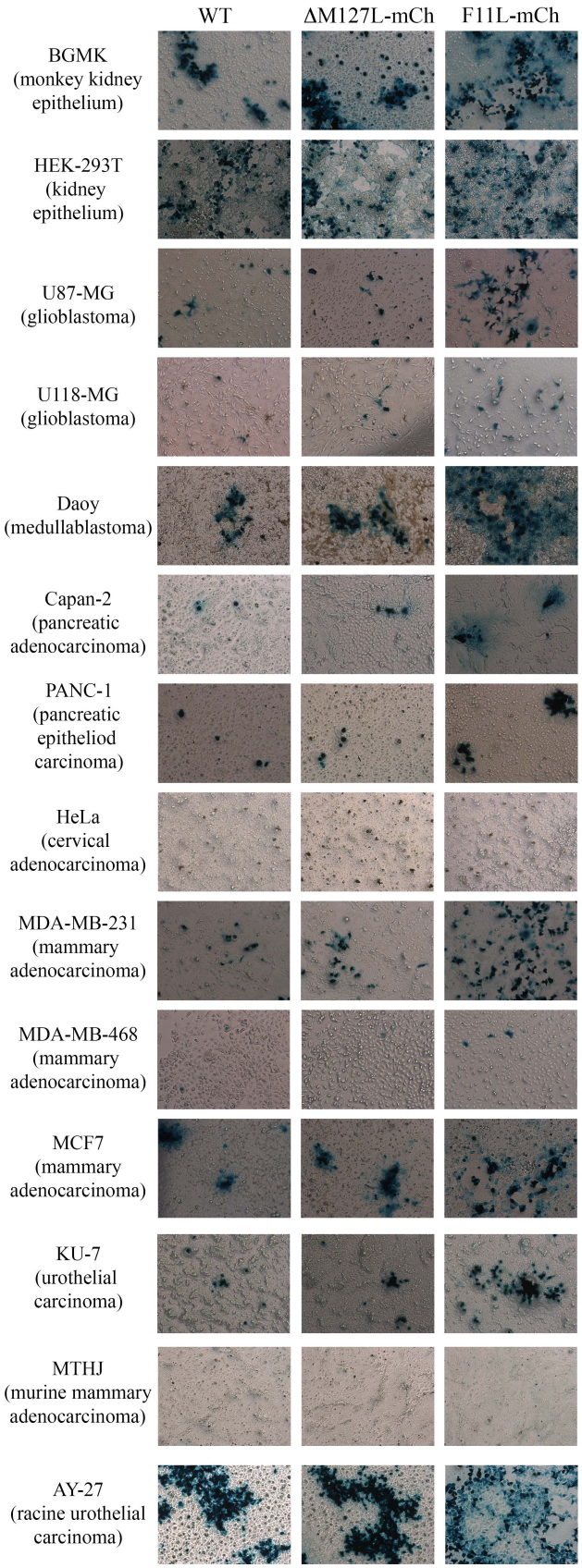

Figure 6.7 Effect of F11L expression on MYXV plaquing properties in a panel of cancer cells: Cells were infected at a MOI = 0.1 with respective viruses and the infection allowed to proceed for 96 h, after which cells were fixed and stained for virus β-galactosidase activity using X-Gal. Cells were then imaged using a Ziess axioskop II at 2.5 X magnification.

their downstream effectors (mDia, ROCK1, Ezrin, LIMK2 or cofilin). **(Figure 6.8)**. This may not be too surprising since we looked at the total levels of these proteins and not the GTP-bound active levels of RhoA or RhoC. F11 is known to bind the GTP-bound active form of RhoA [205].

We also wanted to test whether the F11L dependent increase in virus growth would lead to increased virus-mediated killing of cancer cells. For this, cell viability assays were performed, where 96-well dishes were infected with varying amounts of virus and the cell-viability measured using Alamar blue dye (**Figure 6.9)**. The effect of F11L on MYXV-mediated cell killing varied greatly by cell line and by MOI. In a U87-MG, Daoy, Capan2, PanC1, HeLa, MDA-MB-468, KU-7, or MTHJ cell lines there was no significant difference in the viability of cells infected with F11L-mCh, when compared to WT or ΔM127L-mCh viruses. A significant F11L-dependent decrease in cell viability was observed in BGMK, Hek293T, U118-MG, MDA-MB-231, MCF7, and AY-27 cell lines). These differences tended to be at MOIs where a relatively high fraction, but not all cells, where initially infected (i.e. MOI of 0.1-1).

6.2.4 MYXV F11L-mCh Better Controls Tumor Growth in Xenografted Animals:

These observations lead us to speculate that the F11L expressing MXYV may be more effective than WT MYXV at controlling tumors *in vivo*. To test this hypothesis, we used the xenografted tumor model described in Chapter 5. Once tumors were palpable, three intra-tumoral injections of virus (1×10^6 pfu/injection) were administered over the course of five days. Tumor size was then monitored by caliper measurements. In comparison to mice that received UV-inactivated virus, the tumors grew at significantly slower rates in mice receiving live virus. Furthermore, the tumors of mice treated with F11L-mCh virus grew more slowly than those receiving ΔM127L-mCh virus , with the differences in tumor volume becoming significant by ~ 45 days post implantation **(Figure 6.10A).**

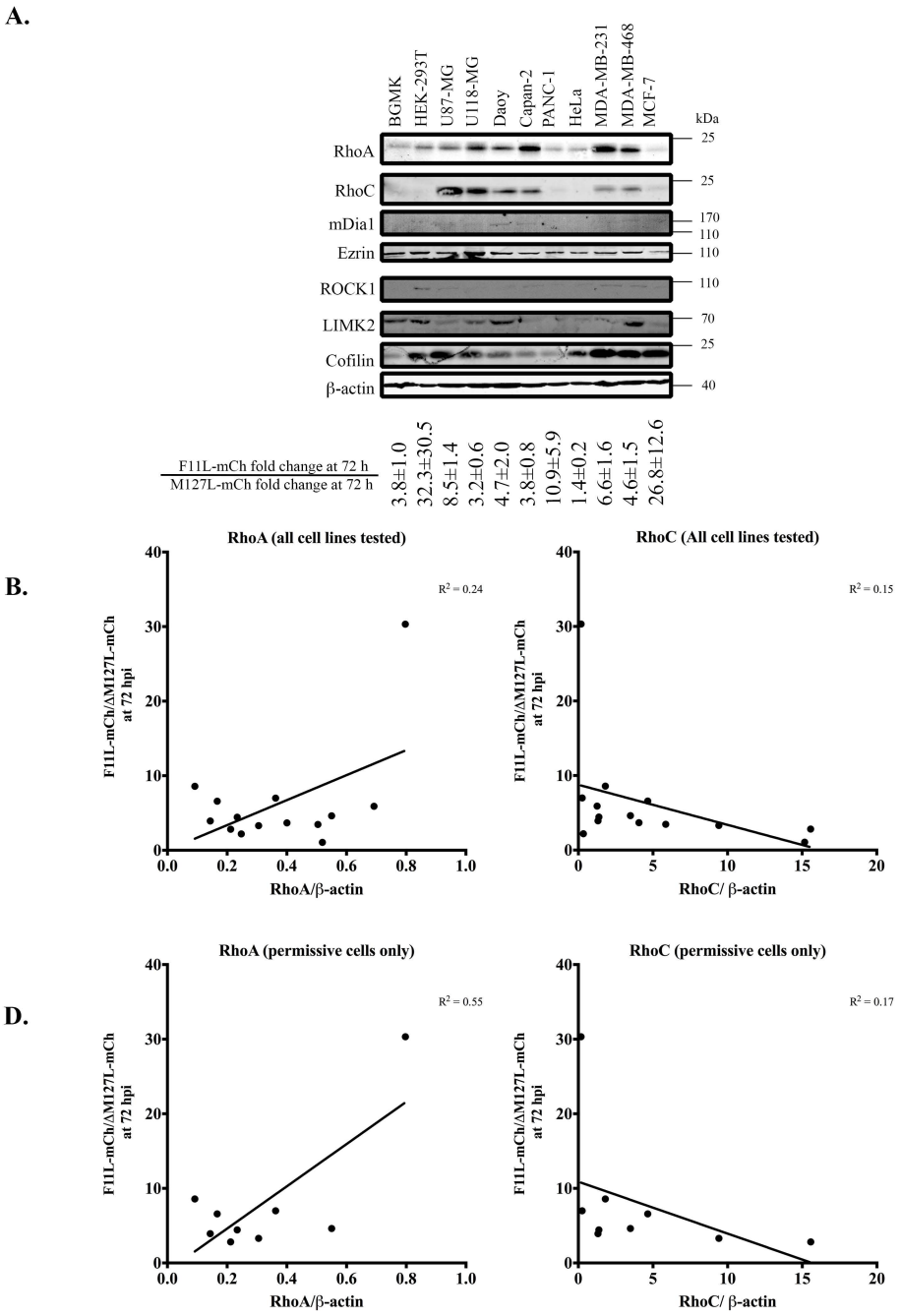

Figure 6.8 : Relationship between cellularproteins linked to actin regulation and the effect of F11L on MYXV growth in cancer cells. (A) Western blot analysis of cancer cell lines. The cells indicated were grown to sub-confluency in the absence of virus, harvested, lysed, and 20 μg of total protein separated using SDS-PAGE gels. Western blotting and infrared imaging was then used to measure the levels of the indicated proteins. The figure also shows the mean fold differences in virus yield at 72 h (±S.E.M.) when F11L-mCh and ΔM127L-mCh were grown on each cell line. These values were calculated from data presented in Figure 6.6. **(B-E)** Correlation between the levels of total RhoA or RhoC (relative to β-actin) and the fold differences in titers observed between F11L-mCh and ΔM127L-mCh at 72 h post-infection. Panels B and C examine all cell lines tested in Figure 6.6. Panels D and E examine only cell lines that supported productive replication of both viruses.

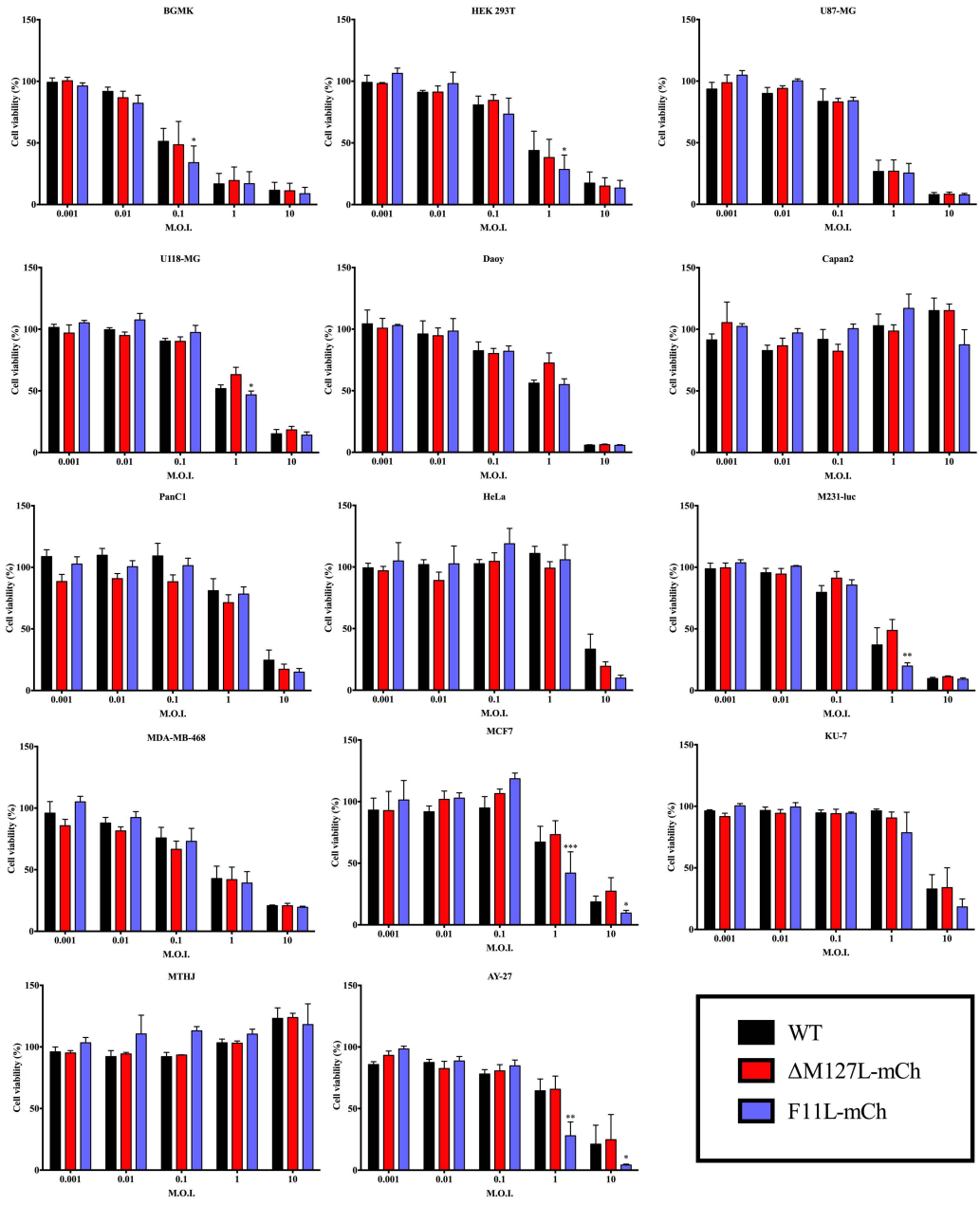

Figure 6.9 Effect of F11L expression on cell-mediated killing of cancer cells by MYXV: 96 well dishes of cells were infected at varying MOIs of virus. The infection was allowed to proceed for 96 h, after which cells were incubated with alamar blue (resaurin salt) for 2 h at 37°C. A Fluorostar Optima plate reader was then used at 544nm excitation/590nm emission filters to read fluorescence generated by live cells metabolizing alamar blue. Signal was then normalized as a percentage of the signal obtained from uninfected cells. The mean plus S.E.M. from three independent experiments are shown. Significance shown represents the comparsion of F11L-mCh infected cells with those infected by ΔM127L-mCh (by two-way ANOVA with Bonferroni post-test)

This delay in tumor growth, translated into a significant increase in the median survival of mice treated with F11L-mCh (86 days post-implantation *versus* 68 days for the ΔM127L-mCh virus; P = 0.015). In contrast, mice receiving UV-inactivated virus had a median survival of 59 days post-implantation, which was significantly different from the mice treated with ΔM127L-mCh (P=0.019) and F11L-mCh (P=0.0001) viruses (**Figure 6.10B).**

Although caliper measurements proved to be much more accurate at tracking tumor size than bioluminescent imaging, we still made some use of the IVIS Spectrum small animal imager to track cancer cells *in vivo*. In this instance mice were imaged only once at 21 days post-tumor implantation for luciferase activity. This was 10 days after the first virus injection. A representative image showing three mice for each group is presented in **Figure 6.11A.**

In contrast to the difficulties that were encountered using luciferase imaging, mCherry imaging of virus appeared to be much more reliable. This is possibly due to the fact that a substrate need not be injected. We found that a mCherry signal was detectable on the first day we imaged, 4 days after the first virus injection. Quantification of this signal showed that there were significantly higher levels of mCherry fluorescence detected in the tumors of F11L-mCh treated mice. About 10 days later the mCherry fluorescence in the ΔM127L-mCh infected mice reached similar levels to those seen in mice infected with F11L-mCh virus. The two viruses then continued to express similar levels for another approximately three weeks. At this point the mCherry levels started to wane and in some cases disappear **(Figure 6.11B).** However, the F11L-mCh virus did seem to persist longer in the treated mice, with one mouse still exhibiting a mCherry signal (and detectible virus in plaque assay) when it reached experimental endpoint 155 days after tumor implantation.

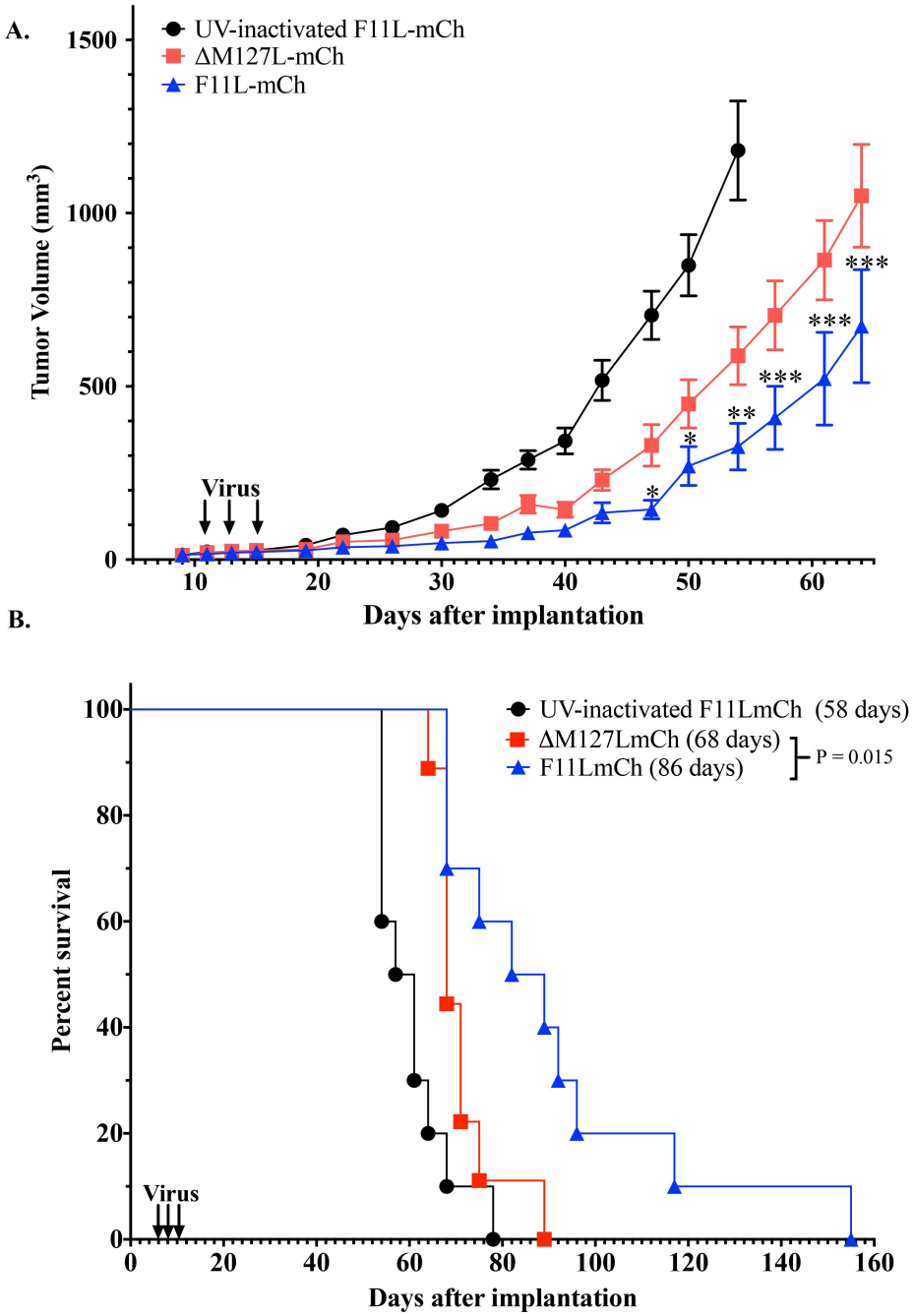

Figure 6.10: F11L expressing MYXV promotes delayed tumor growth and prolongs survival of NIH-III mice bearing xenografted MDA-MB-231 tumors. Luciferase-tagged MDA-MB-231 human breast cancer cells were used to establish tumors in the mammary fat pads of NIH-III mice. Once the tumors were palpable, mice were treated with three intratumoral injections of the indicated mCherry-tagged MYXV (1×106 pfu per injection) administered over a five-day period (9-10 mice per group). **(A)** Tumor growth. Tumor size was measured twice-weekly using calipers and shows the mean tumor volume ± S.E.M.The statistics shown compare the live ΔM127L-mCh and F11L-mCh groups (by 2-way ANOVA). **(B)** Kaplan-Meier survival plot. The fraction of animals surviving at each time point is indicated as well as the median survival times for each cohort (inset). Survival curve comparisons were calculated using the Log-Rank (Mantel-Cox) test built into Prism's software.

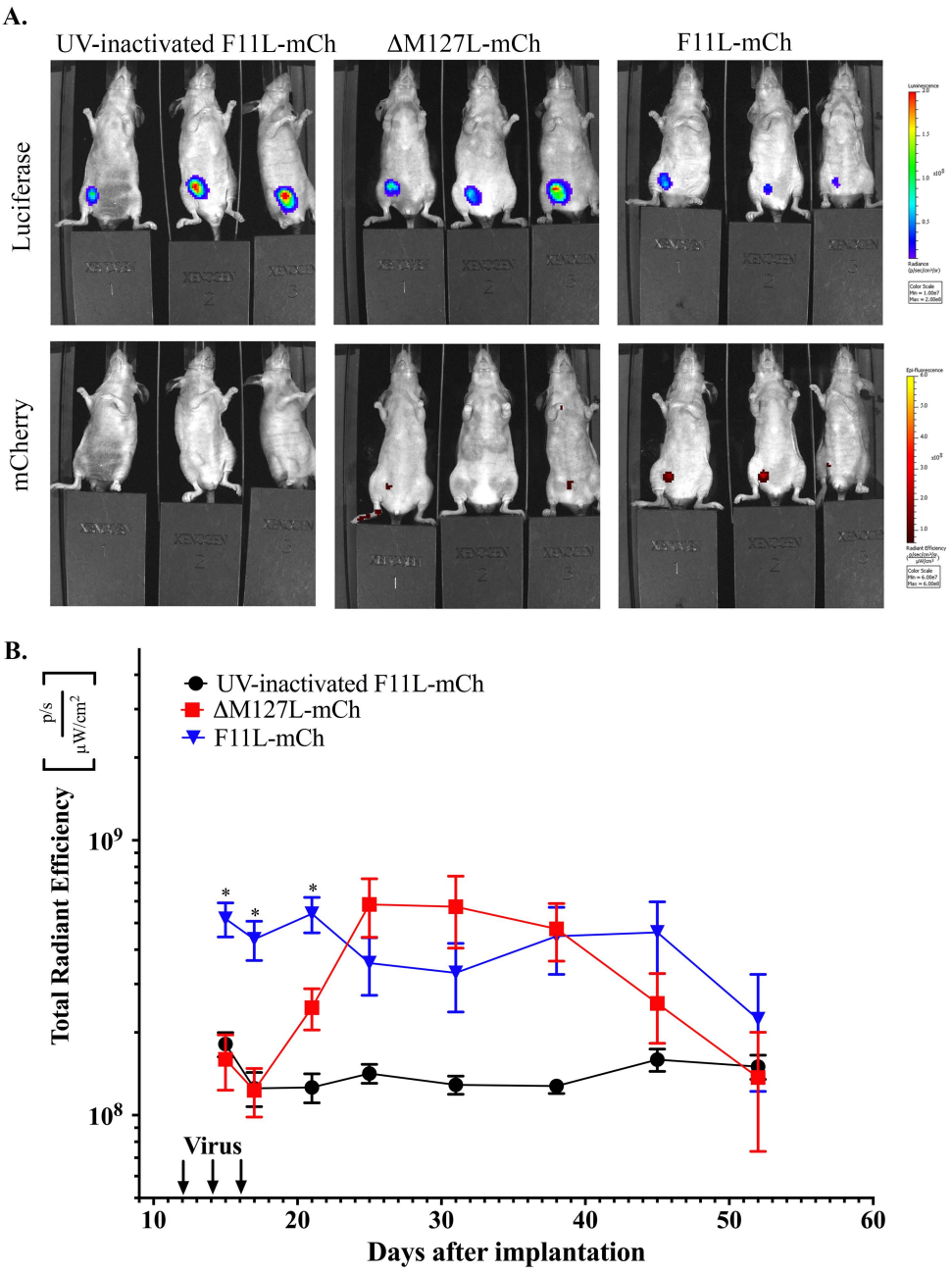

Figure 6.11: Comparison of mCherry expressing recombinant MYXV by IVIS imager: An IVIS Spectum small animal imager was used to follow the same cohort of mice presented in figure 6.10 for cancer cell expressed luciferase activity, or virally expressed mCherry fluorescent protein. **(A)** Representative images of mice at day 21 (10 days after the first virus injection) for luciferase activity (tumor) and mCherry fluorescent protein (virus) **(B)** Quantification of mCherry fluorescent protein signal over time using IVIS imager. Starting at 4 days after the first virus injection, the total radiant efficiency of mCherry signal in tumors were measured for mice at regular intervals until the first UV-inactivated mouse reached endpoint (as determined by caliper measurements) mCherry signal was measured using excitation and emission filters of 570nm and 680nm, respectively.

6.2.5 MYXV F11L-mCh is More Effective at Spreading Between Tumors and Controlling the Growth of a Second Site Tumor:

Lastly, we wanted to see if the superior tumor control demonstrated by the F11L-expressing MXYV was restricted to a single tumor. In particular, we wondered if this virus could also spread more efficiently to a second tumor, one that had not received a direct injection of virus. To investigate this question, we modified the aforementioned tumor model to incorporate a second tumor in another contralateral mammary fat pad. Once tumors were palpable, the tumor on the right-side of the mouse was directly injected with three injections of 5×10^7 pfu of virus, while the left-side tumor was left untreated. The size of both tumors was then monitored for the next six weeks, after which the mice were euthanized, and the tumors and organs assayed for virus by titration. We chose to use this higher dose of virus in order to maximize the likelihood that we would see viral spread from the site of introduction. Six weeks of examination was chosen, because based on previous experiments, the mouse tumor burden should still be well below the safe limits for CCAC regulations (i.e. less than 10% of body mass).

Even at these much higher doses of virus, we observed that tumors injected directly with live F11L-mCh grew at slower rates than those which received injections of the ΔM127L-mCh control virus. By the end of the experiment (52 days post-implantation) the mean injected tumor volume of F11L-mch treated mice was 170 ± 40 mm^3 *versus* 300 ± 50 mm^3 in mice treated with the ΔM127L-mCh . In comparison the tumors in mice treated with UV-inactivated virus were significantly larger than those seen in either live virus-receiving group (830± 130 mm^3) (**Figure 6.12A).**

Treating mice with live virus also delayed the growth of the second uninjected tumor. More interestingly, we observed that in mice injected with the F11L-mCh virus, the untreated tumors were significantly smaller than those animals receiving ΔM127L-mCh virus (540±40 mm^3 *versus* 750±70 mm^3; $P<0.001$). In comparison, the untreated

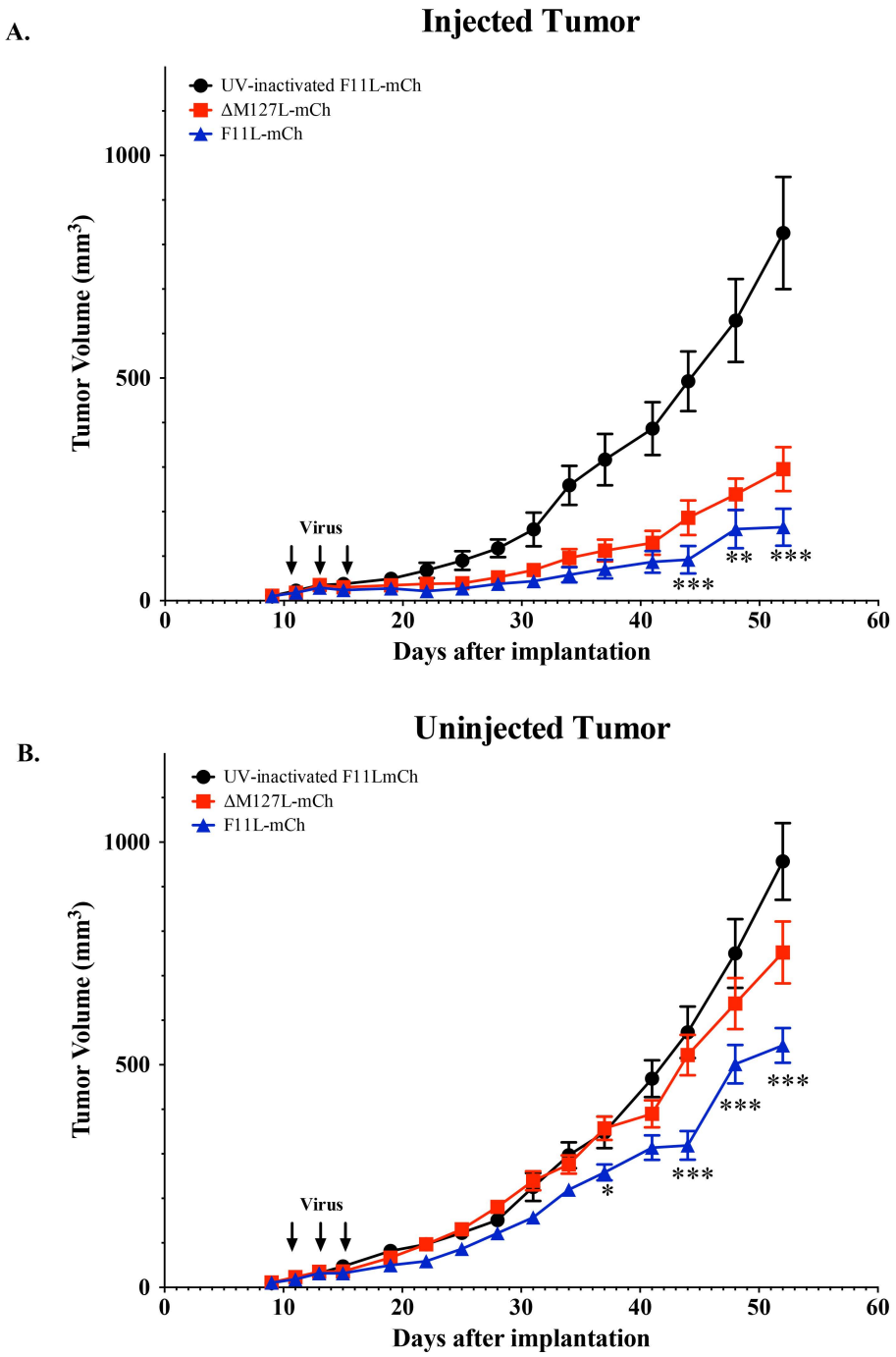

Figure 6.12: MYXV F11L-mCh produces better control of secondary untreated tumors. Two tumors (one in each mammary fat pad) were established in NIH-III mice using MDA-MB-231 cells. Once palpable the right-side tumor was injected with three doses of $5x10^7$ pfu of either ΔM127L-mCh, F11L-mCh, or an equivalent amount of UV-inactivated virus. Tumor growth was monitored by caliper measurements for the next six weeks **(A)** Tumor volume of injected tumor **(B)** Tumor volume of the uninjected tumor. Statistics shown are the results of a two-way ANOVA comparison of ΔM127L-mCh and F11L-mCh groups. For the live-virus groups 10 mice each were used, and UV-inactivated mice used 8 mice.

tumors in mice injected with UV-inactivated virus had grown by this point to a mean tumor volume of 960±90 mm^3 (**Figure 6.12B).**

In an earlier pilot study of this bilateral tumor model, we detected one F11L-mCh treated mouse where the higher dose of virus appeared to cause the eradication of the injected tumor. Furthermore, over the course of several weeks we observed the migration of mCherry signal from the injected tumor, to the second untreated tumor. In this larger scale experiment we did not observe any instances of mCherry signal appearing in the second un-injected tumor. However, the visualization of mCherry signal was confounded by a number of scabs that formed on tumors at later timepoints. These scabs also autofluoresced at wavelengths used to detect a mCherry signal, as signified by the rise in fluorescence in the UV-inactivated group at later times in the experiment (**Figure 6.13B and C).**

However, at early times of the experiment (before ~ day 30) a mCherry signal did seem to be accurately measurable. At these higher doses of virus, the signal in the injected tumors between the two live-virus receiving groups was quite similar **(Figure 6.13B).** Less mCherry fluorescence was detected in the uninjected tumors, and although small differences were observed between the groups that received live viruses those receiving the UV-inactivated virus, at no times were these differences significant (**Figure 6.14B).**

Since mCherry imaging proved less useful in this experiment as it had been in the single-tumor model, we excised the tumors at the conclusion of the study and assayed them for virus using plaque assays. Similar levels of virus were observed in the injected tumors of mice receiving either live F11L-mCh or ΔM127L-mCh (~ 4×10^6 pfu/ g of tumor). There were several logs less virus in the untreated tumors. However, there was still significantly (~10-fold) more F11L-mCh virus detected in the un-injected tumors compared to mice treated with the ΔM127L-mCh virus. We also titered the tumors of the

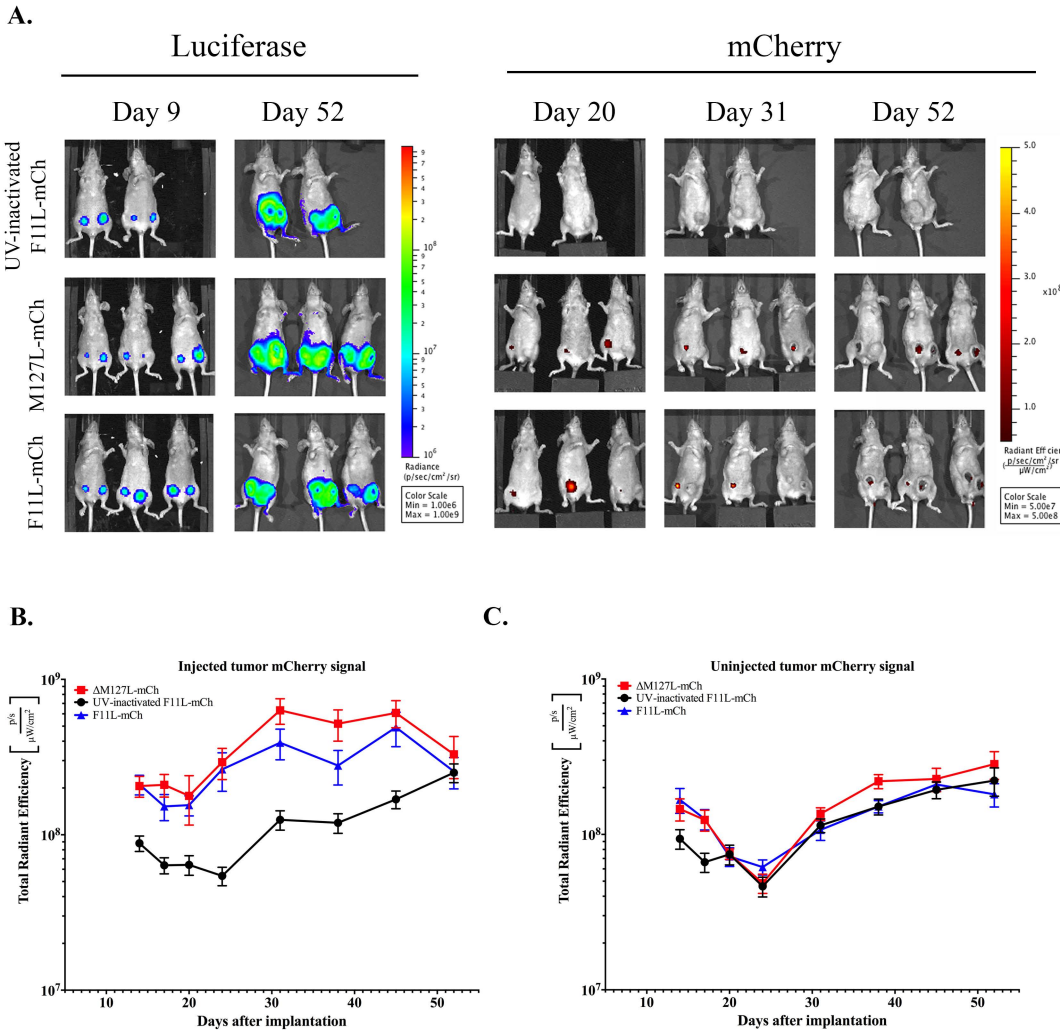

Figure 6.13: Evaluation of the efficacy of F11L⁺ MYXV in a bilateral tumor model by *in vivo* imaging. An IVIS spectrum imager was used to evaluate the same cohort of mice presented in figure 6.11. **(A)** Representative images of the same mice over time. Mice were imaged for cancer luciferase signal at day 9 (1 day before virus injection) and at the end of the experiment. Mice were imaged for mCherry signal at regular intervals. Images at day 20, 31 and 52 are shown. **(B+C)** Quantification of mCherry signal in the injected tumor (B) or uninjected tumor (C). Excitation and emission filters of 570nm and 680nm were used to measure the total radiant efficiency of mCherry signal.

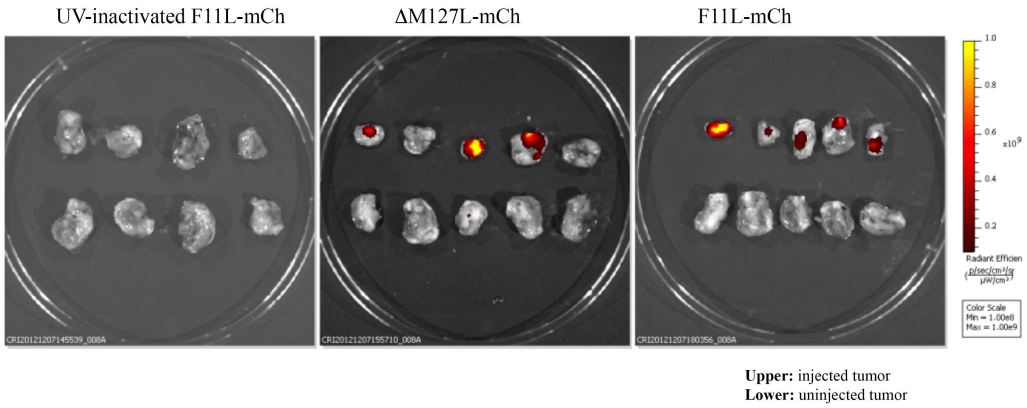

Figure 6.14: Analysis of viral levels in tumors at experimenal endpoint. Six weeks after virus injection mice from figure 6.12 were sacrificed and tumors extracted. **(A)** mCherry fluorescence imaging of tumors at endpoint by IVIS imager. One cage from each treatment was imaged. **(B)** Virus titers in excised tumors. Tumour tissues were recovered from the mice at the experimental endpoint, weighed, and the viruses titered on BGMK cells. The horizontal line denotes the mean titer.

UV-inactivated virus receiving group, and could find no evidence of virus, confirming the UV-inactivation was complete **(Figure 6.14).**

We also assayed for virus in a number of other tissues (brains, lungs, liver, spleen, kidneys) and in blood. No virus was detected in the majority of tissues assayed. The single exception was in the lungs of a mouse that had had been treated with live F11L-mCh, where approximately 300 pfu/organ was recovered. This tissue contained no luciferase signal detectible either by IVIS imaging or by western blot analysis, so whether this reflects trace virus contamination, virus spread to normal tissue, or a small amount of MYXV replicating in a metastatic site composed of MDA-MB-231 cells, is difficult to determine.

6.3 SUMMARY AND BRIEF DISSCUSION:

The oncolytic efficacy of both VACV and reovirus can be improved through increasing the ability of these viruses to spread. Here we asked if an F11L-dependent increase in MYXV spread, seen in rabbit and monkey cells, could enhance MYXV oncolytic activity. We showed that, similar to what we see in rabbit and monkey cells, an F11L-expressing MYXV induced a number of similar cytological alterations in an MDA-MB-231 human breast adenocarcinoma cell line. Furthermore, we showed that this virus grew to higher levels in a number of cancer cell lines. In some instances it was also more effective at killing these cells.

We found that these *in vitro* findings translated into more effective tumor control, and prolonged survival, of NIH-III mice bearing xenografted tumors. Furthermore, I showed that F11L expressing MYXV was better able to spread into and control the growth of a second distant tumor, with ~10-fold more virus being found in these second tumors compared to mice receiving the ΔM127L-mCh control virus. Collectively these show that we could exploit a system, which promotes *Orthopoxvirus* spread to enhance the oncolytic efficacy of a *Leporipoxvirus.*

F11 enhances VACV spread by disrupting the actin cytoskeleton by binding to, and inhibiting, RhoA signaling to mDia1. I showed that the growth of WT and ΔM127L-mCh MYXV, but not F11L-mCh, could be enhanced by siRNA-mediated silencing of this signaling pathway. These could be components that are known to be targets of F11 (RhoA or mDia1) or other genes known to regulate actin structures in cells (RhoC or LIMK2). Furthermore, we could enhance MYXV growth with low levels of latrunculin B, which is a chemical inhibitor of actin polymerization.

It is known that the activation of Rho GTPase pathways is linked to the progression of many cancers. Consequently much research has been directed towards producing pharmacological inhibitors of these pathways (reviewed in [314]). Our work suggests that it might be possible to use these inhibitors to improve MYXV-based oncolytic viral therapies. Since all viruses must overcome barriers to exit, such as those composed of cortical actin, it is possible that pharmacological targeting of Rho GTPase signaling pathways might also enhance the oncolytic activity of other viruses.

CHAPTER 7: DISCUSSION AND FUTURE DIRECTIONS

7.1 MYXV Forms Fewer Actin Projectiles than VACV:

In tissue culture, poxviruses form two types of plaques. The first is the large rapidly spreading cytolytic plaques formed by orthopoxviruses such as VACV. These plaques are often visible within 1-2 days in tissue culture settings. However, plaque assays using other chordopoxviruses (e.g. MYXV) suggest that this rapid spread of VACV may not be typical of all poxviruses. Infecting cell monolayers with other types of poxviruses often does not produce plaques, but rather a clustering of infected cells, sometimes called a focus. Foci take much longer to form, with up to 10 days being reported for some viruses such as Yaba-like disease virus [315].

We started the work presented here by asking why do VACV and MYXV form such drastically different plaques in culture? For VACV, the formation of EVs and actin projectiles has been linked to rapid plaque expansion. Given that VACV mutations, which limit or abolish the formation of EVs and actin projectiles, create smaller more MYXV-like plaques, we wondered if differences in the abilities of these viruses to produce EV and actin projectiles may contribute to differences in plaque size (i.e. might MYXV produce less EV and/or actin projectiles).

We used fluorescent microscopy to study whether VACV and MYXV form actin projectiles in three different cell lines, which support good growth of both viruses (monkey BGMK and rabbit SIRC or RK13). In all cell lines tested, we found that VACV-infected cells produced significantly higher numbers of actin projectiles than in MYXV-infected cells. These observations also held true in human MDA-MB-231 cells and primary cells derived from rabbit corneas. Although cellular factors contribute to actin projectile formation, the fact that this difference in actin projectile frequency was a general phenomenon suggested to us that these differences were a result of viral genetic

differences and not due to differences in how these viruses with engage cellular processes.

We performed a comparison of the MYXV and VACV genomes to look for the presence of MYXV homologs of VACV genes that are important for EV and actin projectile formation. MYXV homologs, often in syntenic positions, were found to the majority of these VACV genes. However, we could find no homolog to VACV F11L and homologs to A36R and B5R were less clear.

7.2 A36/M125 Homologs:

Despite limited sequence similarity, which makes its detection difficult by BLAST P searches, M125R can complement actin projectile formation in an A36R-deficient strain of VACV [219]. This suggests these proteins are orthologs. By making a MYXV M125R-deficient strain we showed that M125R was essential for MYXV actin projectile formation and that transient transfections with plasmids encoding for A36R we could complement this deficiency. This provides additional support for these proteins having homologous functions.

While this M125R-deficient strain of MYXV showed a decrease in plaque size, across various cell lines this did not translate into changes in virus yields. Virus yields of the M125R-deficient MYXV were only tested on BGMK cells. This cell line had one of the smallest differences in plaque size between the WT and mutant virus (Figure 4.1). BGMKs also support lower levels of MYXV actin projectiles than other cell lines such as RK13s (Figure 3.2). It may be that if virus yields were assayed on a cell line that had larger differences in plaque size, and supports higher levels of actin projectile formation, a difference in viral yields may have been observed.

However, while changes in plaque size often correlate with differences in viral yields, it is not unprecedented that plaque size mutants do not show noticeable changes in

viral yields. For example B4R or F5L mutations have been reported to alter VACV plaque size, without changing viral yields[316] (Dobson and Tscharke, unpublished).

7.3 B5/C3/M144 Homologs:

MYXV M144R resembles VACV B5R, but is also related to VACV C3L. C3 and B5 show sequence similarity due to the presence of a set of repeats (SCRs) found in host complement control proteins. Indeed C3 has been implicated in complement control[317]. While B5 is a type I membrane protein found in EV membranes C3 is secreted. Additional analysis of M144 revealed that it had a hydrophobicity profile more similar to B5, and like B5, lacks a secretion profile, suggesting to us that M144 is most likely a B5 homolog.

Recently Bratke *et al*. analyzed the genomes of multiple poxviruses for the presence of B5/C3 homologs[309]. Their analysis classified grouped B5/C3 homologs into three groups. These were the B5-like group, the C3-like group and the "clade II poxvirus group." B5 and C3 like groups were found only in orthopoxviruses, whereas the clade II group was found in capripoxviruses, cervidpoxviruses, suipoxviruses, yatspoxviruses and leporipoxviruses. M144 was grouped into clade II group. Given that the clade II group are found in similar genomic positions as orthopoxviruses B5 (near the right end of the genome), and C3 homologs are found near the left end of orthopoxviruses, the authors suggested that ancestral poxviruses may have encoded a protein more similar to M144. During *Orthopoxvirus* evolution this gene may have been duplicated and one copy (C3) has lost its transmembrane domain and became specialized in complement control [309].

Work with the *Yatapoxvirus,* yaba-like disease virus (YLDV), suggests that *Orthopoxvirus* B5 and these clade II B5 homologs may have some divergent functions. YLDV also forms actin projectiles and its B5 homolog (Y144) associates with WVs/EVs and actin projectiles. However, Y144R was unable to complement actin projectile formation in a B5R-deficient strain of VACV[318]. Both YLDV Y144 and MYXV M144

have regions that align with 3 of the 4 extracellular SCR domains of VACV B5[309,318]. The exception is SCR region 2. The deletion of B5 SCRs causes a reduction in VACV plaque size and actin projectile formation, despite B5 being located in WV membranes[201].While no deletion of this particular region of VACV B5R has been performed, it is possible that these differences could explain why Y144 cannot complement B5 and may also contribute to a difference in plaque size between MYXV and VACV.

Interestingly, genera of poxviruses, which encode clade II B5 homologs (i.e MYXV M144-like), also encode the divergent actin nucleators (i.e. MYXV M125-like). Orthopoxviruses are the only genera that encode B5 and A36 homologs **(Figure 7.1)**. There also exist three genera of *Chordopoxvirinae* (*Avipoxvirus, Molluscipoxvirus,* and *Parapoxvirus*) that lack homologs to any of these genes (A36/M125, B5/M144 or C3) and I would predict that they should be incapable of forming actin projectiles. No experiments have been performed to investigate this possibility but it has been suggested that molluscum contagiosum (the only known *Molluscipoxvirus*) may not form WV or EV, as it lacks a functional homologs to A27L (reviewed in[319]). However, the *Avipoxvirus* fowlpox does form EV and still encodes many homologs of other genes involved in virus exit [109,320]. Phylogenetic analysis groups avipoxviruses, parapoxviruses and molluscipoxviruses into clades separate from other *Chordopoxvirinae*[321]. This suggests two possibilities. First the acquisition of genes needed to direct the assembly of actin projectilles may have occurred subsequent to the ability to produce EV (i.e. after the divergence of what would evolve into the avipoxviruses, parapoxviruses and molluscipoxviruses, but prior to the divergence of the other genera). The second possibility is that avipoxviruses, parapoxviruses and molluscipoxviruses lost genes implicated in production of actin projectiles, after their divergence from other chordopoxviruses.

It appears as though two subtypes of A36 and B5 have evolved – the VACV like system found in orthopoxviruses, and the MYXV like system found in other genera. It is uncertain as to whether this has any biological relevance. While we were able to generate recombinant strains of MYXV that expressed VACV A36R and/or B5R, in addition to their endogenous MYXV counterparts, this expression had no effect on MYXV growth properties. Even in situations where these VACV genes were expressed in MYXV in conjunction with the two other viral proteins required for formation of actin projectiles (A33R and A34R), no alterations in the behaviour of MYXV were seen.

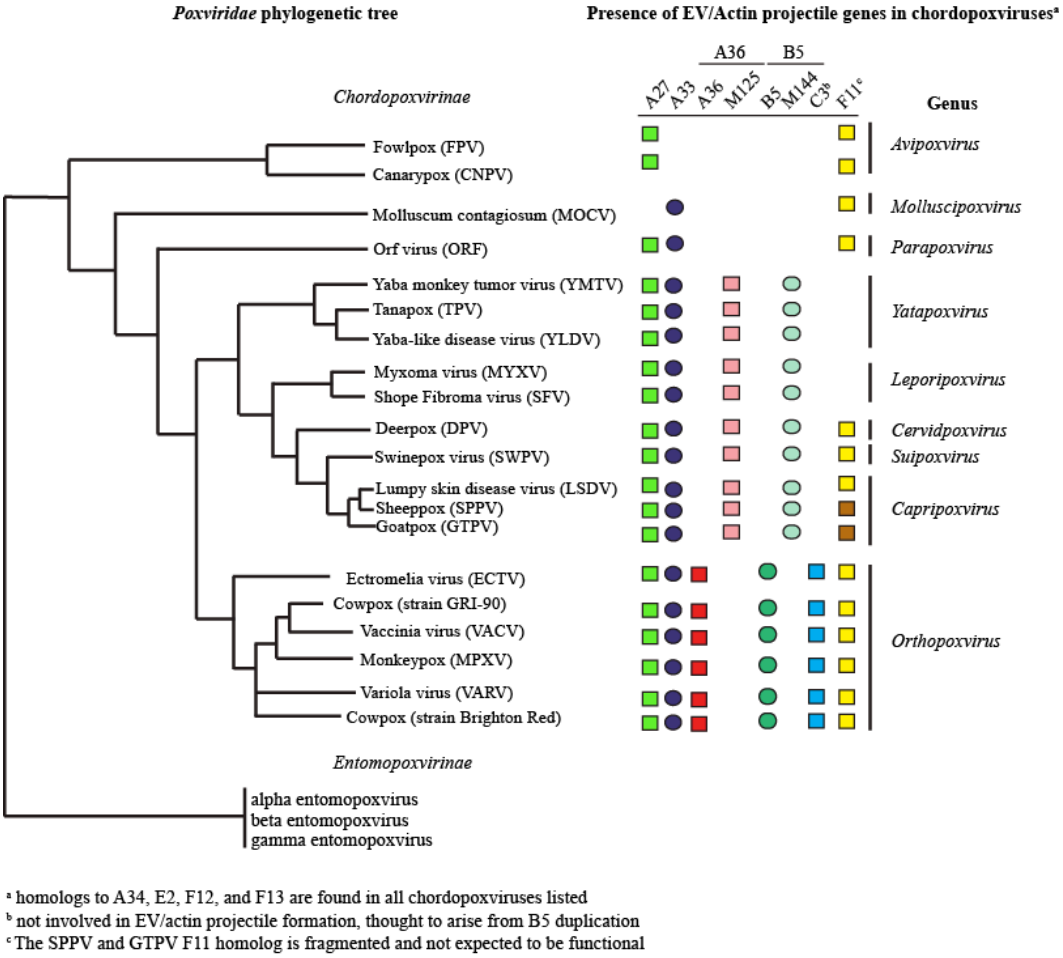

Figure 7.1: Presence of EV/actin projectile genes in Chordopoxviruses NCBI BLAST P analysis was performed to identify homologs of EV/actin projectile genes in chordopoxviruses. The presence of these genes were overlaid on a poxvirus phylogenetic tree as adapted from [1,321]. The following NCBI protein sequences were used as references: YP 233032.1 (VACV A27L), YP 233038.1 (VACV A33R), YP 233039.1 (VACV A34R), YP 233041.1 (VACV A36R), YP 233069.1 (VACV B5R), YP 232907.1 (VACV C3L), YP 232940.1 (VACV E2L), YP 232932.1 (VACV F11L), YP 232933.1 (VACV F12L), YP 232932.1 (VACV F13L), NP 051839.1 (MYXV M125R), NP 051858.1 (MYXV M144R). For VACV the WR genome was used as a reference, for MYXV the Lausanne genome was used as a reference.

7.4 The Role of F11L in Poxvirus Spread:

In contrast to the aforementioned genes, we could not find a MYXV homolog to VACV F11L. F11 promotes both the *in vitro* and *in vivo* spread of VACV[205] and, while not directly involved in forming EV or actin projectiles, it is thought to promote microtubule rearrangement and disrupt cortical actin in such a way as to aid WV reaching the cell periphery [143,204]. VACV F11L mutants show decreased plaque size and reduced actin projectile formation. Thus we sought to investigate whether the absence of an F11L homolog played some role in limiting MYXV spread.

The expression of F11L in MYXV caused a noticeable increase in plaque size. This varied by cell line but ranged from 2-4-fold increases in plaque size by 4 days post-infection. Also, consistent with the observations that F11 promotes detachment of VACV-infected cells[223], we observed that in some cases our F11L expressing MYXV formed a more lytic plaque. This was particularly noticeable in rabbit SIRC cells or in primary cells isolated from rabbit corneas. Live-cell microscopy suggested that this $F11L^{+}$ virus can spread at ~6-7 times faster rate than a control MYXV strain.

Several factors suggested to us that F11L expression enhances MYXV plaque formation in a manner similar to how it is thought to facilitate VACV spread. First, F11L expression had no effect on viral yields under high MOI situations where every cell is presumably infected. However, under low MOI conditions, and more profoundly at later times in infection, we saw that F11L increased MYXV yields. This suggests that F11 is promoting MYXV growth by increasing the ability of the virus to spread, and not simply increasing the amount of virus produced in a single infection.

Relative to wildtype, disruption of M127L decreased the percentage of total virus found in the media of RK13 infected cells **(Figure 3.15)**. This did not appear to be the result of a second site mutation as it was observed with multiple M127L deficient strains. Interestingly, when this experiment was repeated using MDA-MB-231 cells we observed

that the M127L deficient control strains, along with an additional virus which had similar selectable markers but was deficient in M004L/R, all showed similar percentages of virus in the medium as in WT MYXV **(Figure 6.2).** The reasons for these discrepancies remain unclear. Regardless of these oddities, in both cell lines F11L significantly increased the percent of virus in the medium relative to the control virus. This suggests that F11 promotes MYXV spread by increasing virus release.

F11L has also been implicated in promoting cell migration, as shown by the fact that siRNA-mediated silencing of F11L, or mutations in F11L, caused decreased VACV-induced cell motility[205,224]. In wound-healing experiments, the WT and control strains of MYXV behaved much like these F11L mutants, in that they did induce cell motility. In contrast the $F11L^{+}$ MXYV does induce cell migration although not as much as that observed using WT VACV. This is despite the fact that we see similar levels of F11 expression. The VACV MVA strain has mutations or deletions in approximately one third of its genome, including an inactivating mutation in F11L[322]. While MVA does not induce cell migration, repairing F11L does restore some viral mediated-cell movement, but at lower levels than what is seen in WT VACV (strain WR)[225].

RhoA, Rac1 and Cdc42 have all been implicated in supporting cell movement and WT VACV infection does decrease the GTP-bound levels of all three proteins[204]. F11 has been shown to decrease the levels of active RhoA, but not Cdc42 or Rac1, suggesting additional viral gene(s) are responsible for the downregulation of these other Rho GTPases [205]. The presence of such a gene(s) in WT VACV, but not in $F11L^{+}$ MYXV or F11L repaired MVA could explain the remaining differences in the capacity to cause cell movement between the different viruses.

At the cellular level, F11 expression from MYXV caused a number of morphological changes consistent with disruption of the actin cytoskeleton. While infecting cells with either the WT or control strains of MYXV had little effect on cell

surface area or the numbers of actin stress fibers, the presence of F11 caused a "rounding up" of cells and a reduction in stress fibers. At 8 h post-infection, the cell area and number of actin stress fibers in F11L^{+} MYXV-infected cells were similar to those observed in cells infected with WT VACV. This suggests that F11 is probably the only viral factor controlling this phenotype in VACV. It is also in good agreement with the observations that cells infected with F11L-deficient VACV show higher levels of stress fibers and less rounding up of cells [205,223].

F11 homologs are found in most chordopoxviruses. Exceptions are members of the *Yatapoxvirus* and *Leporipoxvirus* genera. Some capripoxviruses (sheeppox and goatpox) encode mutated F11L gene homologs, which likely render them non-functional[323]. Work by Way and colleagues shows that in VACV-infected cells F11 expression correlates with increased actin projectile formation [143,204,205,224], and our work shows that F11 expression from MYXV also increases their formation.

The increase in CEV and consequently increased number of actin projectiles may be the major method whereby F11 contributes to plaque size and viral spread in culture. Work with MVA VACV and fowlpox seems to support this idea. MVA has mutations in EV/actin projectile genes (e.g. A36) [322] and, while fowlpox produces EV[320], it lacks homologs to A33R, A36R/M125R, and B5R/M144R. This suggests that both viruses have deficiencies in actin projectile formation. These defects could explain why presence of F11L homologs in these virus has no effect on viral yields. The repair of F11L in MVA does not alter plaque size or viral yields, despite a partial restoration in cell motility[225], and the disruption of the fowlpox F11L homolog does not alter viral yields[324].

While F11L's role in promoting actin projectiles appears to be important in culture for viral spread, this might not be the same *in vivo*. While F11L promotes VACV spread *in vivo*[205], F11L homologs are found in the *Chordopoxvirus* genera not predicted

to produce actin projectiles (*Avipoxvirus, Molluscipoxvirus*, and *Parapoxvirus*). It may be that *in vivo,* F11s promotion of spread is less dependent on promoting actin projectiles. It would be interesting to investigate the role of F11L in the absence of a viruses ability to induce actin projectile formation (e.g. fowlpox or an A36R-deficient VACV).

7.5 Other Factors may contribute to Differences in Plaque Size Between MYXV and VACV:

F11L can increase MYXV plaque size and elevate the number of actin projectiles. However, F11L^{+} MYXV still exhibited significantly smaller plaques and produced fewer actin projectiles than VACV. This suggests that while the absence of a MYXV F11L homolog can partially explain the differences in plaquing properties between MYXV and VACV, it is not the only factor.

We found that MYXV-expressing VACV A33R, A34R, A36R and B5R, either alone or in combination, produced nearly identical levels of actin projectiles and plaques compared with WT and control MYXV strains. The A36 and B5 proteins seem to be expressed and processed by MYXV-infected cells much like they are in VACV infections. In contrast, A33 and A34 migrate as lower molecular weight band when expressed from MYXV **(Figure 3.5).** Furthermore, using immunofluorescent microscopy MYXV-expressed A33 and A34 do not appear to be as widely distributed in cells compared to what we see with VACV **(Figure 3.8)**. In VACV, B5 has been shown to be important for the proper glycosylation and incorporation of these proteins into WV membranes[173,180]. This suggests that MYXV EV homologs (e.g. M144) may not be able to facilitate incorporation of these proteins into WVs. It would be interesting to examine whether the co-expression of these four proteins alters the migration profile of A33 and A34. If A33 and A34 electrophorese differently, even when VACV B5 and A36 are co-expressed, it would suggest that additional VACV proteins are needed (e.g. F13L, which is important for proper B5 localization[149]). Even if these four proteins are properly

processed and localized when co-expressed, they still do not seem to facilitate noticeable increases in actin projectile formation as evident by co-infection experiments **(Figure 3.11).**

At a recent poxvirus meeting it was noted that the F5L gene also contributes to VACV plaque size, although how it contributes to plaque size remains unknown (Dobson and Tscharke, unpublished). BLAST P searches cannot detect an F5L homolog outside of the *Orthopoxvirus* genus, so it is possible that the absence of a MYXV F5L homolog may also contribute to differences in plaque size between these viruses. However, F5L does not contribute to viral yields, so the absence of a MYXV F5L would not be expected to explain the lower yields of MYXV.

7.6 Differences in Spread Modes of Poxviruses and a Potential Role of F11:

The presence of F11 in many chordopoxviruses would suggest that the acquisition of a F11 homolog occurred early in their evolution. As a corollary, it might be predicted that F11L was lost from the virus(es) that gave rise to the *Yatapoxvirus* and *Leporipoxvirus* families. The absence of a F11 homolog, and lower rate of actin projectile formation could potentially explain some of the differences in the *in vivo* behavior of orthopoxviruses and leporipoxviruses.

Leporipoxvirus infections remain relatively localized in tumor-like lesions and are thought to be spread primarily by arthropod bites. An exception to this is in European rabbits. While MYXV spreads rapidly and systemically through European rabbits, it is thought to be that this may be due to a specific genetic defect in *Oryctolagus* rabbits, which allows MYXV to replicate in leukocytes. These leukocytes are thought to serve as a vehicle to transport MYXV to other organs[75].

Orthopoxvirus infections often behave like MYXV does in European rabbits, i.e. they spread systemically, although this occurs without requiring leukocyte vehicles. This rapid spread could also contribute to the spread of these viruses through aerosols or

abrasions. F11 contributes to intrahost spread of VACV, as F11L-deficient VACV spread less efficiently to the spleen when administered intranasally [205].

The absence of a F11 homolog may cause MYXV to remain localized during infection, which could promote its spread via arthropods bites in its native American lagomorph hosts. It was observed that when it was released into Australia, MYXV became rapidly attenuated. This attenuation was thought to promote virus dissemination by increasing survival and allowing for greater time for virus to be spread via mosquitoes[72,77,80]. MYXV does not replicate in mosquitoes and spread via this mechanism requires relatively high local titers of virus (>10^7 pfu/g)[76,325].

In our bilateral tumor model (Chapter 6) we showed that F11L$^+$ MYXV shows a greater capacity to spread from the site of introduction. This suggests that such a virus may spread better in a rabbit host. However, it is possible that by not encoding an F11L homolog (possibly through a deletion) MYXV can stay near the site of infection. This would reduce the pathogenicity, while allowing the virus to produce titers high enough to promote efficient spread *via* insects. It is noteworthy that yatapoxviruses, which also lack F11L homologs, may also spread through mosquitoes[315].

It would be interesting to test whether the F11$^+$ MYXV exhibits altered pathogenicity. One could envision that this virus may show increased systemic spread in a manner that may not require a leukocyte vehicle. Furthermore, one might predict that this virus would display increased pathogenicity in American lagomorphs.

7.7 Improved Growth of F11L MYXV in Cancer Cells:

While we have shown that the absence of an F11L homolog partially can explain differences in plaquing properties between MXYV and VACV we also developed a useful application for an F11L$^+$ MYXV. While MYXV has shown promise in a number of tumor models it does not spread well between tumors [282]. An improvement in the spread of oncolytic VACV has been obtained by introducing a K151E point mutation into

A34R in VACV strain WR or Wheyth[299-301]. The E_{151} allele is naturally found in the IHD strains of VACV, and appears to account for the increased rates of EV production in these strains[179,182]. Given that our F11L$^+$ strain of MYXV also increased the release of MYXV, we hypothesized that F11L-mCh MYXV might be a more effective oncolytic virus.

We screened a number of cancer cell lines for the effect of F11L on MYXV growth. These assays were done at low MOI, and allowed to go for several days to let multiple rounds of replication occur. Generally, we found that F11L increased the yields of MYXV in a number of cell lines, which were permissive for MYXV (**Figure 6.6).** We also observed that F11L also produced increased β-galactosidase staining at 96 h post-infection, suggesting increased cell-to-cell spread **(Figure 6.5).** The F11L-mediated alterations to the growth properties of MXYV, which we observed in rabbit and monkey cells, were also seen in human MDA-MB-231 adenocarcinomas. Decreased cell area, less stress fibers, along with increased actin projectile frequency and virus released into the were all observed.

7.8 Establishment and Evaluation of MYXV in an Animal Tumor Model:

The superior growth, and in some cases enhanced cell killing, observed with F11L$^+$ MYXV, lead us to speculate that such a virus may be a more effective oncolytic agent in an animal tumor model. We chose an established animal model using immunocompromised NIH-III mice bearing xenografted tumors composed of human MDA-MB-231 cells. This model was chosen for a number of reasons. MDA-MB-231 cells support an intermediate level of MYXV growth and intraperitoneal tumors are not easily curable by MYXV (G. McFadden, personal communication). Our lab was also performing a siRNA screen, using these cells to identify factors that affect MYXV growth in human cancer cells[290]. We found this model had a fairly high success rate of tumor establishment, and was amenable to MYXV treatments. While MYXV treatment

did not appear to result in any cures it did significantly delay tumors growth rates and prolonged survival of mice. We found that the dose of control virus needed to prolong survival in this model ranged between 1×10^5 and 1×10^6 pfu. We did not observe any noticeable signs of virus toxicity in this animal model using doses up to 5×10^7 pfu/injection.

We optimized a number of parameters so that a non-invasive small animal imager could be used to track virus and cancer cells. While IVIS imaging did allow us to detect tumors *via* luciferase activity, and was particularly useful for confirming the presence of tumors at early experiment stages, it was not overly reliable at later stages of the experiment. We sometimes saw that a tumor would not exhibit luciferase activity, despite the presence of a visible tumor. We also noticed that while a tumor may show luciferase activity one day, it might not the next, only to become visible again at a subsequent imaging. Finally, we found that tumor volume did not show a good correlation with luciferase activity (Chapter 5). There are a number of possible reasons for these discrepancies. Luciferase activity is only found in live cancer cells and it is possible that necrotic or virus-killed portions of the tumor were still contributing to tumor volume and thus an overestimation of the proportion of live cells. It is also possible that the luciferase transgene became inactivated in some cell populations as there have been reports of transgenes becoming inactivated after long periods of transplantation[326]. Rearrangements in the tumor architecture, which prevent luciferin delivery, could also have occurred. Regardless, we found that calipers gave us more reliable results.

We also tested a number of fluorescent markers as tools for tracking replicating virus. Of the markers tested, we found that mCherry fluorescent protein gave the best signal to background. This marker was used to track virus in subsequent experiments. While this marker worked well, we did find that when scabs formed on tumors, these scabs autofluoresced in a way that interfered with mCherry imaging. This became a

particular problem as tumors grew larger at later times in the experiment. It is possible that using an even more red-shifted fluorescent protein could avoid such issues.

7.9 Oncolytic Efficacy of F11L$^+$ MYXV:

Using this tumor model, we compared the oncolytic efficacy of the F11L-mCh and ΔM127L-mCh viruses. We administered three doses of 1×10^6 pfu of virus and then monitored tumor growth. We observed that mice receiving live virus showed significant delays in tumor growth, which translated into increased survival. We also observed that the tumors in mice receiving F11L$^+$ MYXV grew at a slower rate than those injected with live control virus. This also translated into increased survival. In a bilateral tumor model, we observed that the F11L$^+$ virus was not only effective at controlling the growth of the injected tumor, but also a second distant tumor. In agreement, we detected ~10-fold more virus in the uninjected tumors of F11L-mCh infected mice at the end of the experiment compared to the control strain. Collectively these data suggest that F11L increases the spread of MXYV and that this can enhance its effectiveness as and oncolytic agent.

We also assayed other organs (brains, lungs, liver, spleen and kidneys), but could find no evidence of MXYV. This suggests that the F11L introduction does not cause viral replication in non-cancerous tissue. The single exception was where we detected ~300 pfu of virus in the lung of a mouse that had been treated with live F11L-mCh virus. This tissue contained no luciferase signal detectable by either IVIS imaging or western blot analysis, so whether this reflects trace virus contamination, virus spread to normal tissues, or a small amount of MYXV replicating in a small metastatic tumor nodule is difficult to determine.

Quantification of *in vivo* mCherry levels in the single tumor model showed that the mCherry levels in tumors of F11L-mCh infected mice were initially significantly

higher than that of ΔM127L-mCh. However, over time the ΔM127L-mCh levels "caught up". This suggests that F11L may increase the efficacy of the virus by promoting its initial rapid spread throughout the tumor. Two other observations seem to support this idea. First, when higher doses of virus were used in the bilateral tumor we observed nearly identical levels of mCherry in the injected tumor, and the differences in the tumor volumes between the live virus groups did not become significant until much later in the experiment. Second, we observed that at the end of the bilateral tumor experiment, similar levels of virus (pfu/g of tumor) were found in the injected tumor.

Like our F11L$^+$ MYXV a VACV A34R K151E mutant showed increased virus release, which are presumably EV. EVs have a number of properties that aid in their immune evasion and intrahost spread (see section 1.8). Given that this A34R mutant showed increased oncolytic efficacy in an immunocompetent host[300,301], one might predict that F11L$^+$ MYXV would also show increased efficacy in an immunocompetent host. Future work should investigate this possibility.

In all cases no cures were observed suggesting that while enhanced spread of F11L increases the oncolytic efficacy of MYXV, the virus could still be made more effective for the treatment of solid tumors.

7.10: Disruption of the actin cytoskeleton as a method of improving oncolysis

F11 disrupts cortical actin by inhibiting RhoA-mDia1 signaling[143,204,205,223,224]. We showed that targeting elements of this pathway, either through siRNA-mediated silencing or pharmacological inhibitors, could mimic the effect of F11 on MYXV growth in MDA-MB-231 cells. Although many inhibitors of actin microfilaments inhibit VACV growth, low concentrations of the actin polymerization inhibitor latrunculin B can overcome the inhibitory effects of RhoA activation on VACV release[204]. We found that the inhibitor could also enhance the numbers of actin projectile formed in MYXV and increase virus yields. Similarly, we found that siRNA-mediated depletion of four genes

whose activation promotes actin polymerization could also enhance MYXV growth. These genes were RhoA, RhoC, LIMK2 and mDia1. The effects of silencing RhoA and mDia1 on MYXV growth may not be surprising, since the disruption of this signaling axis is thought to be the primary way that F11 promotes VACV growth. While RhoA signals primarily to mDia1 and ROCK, we found that a ROCK inhibitor called Y-27632 had little effect on MYXV growth. Similar observations were reported in VACV-infected cells[143].

The three Rho GTPases (RhoA, RhoB and RhoC) show some functional overlaps but also exhibit a number of differences. RhoA seems to be more effective at promoting turnover of cell adhesions at the rear of cells, while RhoC seems to be involved in disrupting tight junctions. Both RhoA and C have been shown to be upregulated in cancers, and have been shown to be important for cell migration. In contrast RhoB is thought have tumor suppressor activities, is often downregulated in cancer cells, and seems to be important for forming cell-adhesions[21,22,327]. RhoC has also been shown to bind mDia1[22], and we found that siRNA-mediated depletion of this gene also enhanced MYXV growth. LIMK is downstream of ROCK and its activation promotes formation of actin stress fibers[328]. This gene was detected in a genome scale siRNA screen in our laboratory, as a factor whose silencing promoted MYXV growth (mDia1 was detected in this screen as well)[290]. My studies confirmed the validity of the hits detected in this screen. Collectively, these data show that targeting factors that lead to actin polymerization can promote MYXV growth. Why inhibiting LIMK, but not its upstream effector ROCK, has an effect on MYXV growth is unknown. LIMK is also regulated by other Rho GTPases (**Figure 1.2)** and it is possible that these factors could limit the effects of F11 disruption of RhoA signaling on LIMK activity.

Disrupting these signaling cascades had little effect on the growth of the F11L$^+$ MYXV, while increasing the growth of WT and a control MYXV strain. This suggests

two things. First, F11 primarily works by inhibiting these pathways. Second, it appears that these pathways can be saturated with genetic or chemical inhibitors, after which additional disruptions do not have any additive effects.

While F11 has been reported to work by targeting the elements of the RhoA/C signaling pathway, we could not find a correlation between the levels of these proteins and the effects of F11 on MYXV growth in cancer cells **(Figure 6.8).** This lack of correlation may not be too surprising, since we only looked at total levels of these proteins, while F11 binds GTP-bound RhoA[205]. It has also recently been shown that F11 can not only bind to active RhoA but also promote its conversion back into a GDP-bound inactive form. This occurs through F11's recruitment of the GAP myosin 9A (Michael Way, personal communication).

The up-regulation and activation of Rho GTPases, or their downstream effectors, has been linked with a number of processes critical to cancer progression including cell-proliferation, cell migration, and invasion, and has been the subject of many reviews [19,22,313,329]. As such, it is widely recognized that elements of this pathway might be useful targets for cancer therapeutics (reviewed in [18]). Indeed, a number of inhibitors against proteins encoded by genes like RhoA, RhoC, mDia1, or LIMK2 are in various states of development [18,314,330-332]. Our work suggests that it may be possible to synergize these new chemotherapeutics with MYXV virotherapy.

Moreover, given that all viruses must overcome the challenge to exit posed by structures like cortical actin layer, and that cancer progression could potentially increase these barriers, this approach may be applicable to increasing the efficacy of other oncolytic viruses. Further work should investigate these possibilities.

8 REFERENCES:

1 in *Virus Taxonomy* (eds M. Q. King Andrew *et al.*) 291-309 (Elsevier, 2012).

2 Roberts, K. L. & Smith, G. L. Vaccinia virus morphogenesis and dissemination. *Trends Microbiol*, doi:S0966-842X(08)00191-1 [pii] 10.1016/j.tim.2008.07.009 [doi] (2008).

3 Moss, B. in *Fields Virology* (eds D. M. Knipe & P. M. Howley) 2906-2945 (Lippincott Williams & Wilkins, 2007).

4 Parsons, J. T., Horwitz, A. R. & Schwartz, M. A. Cell adhesion: integrating cytoskeletal dynamics and cellular tension. *Nat Rev Mol Cell Biol* **11**, 633-643, doi:10.1038/nrm2957 (2010).

5 Schwartz, M. A. & Horwitz, A. R. Integrating adhesion, protrusion, and contraction during cell migration. *Cell* **125**, 1223-1225, doi:10.1016/j.cell.2006.06.015 (2006).

6 Foley, E. A. & Kapoor, T. M. Microtubule attachment and spindle assembly checkpoint signalling at the kinetochore. *Nat Rev Mol Cell Biol* **14**, 25-37, doi:10.1038/nrm3494 (2013).

7 Rago, F. & Cheeseman, I. M. Review series: The functions and consequences of force at kinetochores. *J Cell Biol* **200**, 557-565, doi:10.1083/jcb.201211113 (2013).

8 de Curtis, I. & Meldolesi, J. Cell surface dynamics - how Rho GTPases orchestrate the interplay between the plasma membrane and the cortical cytoskeleton. *J Cell Sci* **125**, 4435-4444, doi:10.1242/jcs.108266 (2012).

9 Porat-Shliom, N., Milberg, O., Masedunskas, A. & Weigert, R. Multiple roles for the actin cytoskeleton during regulated exocytosis. *Cell Mol Life Sci*, doi:10.1007/s00018-012-1156-5 (2012).

10 Wang, J. & Richards, D. A. Spatial regulation of exocytic site and vesicle mobilization by the actin cytoskeleton. *PLoS One* **6**, e29162, doi:10.1371/journal.pone.0029162 (2011).

11 Spencer, V. A., Xu, R. & Bissell, M. J. Gene expression in the third dimension: the ECM-nucleus connection. *J Mammary Gland Biol Neoplasia* **15**, 65-71, doi:10.1007/s10911-010-9163-3 (2010).

12 Fiorentini, C., Falzano, L., Travaglione, S. & Fabbri, A. Hijacking Rho GTPases by protein toxins and apoptosis: molecular strategies of pathogenic bacteria. *Cell Death Differ* **10**, 147-152, doi:10.1038/sj.cdd.4401151 (2003).

13 Street, C. A. & Bryan, B. A. Rho kinase proteins--pleiotropic modulators of cell survival and apoptosis. *Anticancer Res* **31**, 3645-3657 (2011).

14 Taylor, M. P., Koyuncu, O. O. & Enquist, L. W. Subversion of the actin cytoskeleton during viral infection. *Nat Rev Microbiol* **9**, 427-439, doi:10.1038/nrmicro2574 (2011).

15 Orchard, R. C. & Alto, N. M. Mimicking GEFs: a common theme for bacterial pathogens. *Cell Microbiol* **14**, 10-18, doi:10.1111/j.1462-5822.2011.01703.x (2012).

16 Aktories, K. Bacterial protein toxins that modify host regulatory GTPases. *Nat Rev Microbiol* **9**, 487-498, doi:10.1038/nrmicro2592 (2011).

17 Finlay, B. B. Bacterial virulence strategies that utilize Rho GTPases. *Curr Top Microbiol Immunol* **291**, 1-10 (2005).

18 Mardilovich, K., Olson, M. F. & Baugh, M. Targeting Rho GTPase signaling for cancer therapy. *Future Oncol* **8**, 165-177, doi:10.2217/fon.11.143 (2012).

19 Karlsson, R., Pedersen, E. D., Wang, Z. & Brakebusch, C. Rho GTPase function in tumorigenesis. *Biochimica et Biophysica Acta (BBA) - Reviews on Cancer* **1796**, 91-98 (2009).

20 Jaffe, A. B. & Hall, A. Rho GTPases: biochemistry and biology. *Annu Rev Cell Dev Biol* **21**, 247-269, doi:10.1146/annurev.cellbio.21.020604.150721 (2005).

21 Wennerberg, K. & Der, C. J. Rho-family GTPases: it's not only Rac and Rho (and I like it). *J Cell Sci* **117**, 1301-1312, doi:10.1242/jcs.01118 (2004).

22 Wheeler, A. P. & Ridley, A. J. Why three Rho proteins? RhoA, RhoB, RhoC, and cell motility. *Exp Cell Res* **301**, 43-49, doi:10.1016/j.yexcr.2004.08.012 (2004).

23 Cibulka, J., Fraiberk, M. & Forstova, J. Nuclear actin and lamins in viral infections. *Viruses* **4**, 325-347, doi:10.3390/v4030325 (2012).

24 H, L. *et al. Molecular Cell Biology*. 5th edn, (W.H. Freeman and Company, 2004).

25 Fletcher, D. A. & Mullins, R. D. Cell mechanics and the cytoskeleton. *Nature* **463**, 485-492, doi:10.1038/nature08908 (2010).

26 Bunnell, T. M. & Ervasti, J. M. Structural and functional properties of the actin gene family. *Crit Rev Eukaryot Gene Expr* **21**, 255-266 (2011).

27 Lodish, H. *et al.* Section 18.1, The Actin Cytoskeleton. *Molecular Cell Biology. 4th edition*, http://www.ncbi.nlm.nih.gov/books/NBK21493/ (2000).

28 Dominguez, R. & Holmes, K. C. Actin structure and function. *Annu Rev Biophys* **40**, 169-186, doi:10.1146/annurev-biophys-042910-155359 (2011).

29 Goode, B. L. & Eck, M. J. Mechanism and function of formins in the control of actin assembly. *Annu Rev Biochem* **76**, 593-627, doi:10.1146/annurev.biochem.75.103004.142647 (2007).

30 Kerkhoff, E. Actin dynamics at intracellular membranes: the Spir/formin nucleator complex. *Eur J Cell Biol* **90**, 922-925, doi:10.1016/j.ejcb.2010.10.011 (2011).

31 Rotty, J. D., Wu, C. & Bear, J. E. New insights into the regulation and cellular functions of the ARP2/3 complex. *Nat Rev Mol Cell Biol* **14**, 7-12, doi:10.1038/nrm3492 (2013).

32 Campellone, K. G. & Welch, M. D. A nucleator arms race: cellular control of actin assembly. *Nat Rev Mol Cell Biol* **11**, 237-251, doi:10.1038/nrm2867 (2010).

33 Dominguez, R. Actin filament nucleation and elongation factors--structure-function relationships. *Crit Rev Biochem Mol Biol* **44**, 351-366, doi:10.3109/10409230903277340 (2009).

34 Bugyi, B. & Carlier, M. F. Control of actin filament treadmilling in cell motility. *Annu Rev Biophys* **39**, 449-470, doi:10.1146/annurev-biophys-051309-103849 (2010).

35 Pollard, T. D., Blanchoin, L. & Mullins, R. D. Molecular mechanisms controlling actin filament dynamics in nonmuscle cells. *Annu Rev Biophys Biomol Struct* **29**, 545-576, doi:10.1146/annurev.biophys.29.1.545 (2000).

36 Yamashiro, S., Gokhin, D. S., Kimura, S., Nowak, R. B. & Fowler, V. M. Tropomodulins: pointed-end capping proteins that regulate actin filament architecture in diverse cell types. *Cytoskeleton (Hoboken)* **69**, 337-370, doi:10.1002/cm.21031 (2012).

37 Pollard, T. D. Regulation of actin filament assembly by Arp2/3 complex and formins. *Annu Rev Biophys Biomol Struct* **36**, 451-477, doi:10.1146/annurev.biophys.35.040405.101936 (2007).

38 Arpin, M., Chirivino, D., Naba, A. & Zwaenepoel, I. Emerging role for ERM proteins in cell adhesion and migration. *Cell Adh Migr* **5**, 199-206 (2011).

39 Eliáš, M. & Klimeš, V. Rho GTPases: deciphering the evolutionary history of a complex protein family. *Methods Mol Biol* **827**, 13-34, doi:10.1007/978-1-61779-442-1_2 (2012).

40 Heasman, S. J. & Ridley, A. J. Mammalian Rho GTPases: new insights into their functions from in vivo studies. *Nat Rev Mol Cell Biol* **9**, 690-701, doi:10.1038/nrm2476 (2008).

41 Bustelo, X. R., Sauzeau, V. & Berenjeno, I. M. GTP-binding proteins of the Rho/Rac family: regulation, effectors and functions in vivo. *Bioessays* **29**, 356-370, doi:10.1002/bies.20558 (2007).

42 Cherfils, J. & Zeghouf, M. Regulation of small GTPases by GEFs, GAPs, and GDIs. *Physiol Rev* **93**, 269-309, doi:10.1152/physrev.00003.2012 (2013).

43 Ryan, G. L., Watanabe, N. & Vavylonis, D. A review of models of fluctuating protrusion and retraction patterns at the leading edge of motile cells. *Cytoskeleton (Hoboken)* **69**, 195-206, doi:10.1002/cm.21017 (2012).

44 Vega, F. M., Fruhwirth, G., Ng, T. & Ridley, A. J. RhoA and RhoC have distinct roles in migration and invasion by acting through different targets. *J Cell Biol* **193**, 655-665, doi:10.1083/jcb.201011038 (2011).

45 Guilluy, C., Garcia-Mata, R. & Burridge, K. Rho protein crosstalk: another social network? *Trends Cell Biol* **21**, 718-726, doi:10.1016/j.tcb.2011.08.002 (2011).

46 Raftopoulou, M. & Hall, A. Cell migration: Rho GTPases lead the way. *Dev Biol* **265**, 23-32 (2004).

47 Harris, K. P. & Tepass, U. Cdc42 and vesicle trafficking in polarized cells. *Traffic* **11**, 1272-1279, doi:10.1111/j.1600-0854.2010.01102.x (2010).

48 Etienne-Manneville, S. Cdc42--the centre of polarity. *J Cell Sci* **117**, 1291-1300, doi:10.1242/jcs.01115 (2004).

49 Spiering, D. & Hodgson, L. Dynamics of the Rho-family small GTPases in actin regulation and motility. *Cell Adh Migr* **5**, 170-180 (2011).

50 Lessey, E. C., Guilluy, C. & Burridge, K. From mechanical force to RhoA activation. *Biochemistry* **51**, 7420-7432, doi:10.1021/bi300758e (2012).

51 Prasain, N. & Stevens, T. The actin cytoskeleton in endothelial cell phenotypes. *Microvasc Res* **77**, 53-63, doi:10.1016/j.mvr.2008.09.012 (2009).

52 Bartolini, F., Ramalingam, N. & Gundersen, G. G. Actin-capping protein promotes microtubule stability by antagonizing the actin activity of mDia1. *Mol Biol Cell* **23**, 4032-4040, doi:10.1091/mbc.E12-05-0338 (2012).

53 Anitei, M. & Hoflack, B. Bridging membrane and cytoskeleton dynamics in the secretory and endocytic pathways. *Nat Cell Biol* **14**, 11-19, doi:10.1038/ncb2409 (2012).

54 Trifaró, J. M., Gasman, S. & Gutiérrez, L. M. Cytoskeletal control of vesicle transport and exocytosis in chromaffin cells. *Acta Physiol (Oxf)* **192**, 165-172, doi:10.1111/j.1748-1716.2007.01808.x (2008).

55 Ory, S. & Gasman, S. Rho GTPases and exocytosis: what are the molecular links? *Semin Cell Dev Biol* **22**, 27-32, doi:10.1016/j.semcdb.2010.12.002 (2011).

56 Himsworth, C. G., McInnes, C. J., Coulter, L., Everest, D. J. & Hill, J. E. Characterization of a Novel Poxvirus in a North American Red Squirrel (Tamiasciurus hudsonicus). *Journal of Wildlife Diseases* **49**, 173-179, doi:10.7589/2012-02-054 (2013).

57 Tulman, E. R. *et al.* Genome of horsepox virus. *J Virol* **80**, 9244-9258, doi:10.1128/JVI.00945-06 (2006).

58 Carroll, D. S. *et al.* Chasing Jenner's vaccine: revisiting cowpox virus classification. *PLoS One* **6**, e23086, doi:10.1371/journal.pone.0023086 (2011).

59 Currier, J. R. *et al.* Phase I safety and immunogenicity evaluation of MVA-CMDR, a multigenic, recombinant modified vaccinia Ankara-HIV-1 vaccine candidate. *PLoS One* **5**, e13983, doi:10.1371/journal.pone.0013983 (2010).

60 Chen, H. *et al.* Optimisation of prime-boost immunization in mice using novel protein-based and recombinant vaccinia (Tiantan)-based HBV vaccine. *PLoS One* **7**, e43730, doi:10.1371/journal.pone.0043730 (2012).

61 Sekiguchi, S. *et al.* Immunization with a recombinant vaccinia virus that encodes nonstructural proteins of the hepatitis C virus suppresses viral protein levels in mouse liver. *PLoS One* **7**, e51656, doi:10.1371/journal.pone.0051656 (2012).

62 Bais, S., Bartee, E., Rahman, M. M., McFadden, G. & Cogle, C. R. Oncolytic virotherapy for hematological malignancies. *Adv Virol* **2012**, 186512, doi:10.1155/2012/186512 (2012).

63 Gammon, D. B. *et al.* Vaccinia virus-encoded ribonucleotide reductase subunits are differentially required for replication and pathogenesis. *PLoS pathogens* **6**, e1000984, doi:10.1371/journal.ppat.1000984 (2010).

64 Kim, J. H. *et al.* Systemic armed oncolytic and immunologic therapy for cancer with JX-594, a targeted poxvirus expressing GM-CSF. *Mol Ther* **14**, 361-370, doi:S1525-0016(06)00183-3 [pii] 10.1016/j.ymthe.2006.05.008 (2006).

65 McCart, J. A. *et al.* Systemic cancer therapy with a tumor-selective vaccinia virus mutant lacking thymidine kinase and vaccinia growth factor genes. *Cancer Res* **61**, 8751-8757 (2001).

66 Park, B. H. *et al.* Use of a targeted oncolytic poxvirus, JX-594, in patients with refractory primary or metastatic liver cancer: a phase I trial. *Lancet Oncol* **9**, 533-542, doi:S1470-2045(08)70107-4 [pii] 10.1016/S1470-2045(08)70107-4 (2008).

67 Liu, T. C., Hwang, T., Park, B. H., Bell, J. & Kirn, D. H. The targeted oncolytic poxvirus JX-594 demonstrates antitumoral, antivascular, and anti-HBV activities in patients with hepatocellular carcinoma. *Mol Ther* **16**, 1637-1642, doi:mt2008143 [pii] 10.1038/mt.2008.143 (2008).

68 Barrett, J. W. & McFadden, G. in *Poxviruses* (eds A. A. Mercer, A. Schmidt, & O. Weber) 183-201 (Birkhauser Verlag, 2007).

69 Upton, C. & McFadden, G. Tumorigenic poxviruses: analysis of viral DNA sequences implicated in the tumorigenicity of Shope fibroma virus and malignant rabbit virus. *Virology* **152**, 308-321 (1986).

70 Block, W., Upton, C. & McFadden, G. Tumorigenic poxviruses: genomic organization of malignant rabbit virus, a recombinant between Shope fibroma virus and myxoma virus. *Virology* **140**, 113-124 (1985).

71 Upton, C., Macen, J. L., Maranchuk, R. A., DeLange, A. M. & McFadden, G. Tumorigenic poxviruses: fine analysis of the recombination junctions in malignant rabbit fibroma virus, a recombinant between Shope fibroma virus and myxoma virus. *Virology* **166**, 229-239 (1988).

72 Fenner, F. J. & Ratcliffe, F. *Myxomatosis*. (University Press, 1965).

73 Hobbs, J. R. THE OCCURRENCE OF NATURAL AND ACQUIRED IMMUNITY TO INFECTIOUS MYXOMATOSIS OF RABBITS. *Science* **73**, 94-95, doi:10.1126/science.73.1882.94 (1931).

74 Rivers, T. M. INFECTIOUS MYXOMATOSIS OF RABBITS : OBSERVATIONS ON THE PATHOLOGICAL CHANGES INDUCED BY VIRUS MYXOMATOSUM (SANARELLI). *J Exp Med* **51**, 965-976 (1930).

75 Macen, J. L. *et al.* Expression of the myxoma virus tumor necrosis factor receptor homologue and M11L genes is required to prevent virus-induced apoptosis in infected rabbit T lymphocytes. *Virology* **218**, 232-237, doi:10.1006/viro.1996.0183 (1996).

76 Kerr, P. J. Myxomatosis in Australia and Europe: a model for emerging infectious diseases. *Antiviral Res* **93**, 387-415, doi:10.1016/j.antiviral.2012.01.009 (2012).

77 FENNER, F., MARSHALL, I. D. & WOODROOFE, G. M. Studies in the epidemiology of infectious myxomatosis of rabbits. I. Recovery of Australian wild rabbits (Oryctolagus cuniculus) from myxomatosis under field conditions. *J Hyg (Lond)* **51**, 225-244 (1953).

78 Morales, M. *et al.* Genome comparison of a nonpathogenic myxoma virus field strain with its ancestor, the virulent Lausanne strain. *J Virol* **83**, 2397-2403, doi:10.1128/JVI.02189-08 (2009).

79 Best, S. M., Collins, S. V. & Kerr, P. J. Coevolution of host and virus: cellular localization of virus in myxoma virus infection of resistant and susceptible European rabbits. *Virology* **277**, 76-91, doi:10.1006/viro.2000.0505 S0042-6822(00)90505-1 [pii] (2000).

80 Kerr, P. J. *et al.* Evolutionary history and attenuation of myxoma virus on two continents. *PLoS Pathog* **8**, e1002950, doi:10.1371/journal.ppat.1002950 (2012).

81 Dalton, K. P., Nicieza, I., Baragaño, A., Alonso, J. M. & Parra, F. Molecular characterisation of virulence graded field isolates of myxoma virus. *Virol J* **7**, 49, doi:10.1186/1743-422X-7-49 (2010).

82 Mallardo, M., Schleich, S. & Krijnse Locker, J. Microtubule-dependent organization of vaccinia virus core-derived early mRNAs into distinct cytoplasmic structures. *Mol Biol Cell* **12**, 3875-3891 (2001).

83 Carter, G. C. *et al.* Vaccinia virus cores are transported on microtubules. *J Gen Virol* **84**, 2443-2458 (2003).

84 Smith, G. L., Murphy, B. J. & Law, M. Vaccinia virus motility. *Annu Rev Microbiol* **57**, 323-342, doi:10.1146/annurev.micro.57.030502.091037 (2003).

85 Yang, Z. *et al.* Expression profiling of the intermediate and late stages of poxvirus replication. *J Virol* **85**, 9899-9908, doi:10.1128/JVI.05446-11 (2011).

86 JOKLIK, W. K. THE INTRACELLULAR UNCOATING OF POXVIRUS DNA. II. THE MOLECULAR BASIS OF THE UNCOATING PROCESS. *J Mol Biol* **8**, 277-288 (1964).

87 Broyles, S. S. Vaccinia virus transcription. *J Gen Virol* **84**, 2293-2303 (2003).

88 Chakrabarti, S., Sisler, J. R. & Moss, B. Compact, synthetic, vaccinia virus early/late promoter for protein expression. *Biotechniques* **23**, 1094-1097 (1997).

89 Doceul, V., Hollinshead, M., van der Linden, L. & Smith, G. L. Repulsion of Superinfecting Virions: A Mechanism for Rapid Virus Spread. *Science* **327**, 873-876, doi:10.1126/science.1183173 (2010).

90 Condit, R. C., Moussatche, N. & Traktman, P. In a nutshell: structure and assembly of the vaccinia virion. *Adv Virus Res* **66**, 31-124, doi:S0065-3527(06)66002-8 [pii] 10.1016/S0065-3527(06)66002-8 (2006).

91 Szajner, P., Weisberg, A. S., Lebowitz, J., Heuser, J. & Moss, B. External scaffold of spherical immature poxvirus particles is made of protein trimers, forming a honeycomb lattice. *J Cell Biol* **170**, 971-981, doi:10.1083/jcb.200504026 (2005).

92 Cassetti, M. C., Merchlinsky, M., Wolffe, E. J., Weisberg, A. S. & Moss, B. DNA packaging mutant: repression of the vaccinia virus A32 gene results in noninfectious, DNA-deficient, spherical, enveloped particles. *J Virol* **72**, 5769-5780 (1998).

93 Mohandas, A. R. & Dales, S. Involvement of spicules in the formation of vaccinia virus envelopes elucidated by a conditional lethal mutant. *Virology* **214**, 494-502 (1995).

94 Sodeik, B., Griffiths, G., Ericsson, M., Moss, B. & Doms, R. W. Assembly of vaccinia virus: effects of rifampin on the intracellular distribution of viral protein p65. *J Virol* **68**, 1103-1114 (1994).

95 Senkevich, T. G., Weisberg, A. S. & Moss, B. Vaccinia virus E10R protein is associated with the membranes of intracellular mature virions and has a role in morphogenesis. *Virology* **278**, 244-252, doi:10.1006/viro.2000.0656 (2000).

96 Senkevich, T. G., White, C. L., Koonin, E. V. & Moss, B. Complete pathway for protein disulfide bond formation encoded by poxviruses. *Proc Natl Acad Sci U S A* **99**, 6667-6672, doi:10.1073/pnas.062163799 (2002).

97 da Fonseca, F. G., Wolffe, E. J., Weisberg, A. & Moss, B. Characterization of the vaccinia virus H3L envelope protein: topology and posttranslational membrane insertion via the C-terminal hydrophobic tail. *J Virol* **74**, 7508-7517 (2000).

98 Sodeik, B. *et al.* Assembly of vaccinia virus: incorporation of p14 and p32 into the membrane of the intracellular mature virus. *J Virol* **69**, 3560-3574 (1995).

99 Ward, B. M. Visualization and characterization of the intracellular movement of vaccinia virus intracellular mature virions. *J Virol* **79**, 4755-4763, doi:10.1128/JVI.79.8.4755-4763.2005 (2005).

100 Sanderson, C. M., Hollinshead, M. & Smith, G. L. The vaccinia virus A27L protein is needed for the microtubule-dependent transport of intracellular mature virus particles. *J Gen Virol* **81**, 47-58 (2000).

101 Tooze, J., Hollinshead, M., Reis, B., Radsak, K. & Kern, H. Progeny vaccinia and human cytomegalovirus particles utilize early endosomal cisternae for their envelopes. *Eur J Cell Biol* **60**, 163-178 (1993).

102 Schmelz, M. *et al.* Assembly of vaccinia virus: the second wrapping cisterna is derived from the trans Golgi network. *J Virol* **68**, 130-147 (1994).

103 Hiller, G. & Weber, K. Golgi-derived membranes that contain an acylated viral polypeptide are used for vaccinia virus envelopment. *J Virol* **55**, 651-659 (1985).

104 Geada, M. M., Galindo, I., Lorenzo, M. M., Perdiguero, B. & Blasco, R. Movements of vaccinia virus intracellular enveloped virions with GFP tagged to the F13L envelope protein. *J Gen Virol* **82**, 2747-2760 (2001).

105 Ward, B. M. & Moss, B. Vaccinia virus intracellular movement is associated with microtubules and independent of actin tails. *J Virol* **75**, 11651-11663, doi:10.1128/jvi.75.23.11651-11663.2001 (2001).

106 Ward, B. M. & Moss, B. Visualization of intracellular movement of vaccinia virus virions containing a green fluorescent protein-B5R membrane protein chimera. *J Virol* **75**, 4802-4813, doi:10.1128/jvi.75.10.4802-4813.2001 (2001).

107 Moss, B. Poxvirus entry and membrane fusion. *Virology* **344**, 48-54, doi:S0042-6822(05)00601-X [pii] 10.1016/j.virol.2005.09.037 (2006).

108 Meiser, A., Sancho, C. & Krijnse Locker, J. Plasma membrane budding as an alternative release mechanism of the extracellular enveloped form of vaccinia virus from HeLa cells. *J Virol* **77**, 9931-9942 (2003).

109 Boulanger, D., Smith, T. & Skinner, M. A. Morphogenesis and release of fowlpox virus. *J Gen Virol* **81**, 675-687 (2000).

110 Vanderplasschen, A. & Smith, G. L. A novel virus binding assay using confocal microscopy: demonstration that the intracellular and extracellular vaccinia virions bind to different cellular receptors. *J Virol* **71**, 4032-4041 (1997).

111 Chahroudi, A. *et al.* Vaccinia virus tropism for primary hematolymphoid cells is determined by restricted expression of a unique virus receptor. *J Virol* **79**, 10397-10407, doi:10.1128/JVI.79.16.10397-10407.2005 (2005).

112 Moss, B. Poxvirus Cell Entry: How Many Proteins Does it Take? *Viruses* **4**, 688-707 (2012).

113 Schmidt, F. I., Bleck, C. K. & Mercer, J. Poxvirus host cell entry. *Curr Opin Virol* **2**, 20-27, doi:10.1016/j.coviro.2011.11.007 (2012).

114 Chung, C. S., Hsiao, J. C., Chang, Y. S. & Chang, W. A27L protein mediates vaccinia virus interaction with cell surface heparan sulfate. *J Virol* **72**, 1577-1585 (1998).

115 Hsiao, J. C., Chung, C. S. & Chang, W. Cell surface proteoglycans are necessary for A27L protein-mediated cell fusion: identification of the N-terminal region of A27L protein as the glycosaminoglycan-binding domain. *J Virol* **72**, 8374-8379 (1998).

116 Hsiao, J. C., Chung, C. S. & Chang, W. Vaccinia virus envelope D8L protein binds to cell surface chondroitin sulfate and mediates the adsorption of intracellular mature virions to cells. *J Virol* **73**, 8750-8761 (1999).

117 Lin, C. L., Chung, C. S., Heine, H. G. & Chang, W. Vaccinia virus envelope H3L protein binds to cell surface heparan sulfate and is important for intracellular mature virion morphogenesis and virus infection in vitro and in vivo. *J Virol* **74**, 3353-3365 (2000).

118 Chiu, W. L., Lin, C. L., Yang, M. H., Tzou, D. L. & Chang, W. Vaccinia virus 4c (A26L) protein on intracellular mature virus binds to the extracellular cellular matrix laminin. *J Virol* **81**, 2149-2157, doi:10.1128/JVI.02302-06 (2007).

119 Foo, C. H. *et al.* Vaccinia virus L1 binds to cell surfaces and blocks virus entry independently of glycosaminoglycans. *Virology* **385**, 368-382, doi:10.1016/j.virol.2008.12.019 (2009).

120 Bengali, Z., Townsley, A. C. & Moss, B. Vaccinia virus strain differences in cell attachment and entry. *Virology* **389**, 132-140, doi:10.1016/j.virol.2009.04.012 (2009).

121 Bengali, Z., Satheshkumar, P. S. & Moss, B. Orthopoxvirus species and strain differences in cell entry. *Virology* **433**, 506-512, doi:10.1016/j.virol.2012.08.044 (2012).

122 Roberts, K. L. *et al.* Acidic residues in the membrane-proximal stalk region of vaccinia virus protein B5 are required for glycosaminoglycan-mediated disruption of the extracellular enveloped virus outer membrane. *J Gen Virol* **90**, 1582-1591, doi:10.1099/vir.0.009092-0 (2009).

123 Husain, M., Weisberg, A. S. & Moss, B. Resistance of a vaccinia virus A34R deletion mutant to spontaneous rupture of the outer membrane of progeny virions on the surface of infected cells. *Virology* **366**, 424-432, doi:S0042-6822(07)00352-2 [pii] 10.1016/j.virol.2007.05.015 (2007).

124 Mercer, J. *et al.* Vaccinia virus strains use distinct forms of macropinocytosis for host-cell entry. *Proc Natl Acad Sci U S A* **107**, 9346-9351, doi:10.1073/pnas.1004618107 (2010).

125 Mercer, J. & Helenius, A. Vaccinia virus uses macropinocytosis and apoptotic mimicry to enter host cells. *Science* **320**, 531-535, doi:10.1126/science.1155164 (2008).

126 Mercer, J. *et al.* Vaccinia virus strains use distinct forms of macropinocytosis for host-cell entry. *Proceedings of the National Academy of Sciences of the United States of America* **107**, 9346-9351, doi:10.1073/pnas.1004618107 (2010).

127 Schmidt, F. I., Bleck, C. K., Helenius, A. & Mercer, J. Vaccinia extracellular virions enter cells by macropinocytosis and acid-activated membrane rupture. *EMBO J* **30**, 3647-3661, doi:10.1038/emboj.2011.245 (2011).

128 Chang, S. J., Chang, Y. X., Izmailyan, R., Tang, Y. L. & Chang, W. Vaccinia virus A25 and A26 proteins are fusion suppressors for mature virions and determine strain-specific virus entry pathways into HeLa, CHO-K1, and L cells. *Journal of virology* **84**, 8422-8432, doi:10.1128/jvi.00599-10 (2010).

129 Suh, H. N. & Han, H. J. Laminin regulates mouse embryonic stem cell migration: involvement of Epac1/Rap1 and Rac1/cdc42. *Am J Physiol Cell Physiol* **298**, C1159-1169, doi:10.1152/ajpcell.00496.2009 (2010).

130 Smith, G. L., Vanderplasschen, A. & Law, M. The formation and function of extracellular enveloped vaccinia virus. *J Gen Virol* **83**, 2915-2931 (2002).

131 Benhnia, M. R. *et al.* Unusual features of vaccinia virus extracellular virion form neutralization resistance revealed in human antibody responses to the smallpox vaccine. *J Virol* **87**, 1569-1585, doi:10.1128/JVI.02152-12 (2013).

132 Vanderplasschen, A., Mathew, E., Hollinshead, M., Sim, R. B. & Smith, G. L. Extracellular enveloped vaccinia virus is resistant to complement because of incorporation of host complement control proteins into its envelope. *Proc Natl Acad Sci U S A* **95**, 7544-7549 (1998).

133 Dehaven, B. C., Gupta, K. & Isaacs, S. N. The vaccinia virus A56 protein: a multifunctional transmembrane glycoprotein that anchors two secreted viral proteins. *J Gen Virol* **92**, 1971-1980, doi:10.1099/vir.0.030460-0 (2011).

134 Girgis, N. M. *et al.* Cell surface expression of the vaccinia virus complement control protein is mediated by interaction with the viral A56 protein and protects infected cells from complement attack. *Journal of virology* **82**, 4205-4214, doi:10.1128/jvi.02426-07 (2008).

135 Payne, L. G. & Kristenson, K. Mechanism of vaccinia virus release and its specific inhibition by N1-isonicotinoyl-N2-3-methyl-4-chlorobenzoylhydrazine. *J Virol* **32**, 614-622 (1979).

136 Husain, M. & Moss, B. Role of receptor-mediated endocytosis in the formation of vaccinia virus extracellular enveloped particles. *J Virol* **79**, 4080-4089, doi:10.1128/JVI.79.7.4080-4089.2005 (2005).

137 Ulaeto, D., Grosenbach, D. & Hruby, D. E. The vaccinia virus 4c and A-type inclusion proteins are specific markers for the intracellular mature virus particle. *J Virol* **70**, 3372-3377 (1996).

138 Ward, B. M. & Moss, B. Golgi network targeting and plasma membrane internalization signals in vaccinia virus B5R envelope protein. *J Virol* **74**, 3771-3780 (2000).

139 Husain, M. & Moss, B. Intracellular trafficking of a palmitoylated membrane-associated protein component of enveloped vaccinia virus. *J Virol* **77**, 9008-9019 (2003).

140 Ploubidou, A. *et al.* Vaccinia virus infection disrupts microtubule organization and centrosome function. *EMBO J* **19**, 3932-3944, doi:10.1093/emboj/19.15.3932 (2000).

141 Leite, J. A. *et al.* A-type inclusion bodies: a factor influencing cowpox virus lesion pathogenesis. *Arch Virol* **156**, 617-628, doi:10.1007/s00705-010-0900-0 (2011).

142 Howard, A. R., Weisberg, A. S. & Moss, B. Congregation of orthopoxvirus virions in cytoplasmic A-type inclusions is mediated by interactions of a bridging protein (A26p) with a matrix protein (ATIp) and a virion membrane-associated protein (A27p). *J Virol* **84**, 7592-7602, doi:10.1128/JVI.00704-10 (2010).

143 Arakawa, Y., Cordeiro, J. V., Schleich, S., Newsome, T. P. & Way, M. The release of vaccinia virus from infected cells requires RhoA-mDia modulation of cortical actin. *Cell Host Microbe* **1**, 227-240, doi:S1931-3128(07)00072-8 [pii] 10.1016/j.chom.2007.04.006 (2007).

144 Wagenaar, T. R. & Moss, B. Expression of the A56 and K2 proteins is sufficient to inhibit vaccinia virus entry and cell fusion. *Journal of virology* **83**, 1546-1554, doi:10.1128/jvi.01684-08 (2009).

145 Blasco, R. & Moss, B. Extracellular vaccinia virus formation and cell-to-cell virus transmission are prevented by deletion of the gene encoding the 37,000-Dalton outer envelope protein. *J Virol* **65**, 5910-5920 (1991).

146 Engelstad, M., Howard, S. T. & Smith, G. L. A constitutively expressed vaccinia gene encodes a 42-kDa glycoprotein related to complement control factors that forms part of the extracellular virus envelope. *Virology* **188**, 801-810, doi:0042-6822(92)90535-W [pii] (1992).

147 Wolffe, E. J., Isaacs, S. N. & Moss, B. Deletion of the vaccinia virus B5R gene encoding a 42-kilodalton membrane glycoprotein inhibits extracellular virus envelope formation and dissemination. *J Virol* **67**, 4732-4741 (1993).

148 Lorenzo, M. M., Galindo, I., Griffiths, G. & Blasco, R. Intracellular localization of vaccinia virus extracellular enveloped virus envelope proteins individually expressed using a Semliki Forest virus replicon. *J Virol* **74**, 10535-10550 (2000).

149 Husain, M. & Moss, B. Vaccinia virus F13L protein with a conserved phospholipase catalytic motif induces colocalization of the B5R envelope glycoprotein in post-Golgi vesicles. *J Virol* **75**, 7528-7542, doi:10.1128/jvi.75.16.7528-7542.2001 (2001).

150 Blot, G., Janvier, K., Le Panse, S., Benarous, R. & Berlioz-Torrent, C. Targeting of the human immunodeficiency virus type 1 envelope to the trans-Golgi network through binding to TIP47 is required for env incorporation into virions and infectivity. *J Virol* **77**, 6931-6945 (2003).

151 Lopez-Vergès, S. *et al.* Tail-interacting protein TIP47 is a connector between Gag and Env and is required for Env incorporation into HIV-1 virions. *Proc Natl Acad Sci U S A* **103**, 14947-14952, doi:10.1073/pnas.0602941103 (2006).

152 Chen, Y. *et al.* Vaccinia virus p37 interacts with host proteins associated with LE-derived transport vesicle biogenesis. *Virol J* **6**, 44, doi:10.1186/1743-422X-6-44 (2009).

153 Honeychurch, K. M., Yang, G., Jordan, R. & Hruby, D. E. The vaccinia virus F13L YPPL motif is required for efficient release of extracellular enveloped virus. *J Virol* **81**, 7310-7315, doi:JVI.00034-07 [pii] 10.1128/JVI.00034-07 (2007).

154 Grosenbach, D. W. *et al.* Immune responses to the smallpox vaccine given in combination with ST-246, a small-molecule inhibitor of poxvirus dissemination. *Vaccine* **26**, 933-946, doi:S0264-410X(07)01437-5 [pii] 10.1016/j.vaccine.2007.11.095 (2008).

155 Jordan, R. *et al.* Single-dose safety and pharmacokinetics of ST-246, a novel orthopoxvirus egress inhibitor. *Antimicrob Agents Chemother* **52**, 1721-1727, doi:AAC.01303-07 [pii] 10.1128/AAC.01303-07 (2008).

156 Nalca, A. *et al.* Evaluation of orally delivered ST-246 as postexposure prophylactic and antiviral therapeutic in an aerosolized rabbitpox rabbit model. *Antiviral Res* **79**, 121-127, doi:S0166-3542(08)00245-3 [pii] 10.1016/j.antiviral.2008.03.005 (2008).

157 Quenelle, D. C. *et al.* Efficacy of delayed treatment with ST-246 given orally against systemic orthopoxvirus infections in mice. *Antimicrob Agents Chemother* **51**, 689-695, doi:AAC.00879-06 [pii] 10.1128/AAC.00879-06 (2007).

158 Quenelle, D. C. *et al.* Synergistic efficacy of the combination of ST-246 with CMX001 against orthopoxviruses. *Antimicrob Agents Chemother* **51**, 4118-4124, doi:AAC.00762-07 [pii] 10.1128/AAC.00762-07 (2007).

159 Sbrana, E. *et al.* Efficacy of the antipoxvirus compound ST-246 for treatment of severe orthopoxvirus infection. *Am J Trop Med Hyg* **76**, 768-773, doi:76/4/768 [pii] (2007).

160 Yang, G. *et al.* An orally bioavailable antipoxvirus compound (ST-246) inhibits extracellular virus formation and protects mice from lethal orthopoxvirus Challenge. *J Virol* **79**, 13139-13149, doi:79/20/13139 [pii] 10.1128/JVI.79.20.13139-13149.2005 (2005).

161 Husain, M. & Moss, B. Similarities in the induction of post-Golgi vesicles by the vaccinia virus F13L protein and phospholipase D. *J Virol* **76**, 7777-7789 (2002).

162 Engelstad, M. & Smith, G. L. The vaccinia virus 42-kDa envelope protein is required for the envelopment and egress of extracellular virus and for virus virulence. *Virology* **194**, 627-637, doi:S0042-6822(83)71302-4 [pii] 10.1006/viro.1993.1302 (1993).

163 Dodding, M. P., Newsome, T. P., Collinson, L. M., Edwards, C. & Way, M. An E2-F12 complex is required for intracellular enveloped virus morphogenesis during vaccinia infection. *Cellular microbiology* **11**, 808-824, doi:10.1111/j.1462-5822.2009.01296.x (2009).

164 Domi, A., Weisberg, A. S. & Moss, B. Vaccinia virus E2L null mutants exhibit a major reduction in extracellular virion formation and virus spread. *J Virol* **82**, 4215-4226, doi:JVI.00037-08 [pii] 10.1128/JVI.00037-08 (2008).

165 Morgan, G. W. *et al.* Vaccinia protein F12 has structural similarity to kinesin light chain and contains a motor binding motif required for virion export. *PLoS pathogens* **6**, e1000785, doi:10.1371/journal.ppat.1000785 (2010).

166 Chan, W. M., Kalkanoglu, A. E. & Ward, B. M. The inability of vaccinia virus A33R protein to form intermolecular disulfide-bonded homodimers does not affect the production of infectious extracellular virus. *Virology* **408**, 109-118, doi:10.1016/j.virol.2010.09.021 (2010).

167 Chan, W. M. & Ward, B. M. There is an A33-dependent mechanism for the incorporation of B5-GFP into vaccinia virus extracellular enveloped virions. *Virology* **402**, 83-93, doi:10.1016/j.virol.2010.03.017 (2010).

168 Katz, E., Ward, B. M., Weisberg, A. S. & Moss, B. Mutations in the vaccinia virus A33R and B5R envelope proteins that enhance release of extracellular virions and eliminate formation of actin-containing microvilli without preventing tyrosine phosphorylation of the A36R protein. *J Virol* **77**, 12266-12275 (2003).

169 Ward, B. M., Weisberg, A. S. & Moss, B. Mapping and functional analysis of interaction sites within the cytoplasmic domains of the vaccinia virus A33R and A36R envelope proteins. *J Virol* **77**, 4113-4126 (2003).

170 Wolffe, E. J., Weisberg, A. S. & Moss, B. The vaccinia virus A33R protein provides a chaperone function for viral membrane localization and tyrosine phosphorylation of the A36R protein. *J Virol* **75**, 303-310, doi:10.1128/jvi.75.1.303-310.2001 (2001).

171 Roper, R. L., Wolffe, E. J., Weisberg, A. & Moss, B. The envelope protein encoded by the A33R gene is required for formation of actin-containing microvilli and efficient cell-to-cell spread of vaccinia virus. *J Virol* **72**, 4192-4204 (1998).

172 Roper, R. L., Payne, L. G. & Moss, B. Extracellular vaccinia virus envelope glycoprotein encoded by the A33R gene. *J Virol* **70**, 3753-3762 (1996).

173 Breiman, A., Carpentier, D. C., Ewles, H. A. & Smith, G. L. Transport and stability of the vaccinia virus A34 protein is affected by the A33 protein. *J Gen Virol* **94**, 720-725, doi:10.1099/vir.0.049486-0 (2013).

174 Chan, W. M. & Ward, B. M. Increased interaction between vaccinia virus proteins A33 and B5 is detrimental to infectious extracellular enveloped virion production. *J Virol* **86**, 8232-8244, doi:10.1128/JVI.00253-12 (2012).

175 Chan, W. M. & Ward, B. M. The A33-dependent incorporation of B5 into extracellular enveloped vaccinia virions is mediated through an interaction between their lumenal domains. *J Virol* **86**, 8210-8220, doi:10.1128/JVI.00249-12 (2012).

176 Earley, A. K., Chan, W. M. & Ward, B. M. The vaccinia virus B5 protein requires A34 for efficient intracellular trafficking from the endoplasmic reticulum to the site of wrapping and incorporation into progeny virions. *J Virol* **82**, 2161-2169, doi:10.1128/JVI.01971-07 (2008).

177 Wolffe, E. J., Katz, E., Weisberg, A. & Moss, B. The A34R glycoprotein gene is required for induction of specialized actin-containing microvilli and efficient cell-to-cell transmission of vaccinia virus. *J Virol* **71**, 3904-3915 (1997).

178 McIntosh, A. A. & Smith, G. L. Vaccinia virus glycoprotein A34R is required for infectivity of extracellular enveloped virus. *J Virol* **70**, 272-281 (1996).

179 Blasco, R., Sisler, J. R. & Moss, B. Dissociation of progeny vaccinia virus from the cell membrane is regulated by a viral envelope glycoprotein: effect of a point mutation in the lectin homology domain of the A34R gene. *J Virol* **67**, 3319-3325 (1993).

180 Breiman, A. & Smith, G. L. Vaccinia virus B5 protein affects the glycosylation, localization and stability of the A34 protein. *J Gen Virol* **91**, 1823-1827, doi:10.1099/vir.0.020677-0 (2010).

181 Perdiguero, B., Lorenzo, M. M. & Blasco, R. Vaccinia virus A34 glycoprotein determines the protein composition of the extracellular virus envelope. *J Virol* **82**, 2150-2160, doi:JVI.01969-07 [pii] 10.1128/JVI.01969-07 (2008).

182 Horsington, J. *et al.* A36-dependent Actin Filament Nucleation Promotes Release of Vaccinia Virus. *PLoS Pathog* **9**, e1003239 (2013).

183 Humphries, A. C. *et al.* Clathrin potentiates vaccinia-induced actin polymerization to facilitate viral spread. *Cell Host Microbe* **12**, 346-359, doi:10.1016/j.chom.2012.08.002 (2012).

184 Johnston, S. C. & Ward, B. M. Vaccinia virus protein F12 associates with intracellular enveloped virions through an interaction with A36. *J Virol* **83**, 1708-1717, doi:10.1128/JVI.01364-08 (2009).

185 Newsome, T. P., Weisswange, I., Frischknecht, F. & Way, M. Abl collaborates with Src family kinases to stimulate actin-based motility of vaccinia virus. *Cell Microbiol* **8**, 233-241, doi:CMI613 [pii] 10.1111/j.1462-5822.2005.00613.x (2006).

186 Herrero-Martinez, E., Roberts, K. L., Hollinshead, M. & Smith, G. L. Vaccinia virus intracellular enveloped virions move to the cell periphery on microtubules in the absence of the A36R protein. *J Gen Virol* **86**, 2961-2968, doi:86/11/2961 [pii] 10.1099/vir.0.81260-0 (2005).

187 Ward, B. M. & Moss, B. Vaccinia virus A36R membrane protein provides a direct link between intracellular enveloped virions and the microtubule motor kinesin. *J Virol* **78**, 2486-2493 (2004).

188 van Eijl, H., Hollinshead, M. & Smith, G. L. The vaccinia virus A36R protein is a type Ib membrane protein present on intracellular but not extracellular enveloped virus particles. *Virology* **271**, 26-36, doi:10.1006/viro.2000.0260 S0042-6822(00)90260-5 [pii] (2000).

189 Frischknecht, F. *et al.* Actin-based motility of vaccinia virus mimics receptor tyrosine kinase signalling. *Nature* **401**, 926-929, doi:10.1038/44860 (1999).

190 Rottger, S., Frischknecht, F., Reckmann, I., Smith, G. L. & Way, M. Interactions between vaccinia virus IEV membrane proteins and their roles in IEV assembly and actin tail formation. *J Virol* **73**, 2863-2875 (1999).

191 Sanderson, C. M., Frischknecht, F., Way, M., Hollinshead, M. & Smith, G. L. Roles of vaccinia virus EEV-specific proteins in intracellular actin tail formation and low pH-induced cell-cell fusion. *J Gen Virol* **79 (Pt 6)**, 1415-1425 (1998).

192 Wolffe, E. J., Weisberg, A. S. & Moss, B. Role for the vaccinia virus A36R outer envelope protein in the formation of virus-tipped actin-containing microvilli and cell-to-cell virus spread. *Virology* **244**, 20-26, doi:S0042-6822(98)99103-6 [pii] 10.1006/viro.1998.9103 (1998).

193 Parkinson, J. E. & Smith, G. L. Vaccinia virus gene A36R encodes a M(r) 43-50 K protein on the surface of extracellular enveloped virus. *Virology* **204**, 376-390, doi:S0042-6822(84)71542-X [pii] 10.1006/viro.1994.1542 (1994).

194 Turner, P. C. & Moyer, R. W. The vaccinia virus fusion inhibitor proteins SPI-3 (K2) and HA (A56) expressed by infected cells reduce the entry of superinfecting virus. *Virology* **380**, 226-233, doi:10.1016/j.virol.2008.07.020 (2008).

195 Wagenaar, T. R., Ojeda, S. & Moss, B. Vaccinia virus A56/K2 fusion regulatory protein interacts with the A16 and G9 subunits of the entry fusion complex. *Journal of virology* **82**, 5153-5160, doi:10.1128/jvi.00162-08 (2008).

196 Newsome, T. P., Scaplehorn, N. & Way, M. SRC mediates a switch from microtubule- to actin-based motility of vaccinia virus. *Science* **306**, 124-129, doi:10.1126/science.1101509 1101509 [pii] (2004).

197 Katz, E., Wolffe, E. & Moss, B. Identification of second-site mutations that enhance release and spread of vaccinia virus. *J Virol* **76**, 11637-11644 (2002).

198 Mathew, E. C., Sanderson, C. M., Hollinshead, R. & Smith, G. L. A mutational analysis of the vaccinia virus B5R protein. *J Gen Virol* **82**, 1199-1213 (2001).

199 Mathew, E. C. *et al.* The effects of targeting the vaccinia virus B5R protein to the endoplasmic reticulum on virus morphogenesis and dissemination. *Virology* **265**, 131-146, doi:10.1006/viro.1999.0023 S0042-6822(99)90023-5 [pii] (1999).

200 Herrera, E., Lorenzo, M. M., Blasco, R. & Isaacs, S. N. Functional analysis of vaccinia virus B5R protein: essential role in virus envelopment is independent of a large portion of the extracellular domain. *J Virol* **72**, 294-302 (1998).

201 Mathew, E., Sanderson, C. M., Hollinshead, M. & Smith, G. L. The extracellular domain of vaccinia virus protein B5R affects plaque phenotype, extracellular enveloped virus release, and intracellular actin tail formation. *J Virol* **72**, 2429-2438 (1998).

202 Katz, E., Wolffe, E. J. & Moss, B. The cytoplasmic and transmembrane domains of the vaccinia virus B5R protein target a chimeric human immunodeficiency virus type 1 glycoprotein to the outer envelope of nascent vaccinia virions. *J Virol* **71**, 3178-3187 (1997).

203 Isaacs, S. N., Wolffe, E. J., Payne, L. G. & Moss, B. Characterization of a vaccinia virus-encoded 42-kilodalton class I membrane glycoprotein component of the extracellular virus envelope. *J Virol* **66**, 7217-7224 (1992).

204 Arakawa, Y., Cordeiro, J. V. & Way, M. F11L-mediated inhibition of RhoA-mDia signaling stimulates microtubule dynamics during vaccinia virus infection. *Cell Host Microbe* **1**, 213-226, doi:S1931-3128(07)00073-X [pii] 10.1016/j.chom.2007.04.007 (2007).

205 Cordeiro, J. V. *et al.* F11-mediated inhibition of RhoA signalling enhances the spread of vaccinia virus in vitro and in vivo in an intranasal mouse model of infection. *PLoS One* **4**, e8506, doi:10.1371/journal.pone.0008506 (2009).

206 Zhang, W. H., Wilcock, D. & Smith, G. L. Vaccinia virus F12L protein is required for actin tail formation, normal plaque size, and virulence. *J Virol* **74**, 11654-11662 (2000).

207 van Eijl, H., Hollinshead, M., Rodger, G., Zhang, W. H. & Smith, G. L. The vaccinia virus F12L protein is associated with intracellular enveloped virus particles and is required for their egress to the cell surface. *J Gen Virol* **83**, 195-207 (2002).

208 Husain, M., Weisberg, A. & Moss, B. Topology of epitope-tagged F13L protein, a major membrane component of extracellular vaccinia virions. *Virology* **308**, 233-242 (2003).

209 Borrego, B., Lorenzo, M. M. & Blasco, R. Complementation of P37 (F13L gene) knock-out in vaccinia virus by a cell line expressing the gene constitutively. *J Gen Virol* **80 (Pt 2)**, 425-432 (1999).

210 Roper, R. L. & Moss, B. Envelope formation is blocked by mutation of a sequence related to the HKD phospholipid metabolism motif in the vaccinia virus F13L protein. *J Virol* **73**, 1108-1117 (1999).

211 Wagenaar, T. R. & Moss, B. Association of vaccinia virus fusion regulatory proteins with the multicomponent entry/fusion complex. *Journal of virology* **81**, 6286-6293, doi:10.1128/jvi.00274-07 (2007).

212 Zhou, J., Sun, X. Y., Fernando, G. J. & Frazer, I. H. The vaccinia virus K2L gene encodes a serine protease inhibitor which inhibits cell-cell fusion. *Virology* **189**, 678-686 (1992).

213 Turner, P. C. & Moyer, R. W. Orthopoxvirus fusion inhibitor glycoprotein SPI-3 (open reading frame K2L) contains motifs characteristic of serine proteinase inhibitors that are not required for control of cell fusion. *J Virol* **69**, 5978-5987 (1995).

214 Hollinshead, M. *et al.* Vaccinia virus utilizes microtubules for movement to the cell surface. *J Cell Biol* **154**, 389-402 (2001).

215 Rietdorf, J. *et al.* Kinesin-dependent movement on microtubules precedes actin-based motility of vaccinia virus. *Nat Cell Biol* **3**, 992-1000, doi:10.1038/ncb1101-992 ncb1101-992 [pii] (2001).

216 Doceul, V., Hollinshead, M., Breiman, A., Laval, K. & Smith, G. L. Protein B5 is required on extracellular enveloped vaccinia virus for repulsion of superinfecting virions. *J Gen Virol* **93**, 1876-1886, doi:10.1099/vir.0.043943-0 (2012).

217 Scaplehorn, N. *et al.* Grb2 and Nck act cooperatively to promote actin-based motility of vaccinia virus. *Curr Biol* **12**, 740-745, doi:S0960982202008126 [pii] (2002).

218 Frischknecht, F. *et al.* Tyrosine phosphorylation is required for actin-based motility of vaccinia but not Listeria or Shigella. *Curr Biol* **9**, 89-92, doi:S0960-9822(99)80020-7 [pii] (1999).

219 Dodding, M. P. & Way, M. Nck- and N-WASP-dependent actin-based motility is conserved in divergent vertebrate poxviruses. *Cell Host Microbe* **6**, 536-550, doi:S1931-3128(09)00379-5 [pii] 10.1016/j.chom.2009.10.011 (2009).

220 Moreau, V. *et al.* A complex of N-WASP and WIP integrates signalling cascades that lead to actin polymerization. *Nat Cell Biol* **2**, 441-448, doi:10.1038/35017080 (2000).

221 Reeves, P. M. *et al.* Disabling poxvirus pathogenesis by inhibition of Abl-family tyrosine kinases. *Nat Med* **11**, 731-739, doi:10.1038/nm1265 (2005).

222 Guerra, S., Aracil, M., Conde, R., Bernad, A. & Esteban, M. Wiskott-Aldrich syndrome protein is needed for vaccinia virus pathogenesis. *J Virol* **79**, 2133-2140, doi:10.1128/JVI.79.4.2133-2140.2005 (2005).

223 Morales, I. *et al.* The vaccinia virus F11L gene product facilitates cell detachment and promotes migration. *Traffic* **9**, 1283-1298, doi:TRA762 [pii] 10.1111/j.1600-0854.2008.00762.x (2008).

224 Valderrama, F., Cordeiro, J. V., Schleich, S., Frischknecht, F. & Way, M. Vaccinia virus-induced cell motility requires F11L-mediated inhibition of RhoA signaling. *Science* **311**, 377-381, doi:311/5759/377 [pii] 10.1126/science.1122411 (2006).

225 Zwilling, J., Sliva, K., Schwantes, A., Schnierle, B. & Sutter, G. Functional F11L and K1L genes in modified vaccinia virus Ankara restore virus-induced cell motility but not growth in human and murine cells. *Virology* **404**, 231-239, doi:10.1016/j.virol.2010.05.008 (2010).

226 Way, M. Interaction of vaccinia virus with the actin cytoskeleton. *Folia Microbiol (Praha)* **43**, 305-310 (1998).

227 Sanderson, C. M., Way, M. & Smith, G. L. Virus-induced cell motility. *J Virol* **72**, 1235-1243 (1998).

228 Dulbecco, R. Production of Plaques in Monolayer Tissue Cultures by Single Particles of an Animal Virus. *Proc Natl Acad Sci U S A* **38**, 747-752 (1952).

229 PADGETT, B. L., MOORE, M. S. & WALKER, D. L. Plaque assays for myxoma and fibroma viruses and differentiation of the viruses by plaque form. *Virology* **17**, 462-469 (1962).

230 SCHWERDT, P. R. & SCHWERDT, C. E. A plaque assay for myxoma virus infectivity. *Proc Soc Exp Biol Med* **109**, 717-721 (1962).

231 WOODROOFE, G. M. & FENNER, F. VIRUSES OF THE MYXOMA-FIBROMA SUBGROUP OF THE POXVIRUSES. I. PLAQUE PRODUCTION IN CULTURED CELLS, PLAQUE-REDUCTION TESTS, AND CROSS-PROTECTION TESTS IN RABBITS. *Aust J Exp Biol Med Sci* **43**, 123-142 (1965).

232 HANAFUSA, H., HANAFUSA, T. & KAMAHORA, J. Transformations of myxoma into vaccinia or ectromelia virus in tissue culture. *Nature* **184(Suppl 15)**, 1152-1153 (1959).

233 PORTERFIELD, J. S. & ALLISON, A. C. Studies with poxviruses by an improved plaque technique. *Virology* **10**, 233-244 (1960).

234 NOYES, W. F. A simple technic for demonstrating plaque formation with virus of vaccinia. *Proc Soc Exp Biol Med* **83**, 426-429 (1953).

235 Villa, N. Y. *et al.* Myxoma and vaccinia viruses exploit different mechanisms to enter and infect human cancer cells. *Virology* **401**, 266-279, doi:10.1016/j.virol.2010.02.027 (2010).

236 Purcell, D. A. & Clarke, J. K. Some aspects of the morphogenesis of myxoma virus in vivo. *Arch Gesamte Virusforsch* **39**, 369-375 (1972).

237 PADGETT, B. L., WRIGHT, M. J., JAYNE, A. & WALKER, D. L. ELECTRON MICROSCOPIC STRUCTURE OF MYXOMA VIRUS AND SOME REACTIVABLE DERIVATIVES. *J Bacteriol* **87**, 454-460 (1964).

238 CHAPPLE, P. J. & WESTWOOD, J. C. ELECTRON MICROSCOPY OF MYXOMA VIRUS. *Nature* **199**, 199-200 (1963).

239 Duteyrat, J. L., Gelfi, J. & Bertagnoli, S. Ultrastructural study of myxoma virus morphogenesis. *Archives of Virology* **151**, 2161-2180, doi:10.1007/s00705-006-0791-2 (2006).

240 KATO, S., TAKAHASHI, M., MIYAMOTO, H. & KAMAHORA, J. SHOPE FIBROMA AND RABBIT MYXOMA VIRUSES. I. AUTORADIOGRAPHIC AND CYTOIMMUNOLOGICAL STUDIES ON "B" TYPE INCLUSIONS. *Biken J* **6**, 127-134 (1963).

241 FARRANT, J. L. & FENNER, F. A comparison of the morphology of vaccinia and myxoma viruses. *Aust J Exp Biol Med Sci* **31**, 121-125 (1953).

242 Zachertowska, A., Brewer, D. & Evans, D. H. MALDI-TOF mass spectroscopy detects the capsid structural instabilities created by deleting the myxoma virus cuprozinc SOD1 homolog M131R. *J Virol Methods* **122**, 63-72, doi:S0166-0934(04)00234-4 [pii] 10.1016/j.jviromet.2004.08.004 (2004).

243 Zachertowska, A., Brewer, D. & Evans, D. H. Characterization of the major capsid proteins of myxoma virus particles using MALDI-TOF mass spectrometry. *J Virol Methods* **132**, 1-12, doi:S0166-0934(05)00276-4 [pii] 10.1016/j.jviromet.2005.08.015 (2006).

244 Cao, J. X. & McFadden, G. Characterization of the myxoma virus M118L protein: a novel essential poxvirus IMV-associated protein. *Virus Genes* **23**, 303-313 (2001).

245 Katze, M. G., He, Y. & Gale, M. Viruses and interferon: a fight for supremacy. *Nat Rev Immunol* **2**, 675-687, doi:10.1038/nri888 (2002).

246 Croft, M., Benedict, C. A. & Ware, C. F. Clinical targeting of the TNF and TNFR superfamilies. *Nat Rev Drug Discov* **12**, 147-168, doi:10.1038/nrd3930 (2013).

247 Wang, F. *et al.* RIG-I mediates the co-induction of tumor necrosis factor and type I interferon elicited by myxoma virus in primary human macrophages. *PLoS Pathog* **4**, e1000099, doi:10.1371/journal.ppat.1000099 (2008).

248 Wang, F. *et al.* Disruption of Erk-dependent type I interferon induction breaks the myxoma virus species barrier. *Nat Immunol* **5**, 1266-1274, doi:ni1132 [pii] 10.1038/ni1132 (2004).

249 Dai, P. *et al.* Myxoma virus induces type I interferon production in murine plasmacytoid dendritic cells via a TLR9/MyD88-, IRF5/IRF7-, and IFNAR-dependent pathway. *J Virol* **85**, 10814-10825, doi:10.1128/jvi.00104-11 (2011).

250 Cao, H. *et al.* Innate immune response of human plasmacytoid dendritic cells to poxvirus infection is subverted by vaccinia E3 via its Z-DNA/RNA binding domain. *PLoS One* **7**, e36823, doi:10.1371/journal.pone.0036823 (2012).

251 Wang, F. *et al.* Myxoma virus selectively disrupts type I interferon signaling in primary human fibroblasts by blocking the activation of the Janus kinase Tyk2. *Virology* **387**, 136-146, doi:S0042-6822(09)00098-1 [pii] 10.1016/j.virol.2009.02.013 (2009).

252 Alcamí, A. & Smith, G. L. Soluble interferon-gamma receptors encoded by poxviruses. *Comp Immunol Microbiol Infect Dis* **19**, 305-317 (1996).

253 Mossman, K., Upton, C. & McFadden, G. The myxoma virus-soluble interferon-gamma receptor homolog, M-T7, inhibits interferon-gamma in a species-specific manner. *J Biol Chem* **270**, 3031-3038 (1995).

254 Schreiber, M. & McFadden, G. The myxoma virus TNF-receptor homologue (T2) inhibits tumor necrosis factor-alpha in a species-specific fashion. *Virology* **204**, 692-705, doi:10.1006/viro.1994.1585 (1994).

255 Bartee, E., Mohamed, M. R., Lopez, M. C., Baker, H. V. & McFadden, G. The addition of tumor necrosis factor plus beta interferon induces a novel synergistic antiviral state against poxviruses in primary human fibroblasts. *J Virol* **83**, 498-511, doi:10.1128/JVI.01376-08 (2009).

256 Bartee, E. & McFadden, G. Human cancer cells have specifically lost the ability to induce the synergistic state caused by tumor necrosis factor plus interferon-beta. *Cytokine* **47**, 199-205, doi:10.1016/j.cyto.2009.06.006 (2009).

257 Reed, J. C. Dysregulation of apoptosis in cancer. *J Clin Oncol* **17**, 2941-2953 (1999).

258 Yu, H., Pardoll, D. & Jove, R. STATs in cancer inflammation and immunity: a leading role for STAT3. *Nat Rev Cancer* **9**, 798-809, doi:10.1038/nrc2734 (2009).

259 Bukur, J., Jasinski, S. & Seliger, B. The role of classical and non-classical HLA class I antigens in human tumors. *Semin Cancer Biol* **22**, 350-358, doi:10.1016/j.semcancer.2012.03.003 (2012).

260 Dunn, G. P., Old, L. J. & Schreiber, R. D. The immunobiology of cancer immunosurveillance and immunoediting. *Immunity* **21**, 137-148, doi:10.1016/j.immuni.2004.07.017 (2004).

261 Gao, J. Q., Okada, N., Mayumi, T. & Nakagawa, S. Immune cell recruitment and cell-based system for cancer therapy. *Pharm Res* **25**, 752-768, doi:10.1007/s11095-007-9443-9 (2008).

262 Lippitz, B. E. Cytokine patterns in patients with cancer: a systematic review. *Lancet Oncol* **14**, e218-228, doi:10.1016/S1470-2045(12)70582-X (2013).

263 Andrewes, C. H. & Chaproniere, D. M. Propagation of rabbit myxoma and fibroma viruses in a guinea pig sarcoma. *Virology* **4**, 346-350 (1957).

264 Sypula, J., Wang, F., Ma, Y., Bell, J. & McFadden, G. Myxoma virus tropism in human tumor cells. *Gene Therapy and Molecular Biology* **8**, 103-114 (2004).

265 Kim, M. *et al.* The viral tropism of two distinct oncolytic viruses, reovirus and myxoma virus, is modulated by cellular tumor suppressor gene status. *Oncogene* **29**, 3990-3996, doi:10.1038/onc.2010.137 (2010).

266 Werden, S. J. & McFadden, G. The role of cell signaling in poxvirus tropism: the case of the M-T5 host range protein of myxoma virus. *Biochim Biophys Acta* **1784**, 228-237, doi:S1570-9639(07)00187-2 [pii] 10.1016/j.bbapap.2007.08.001 (2008).

267 Werden, S. J., Barrett, J. W., Wang, G., Stanford, M. M. & McFadden, G. M-T5, the ankyrin repeat, host range protein of myxoma virus, activates Akt and can be functionally replaced by cellular PIKE-A. *J Virol* **81**, 2340-2348, doi:JVI.01310-06 [pii] 10.1128/JVI.01310-06 (2007).

268 Wang, G. *et al.* Infection of human cancer cells with myxoma virus requires Akt activation via interaction with a viral ankyrin-repeat host range factor. *Proc Natl Acad Sci U S A* **103**, 4640-4645, doi:0509341103 [pii] 10.1073/pnas.0509341103 (2006).

269 Stanford, M. M., Barrett, J. W., Nazarian, S. H., Werden, S. & McFadden, G. Oncolytic virotherapy synergism with signaling inhibitors: Rapamycin increases myxoma virus tropism for human tumor cells. *J Virol* **81**, 1251-1260, doi:JVI.01408-06 [pii] 10.1128/JVI.01408-06 (2007).

270 Nicholson, K. M. & Anderson, N. G. The protein kinase B/Akt signalling pathway in human malignancy. *Cell Signal* **14**, 381-395 (2002).

271 Weichhart, T. & Säemann, M. D. The PI3K/Akt/mTOR pathway in innate immune cells: emerging therapeutic applications. *Ann Rheum Dis* **67 Suppl 3**, iii70-74, doi:10.1136/ard.2008.098459 (2008).

272 Werden, S. J. *et al.* The myxoma virus m-t5 ankyrin repeat host range protein is a novel adaptor that coordinately links the cellular signaling pathways mediated by Akt and Skp1 in virus-infected cells. *J Virol* **83**, 12068-12083, doi:10.1128/JVI.00963-09 (2009).

273 Johnston, J. B. *et al.* Myxoma virus M-T5 protects infected cells from the stress of cell cycle arrest through its interaction with host cell cullin-1. *J Virol* **79**, 10750-10763, doi:10.1128/JVI.79.16.10750-10763.2005 (2005).

274 Stanford, M. M. & McFadden, G. Myxoma virus and oncolytic virotherapy: a new biologic weapon in the war against cancer. *Expert Opin Biol Ther* **7**, 1415-1425, doi:10.1517/14712598.7.9.1415 (2007).

275 Thirukkumaran, C. M. & Morris, D. G. Oncolytic virotherapy for multiple myeloma: past, present, and future. *Bone Marrow Res* **2011**, 632948, doi:10.1155/2011/632948 (2011).

276 Chan, W. M. *et al.* Myxoma and vaccinia viruses bind differentially to human leukocytes. *J Virol* **87**, 4445-4460, doi:10.1128/JVI.03488-12 (2013).

277 Bartee, E., Chan, W. M., Moreb, J. S., Cogle, C. R. & McFadden, G. Selective purging of human multiple myeloma cells from autologous stem cell transplantation grafts using oncolytic myxoma virus. *Biol Blood Marrow Transplant* **18**, 1540-1551, doi:10.1016/j.bbmt.2012.04.004 (2012).

278 Madlambayan, G. J. *et al.* Acute myeloid leukemia targeting by myxoma virus in vivo depends on cell binding but not permissiveness to infection in vitro. *Leuk Res* **36**, 619-624, doi:10.1016/j.leukres.2012.01.020 (2012).

279 Rahman, M. M., Madlambayan, G. J., Cogle, C. R. & McFadden, G. Oncolytic viral purging of leukemic hematopoietic stem and progenitor cells with Myxoma virus. *Cytokine Growth Factor Rev* **21**, 169-175, doi:10.1016/j.cytogfr.2010.02.010 (2010).

280 Kim, M. *et al.* Myxoma virus targets primary human leukemic stem and progenitor cells while sparing normal hematopoietic stem and progenitor cells. *Leukemia* **23**, 2313-2317, doi:10.1038/leu.2009.219 (2009).

281 Chaproniere, D. M. & Andrewes, C. H. Cultivation of rabbit myxoma and fibroma viruses in tissues of nonsusceptible hosts. *Virology* **4**, 351-365 (1957).

282 Lun, X. *et al.* Myxoma virus is a novel oncolytic virus with significant antitumor activity against experimental human gliomas. *Cancer Res* **65**, 9982-9990, doi:10.1158/0008-5472.CAN-05-1201 (2005).

283 Lun, X. Q. *et al.* Targeting human medulloblastoma: oncolytic virotherapy with myxoma virus is enhanced by rapamycin. *Cancer Res* **67**, 8818-8827, doi:67/18/8818 [pii] 10.1158/0008-5472.CAN-07-1214 (2007).

284 Wu, Y. *et al.* Oncolytic efficacy of recombinant vesicular stomatitis virus and myxoma virus in experimental models of rhabdoid tumors. *Clin Cancer Res* **14**, 1218-1227, doi:10.1158/1078-0432.CCR-07-1330 (2008).

285 Stanford, M. M. *et al.* Myxoma virus oncolysis of primary and metastatic B16F10 mouse tumors in vivo. *Mol Ther* **16**, 52-59, doi:10.1038/sj.mt.6300348 (2008).

286 Lun, X. *et al.* Myxoma virus virotherapy for glioma in immunocompetent animal models: optimizing administration routes and synergy with rapamycin. *Cancer Res* **70**, 598-608, doi:10.1158/0008-5472.CAN-09-1510 (2010).

287 Werden, S. J. & McFadden, G. Pharmacological manipulation of the akt signaling pathway regulates myxoma virus replication and tropism in human cancer cells. *J Virol* **84**, 3287-3302, doi:10.1128/JVI.02020-09 (2010).

288 Zemp, F. J. *et al.* Treating brain tumor-initiating cells using a combination of myxoma virus and rapamycin. *Neuro Oncol*, doi:10.1093/neuonc/not035 (2013).

289 Thomas, D. L. *et al.* Myxoma virus combined with rapamycin treatment enhances adoptive T cell therapy for murine melanoma brain tumors. *Cancer Immunol Immunother* **60**, 1461-1472, doi:10.1007/s00262-011-1045-z (2011).

290 Teferi, W. M., Dodd, K., Maranchuk, R., Favis, N. & Evans, D. H. A whole-genome RNA interference screen for human cell factors affecting myxoma virus replication. *J Virol*, doi:10.1128/jvi.02617-12 (2013).

291 Kaur, B., Cripe, T. P. & Chiocca, E. A. "Buy one get one free": armed viruses for the treatment of cancer cells and their microenvironment. *Curr Gene Ther* **9**, 341-355 (2009).

292 Del Vecchio, M. *et al.* Interleukin-12: biological properties and clinical application. *Clin Cancer Res* **13**, 4677-4685, doi:10.1158/1078-0432.CCR-07-0776 (2007).

293 Parker, J. N. *et al.* Engineered herpes simplex virus expressing IL-12 in the treatment of experimental murine brain tumors. *Proc Natl Acad Sci U S A* **97**, 2208-2213, doi:10.1073/pnas.040557897 (2000).

294 Hellums, E. K. *et al.* Increased efficacy of an interleukin-12-secreting herpes simplex virus in a syngeneic intracranial murine glioma model. *Neuro Oncol* **7**, 213-224, doi:10.1215/S1152851705000074 (2005).

295 Stanford, M. M., Barrett, J. W., Gilbert, P. A., Bankert, R. & McFadden, G. Myxoma virus expressing human interleukin-12 does not induce myxomatosis in European rabbits. *J Virol* **81**, 12704-12708, doi:10.1128/JVI.01483-07 (2007).

296 Liu, J. *et al.* Myxoma virus expressing interleukin-15 fails to cause lethal myxomatosis in European rabbits. *J Virol* **83**, 5933-5938, doi:10.1128/JVI.00204-09 (2009).

297 Aboody, K. S. *et al.* Neural stem cells display extensive tropism for pathology in adult brain: evidence from intracranial gliomas. *Proc Natl Acad Sci U S A* **97**, 12846-12851, doi:10.1073/pnas.97.23.12846 (2000).

298 Josiah, D. T. *et al.* Adipose-derived stem cells as therapeutic delivery vehicles of an oncolytic virus for glioblastoma. *Mol Ther* **18**, 377-385, doi:10.1038/mt.2009.265 (2010).

299 Shmulevitz, M., Gujar, S. A., Ahn, D. G., Mohamed, A. & Lee, P. W. Reovirus variants with mutations in genome segments S1 and L2 exhibit enhanced virion infectivity and superior oncolysis. *J Virol* **86**, 7403-7413, doi:10.1128/jvi.00304-12 (2012).

300 Kirn, D. H., Wang, Y., Liang, W., Contag, C. H. & Thorne, S. H. Enhancing poxvirus oncolytic effects through increased spread and immune evasion. *Cancer Res* **68**, 2071-2075, doi:68/7/2071 [pii] 10.1158/0008-5472.CAN-07-6515 (2008).

301 Thirunavukarasu, P. *et al.* A Rationally Designed A34R Mutant Oncolytic Poxvirus: Improved Efficacy in Peritoneal Carcinomatosis. *Mol Ther*, doi:10.1038/mt.2013.27 (2013).

302 Griffith, M., Trinkause-Randall, V., Watsky, M. A., Liu, C. Y. & Sheardown, H. in *Methods in tissue engineering* (ed A. and R. P. Lanza Atala) 131-140 (Academic Press, 2002).

303 Chan, K. Y. & Haschke, R. H. Isolation and culture of corneal cells and their interactions with dissociated trigeminal neurons. *Experimental eye research* **35**, 137-156 (1982).

304 Katsafanas, G. C. & Moss, B. Colocalization of Transcription and Translation within Cytoplasmic Poxvirus Factories Coordinates Viral Expression and Subjugates Host Functions. *Cell Host & Microbe* **2**, 221-228, doi:10.1016/j.chom.2007.08.005 (2007).

305 Opgenorth, A., Graham, K., Nation, N., Strayer, D. & McFadden, G. Deletion analysis of two tandemly arranged virulence genes in myxoma virus, M11L and myxoma growth factor. *J Virol* **66**, 4720-4731 (1992).

306 Bennett, C. J., Webb, M., Willer, D. O. & Evans, D. H. Genetic and phylogenetic characterization of the type II cyclobutane pyrimidine dimer photolyases encoded by Leporipoxviruses. *Virology* **315**, 10-19 (2003).

307 Barry, M. *et al.* The myxoma virus M-T4 gene encodes a novel RDEL-containing protein that is retained within the endoplasmic reticulum and is important for the productive infection of lymphocytes. *Virology* **239**, 360-377, doi:10.1006/viro.1997.8894 (1997).

308 Smallwood, S. E., Rahman, M. M., Smith, D. W. & McFadden, G. Myxoma virus: propagation, purification, quantification, and storage. *Curr Protoc Microbiol* **Chapter 14**, Unit 14A 11, doi:10.1002/9780471729259.mc14a01s17 (2010).

309 Bratke, K. A., McLysaght, A. & Rothenburg, S. A survey of host range genes in poxvirus genomes. *Infection, Genetics and Evolution* **14**, 406-425, doi:http://dx.doi.org/10.1016/j.meegid.2012.12.002 (2013).

310 Tung, C. H. *et al.* In vivo imaging of beta-galactosidase activity using far red fluorescent switch. *Cancer Res* **64**, 1579-1583 (2004).

311 Gong, H. *et al.* beta-Galactosidase activity assay using far-red-shifted fluorescent substrate DDAOG. *Anal Biochem* **386**, 59-64, doi:10.1016/j.ab.2008.11.031 (2009).

312 Payne, L. G. & Kristensson, K. The effect of cytochalasin D and monensin on enveloped vaccinia virus release. *Arch Virol* **74**, 11-20 (1982).

313 Scott, R. W. & Olson, M. F. LIM kinases: function, regulation and association with human disease. *J Mol Med (Berl)* **85**, 555-568, doi:10.1007/s00109-007-0165-6 (2007).

314 Scott, R. W. *et al.* LIM kinases are required for invasive path generation by tumor and tumor-associated stromal cells. *J Cell Biol* **191**, 169-185, doi:10.1083/jcb.201002041 (2010).

315 Mercer, A., Schmidt, A., Weber, O. & Smith, G. in *Poxviruses Birkhäuser Advances in Infectious Diseases* 113-125 (Birkhäuser Basel, 2007).

316 Burles, K. A. & University of Alberta. Dept. of Medical Microbiology and Immunology. (2012).

317 Mullick, J. *et al.* Identification of complement regulatory domains in vaccinia virus complement control protein. *J Virol* **79**, 12382-12393, doi:10.1128/JVI.79.19.12382-12393.2005 (2005).

318 Law, M., Hollinshead, M., Lee, H. J. & Smith, G. L. Yaba-like disease virus protein Y144R, a member of the complement control protein family, is present on enveloped virions that are associated with virus-induced actin tails. *J Gen Virol* **85**, 1279-1290 (2004).

319 Senkevich, T. G., Koonin, E. V., Bugert, J. J., Darai, G. & Moss, B. The genome of molluscum contagiosum virus: analysis and comparison with other poxviruses. *Virology* **233**, 19-42, doi:10.1006/viro.1997.8607 (1997).

320 Ogawa, R., Calvert, J. G., Yanagida, N. & Nazerian, K. Insertional inactivation of a fowlpox virus homologue of the vaccinia virus F12L gene inhibits the release of enveloped virions. *J Gen Virol* **74 (Pt 1)**, 55-64 (1993).

321 Hughes, A. L., Irausquin, S. & Friedman, R. The evolutionary biology of poxviruses. *Infect Genet Evol* **10**, 50-59, doi:10.1016/j.meegid.2009.10.001 (2010).

322 Antoine, G., Scheiflinger, F., Dorner, F. & Falkner, F. G. The complete genomic sequence of the modified vaccinia Ankara strain: comparison with other orthopoxviruses. *Virology* **244**, 365-396, doi:10.1006/viro.1998.9123 (1998).

323 Tulman, E. R. *et al.* The genomes of sheeppox and goatpox viruses. *J Virol* **76**, 6054-6061 (2002).

324 Boulanger, D., Baier, R., Erfle, V. & Sutter, G. Generation of recombinant fowlpox virus using the non-essential F11L orthologue as insertion site and a rapid transient selection strategy. *J Virol Methods* **106**, 141-151 (2002).

325 FENNER, F., DAY, M. F. & WOODROOFE, G. M. Epidemiological consequences of the mechanical transmission of myxomatosis by mosquitoes. *J Hyg (Lond)* **54**, 284-303 (1956).

326 Palmer, T. D., Rosman, G. J., Osborne, W. R. & Miller, A. D. Genetically modified skin fibroblasts persist long after transplantation but gradually inactivate introduced genes. *Proc Natl Acad Sci U S A* **88**, 1330-1334 (1991).

327 Ridley, A. J. RhoA, RhoB and RhoC have different roles in cancer cell migration. *J Microsc*, doi:10.1111/jmi.12025 (2013).

328 Bernard, O. Lim kinases, regulators of actin dynamics. *Int J Biochem Cell Biol* **39**, 1071-1076, doi:10.1016/j.biocel.2006.11.011 (2007).

329 McHenry, P. R. & Vargo-Gogola, T. Pleiotropic functions of Rho GTPase signaling: a Trojan horse or Achilles' heel for breast cancer treatment? *Curr Drug Targets* **11**, 1043-1058 (2010).

330 Harrison, B. A. *et al.* Novel class of LIM-kinase 2 inhibitors for the treatment of ocular hypertension and associated glaucoma. *J Med Chem* **52**, 6515-6518, doi:10.1021/jm901226j (2009).

331 Gauvin, T. J., Fukui, J., Peterson, J. R. & Higgs, H. N. Isoform-selective chemical inhibition of mDia-mediated actin assembly. *Biochemistry* **48**, 9327-9329, doi:10.1021/bi901354z (2009).

332 Shang, X. *et al.* Rational design of small molecule inhibitors targeting RhoA subfamily Rho GTPases. *Chem Biol* **19**, 699-710, doi:10.1016/j.chembiol.2012.05.009 (2012).

APPENDIX: SUPPORTING METHODOLOGY AND DATA

Generation of polyclonal antibodies:

Polyclonal antibodies against A34 (Y_{101}-A_{140}) and A36 (T_{142}-E_{214}) were generated as follows; corresponding regions of the genes were PCR amplified and Topo-cloned as outlined in section 2.1. The resulting clones were digested with *BamHI* and *EcoRI,* and the desired regions subcloned into pGEX-2T (Promega). This generated regions of A34R or A36R which were fused with an N-terminal glutathione-S-transferase (GST) tag, and under the control of an IPTG-inducible promoter. These plasmids were then transformed into the BL21 **(**F^- *ompT hsdS*$_B$ *(*$r_B^-m_B^-$*) gal dcm rne131 (DE3))* protein expression strain of *E.coli*.

To express protein, 5 L of bacterial culture were grown to an OD_{600} of 0.6 in LB. Protein expression was induced with 1mM IPTG addition and, 3 h later, bacterial cells pelleted. The bacteria were then lysed using BugBuster lysis buffer (2mL/g of bacteria) containing 10 U/mL benzonase and r-lysozyme (Novagen). Following centrifugation and filtration, the soluble protein was loaded onto a GST-affinity column (GE) and purified using an AKTA HPLC. Columns were washed with 5 column-volumes of buffer containing 150mM NaCl and 20mM $NaPO_4$ pH 7.3. Protein was then eluted using 10mM glutathione in 50mM Tris pH 8.0, and collected in 1 mL fractions. Fractions containing the desired protein were pooled, as determined by SDS-PAGE and OD_{260} values, dialyzed overnight into PBS, and then protein concentration determined by a Bradford assay. **Figure A.1 A&B** shows SDS-PAGE gels of the purified protein. The purified proteins were sent to ProSci Incorporated (Poway CA, USA), which immunized 4 rabbits with each immunogen. Following the third bleed, viral lysates were screened for reactivity to viral lysates. Serum from one rabbit for each protein was selected for subsequent use **(Figure A.1 C&D).**

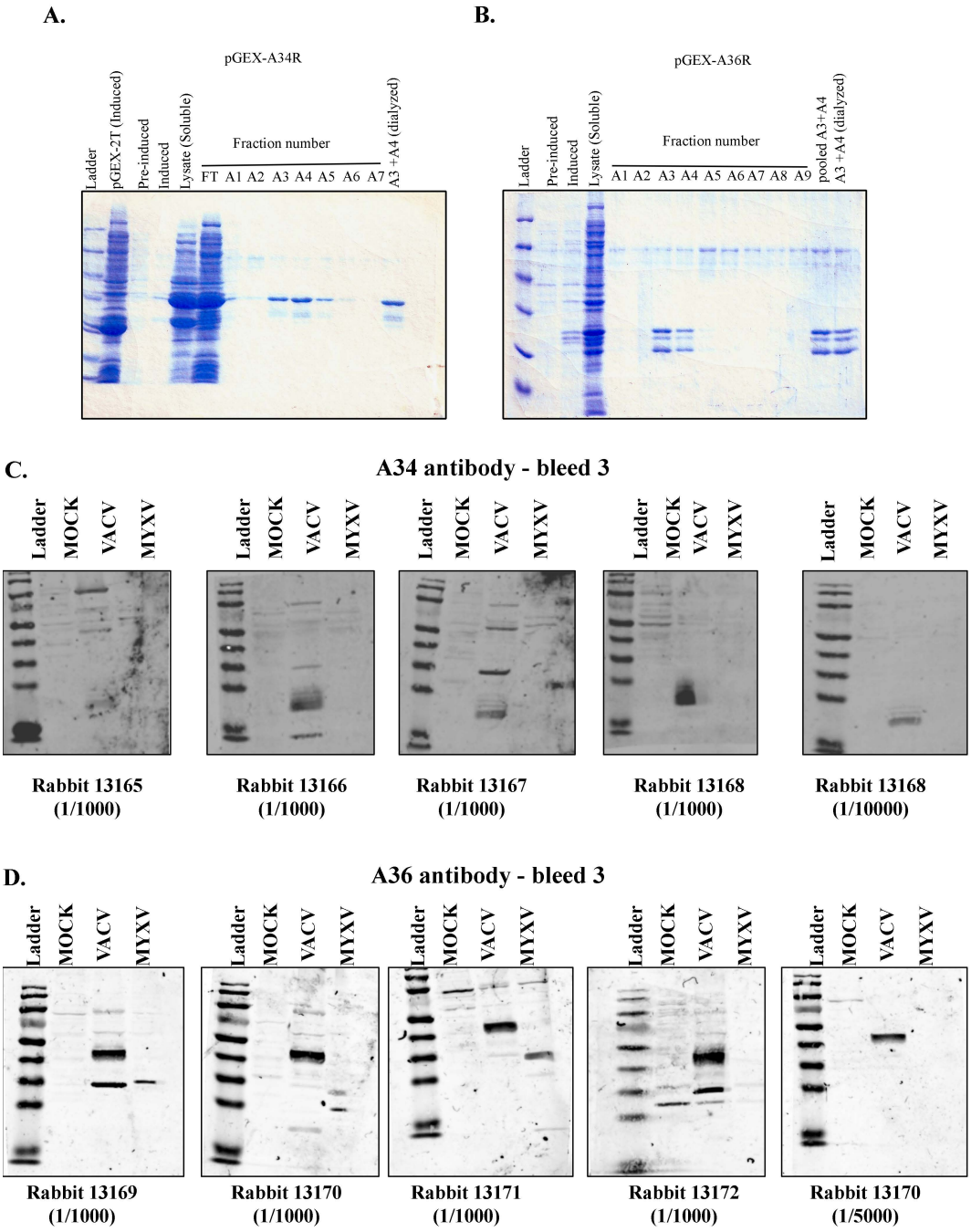

Figure A.1: Production of polyclonal antibodies against VACV A34 and A36. (A+B): Coomassie blue stained SDS-PAGE gels of GST-fusion protein following GST-affinity purification as described in text **(A)** A34 **(B)** A36 **(C+D)** Analysis of anti-sera against viral lysates following bleed 3 of immunized rabbits. Lysates were prepared from BGMK cells that had been infected with WT VACV or MYXV for 24 h at a MOI=5. (C) A34-serum from rabbit 13168 was selected for subsequent use, and conditions optimized (right) (D) A36-serum from rabbit 13170 was selected for subsequent use and conditions optimized (right)

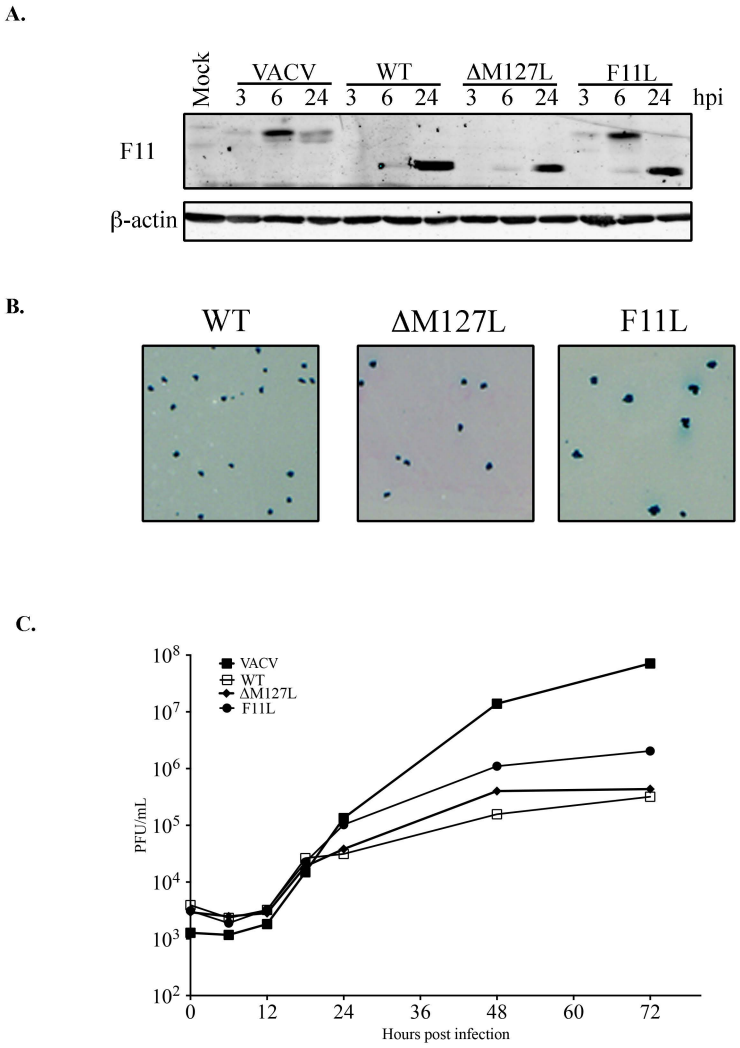

Figure A.2: Characterization of F11L MYXV lacking mCherry fluorescent protein: An F11L expressing strain of MYXV was generated similarly to that used in experiments depicted in Chapters 3 and 6, however this virus lacked mCherry fluorescent protein. (A) western blot analysis of recombinants. BGMK cells were infected at MOI of 5 with respective viruses, harvested at indicated times, and western blot analysis performed using antibodies against F11 and actin. (B) Plaque morphology at 4 days post-infection (C) Analysis of the growth properties of virus. BGMK cells were infected at MOI of 0.01, harvested at indicated times, and titered on BGMK cells. Mean + S.E.M. from three independent experiments are shown.

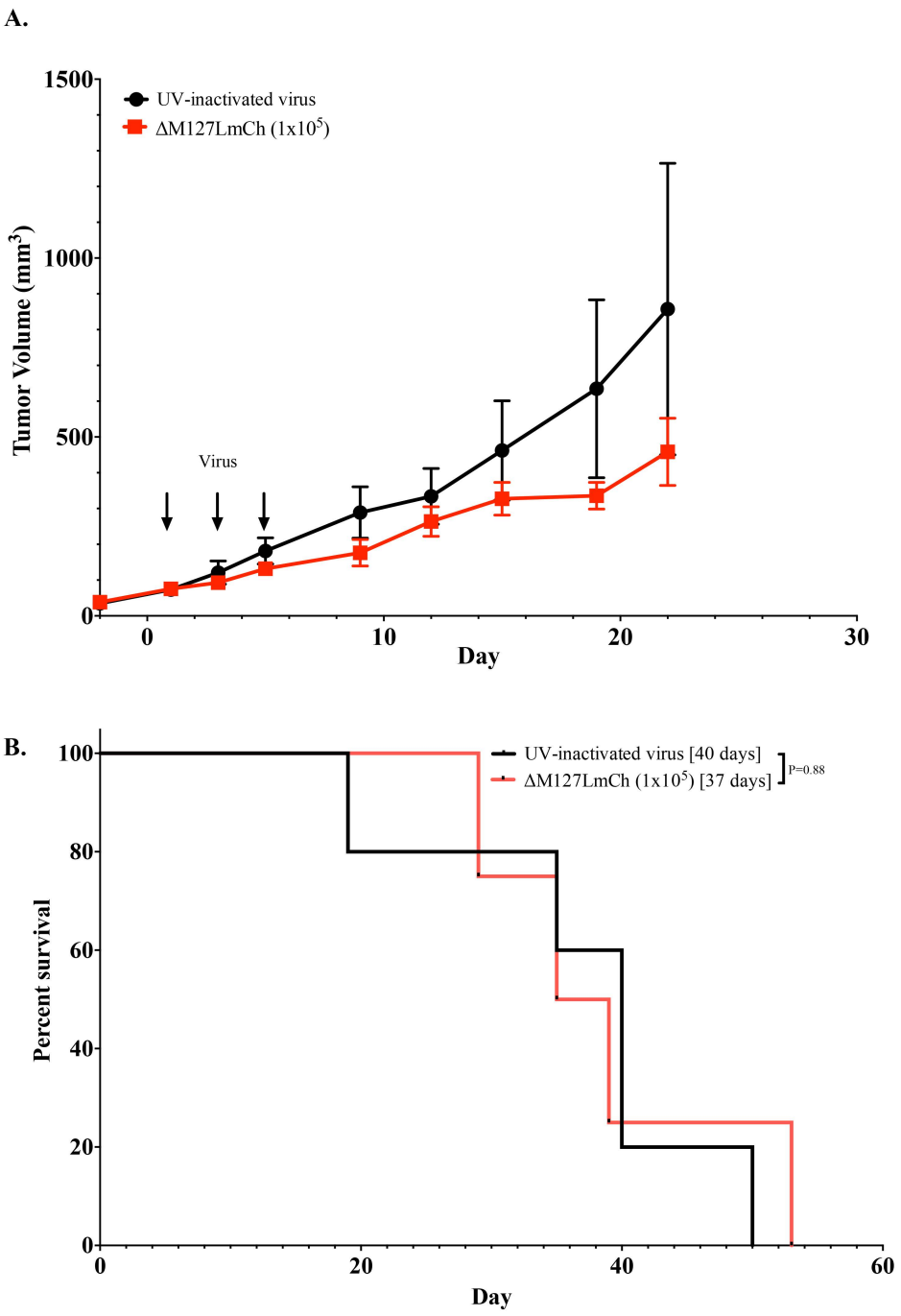

Figure A.3: Evaluation of oncolytic MYXV using 10^5 pfu dose of virus: The experimental setup was similar to that shown in single tumor models depicted in Chapters 5 and 6 except doses of 10^5 pfu were administered. UV n=5, Live virus n=4. **(A)** Tumor growth. Tumor size was measured twice-weekly using calipers and shows the mean tumor volume ± S.E.M. **(B)** Kaplan-Meier survival plot. The fraction of animals surviving at each time point is indicated as well as the median survival times for each cohort (inset). Survival curve comparisons were calculated using the Log-Rank (Mantel-Cox) test built into Prism's software.

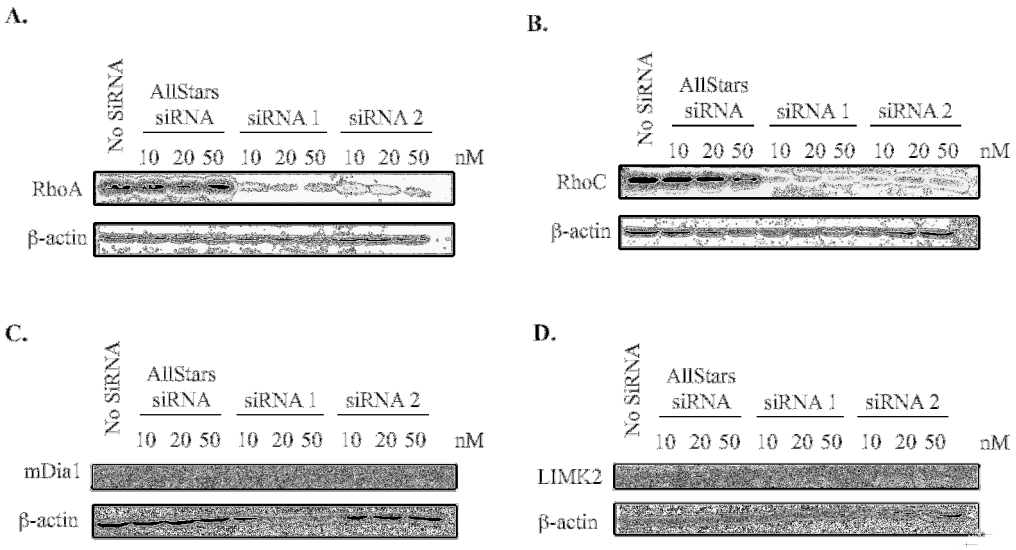

Figure A4: Optimization of conditions for siRNA-mediating silencing of RhoA, RhoC, mDia1, LIMK2 in MDA-MB-231 cells. MDA-MB-231 cells were transfected with given siRNAs at either 10, 20 or 50 nM concentration. After 48 h cells were harvested, lysed, and western blotted using antibodies against either RhoA (A), RhoC (B), mDia1 (C) or LIMK2 (D), along with antibodies against β-actin. In parallel to these reactions cells were transfected with similar concentrations of a non-targetting AllStars siRNA control. From these conditions it was decided that all siRNA experiments, shown in Figure 6.5, would be done using 10 nM concentrations.